MATHEMATICAL MODELING OF HIV-TB CO-INFECTION WITH OPTIMAL CONTROL: A CAPUTO FRACTIONAL APPROACH

Abdurkadir Edeo Gemeda

A Dissertation Submitted to the Department of Applied Mathematics, College of Applied Natural Science

Presented in Partial Fulfillment of the Requirement for the Degree of Doctor of Philosophy in Applied Mathematics

School of Graduate Studies
Adama Science and Technology University

December, 2025
Adama, Ethiopia

Mathematical Modeling of HIV-TB Co-infection with Optimal Control: A Caputo Fractional Approach

Abdurkadir Edeo Gemeda

Supervisor: Dr. Legese Lemecha Obsu
Co-Supervisors: Dr. Eshetu Dadi Gurmu
Dr. Shambel Tadesse Degefa

A Dissertation Submitted to the Department of Applied Mathematics, College of Applied Natural Science

Presented in Partial Fulfillment of the Requirement for the Degree of Doctor of Philosophy in Applied Mathematics

School of Graduate Studies
Adama Science and Technology University

December, 2025
Adama, Ethiopia

DECLARATION

I declare that this dissertation entitled **"Mathematical Modeling of HIV-TB Co-infection with Optimal Control: A Caputo Fractional Approach"** is my own work and has not been submitted to any university for similar purpose. The references used in this proposal are duly recognized by proper citations.

Abdurkadir Edeo Gemeda	_____	_____
Student name	Signature	Date

RECOMMENDATION

We, the supervisors of this dissertation, hereby certify that we have read and revised the dissertation entitled "**Mathematical Modeling of HIV-TB Co-infection with Optimal Control: A Caputo Fractional Approach**" prepared under our guidance by **Abdurkadir Edeo Gemeda** submitted in partial fulfillment of the requirements for the degree of Doctor of Philosophy in Applied Mathematics. Therefore, we recommend the submission of the dissertation to the department for further review and defense.

Main Supervisor	Signature	Date
Co-Supervisor 1	Signature	Date
Co-Supervisor 2	Signature	Date

APPROVAL PAGE

We hereby certify that the recommendations and suggestions made by the board of examiners are appropriately incorporated into the final version of the dissertation entitled "**Mathematical Modeling of HIV-TB Co-infection with Optimal Control: A Caputo Fractional Approach**" by **Abdurkadir Edeo Gemeda**.

Main Supervisor	Signature	Date
Co-Supervisor 1	Signature	Date
Co-Supervisor 2	Signature	Date

We, the undersigned, members of the Board of Examiners of the dissertation open defense by **Abdurkadir Edeo Gemeda** have read and evaluated the dissertation entitled "**Mathematical Modeling of HIV-TB Co-infection with Optimal Control: A Caputo Fractional Approach**" and examined the candidate during open defense. This is, therefore, to certify that the dissertation is accepted for partial fulfillment of the requirement of the degree of Doctor of Philosophy in Applied Mathematics.

Chair person	Signature	Date
Internal Examiner 1	Signature	Date
Internal Examiner 2	Signature	Date
External Examiner 1	Signature	Date
External Examiner 2	Signature	Date

Finally, approval and acceptance of the dissertation is contingent upon submission of its final copy to the School of Postgraduate Studies (SPGS) through the candidate's Department Graduate Council (DGC) and College Graduate Committee (CGC).

Department Head	Signature	Date
College Dean	Signature	Date
School of Postgraduate Studies, Dean	Signature	Date

ACKNOWLEDGMENTS

First and foremost, I wish to convey my profound gratitude to Almighty God for blessing me with the chance to engage in daily activities and relish the invigorating freshness of the air. I am especially grateful to my supervisors, Dr. Legesse Lemecha, Dr. Eshetu Dadi, and Dr. Shambel Tadese whose inspiration and invaluable guidance have been pivotal in my journey through scientific research. I greatly appreciate their support, which has spanned from the initial selection of my research title to the comprehensive review of this dissertation, significantly enhancing its quality. Their insightful advice on the organization and themes of the dissertation has been instrumental in bringing it to completion.

I would also like to extend my heartfelt thanks to Arsi University for its generous financial support of my educational and research pursuits, allowing me to engage fully in this academic program. Furthermore, I am deeply grateful to Adama Science and Technology University for fostering an exceptional environment for learning and research throughout my studies. Last, but not least, I wish to express my deepest gratitude to my spouse Makida Biftu, my children Sena, Mersen, Aziza and Bilal, and all my friends for their patience and steadfast support during the development of this dissertation.

TABLE OF CONTENTS

LIST OF TABLES

LIST OF FIGURES

ABBREVIATIONS AND ACRONYMS

AIDS	Acquired Immune Deficiency Syndrome
ART	Antiretroviral Therapy
BCG	Bacille Calmette-Guerin
CCOHS	Canadian Center for Occupational Health and Safety
CIDRAP	Center for Infectious Disease Research and Policy
DR-TB	Drug-Resistant Tuberculosis
ECDC	Ethiopian Center for Disease Control
ENA	Ethiopian News Agency
EPHI	Ethiopian Public Health Institute
FDEs	Fractional Differential Equations
FOCP	Fractional Order Control Problem
HIV	Human Immunodeficiency Virus
IPT	Isoniazid Preventive Therapy
IRIS	Immune Reconstitution Inflammatory Syndrome
MDR-TB	Multi Drug-Resistant Tuberculosis
PEP	Post-Exposure Prophylaxis
PLHIV	People Living with HIV
PrEP	Pre-Exposure Prophylaxis
RR-TB	Rifampiicin-Resistant Tuberculosis
TB	Tuberculosis
TBCAB	Global TB Community Advisory Board
TPT	TB Preventive Therapy
UNAIDS	United Nations Programme on HIV/AIDS
WHO	World Health Organization
XDR-TB	Extensively Drug-Resistant Tuberculosis

ABSTRACT

Human immunodeficiency virus (HIV) and tuberculosis (TB) remain among the most devastating infectious diseases worldwide, particularly in sub-Saharan Africa. The interaction between these diseases through co-infection produce significant challenges for effective disease management. HIV compromises the immune system which increases risk of developing active TB, while TB exacerbates the progression of HIV to AIDS. Understanding the dynamics of these diseases and evaluating the impact of intervention strategies is therefore essential for effective control. In this dissertation, we develop and analyze a series of Caputo fractional order mathematical models to study the transmission dynamics of HIV, TB, and their co-infections. First, an HIV/AIDS model incorporating PrEP and drug-resistant strain is proposed. Analysis shows that reducing transmission rate, PrEP discontinuation rate, and drug resistance development rate, while increasing PrEP uptake and detection rates of symptomatic cases, significantly decreases HIV prevalence. Next, a TB model is formulated to investigate the impact of vaccination and treatment interventions. The finding indicates that increased vaccination and treatment rates, coupled with reduced effective contact, substantially decrease TB prevalence. Extending this model into a Caputo fractional optimal control framework, we proposed and analyzed seven different intervention strategies: prevention alone, vaccination alone, treatment alone, prevention combined with vaccination, prevention combined with treatment, vaccination combined with treatment, and all three combined together, among which vaccination alone emerges as the most cost-effective intervention strategy. Finally, two HIV-TB co-infection models are developed, with parameters estimated using real-data obtained from Ethiopia. An optimal control analysis demonstrates that simultaneous HIV and TB treatment strategy yields the most effective reduction in disease burden at minimal cost. Numerical simulations across models support the analytical findings, and stability analyses confirm that the disease-free equilibrium is locally asymptotically stable when all the eigenvalues of the linearized matrix satisfy the Matignon's fractional stability criterion and globally stable whenever the constructed Lyapunov functions monotonically decay to zero. Overall, the dissertation illustrates the importance of Caputo fractional-order models and fractional optimal control theory in understanding the complex dynamics of HIV, TB, and their co-infection and provides valuable insights for designing cost-effective public health strategies with long-term policy effects in Ethiopia and similar burden regions.

Keywords: HIV; TB; HIV-TB co-infection; Caputo fractional approach; Vaccination; Treatment therapies; PrEP; ART; Drug-resistant strains; Numerical simulations

CHAPTER 1

INTRODUCTION

This chapter provides a concise overview of the background regarding infectious diseases and their global health impacts. It specifically examines the dynamics of HIV and TB, along with their co-infections, and evaluates the limitations of current intervention strategies aimed at combating these diseases. Additionally, the chapter presents the applications and constraints of classical epidemic models, as well as the refinements demonstrated by advanced mathematical models. Furthermore, it discusses the theoretical foundations, rationale, and applications of fractional order modeling, highlighting its advantages over integer-order modeling. The chapter also addresses the conceptual framework and identifies gaps in the co-infection modeling of fractional optimal control problems. Finally, it articulates the statement of the problem, outlines the objectives of the study, and underscores the significance, delimitation, and scope of the proposed research.

1.1 Background of the Study

1.1.1 Infectious Disease and Global Burden

Infectious diseases are brought on by pathogenic microorganisms such as bacteria, viruses, fungi, and parasites, and they can spread by direct contact, air droplets, and contaminated surfaces, among other ways. Globally, these diseases affect millions of people and are a major cause of morbidity and mortality (Michuad, 2009; CIDRAP, 2024). The WHO reported that Malaria, TB, and HIV are among the top causes of deaths. Approximately 630,000 individuals lost their lives due to HIV-related causes in 2024, and 1.3 million people contracted the virus. In the same year, 40.8 million individuals worldwide were living with HIV, with 65% of those in the WHO African Region (ContagionLive, 2020; WHO, 2025b, 2025d; UNAIDS, 2025a).

According to the WHO's 2024 Global Tuberculosis Report, 8.2 million individuals had a new TB diagnosis in 2023, the most since 1995. Among these, TB killed 1.25 million people including 161,000 HIV-positive individuals. The intertwined challenges associated with HIV and TB are highlighted in recent WHO and UNAIDS reports. For instance, about one-third of all AIDS-related deaths are caused by tuberculosis, which continued to be a major cause of deaths for PLHIV. Despite advancements, only 58% of co-infected individuals with HIV/AIDS and TB received antiretroviral treatment in 2023. The studies also alert readers about possible obstacles caused by financial cuts, which have disrupted TB/HIV care and could lead to a recurrence of TB cases (AfricaNews, 2024; TBCAB, 2025; UNAIDS, 2025b).

The impact of infectious diseases extends beyond individual health, straining healthcare systems, economies, and societal structures, particularly in low- and middle-income countries. Moreover, emerging infectious diseases continue to challenge global health security. Effective prevention and control strategies are essential, including vaccination, improved sanitation, and public health education. Understanding the complex dynamics of disease transmission and the factors that contribute to outbreaks is crucial for developing targeted interventions and mitigating the impact of infectious diseases on global health (Wired, 2020; Annual, 2022).

1.1.2 Dynamics of HIV, TB and their Co-infection

HIV Dynamics

The human immunodeficiency virus (HIV) impacts the immune system by damaging white blood cells, which impairs its function. In the initial weeks following infection, individuals may remain asymptomatic or experience flu-like symptoms such as fever, headache, rash, sore throat, diarrhea, and lymphadenopathy. The infection progresses through three distinct stages: the acute phase, characterized by a high risk of transmission and rapid virus spread; the chronic phase, also known as clinical latency, where viral replication slows down; and the final stage, AIDS, which is diagnosed when an individual's CD4+ count falls below 200 cells/mm^3. This stage results in significant immunocompromise, making individuals susceptible to opportunistic infections (HIV-info.NIH.gov, 2021).

According to WHO (2023b), HIV transmission occurs through the exchange of specific bodily fluids, and can also be transmitted from mother to child during pregnancy and childbirth. Importantly, routine social interactions such as kissing, hugging, handshakes, and sharing food or beverages do not spread HIV. This understanding highlights that HIV is a preventable disease.

An HIV prevention, control, and treatment strategies encompass a multifaceted approach aimed at reducing transmission and improving health outcomes for those affected. Primary prevention methods include the promotion of safe sex practices, such as consistent condom use and the use of PrEP, which has been shown to significantly lower the risk of acquiring HIV among high-risk populations(HIVinfo.NIH.gov, 2025).

Regular HIV testing and counseling are vital for early detection and linking individuals to care, allowing for timely initiation of ART. For those living with HIV, ART serves as the cornerstone of treatment, effectively suppressing viral load to undetectable levels and improving immune function, which also helps prevent transmission. Moreover, integrating services like HIV and TB screening is crucial for providing comprehensive care, especially in resource-limited settings. Together, these strategies form a holistic approach to addressing the HIV epidemic, focusing on both prevention and the sustained health of affected individuals (WHO, 2025e).

The impact of increasing PrEP coverage on HIV/AIDS transmission in Brazil has been examined in (Moya et al., 2024) using a mathematical model that included case diagnosis for PrEP entry. The findings indicated that higher PrEP coverage significantly reduces HIV incidence and increases the number of cases avoided.

Current HIV/AIDS interventions are limited by unequal access to PrEP for marginalized communities and the emergence of drug-resistant HIV strains, which threaten the effectiveness of ART. These issues arise from economic, geographic, and racial barriers, stigma, and inadequate culturally competent healthcare (AIDSMAP, 2019, 2022).

TB Dynamics

Tuberculosis (TB), caused by the rod-shaped bacterium Mycobacterium tuberculosis, is an infectious airborne disease primarily affecting the lungs, although it can also impact the skin, spine, brain, and kidneys. Transmission occurs through the cough, sneeze, or saliva of infected individuals. Symptoms of active TB include a persistent cough (sometimes with blood), chest pain, weakness, fatigue, weight loss, fever, and night sweats, which can vary depending on the affected body part (WHO, 2023a).

Tuberculosis exists in two stages: latent TB infection, where individuals are asymptomatic and non-infectious despite positive test results, and active TB, which occurs when the immune system fails to fight the bacteria, leading to illness and potential transmission. Latent TB may progress to active TB through two mechanisms: endogenous reactivation, where the dormant bacteria become active due to immune system instability, and exogenous reinfection, which arises from recent exposure to infectious sources such as individuals with active TB (CDC, 2020; Wangari & Stone, 2018).

Individuals who recover from TB may not develop lasting immunity, leading to potential recurrence of the disease either through relapse of the original Mycobacterium tuberculosis strain or reinfection with a different strain. This phenomenon is referred to as recurrent TB. Preventing TB involves several strategies, including seeking prompt medical attention for symptoms like prolonged cough, fever, or unexplained weight loss, which can enhance recovery and limit transmission. Testing is particularly important for high-risk populations, such as individuals with HIV or those in contact with TB patients (Chaisson & Churchyard, 2010; WHO, 2023c).

Adhering to the full course of TB treatment, practicing good hygiene (e.g., wearing masks, proper tissue disposal), and implementing infection control measures like adequate ventilation in healthcare settings are essential for reducing TB transmission. Treatment of TB is achievable with antibiotics such as isoniazid, rifampin, pyrazinamide, ethambutol, and streptomycin, which must be taken daily for four to six months. Premature discontinuation or improper use of these medications can lead to drug-resistant TB, which necessitates more complex and toxic treatment regimens. DR-TB refers to strains resistant to at least one first-line anti-TB medication, while MDR-TB is resistant to at least isoniazid and rifampicin, the two most effective anti-TB drugs (CDC, 2012; WHO, 2018).

Moreover, XDR-TB is a severe form of TB that is resistant to at least four core anti-TB drugs: isoniazid, rifampicin, fluoroquinolones, and aminoglycosides. This resistance presents significant treatment challenges and increases the risk of transmission among individuals. Treatment for XDR-TB is complex, often requiring lengthy regimens with less effective and more toxic medications. Its emergence is a major public health concern, as it limits effective treatment options and is associated with higher morbidity and mortality rates (WHO, 2024b).

Drug-resistant TB, particularly MDR-TB and XDR-TB, presents significant challenges for both treatment and modeling efforts. The development of drug resistance typically arises from human error, such as mismanagement of TB treatment, non-adherence to treatment, or the use of poor-quality drugs. Accurate modeling of drug-resistant TB is constrained by data limitations, variations in transmission dynamics, and the need to account for socioeconomic factors. Treatment outcomes for MDR-TB and XDR-TB are less favorable, requiring longer, more complex regimens with more side effects. Models evaluating intervention strategies must consider factors like improved diagnostics, access to second-line treatments, and adherence programs. The WHO estimates that 410,000 people developed MDR/RR-TB in 2022, with a treatment success rate of only 63%. Addressing these challenges is essential for devising effective public health strategies to combat DR-TB (WHO, 2024c; CCOHS, 2025).

The study by Oshinubi et al. (2023) focused on TB transmission in East African countries, incorporating vaccination and treatment into a deterministic mathematical model. The findings suggested that minimizing contact with infected individuals and increasing vaccination rates with high-efficacy vaccines can lower TB prevalence. The model used real data from Uganda and Rwanda to predict disease dynamics and found that increasing treatment availability significantly reduces the TB burden.

HIV-TB Co-infection Dynamics

The simultaneous presence of HIV and TB in an individual's body is referred to as HIV-TB co-infection. This combination is particularly dangerous, as each disease exacerbates the progression of the other. PLHIV are approximately 16 times more likely to develop active TB due to their compromised immune systems. If left untreated, this co-infection can significantly decrease life expectancy, with nearly all HIV-positive individuals suffering from TB facing a high risk of mortality (Singh et al., 2021; WHO, 2023c).

Multiple mechanisms through which TB reactivation contributes to HIV-TB co-infection has been outlined in (Azevedo-Pereira et al., 2023; CDC, 2025b). HIV weakens the immune system by depleting CD4+ T cells, increasing the risk of latent TB infections becoming active. Individuals with active TB are more infectious, raising co-infection risks among HIV-positive populations. Moreover, complications from overlapping TB and HIV treatment regimens can hinder management and adherence. High co-prevalence rates in sub-Saharan Africa, alongside socioeconomic challenges like poverty and limited healthcare access, further exacerbate the risk of co-infection. After ensuring that PLHIV are routinely screened for TB infection, appropriate treatment for either latent TB infection or active TB has to be initiated (CDC, 2020).

Furthermore, the studies in Letang et al. (2020); Navasardyan et al. (2024) highlighted several significant limitations in managing HIV-TB co-infection interventions. Diagnostic challenges arise from overlapping symptoms and the limited sensitivity of traditional tools, leading to delays in accurate diagnoses, particularly in immunocompromised individuals. The complexity of treatment is increased by drug interactions between ART and anti-TB medications, requiring careful monitoring. Access and equity issues are pronounced in low-resource settings, where socioeconomic disparities, geographic barriers, and stigma hinder individuals from seeking integrated care. Additionally, stigma and discrimination further discourage testing and treatment, complicating public health efforts.

Moreover, inadequate funding constrains the implementation of comprehensive programs, affecting prevention, diagnosis, and treatment. Poorly coordinated healthcare

systems and a lack of public awareness also contribute to fragmented services and misconceptions. Addressing these limitations requires improved diagnostics, increased access to integrated services, enhanced public awareness, and adequate funding to reduce the impact of HIV-TB co-infection on affected populations (Sester et al., 2010).

1.1.3 Mathematical Modeling in Epidemiology

Classical Epidemic Models

Classical epidemic models, such as the SIR and SEIR, are essential in epidemiology for understanding and predicting the spread of infectious diseases. The SIR model, developed by Kermack and McKendrick in 1927, categorizes a population into Susceptible (S), Infected (I), and Recovered (R) compartments, modeling disease spread through differential equations. It assumes a closed population with homogeneous mixing and permanent immunity. The SEIR model extends SIR by adding an Exposed (E) compartment for individuals who are infected but not yet infectious, making it suitable for diseases with a latency period. Both models rely on transmission and recovery rates, with SEIR including a rate for exposed individuals becoming infectious (Ozanne et al., 2019; Lee, 2025).

While foundational in epidemiology, SIR and SEIR models, have several limitations rooted in their mathematical formulation. They are deterministic, failing to capture the inherent stochasticity of disease spread, particularly in small populations or at the early stages of an outbreak. A key assumption is homogeneous mixing, which posits that all individuals have an equal probability of contact, an oversimplification because, in reality, social interactions are often structured and influenced by factors such as geography, social networks, and behavior. For instance, people tend to interact more frequently with family, friends, and colleagues rather than randomly with everyone in the population. Furthermore, they typically consider closed populations, ignoring migration and demographic changes. The models also lack individual-level detail, assuming uniform susceptibility and infectiousness. These simplifications can limit their accuracy in reflecting the complex dynamics of real-world epidemics (Chen et al., 2020; J. Wang, 2020; Roberto Telles et al., 2021).

Advanced Mathematical Modeling

Advanced mathematical epidemic models address the limitations of classical epidemic models by incorporating heterogeneous mixing, stochasticity, and other complexities. Heterogeneous mixing is modeled using network-based approaches, where

individuals are nodes connected by edges representing contacts, allowing for varied interaction patterns based on social structures or spatial locations. These network models can describe real-world systems more accurately. Stochastic models account for randomness in disease transmission, recovery, births, and deaths, which is particularly important when the number of infected individuals is small. Stochasticity is introduced through continuous-time Markov chains or stochastic differential equations (Allen, 2017; Y. Wang et al., 2023).

Other advancements include incorporating within-host kinetics to account for variations in infectivity and virulence, and integrating geographical scales to address local heterogeneities. Machine learning, network analysis, and Bayesian inference are also used to analyze large datasets and improve parameter estimation in complex models. These advanced models provide a more realistic and nuanced understanding of epidemic dynamics, though they also present challenges related to data quality, model complexity, and interpretability (Crepey et al., 2022).

1.1.4 Gaps in Co-infection Modeling

Theoretical Gaps

Existing integer-order models for HIV-TB co-infection acknowledge several limitations. Despite their widespread use, they often fall short of capturing the intricacies of co-infection. A major concern is their neglect of memory effects in treatment efficacy. These models assume instantaneous responses to interventions and overlook delays and historical influences which may significantly impact patient outcomes. This simplification leads to inaccurate predictions, failing to account for the lingering effects of prior treatments on current disease dynamics. Additionally, these models often oversimplify the complex interactions between HIV and TB, such as the heightened susceptibility to TB reactivation in HIV-positive individuals. Consequently, inherent nonlinearities in co-infection dynamics may be overlooked, resulting in overly simplistic conclusions regarding the relationship between the two diseases (Roeger et al., 2009; Georgiev, 2023).

Integer-order models typically assume homogeneity within populations, disregarding the variability in individual treatment responses due to factors like genetics and social determinants of health. This limits their applicability in diverse settings. Furthermore, these models rely on static parameters that fail to capture the changing epidemiological landscape, particularly in response to interventions such as ART or TB vaccination programs. As a result, predictions may become outdated, failing to effectively inform public health strategies. Recent studies indicate that fractional-order

models can address these limitations by incorporating memory effects and non-local interactions. By representing time-dependent dynamics, fractional-order models offer more accurate depiction of delayed and gradual treatment effects in disease progression (Fouladi et al., 2022; Raza et al., 2025).

The restricted applications of fractional-order models highlight a significant gap in current research on mathematical modeling of HIV-TB co-infection. Fractional-order models have the potential to better reflect real-world scenarios, accommodating delayed responses and acknowledging individual patient variability. Although some studies have explored fractional-order models for HIV or TB separately, research specifically addressing the unique dynamics of HIV-TB co-infection remains sparse (Barakat et al., 2023; Riaz et al., 2024; Mumbu et al., 2025; Saqib et al., 2025).

Another gap in co-infection modeling is the one pertaining to different biological and clinical time scales of TB infection and HIV progression, which falls under the category of theoretical gaps. It is related to the limitations in modeling techniques and frameworks that fail to account for the complex, multi-time scale dynamics of co-infections, rather than a direct implementation or operational aspect of epidemiological strategies. This gap specifically addresses the need for more complex theoretical models to better comprehend the difficulties associated with co-infection in those diseases that progress at different rates and to effectively depict how these rates affect the dynamics of the diseases. The difficulties in modeling HIV and TB co-infections because of their different models of transmission are addressed in a paper by Roeger et al. (2009). The study emphasizes how challenging it is to capture the combined dynamics of these illnesses, which are made more difficult by the unknown proportion of people who are susceptible to both infections. This work underscores the need for models that address the multi-time scale dynamics inherent in HIV-TB co-infection.

Epidemiological Gaps

Cost-effective control strategies are vital for managing HIV-TB co-infection, optimizing healthcare resources, and improving patient outcomes. These strategies seek to maximize the impact of interventions while minimizing costs, which is particularly important in resource-limited settings. For instance, integrating ART with preventive treatments for TB has shown promise in reducing co-infection rates. Mathematical models that incorporate factors such as treatment adherence, patient demographics, and socio-economic conditions can help healthcare providers allocate resources to interventions with the highest return on investment. Studies in Brazil and South Africa have demonstrated up to a 90% reduction in TB risk among HIV-infected patients receiving both ART and IPT (Houben et al., 2014; Shayo et al., 2017).

Implementing cost-effective strategies reduce the overall disease burden, alleviating pressure on healthcare systems. Real-world validation of models ensures they reflect actual disease dynamics, enabling more accurate predictions and informed decision-making. For example, a study in Ethiopia developed an optimal HIV/AIDS-TB co-infection model, revealing that concurrently applying HIV/AIDS prevention efforts and TB case finding is the most cost-effective strategy. Similarly, integrating TB and HIV treatment can lower costs by utilizing existing TB care services to make ART accessible (Smith et al., 2015; Kim et al., 2018; Ayele et al., 2024).

In summary, cost-effective control strategies, validated against real-world data, are essential for improving healthcare delivery, enhancing patient outcomes, and ensuring the sustainability of health systems. These strategies serve as crucial components of a comprehensive public health approach to managing HIV-TB co-infection.

Numerous studies on HIV-TB co-infection dynamics predominantly utilize integer-order mathematical models, which often fall short of capturing the intricacies of the co-infection. Furthermore, many studies fail to consider essential factors such as vaccination, drug-resistant strains, PrEP, ART, and TPT, diminishing their applicability to real-world scenarios. They also lack the ability to explore fractional-order optimal control strategies that could minimize the number of individuals infected while ensuring cost-effective implementation.

Compared to other fractional operators, the Caputo fractional operator has a number of advantages, which make it mathematically and epidemiologically suitable for modeling infectious diseases like HIV-TB co-infection. Unlike the Riemann-Liouville operator, it provides clarity in epidemiological scenarios by allowing for straightforward classical initial conditions and successfully incorporating memory effects. Compared to the Atangana-Baleanu operator, it is more flexible in managing nonlinear dynamics, allowing for robust fractional coefficients that can be adjusted to different population dynamics. When compared to the Caputo-Fabrizio operator, the Caputo operator demonstrates greater versatility across diverse initial-value problems, as the Caputo-Fabrizio's exponential kernel may limit its applicability in some contexts. Furthermore, unlike the Grunwald-Letnikov operator, the Caputo operator minimizes computational complexity and simplifies model implementation. It is a popular and reliable choice for researchers in infectious disease modeling because of its rigorous empirical validation in the literature, which also shows consistent alignment with observed data (Akuka et al., 2024; E. Alsubaie et al., 2024).

Motivated by these gaps and the superiority of Caputo operator in modeling infectious diseases, our dissertation develops and analyzes Caputo fractional-order mathematical models that incorporate critical interventions like PrEP, ART, vaccination

and TPT to effectively describe the transmission dynamics of HIV, TB and their co-infection. We also perform fractional optimal control and cost-effectiveness analysis to identify the most efficient and cost-effective intervention strategies that minimize disease burden and cost of implementations, using empirical data obtained from Ethiopia. Ultimately, our models provide a comprehensive framework for understanding and managing HIV-TB co-infections, informing targeted public health policies.

1.2 Statement of the Problem

Human immunodeficiency virus (HIV), tuberculosis (TB), and their co-infections are major global health challenges, with sub-Saharan Africa facing a burden of over 50% of cases and 60% of deaths. In Ethiopia, TB incidence has increased by 16%, with approximately 188,000 new cases and 25,000 deaths in 2024. In the same year, 11,000 Ethiopians have lost their live due to HIV with 610,000 PLHIV (Mekonen et al., 2024; ENA, 2025; EPHI, 2025). The rise of MDR-TB in the country, linked to factors such as limited diagnostic access, treatment adherence, and malnutrition is inadequately addressed in existing models (Kheiri & Jafari, 2018; Inayaturohmat et al., 2024).

The core problem is that existing mathematical models of HIV-TB co-infection neglect to take into account memory effects, drug resistance, and combined intervention strategies utilizing optimal control, resulting in inaccurate predictions and ineffective policy recommendations. Therefore, motivated by these gaps, this dissertation develops and analyzes four fractional-order mathematical models in Caputo sense. These include a model for HIV/AIDS transmission dynamics incorporating PrEP and drug-resistant strains, a model for TB transmission dynamics with optimal control that considers vaccination and two lines of treatment modalities, and two integrated models for HIV-TB co-infection. The first co-infection model incorporates ART for HIV and vaccination for TB, while the later includes treatment regimens for both diseases and extends to optimal control problems.

1.3 Objectives of the Study

1.3.1 General Objective

The general objective of this study is to develop and analyze Caputo fractional-order mathematical models with optimal control to accurately describe the transmission dynamics of HIV, TB and their co-infection, and to identify cost-effective intervention strategies.

1.3.2 Specific Objectives

The specific objectives of this study are to:

1. formulate Caputo fractional-order mathematical models for HIV, TB and their co-infection incorporating key epidemiological factors such as PrEP, ART, TPT, vaccination, and drug-resistant strains,

2. analyze the qualitative properties of the formulated models including non-negativity, boundedness, existence and uniqueness of the solutions, equilibrium points, and stability,

3. estimate model parameters using real-world HIV and TB data from Ethiopia, and perform sensitivity analyses,

4. derive and analyze optimal control and cost-effectiveness strategies to minimize disease burden and costs of intervention, in fractional-order settings.

1.4 Significance of the Study

A well studied and organized dissertation on HIV, TB and their co-infection provides strong information on how to design appropriate control and preventive measures in order to bring a long term solution. Thus, the outcomes of this study are helpful to:

(a) introduce fractional-order epidemic modeling methodology to improve the understanding of the epidemiology and transmission of HIV, TB and their co-infection,

(b) integrate PrEP, ART, TPT, vaccination, and drug-resistant strains into a fractional-order framework,

(c) incorporate estimation of model parameters using real-world HIV and TB data from Ethiopia into fractional-order settings, improve decision making at strategic level and adds the advantage of interpreting the situation of HIV, TB and their co-infection,

(d) recommend efficient and cost-effective mitigation strategies for TB and HIV-TB co-infection, utilizing insights from fractional-order optimal control models to inform policy makers in their efforts to reduce diseases burden,

(e) motivate other researchers for further study and mathematical analysis.

1.5 Scope of the Study

This dissertation focuses on developing novel deterministic fractional-order mathematical models to enhance the understanding of HIV/AIDS, TB and their co-infection. The primary aim is to create various models with homogeneous population that incorporate critical interventions such as PrEP, ART, TPT and vaccination. It also considers crucial diseases stages like asymptomatic, latency and drug-resistant compartments. Additionally, the research will explore optimal control strategies that are used to mitigate the diseases with a minimal cost of interventions. Employing a data-driven approach, the models will utilize parameter estimation specifically from Ethiopia to ensure the findings are relevant and applicable to the local context. Ultimately, this research aspires to provide insights that can inform targeted public health interventions, focusing on minimizing disease burden while ensuring cost-effective strategies.

1.6 Delimitation of the study

While the scope of this dissertation is comprehensive, it is essential to delineate its boundaries. The research is geographically focused on Ethiopia, which may limit the generalizability of the findings to other regions with different epidemiological or socio-economic contexts. The primary emphasis was on HIV/AIDS, TB, and their co-infections, other infectious diseases or co-infections have not been addressed within this study. Although the dissertation aims to improve upon existing models, it lacks to consider heterogeneous population as it did not encompass all possible factors affecting disease dynamics, such as behavioral conditions, socio-economic status, environmental influences or healthcare system capacities beyond treatment adherence.

1.7 Organization of the dissertation

This dissertation consists of eight chapters. Chapter one provides an overview of our work, including a discussion of some pertinent biological and epidemiological issues that prompted it. Chapter two is a brief discussion of pertinent and previously linked literature. Chapter three outlines the methodology employed in this dissertation. A deterministic fractional order mathematical model for the dynamics of HIV/AIDS transmission is developed in chapter four.

Chapter five develops a mathematical model for TB using the Caputo approach that takes into account two treatment options and immunization. The developed model is further expanded into an optimum control issue with the intervention of continuous

controls. Chapter six proposes and analyzes a novel fractional order mathematical model that takes into account TB vaccine and treatment regimens for both in the sense of Caputo derivatives for the co-dynamics of HIV and TB. The HIV and TB co-infection model with optimal management, which takes into account both diseases' treatments, is constructed and examined in chapter seven. We conclude the dissertation by providing summary, conclusion and recommendations in chapter eight.

CHAPTER 2

LITERATURE REVIEW

Numerous mathematical studies have been widely conducted on HIV, TB and their co-infection to understand the characteristics of their transmission and how to combat them. In this regard, mathematical modeling and optimal control plays a significant contribution. In this chapter, we present brief review of related literature on mathematical modeling and optimal control that are directly related to the objectives of the study.

2.1 Existing Mathematical Models for HIV, TB and their Co-infection

2.1.1 HIV/AIDS Models

The study by Shukla (2025) demonstrated that migration patterns significantly impact HIV transmission, and evaluated disparities in treatment access among migrant populations. Furthermore, Cassels et al. (2008) has also explored the impact of interventions such as social distancing and vaccination on managing HIV spread during pandemics.

Deterministic integer-order models incorporating PrEP indicate that increasing PrEP coverage, along with enhancing compliance among current PrEP users can significantly reduce HIV incidence and improve treatment adherence among high-risk populations (Gutowska et al., 2022). In (Moya et al., 2024), the authors studied the influence of PrEP and PEP in contexts of undiagnosed and undetectable individuals. Additionally, models that consider non-adherence to HIV management guidelines highlight its role in spreading the virus, especially among infected newborns. Combining strategies like PrEP and condom use with ART adherence can notably reduce HIV transmission, though the assumption of homogeneity in these models may overlook

important variations in risk factors across demographics (Baggaley et al., 2011; Silva & Torres, 2017).

Research examining adherence to ART underscored its critical role in managing HIV, with findings suggesting that improved adherence significantly reduces viral loads and transmission potential (Lai et al., 2023). A study by Frankline et al. (2018) developed a mathematical model with ART adherence, showing that the disease can be kept under control if test and treat strategies are upscaled and adherence to treatment is emphasized. Furthermore, some models incorporate the effects of drug resistance, showing that incomplete adherence to ART can drive the selection of resistant variants.

On the other hand, Ajao et al. (2023) formulated and analyzed a classical order mathematical model to understand the transmission dynamics and control of HIV infection. The findings of this study revealed that increasing the fraction of detected individuals that are receiving treatment increases the population of latent class and reduces that of AIDS class by reducing the viral load to an undetected level. But, the main draw back of this study is that fails to investigate whether or not the mortality and morbidity of HIV infection is affected by factors like geographical distribution, age structure and other opportunistic disease such as TB, diabetes and cancers. The study also lacks to draw enough information such as hereditary properties of the infection as it did not consider a fractional order operator.

In Naik et al. (2020), the authors developed a nonlinear Caputo-type fractional order epidemic model with five compartments to analyze HIV transmission dynamics. They established model equilibria and stability using the fractional Routh-Hurwitz criterion and LaSalle invariant principle, showing that a disease-free state occurs when $\mathcal{R}_0 < 1$ and disease spread happens when $\mathcal{R}_0 > 1$. The study also utilized a Lyapunov functional approach to discuss global dynamics at the endemic equilibrium and formulated a fractional optimal control problem, incorporating strategies such as condom use, treatment for aware infectives, and awareness campaigns for unaware individuals. Simulation results indicated that these combined control measures significantly improve the quality of life for HIV patients and reduce AIDS cases. However, the study notably neglects the HIV-TB co-infected population.

Mathematical modeling studies on HIV/AIDS offer valuable insights into transmission dynamics, intervention strategies, and the impact of various factors on the epidemic. A study by de Oliveira et al. (2022) integrated social determinants of health (SDH) into a mathematical model of HIV/AIDS, highlighting their role in disease transmission and maintenance. It demonstrated how factors like employment, poverty, education, drug, alcohol abuse, and condom use influence HIV/AIDS incidence and mortality rates, underscoring the significance of SDH in understanding and addressing

the occurrence of diseases.

A novel fractal-fractional mathematical model for HIV/AIDS transmission, incorporating fractal-fractional operators to account for memory effects, spatial heterogeneity, and anomalous diffusion has been introduced in (M. Khan et al., 2025). This approach offers a more accurate representation of HIV/AIDS dynamics, emphasizing the importance of reducing contact rates, enhancing preventive measures, ensuring timely treatment and behavioral interventions.

The above cited studies on HIV/AIDS dynamics exhibit several limitations that may impact their findings. Many deterministic models assume homogeneity within populations, potentially overlooking critical demographic variations in risk factors, treatment access, and adherence patterns. The reliance on simplified mathematical abstractions may not fully capture the intricacies of human behavior, migration patterns, and the social determinants of health that influence HIV transmission. Moreover, the effectiveness of interventions like PrEP and ART in real-world settings may vary due to factors such as stigma, healthcare infrastructure, and socioeconomic disparities, which are not always adequately represented in these models.

2.1.2 Mathematical Models of Tuberculosis

Mathematical modeling plays a crucial role in understanding and combating tuberculosis, with recent literature focusing on various aspects of the disease. For instance, in (S. Ullah, Ullah, et al., 2020) an integer order mathematical model featuring six epidemiological compartments is presented to analyze TB transmission dynamics and propose effective control measures. The authors have also developed a control model that includes three time-dependent strategies: isolation, vaccination, and treatment. Simulation results revealed that relying on separate strategies has limitations in controlling the disease, while implementing all measures simultaneously significantly reduces TB infections in society. However, a notable drawback of the study is its failure to incorporate fractional operators with local and non-local kernels, which could provide deeper insights into the disease dynamics.

Similarly, M. A. Khan et al. (2020) formulated a novel fractional model to examine the dynamics of TB across two age groups: children and adults. Each group is further divided into three subclasses: susceptible, latently infected, and actively infected. The study's graphical results indicate that increasing chemoprophylaxis and treatment rates effectively reduces the number of TB infections in both age groups. Additionally, a decrease in the fractional order parameter significantly lowers the infective TB population. However, a key limitation of the study is its failure to explore the optimal control strategies that could minimize TB infections in both children and adults.

On the other hand, Guo & Zhang (2023) developed a five-compartment age-structured mathematical model for tuberculosis (TB) infection, incorporating vaccination to better understand TB spread and suggest control measures in China. Through sensitivity analysis, the study identified several key parameters influencing the basic reproduction number $\mathcal{R}_0$. The findings indicate that reducing transmission rates, alongside improving treatment and vaccine efficacy, significantly lowers $\mathcal{R}_0$ and consequently decreases the number of new TB cases. However, the study has notable limitations, as it does not incorporate fractional operators or a treatment compartment, and it overlooks the impact of drug-resistant TB, which adversely affects treatment success rates.

A significant area of research focuses on the emergence and spread of DR-TB, including MDR-TB and XDR-TB strains. These models consider factors such as treatment adherence and the fitness costs associated with drug resistance. A systematic review highlighted that many models of DR-TB lack bacterial heterogeneity, which could affect predictions of resistance prevalence. Models often stratify the infectious compartment based on sputum smear status or healthcare-related factors (Ronoh et al., 2016; Suddin & Bano, 2021; Fuller et al., 2024).

Optimal control theory is increasingly applied to TB models to determine the most effective and cost-effective intervention strategies. For instance, although they fail to account for their memory effects, Ayele et al. (2024); Alfiniyah et al. (2024) have proposed optimal control strategies to assess intervention effectiveness, incorporating factors such as vaccination, treatment, and prevention efforts.

The study by Avilov et al. (2022) on TB modeling utilized routine notification data to analyze the progression of active pulmonary TB, distinguishing stages based on bacterioexcretion. It compared parallel and serial schemes for TB progression, with the former assuming predefined infectiousness and the latter treating all cases as initially non-infectious. Parameterized with data from Moscow, the research offers valuable insights into the dynamics of early-stage untreated TB.

Furthermore, Elaydi & Lozi (2024) explored the global dynamics of discrete mathematical models of TB, investigating both SEI and SEIT models. The study highlighted the importance of latent infections in TB spread and the potential impact of public health interventions. It has been shown that the disease-free equilibrium is globally asymptotically stable if a certain reproduction number is less than or equal to unity, and unstable otherwise.

Moreover, Alfiniyah et al. (2024) developed another model to capture TB transmission among smokers, integrating smoking behavior and case detection, which are often under explored in existing models. The study found that smoking significantly increases TB transmission rates and that targeted control measures, including social

distancing for smokers, TB screening in high-risk populations, and TB treatment in low-income communities, can effectively reduce TB infections.

The above studies highlight significant limitations in TB modeling, including lack of accounting for memory and hereditary effects, failure to explore effective optimal control strategies, and omission of treatment compartments and drug-resistant TB. These gaps underscore the need for more comprehensive models that integrate fractional dynamics, effective control measures, and the complexities of drug resistance to improve TB control efforts.

2.1.3 Mathematical Models for HIV-TB Co-infection

Several researchers have worked to understand the transmission dynamics of HIV-TB co-infection and assess the effectiveness of various control measures. For example, Bhunu et al. (2009) found that treating AIDS cases significantly reduces TB progression, while treating TB delays the onset of AIDS. Whereas, Kumar & Jain (2018) indicated that early ART initiation during TB treatment is more effective in reducing disease-induced deaths and that treating TB-only infected individuals is very effective in reducing the total infected population. A study by Mwangi et al. (2024) has also emphasized the importance of consistent HIV treatment to reduce HIV-TB co-infection. Additionally, Zahli et al. (2024) investigated the role of treatment in reducing the expansion of both TB and HIV infection, formulating a new non-linear compartmental system to study the dynamics of the diseases. Furthermore, Vincent (2022) suggested that increasing HIV interventions reduces cases of latent TB progressing to active TB.

Studies have also applied optimal control theory to determine the most efficient and cost-effective intervention strategies for HIV-TB co-infection. For instance, Silva & Torres (2015) used optimal control theory, showing that simultaneous or separate treatment for TB and HIV reduces the number of individuals with active TB and AIDS, though TB-only treatment without HIV treatment may lead to severe HIV stages. In their study, Seidu et al. (2023) have also identified that combining preventive and curative measures with skills training is the most cost-effective strategy. A study in Ethiopia developed an optimal HIV/AIDS-TB co-infection model, concluding that applying HIV/AIDS prevention efforts and TB case finding concurrently is the most cost-effective strategy (Ayele et al., 2024).

Some of the existing models (Aggarwal et al., 2021; Saranya Devi et al., 2025; Farman et al., 2020) have also employed fractional calculus to account for the memory effects and complexities associated with the co-infection. Other studies (Adeyemo et al., 2023; Ahmed et al., 2022; Bhattacharjee, 2023; Awoke & Semu, 2018) formulated and analyzed a deterministic first-order mathematical model to describe the flow dynamics

of HIV-TB co-infection.

Furthermore, in Pooranagangadevi & Padmapriyadarsini (2022) the authors have explored the complexities of managing co-infection with HIV and TB. Findings highlight significant pharmacokinetic interactions between ART and anti-TB medications, underscoring the necessity for careful monitoring to prevent adverse effects. It advocates for integrated treatment strategies and recommends starting ART within two weeks of initiating anti-TB treatment to enhance patient outcomes. The effectiveness of rifampicin is emphasized when administered throughout the treatment course, along with strategies to improve treatment adherence.

While the reviewed studies offer valuable insights into HIV-TB co-infection dynamics and control strategies, they exhibit several limitations. Many models focus on specific interventions without adequately addressing the complexities of latent infections, which can significantly influence disease transmission. For instance, several studies overlook the role of latent TB treatment and its impact on progression to active disease. Additionally, some models lack the application of optimal control strategies to identify the most effective intervention combinations, potentially limiting their cost-effectiveness analyses. Furthermore, the reliance on deterministic models may not fully capture the inherent stochastic nature of disease spread, and the use of specific mathematical methods can restrict generalizability across different populations or settings. Overall, these limitations suggest a need for more comprehensive approaches that integrate a wider range of factors influencing TB-HIV co-infection dynamics.

2.2 Memory Effects and Hereditary Factors in Disease Modeling

Memory and hereditary properties are crucial in biological processes, influencing system dynamics, although they require complex mathematical models for accurate representation. Memory effects describe how a biological system's current state depends on its past. For example, the immune system's response to a pathogen is shaped by prior encounters, and behavioral changes during epidemics are influenced by past experiences. Hereditary properties involve the transmission of traits across generations, impacting biological systems. In infectious diseases, host genetics influence susceptibility and infectivity, while vertical transmission introduces a hereditary component. Mathematical models can incorporate memory through mechanisms like hysteresis, where the system's behavior depends on its history, or by using non-Markovian processes that consider past states. They also incorporate hereditary properties through genetic parameters that affect disease transmission (Grassly & Fraser, 2008; Barros et

al., 2021).

In infectious disease modeling, memory and hereditary properties play a critical role in influencing disease dynamics through past exposures, immune responses, and behavioral changes. Memory effects in the immune system's responses, affect the speed and effectiveness of the immune response influencing disease progression and transmission. Behavioral adaptations, such as increased hygiene or social distancing, are also informed by past experiences with diseases, while non-pharmaceutical interventions like mask mandates and lockdowns modify contact patterns based on recent infection histories. On the hereditary side, genetic factors significantly impact an individual's susceptibility and infectivity, with heritable variations affecting the likelihood of infection and transmission. Additionally, vertical transmission of infectious diseases from parent to offspring introduces further hereditary effects that shape long-term disease patterns (Agarwal et al., 2024; Chen-Charpentier, 2025).

Treatment adherence history and drug resistance can indeed be integrated into memory effects within infectious disease modeling. A patient's past adherence to treatment influences future adherence behaviors, impacting therapy effectiveness. Mathematical models show that individuals who were previously non-adherent are likely to remain so, as it can be difficult for them to change their habit and start following the prescribed regimen (Nande, 2021). This can lead to persistent infection and increased transmission, as suboptimal treatment may not fully suppress the pathogen.

Furthermore, as it was indicated in the studies by Lavi et al. (2012); Sun & Hu (2018), the development of drug resistance is intrinsically linked to treatment history. Non-adherence fosters an environment conducive to the emergence of resistant strains, complicating future interventions. Models incorporating these factors can provide nuanced insights into disease dynamics, accounting for the accumulated effects of treatment history and resistance. These models help predict treatment outcomes and inform public health strategies for improving adherence and managing drug resistance. For instance, long-acting therapies are being explored to address adherence issues, though their impact on resistance evolution requires careful modeling.

2.3 Fractional-Order Epidemiological Models

Fractional order modeling has its historical roots in the correspondence between Leibniz and L'Hôpital in 1695, igniting interest in derivatives of non-integer order. Its theoretical foundations were further developed in the 20th century by mathematicians like Niels Henrik Abel, along with significant contributions from Liouville, Riemann, and Caputo. Fractional calculus extends traditional calculus by introducing

non-integer order derivatives and integrals, allowing for more accurate representations of processes exhibiting memory effects and non-local behavior (David et al., 2011). The Liouville–Caputo Derivative, the Riemann–Liouville Derivative, and the Grünwald–Letnikov Derivatives are the most common fractional operators considered in the literature.

The choice of operator affects the model's behavior and suitability for specific applications. For instance, the Liouville–Caputo derivative is advantageous in scenarios where initial conditions are critical, such as in control systems and infectious diseases dynamics. In contrast, the Riemann–Liouville derivative may be preferred in theoretical explorations due to its broader applicability, despite its complexity in initial conditions. The Grünwald–Letnikov derivative excels in numerical implementations, making it valuable for computational modeling (Pratap et al., 2024).

2.4 Comparative Analysis: Integer-Order versus Fractional-Order Models

Recent applications of fractional calculus demonstrate its versatility across various fields, including science, engineering, fluid mechanics, biology, and finance. Studies indicate that fractional-order models outperform traditional integer-order models in simulating disease dynamics, offering valuable insights for public health interventions. This advantage arises from their ability to capture memory and hereditary properties inherent in biological processes. Unlike integer-order derivatives, which focus solely on the current state, fractional derivatives account for a system's entire past evolution, making them more suitable for complex biological phenomena. As a result, fractional-order models provide more accurate simulations, reducing errors and enhancing the understanding of complex biological behaviors. Their non-local, time-dependent nature allows for a more comprehensive representation of biological dynamics, particularly in infectious diseases, leading to more reliable predictions (Matlob & Jamali, 2019; Fouladi et al., 2022; Ali, 2024; Rahman et al., 2024).

Research on fractal-fractional dynamics in infectious diseases like TB and HIV/AIDS has yielded promising results, demonstrating the models' capacity to capture complex behaviors and memory effects inherent in biological systems. For instance, a study on TB lung lesions revealed that fractal-fractional analysis could differentiate between healthy and diseased tissue, improving predictions of treatment outcomes based on lesion characteristics. Similarly, in HIV, TB and their co-infection dynamics, models incorporating memory effects showed enhanced accuracy in forecasting the spread of the diseases and the impacts of treatment interventions (A. Khan et al., 2024; M. Khan

et al., 2025; Sado et al., 2025; Aggarwal et al., 2021; Dwivedi et al., 2025; El-Mesady et al., 2025; Farman et al., 2020; M. A. Khan et al., 2020).

However, these advancements come with notable limitations. The complexity of solving nonlinear equations often necessitates numerical methods, which can introduce approximations that may affect accuracy. Additionally, achieving precise solutions can be challenging due to the intricate nature of fractional calculus, leading to difficulties in model validation. Issues such as small sample sizes and the inherent variability of individual immune responses in HIV patients can also affect the generalizability of findings, highlighting the need for larger-scale studies to validate these models. Furthermore, while these models offer valuable insights, they require further refinement and calibration against real-world data to enhance their applicability in clinical settings, emphasizing the importance of interdisciplinary approaches in advancing research in TB, HIV/AIDS and their co-infection (S. Ullah et al., 2023; Anjam et al., 2024; S. Ullah, Khan, et al., 2020).

2.5 Fractional Optimal Control and cost-effectiveness analysis in Infectious Diseases control

Fractional optimal control offers a promising conceptual framework for managing infectious diseases, particularly HIV, TB, and their co-infection, by incorporating memory effects and hereditary properties into control strategies. Recent mathematical modeling perspectives emphasize the use of fractional derivatives, often in the Caputo or Atangana-Baleanu-Caputo (ABC) sense, to better capture the complex dynamics of disease transmission and treatment responses. These models often include control variables representing interventions such as prevention, treatment, and behavior modification, aiming to minimize the cost of interventions while maximizing their effectiveness (Kheiri & Jafari, 2018; Dwivedi et al., 2025; El-Mesady et al., 2025).

Studies have explored optimal control strategies for TB, HIV and their co-infection, often employing Pontryagin's Maximum Principle to derive necessary conditions for optimality. For instance, research on TB incorporates controls for restricting individual contact, treatment, and sensitization, while HIV models consider condom use, ART treatment, and behavioral changes. Co-infection models address TB preventive therapy, vaccination, and antiretroviral treatment. These studies highlight the potential of fractional optimal control to design more effective and cost-efficient intervention strategies, but also acknowledge challenges in numerical computation and the need for further validation against real-world data. The use of fractional-order models can lead to a better understanding of the dynamics of these diseases and potentially more

effective intervention strategies (Rosa & Torres, 2018; Sweilam et al., 2019; Ayele et al., 2024). In Mallela et al. (2016) the authors developed a mathematical model to assess the effects of early and late HIV treatment during TB therapy, revealing that co-infection programs alone may be insufficient for disease eradication and additional interventions targeting individuals infected with a single disease are necessary. The study also formulated an optimal control problem to minimize the cumulative burden of co-infection, highlighting the significance of both the strength and timing of ART.

Moreover, in Maina et al. (2025) an age-structured mathematical model with optimal control for HIV-TB co-infection in Kenya has been developed, showing that ART adherence is the best intervention in earlier stage of HIV and latent TB co-infection, while TB treatment is more effective in later stage of HIV and active TB co-infection. The study also found that viral load suppression is most effective for children, and TB prevention is most effective for adults.

To sum up, existing mathematical studies on HIV/AIDS, TB, and their co-infection neglect to include memory effects of the diseases and combined intervention strategies utilizing the insights from fractional optimal control and cost-effectiveness analysis, leading to inaccurate predictions and inadequate policy recommendations. Thus, derived by these gaps, this dissertation develops and analyzes Caputo fractional mathematical models with optimal control and cost-effective analysis for HIV/AIDS, TB, and their co-infection, incorporating key epidemiological factors such as PrEP, ART, vaccination, treatment adherence, and drug resistance.

CHAPTER 3

RESEARCH METHODOLOGY

In this chapter, we present the methods and materials used to attain the general and specific objectives stated in section (1.3). For this, we briefly discuss: the study area and period, sources of data, data collection techniques, method of data analysis, and mathematical procedures.

3.1 Study Area and Period

This study is conducted in Ethiopia, from November 2023 to December 2025. It develops and analyzes Caputo fractional-order mathematical models with optimal control to accurately describe the transmission dynamics of HIV, TB, and their co-infection and to identify cost-effective intervention strategies.

3.2 Sources of Data

For successful accomplishment of this study, we collect secondary information both from published and unpublished documents including Ethiopian Public Health Institute (EPHI), Ethiopian Federal Ministry of Health (EFMH) and WHO/UNAIDS reports on the updated status of HIV, TB, and their co-infection.

3.3 Data Collection

Numerical data were collected from secondary sources of information. These data played an important role in increasing the validity, accuracy and reliability of the research. For estimating some of the model parameters, we used a time series real data on HIV and TB incidences collected on yearly records of patients from 2016-2023 GC, which we obtained from Ethiopian Federal Ministry of Health. We used previously

published articles in reputable journals to obtain values of the remaining parameters, while some of them are also assumed. Data showing the global burden of HIV, TB, and their co-infection were collected from WHO/UNAIDS reports. We also used data from EPHI to see the burden of these diseases in Ethiopia. To choose the values of coefficients for the integrand of objective functions while simulating fractional optimal control problems, we followed WHO recommendations.

3.4 Data Analysis

Data analysis is the process of analyzing collected data to outdraw meaningful insights. The techniques focus on the statistical, or mathematical analysis of the data sets, using computational techniques and algorithm. As our data points are taken over time, we used time series analysis to estimate values of model parameters and validate our models by employing the least square techniques.

The least squares technique is a numerical method used to minimize the differences between real data and simulated data by a model. It adjusts the values of model parameters or performs parameter estimation to minimize the sum of squared residuals. We used a Matlab function called 'fminunc' and a Python optimization toolbox called 'minimize,' which serve as numerical tools to effectively implement the least squares technique when dealing with complex models or high-dimensional data. The Matlab algorithm for the least square technique called 'fminunc' to fit model (4.3) to HIV data is given under Appendix (B.1). Whereas, the Python algorithm for the least square technique called 'minimize' to fit model (6.24) to TB data is given under Appendix (B.3).

The study involved both qualitative and quantitative analysis. The numerical simulations have been performed using Adams-Bash forth predictor–corrector method implemented in (Diethelm et al., 2002) and (Naik et al., 2020; Mahata et al., 2022) with the help of GNU OCTAVE/MATLAB software and the results are displayed in the form of graphs or figures.

3.5 Mathematical Procedures

In this section, we discuss the mathematical procedures we used in order to achieve the objectives of our study. We outlined the model formulations based on biological and epidemiological assumptions relevant to HIV/AIDS, TB and their co-infection. We constructed compartmental models addressing HIV transmission, including asymptomatic undiagnosed cases, drug-resistant strains, and PrEP users, alongside TB transmission

model with optimal control that incorporates latency, drug resistance, vaccination, and two lines of treatment modalities.

We also formulated two HIV-TB co-infection models, considering latency periods and treatment therapies. The fist co-infection model considers vaccination for TB and therapies for both, whereas the second co-infection model incorporates treatment for both and extension to optimal control problem. We justify the shift from integer-order to fractional-order modeling, favoring the Caputo fractional derivative for its advantages.

We have ensured well-posedness through proofs of biological feasibility, demonstrating non-negativity and boundedness, while establishing the existence and uniqueness of solutions for systems of Caputo fractional differential equations. The basic reproduction number is computed via the next-generation matrix approach, and we classified disease-free and endemic equilibria. For stability analysis we have employed Jacobian matrix techniques for local stability, along with the fractional Routh-Hurwitz stability criterion and appropriate Lyapunov functions for global stability.

Parameter estimation and model fitting are conducted using real epidemiological data from Ethiopia, applying non-linear least squares methods. Global sensitivity analysis has been carried out using the normalized forward sensitivity analysis to highlight key parameters affecting disease dynamics and control effectiveness. Numerical simulations were performed by leveraging the fractional Adams-Bashforth-Moulton PECE technique, considering sensitivity of $\mathcal{R}_0$ to model parameters.

For optimal control and cost-effectiveness analysis, we formulated fractional optimal control problems focusing on prevention, vaccination and treatment for TB model, and treatment thrapies for the second co-infection model, by proving the existence of optimal controls and deriving necessary conditions through Pontryagin's principles. Finally, we analyzed the cost-effectiveness of various intervention strategies for these two models and provided evidence-based recommendations for health policymakers based on simulation and control outcomes.

CHAPTER 4

FRACTIONAL-ORDER MODELING OF HIV/AIDS DYNAMICS WITH PrEP AND DRUG RESISTANT

This chapter investigates a Caputo approach mathematical model of HIV/AIDS transmission dynamics considering six disease compartments: Susceptibles, Pre-Exposure Prophylaxis, asymptomatic infectious, symptomatic infectious, Drug Resistant Strain and the AIDS compartments. The basic properties of the model and stability of the model equilibria are carried out. Furthermore, the numerical simulations of the model has been performed to assist the analytical results.

4.1 Mathematical Model Formulation

This section presents a Caputo fractional order mathematical model for HIV/AIDS transmission dynamics that considers the PrEP users and drug resistant strain of HIV. Based on the epidemiological context of the disease, we categorize the study population into six distinct compartments: susceptible individuals S(t), who are currently healthy but at risk of future infection; PrEP users P(t) who are taking specific antiretroviral medications that can reduce the risk of contracting HIV; asymptomatic, undiagnosed infectious individuals E(t); symptomatic, diagnosed infectious individuals I(t) with poor adherence to ART; HIV drug resistant class R(t) which is populated by treatment failure from symptomatic infectious class and the AIDS class A(t) consisting of those individuals with CD+ count of less than 200cells/mm^3. The total human population at time t is represented by the equation:

$$N(t) = S(t) + P(t) + E(t) + I(t) + R(t) + A(t).$$

Based on HIV viral load, the order of the proposed compartments from lowest to highest viral load is as follows: asymptomatic, undiagnosed infectious class E(t) generally has a lower viral load. The symptomatic, diagnosed infectious class I(t) which show non-adherence to ART may exhibit higher viral loads than E(t) but less than R(t). Individuals in the class with ART drug-resistant strain R(t) have elevated high viral loads than those in I(t) due to ineffective ART. Finally, the AIDS class A(t) has very high viral loads, making these individuals highly infectious, if left untreated (CDC, 2025a; HIVinfo, 2025).

We formulate the model based on the following basic model assumptions: Past states influence current transmission dynamics via Caputo fractional derivatives. Fraction γ of symptomatic individuals receive ART, with potential waning adherence which may arise due to their non-adherence behavior to ART. The fractional-order σ captures variable latency periods possibly (8-10 years), and the non-instantaneous drug resistance development rate which occurs over a period of time. The population is continuously recruited into susceptible compartments, either by immigration or birth, at a constant rate Λ. A force of infection, specified by $\lambda = \beta(t)\left(\rho_1 \frac{E}{N} + \rho_2 \frac{I}{N} + \rho_3 \frac{R}{N} + \frac{A}{N}\right)$, infects susceptible individuals when they come into contact with those who belong to the infectious compartments E, I, R, A.

In the above expression for λ, $\beta(t) = \beta_0 e^{-q(I+A)}$ represents a behavioral feedback that incorporates a prevalence-dependent risk reduction. This exponential decay, which is a reasonable assumption in behavioral epidemiology, illustrates how the transmission rate falls as the number of affected people rises. By adopting safer habits, the population may lower the chance of transmission overall. The baseline transmission rate β_0 and a behavioral response sensitivity q needs to be precisely calibrated using empirical data.

The modification parameters $\rho_1, \rho_2, \rho_3 \in (0, 1)$ respectively describe the transmission levels of the disease in E, I, R compartments relative to those in the A compartment. Based on the viral load of each compartment discussed above, we adjust the values for these modification parameters as $\rho_1 < \rho_2 < \rho_3$, assuming that lower viral load results in low infectiousness level. On the other hand, the AIDS group A is assigned the highest infectivity level (a base value of 1) since this class has a higher viral load than others.

We assume that small fraction of symptomatic infectious individuals will move to AIDS compartment at a rate $(1 - \phi\gamma)\theta_1$ and the remaining $\phi\gamma\theta_1$ will move to the drug resistant class. Here ϕ, γ respectively denotes the drug resistance development rate, fraction of symptomatic cases receiving ART. The parameter θ_1 represents the non-adherence rate of ART treatment for individuals in I class. The population is considered

to be homogeneous with regard to all epidemiological and biological factors.

The product $\phi\gamma$, which represents the combined effect of the drug resistance development rate (ϕ) and the fraction of symptomatic cases receiving ART (γ), is epidemiologically valid but requires careful interpretation. It highlights the interaction between ART coverage and drug resistance emergence, as higher ART coverage can amplify the effects of drug resistance development. However, this multiplicative relationship may oversimplify the complex dynamics at play, and its impact is context-dependent, influenced by factors such as access to second-line treatments, viral load monitoring, and the prevalence of transmitted drug resistance. Additionally, the model should account for adherence levels, as poor adherence can significantly increase the risk of drug resistance. Overall, while $\phi\gamma$ serves as a useful starting point for modeling HIV/AIDS dynamics, more nuanced approaches that incorporate these complexities are recommended (Phillips et al., 2017; Lai et al., 2023).

We also assume that only individuals from the symptomatic, diagnosed infectious class with poor adherence and those from a class with drug-resistant strain progress to the AIDS class. It is well-documented that symptomatic individuals with poor adherence to ART and those harboring drug-resistant strains experience accelerated progression to AIDS, due to higher viral loads and declining CD4+ T cell counts. However, asymptomatic individuals can also progress to AIDS if untreated; the CDC notes that the chronic asymptomatic stage will eventually advance to AIDS without intervention. Therefore, it is essential to recognize that progression to AIDS can occur in undiagnosed asymptomatic individuals, albeit less frequently (Habtemariam et al., 2008; ASHM, 2024). Figure (4.1) displays the schematic diagram of the developed model.

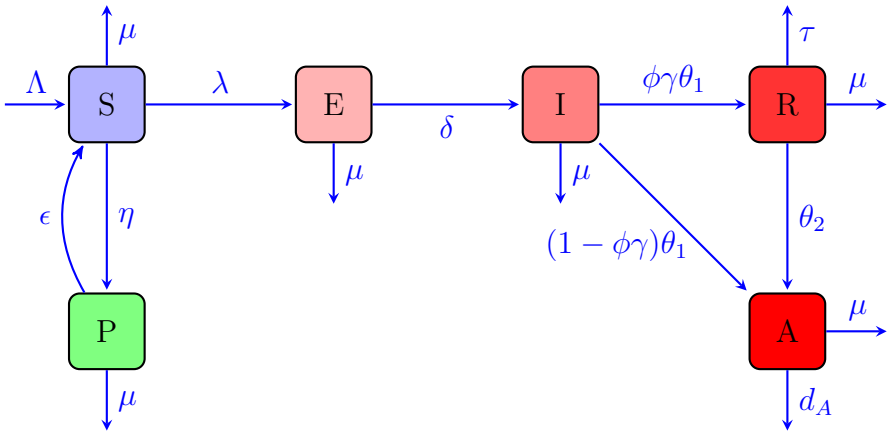

Figure 4.1: Schematic Diagram of HIV/AIDS Model

The parameters η, ϵ respectively denotes the PrEP initiation and discontinuation rates, and θ_2 denotes the non-adherence rate of ART treatment for individuals in R class.

The parameter μ represents the natural mortality rate and τ stands for additional mortality rate due to drug resistant strain. We assume that $\tau > \mu$ due to limited salvage therapies. Furthermore, the parameter δ represents detection rate at which people know they are HIV-positive. Individuals in the AIDS compartments are subject to AIDS associated death at a rate d_A.

An integer-order systems of differential equations corresponding to Figure (4.1) is written as

$$\begin{cases} \frac{dS}{dt} = \Lambda + \epsilon P - \lambda S - (\mu + \eta)S, \\ \frac{dP}{dt} = \eta S - (\mu + \epsilon)P, \\ \frac{dE}{dt} = \lambda S - (\mu + \delta)E, \\ \frac{dI}{dt} = \delta E - (\mu + \theta_1)I, \\ \frac{dR}{dt} = \phi\gamma\theta_1 I - (\mu + \tau + \theta_2)R, \\ \frac{dA}{dt} = (1 - \phi\gamma)\theta_1 I + \theta_2 R - (\mu + d_A)A, \end{cases} \tag{4.1}$$

With the initial conditions given as

$$\begin{aligned} S(0) = S_0 \geq 0,\ P(0) = P_0 \geq 0,\ E(0) = E_0 > 0, \\ I(0) = I_0 > 0,\ R(0) = R_0 \geq 0,\ A(0) = A_0 > 0. \end{aligned} \tag{4.2}$$

Fractional-order derivatives in infectious disease modeling reflect a system with memory, indicating that the current state depends on both present conditions and historical states. This is particularly important in understanding how past infections, treatments, and interventions influence disease spread. The use of fractional derivatives in general, also implies non-local interactions, where the effects of changes in infection or recovery rates are felt over time, allowing for delayed responses to interventions like vaccination or isolation. Additionally, fractional-order models can account for population heterogeneity, capturing varying responses among different sub populations. They also represent diffusion-like behavior, where infection spread is not uniform and may exhibit slower characteristics compared to traditional models. Finally, the introduction of fractional derivatives can lead to complex dynamics, including oscillations and long-term trends, reflecting the multifaceted nature of real-life disease dynamics influenced by factors such as seasonality and social behavior. This can offer a more realistic representation of the biological processes underlying disease transmission and control compared to traditional integer-order models (Agarwal et al., 2024).

For this study, the Caputo fractional derivative with order $\sigma \in (0, 1)$ was employed since it allows the model solution to be derived with the use of local initial conditions, and its memorability makes it possible to estimate the model parameters more

accurately than the integer-order model. Given this advantage, we use the Caputo fractional derivative to assess how PrEP, ART, and drug-resistant accumulation affect the prevalence of HIV/AIDS in Ethiopia. Thus, by taking the above fact into account, the following system of nonlinear differential equations defines the Caputo fractional derivative of order σ for HIV/AIDS transmission dynamics:

$$\begin{cases} {}_0^C D_t^\sigma S(t) = \Lambda + \epsilon P - \lambda S - (\mu + \eta)S, \\ {}_0^C D_t^\sigma P(t) = \eta S - (\mu + \epsilon)P, \\ {}_0^C D_t^\sigma E(t) = \lambda S - (\mu + \delta)E, \\ {}_0^C D_t^\sigma I(t) = \delta E - (\mu + \theta_1)I, \\ {}_0^C D_t^\sigma R(t) = \phi\gamma\theta_1 I - (\mu + \tau + \theta_2)R, \\ {}_0^C D_t^\sigma A(t) = (1 - \phi\gamma)\theta_1 I + \theta_2 R - (\mu + d_A)A, \quad 0 < \sigma \leq 1, \end{cases} \tag{4.3}$$

with the initial conditions given as in equation (4.2).

Remark 4.1 *Each model parameters in system (4.3) are non-negative and they all depend on σ. The force of infection λ also depends on σ.*

The fifth equation of system (4.3) represents the fractional- order HIV drug resistant compartment. Here the term $\phi\gamma\theta_1 I$ stands for the fractional resistance generation term and the term $(\mu + \tau + \theta_2)R$ represents the fractional removal term.

Table 4.1: Description of model parameters.

Parameters	Descriptions
Λ	constant recruitment rate
β_0	base line transmission rate
μ	natural death rate
η	PrEP initiation rate
ϵ	PrEP discontinuation rate
θ_1	ART non-adherence rate for I class
θ_2	ART non-adherence rate for R class
γ	fraction of symptomatic cases receiving ART
ϕ	drug-resistance development rate
δ	detection rate of symptomatic cases
τ	additional mortality rate due to drug-resistance
d_A	AIDS induced death rate
q	behavioral response sensitivity
ρ_1, ρ_2, ρ_3	modification parameters

4.2 Model Analysis

4.2.1 Epidemiological Well-Possdness of the Model

Theorem 4.1 *For all $t \geq 0$, all the solution components $S(t)$, $P(t)$, $E(t)$, $I(t)$, $R(t)$ and $A(t)$ of system (4.3) are non-negative and bounded. Additionally, the closed region*

$$\mathcal{D} = \left\{ (S, P, E, I, R, A) \in \mathbb{R}_+^6 : 0 < N \leq \frac{\Lambda}{\mu} \right\}$$

is positively invariant.

Proof. Using similar techniques in Mahata et al. (2022); Tanvi A. (2021); Oshinubi et al. (2023) we obtain;

$$ {}_0^C D_t^\sigma S(t)|_{S=0} = \Lambda + \epsilon P \geq 0 \ , \ {}_0^C D_t^\sigma P(t)|_{P=0} = \eta S \geq 0 \ , \ {}_0^C D_t^\sigma E(t)|_{E=0} = \lambda S \geq 0,$$
$$ {}_0^C D_t^\sigma I(t)|_{I=0} = \delta E \geq 0 \ , \ {}_0^C D_t^\sigma R(t)|_{R=0} = \phi\gamma\theta_1 I \geq 0 \ , \ {}_0^C D_t^\sigma A(t)|_{A=0} = (1-\phi\gamma)\theta_1 I + \theta_2 R \geq 0.$$

Therefore, the vector field $Q = (S, P, E, I, R, A))^T$ points into $\mathbb{R}_+^6$ on each sextant enclosing the non-negative region. Based on this, the fact that all of the initial conditions in (4.2) are non-negative, we conclude that all solution components of system (4.3) are non-negative.

Now, we show the boundedness. Thus, if we add all the equations in (4.3) we get:

$$ {}_0^C D_t^\sigma N(t) = \Lambda - \mu N(t) - (\tau R + d_A A) \leq \Lambda - \mu N(t)$$

which after some rearrangement gives

$$ {}_0^C D_t^\sigma N(t) + \mu N(t) \leq \Lambda \tag{4.4}$$

Carrying out Laplace transform from (Pudlubny, 1999) on both sides of the inequality (4.4) we have,

$$\mathcal{L}\{ {}_0^C D_t^\sigma N(t)\} + \mu\mathcal{L}\{N(t)\} \leq \Lambda\mathcal{L}\{1\},$$

and this gives

$$s^\sigma N(s) - \sum_{k=0}^{n-1} s^{\sigma-k-1} N^{(k)}(0) + \mu N(s) \leq \Lambda \frac{1}{s} \tag{4.5}$$

As $0 < \sigma \leq 1$, we take $n = 1$ to obtain:

$$s^\sigma N(s) - s^{\sigma-1} N(0) + \mu N(s) \leq \Lambda \frac{1}{s}, \quad (s^\sigma + \mu) N(s) \leq \Lambda s^{-1} + N_0 s^{\sigma-1},$$

$$N(s) \leq \Lambda \frac{s^{-1}}{s^{\sigma}+\mu} + N_0 \frac{s^{\sigma-1}}{s^{\sigma}+\mu} \tag{4.6}$$

Taking out the inverse Laplace transform on each sides of (4.6) we get;

$$N(t) \leq \Lambda \mathcal{L}^{-1}\{\frac{s^{-1}}{s^{\sigma}+\mu}\} + N_0 \mathcal{L}^{-1}\{\frac{s^{\sigma-1}}{s^{\sigma}+\mu}\} \tag{4.7}$$

Considering the relation

$$\mathcal{L}^{-1}\{\frac{s^{\psi-\beta}}{s^{\psi}-\lambda}\} = t^{\beta-1}E_{\psi,\beta}(\lambda t^{\psi})$$

and comparing its exponents with that of inequality (4.6) we get $\beta = \psi + 1$ for the first term, $\beta = 1, \psi = \sigma$ for the second term and $\lambda = -\mu$. Hence, we arrive at

$$\begin{aligned} N(t) &\leq \Lambda t^{\sigma+1-1} E_{\sigma,\sigma+1}(-\mu t^{\sigma}) + N_0 t^{1-1} E_{\sigma,1}(-\mu t^{\sigma}) \\ &= \Lambda t^{\sigma} E_{\sigma,\sigma+1}(-\mu t^{\sigma}) + N_0 E_{\sigma,1}(-\mu t^{\sigma}) \end{aligned} \tag{4.8}$$

Utilizing the properties of Mittag-Leffler function (Pudlubny, 1999) we have,

$$E_{p,q}(z) = zE_{p,p+q}(z) + \frac{1}{\Gamma(q)},$$

and

$$E_{p,p+q}(z) = \frac{1}{z}\left(E_{p,q}(z) - \frac{1}{\Gamma(q)}\right) \tag{4.9}$$

Replacing $p = \sigma$, $q = 1$ and $z = -\mu t^{\sigma}$ in equation (4.9) we get

$$\begin{aligned} E_{\sigma,\sigma+1}(-\mu t^{\sigma}) &= \frac{1}{-\mu t^{\sigma}}\left(E_{\sigma,1}(-\mu t^{\sigma}) - \frac{1}{\Gamma(1)}\right) \\ &= \frac{1}{-\mu t^{\sigma}}\left(E_{\sigma,1}(-\mu t^{\sigma}) - 1\right) \ , \ \Gamma(1) = 1 \end{aligned} \tag{4.10}$$

Substituting (4.10) in (4.8) we have

$$\begin{aligned} N(t) &\leq \Lambda t^{\sigma} E_{\sigma,\sigma+1}(-\mu t^{\alpha}) + N_0 E_{\sigma,1}(-\mu t^{\sigma}) \\ = (\Lambda t^{\sigma})\left(\frac{1}{-\mu t^{\sigma}}\right)&\left(E_{\sigma,1}(-\mu t^{\sigma}) - 1\right) + N_0 E_{\sigma,1}(-\mu t^{\sigma}) \\ &= N_0 E_{\sigma,1}(-\mu t^{\sigma}) - \frac{\Lambda}{\mu} E_{\sigma,1}(-\mu t^{\sigma}) + \frac{\Lambda}{\mu} \\ &= \left(N_0 - \frac{\Lambda}{\mu}\right) E_{\sigma,1}(-\mu t^{\sigma}) + \frac{\Lambda}{\mu} \end{aligned} \tag{4.11}$$

Therefore, if $N_0 \leq \frac{\Lambda}{\mu}$, then

$$\limsup_{t\to\infty}(N(t)) \leq \frac{\Lambda}{\mu}$$

Hence, $\frac{\Lambda}{\mu}$ bounded $N(t)$ from above and we have $0 < N(t) \leq \frac{\Lambda}{\mu}$, meaning that all the solution components are bounded. Consequently, the closed region

$$\mathcal{D} = \left\{(S, P, E, I, R, A) \in \mathbb{R}^6_+ : 0 < N \leq \frac{\Lambda}{\mu}\right\}$$

is positively invariant since every solution that begins in $\mathbb{R}^6_+$ stays in $\mathbb{R}^6_+$.

Non-negativity and boundedness are essential for ensuring that epidemiological models yield accurate and biologically relevant predictions. Non-negativity prevents negative population values, accurately reflecting population dynamics, while boundedness maintains the dynamics within reasonable limits. Together, these features improve the model's reliability, making it a valuable tool for analyzing disease transmission and informing public health planning.

4.2.2 Mathematical Well-Possdness of the Model

Our primary objective here is to show that the solution to system (4.3) exists and is unique.
Thus, we rewrite equation (4.3) as

$$^{C}_{0}D^{\sigma}_{t}V_j(t) = \mathcal{F}_j(t, V_j), \tag{4.12}$$

with the initial conditions as in (4.2) for each $j = 1, 2, \cdots, 6$ where,

$$V_1 = S,\ V_2 = P,\ V_3 = E,\ V_4 = I\ ,\ V_5 = R,\ V_6 = A$$

and $\mathcal{F}_j(t, V_j)$ denotes the j^{th} equation on the right hand sides of equation (4.3). Taking integral transform on each sides of equation (4.12) and for each $j = 1, 2, \cdots, 6$ we obtain

$$V_j(t) = V_j(0) + \frac{1}{\Gamma(\sigma)}\int_0^t (t-\rho)^{\sigma-1}\mathcal{F}_j(\rho, V_j(\rho))d\rho \tag{4.13}$$

Lemma 4.1 *The kernels $\mathcal{F}_k$ are Lipschitz with corresponding Lipschitz constants G_k for each $k = 1, 2, \cdots, 6$. They are contractions as long as $0 < G_k < 1$; where,*
$G_1 = a_1+\mu+\eta,\ G_2 = \mu+\epsilon,\ \ G_3 = \mu+\delta,\ \ G_4 = \mu+\theta_1,\ \ G_5 = \mu+\tau+\theta_2,\ \ G_6 = \mu+d_A.$

Proof. The proof follows similar techniques in Mahata et al. (2022). Thus, with the above definitions for $V_j's,\ j = 1, 2, \cdots, 6$, for V_1 and V_1^* we have;

$||\mathcal{F}_1(t,V_1)-\mathcal{F}_1(t,V_1^*)|| = ||-(\lambda(t)+\mu+\eta)(V_1-V_1^*)|| \leq (||\lambda(t)||+\mu+\eta)||V_1-V_1^*||$. Assume that $G_1 = a_1+\mu+\eta$, where $\lambda(t) \leq a_1$ is a bounded function. Then, $||\mathcal{F}_1(t,V_1)-\mathcal{F}_1(t,V_1^*)|| \leq G_1||V_1-V_1^*||$. Hence, the kernel $\mathcal{F}_1$ is Lipschitz with a Lipschitz constant G_1 and contraction provided that $0 < G_1 < 1$. In the same way, we can show that the kernels $\mathcal{F}_j$ for $j = 2,3,\cdots,6$ are Lipschitz with a Lipschitz constant G_j and are contractions provided that $0 < G_j < 1$.

Theorem 4.2 *If for each $j = 1,2,\cdots,6$ the inequality $\frac{t^\sigma G_j}{\Gamma(\sigma+1)} < 1$ is satisfied, then system (4.3), subject to initial conditions (4.2), has at least one solution.*

Proof. Assume $V_j's$ are as defined in (4.12). Following Mahata et al. (2022); Oshinubi et al. (2023), for $j = 1,2,\cdots,6$, define the following recursive patterns:

$$\Omega_{j_n}(t) = V_{j_n}(t) - V_{j_{n-1}}(t) = \frac{1}{\Gamma(\sigma)}\int_0^t (\mathcal{F}_j(\rho,V_{j_{n-1}}) - \mathcal{F}_j(\rho,V_{j_{n-2}}))(t-\rho)^{\sigma-1}d\rho, \quad (4.14)$$

with the initial conditions as in equation (4.2).
After making some algebraic adjustments and by applying the lipschitz condition from Lemma (4.1), we get

$$||V_{j_n}(t) - V_{j_{n-1}}(t)|| \leq ||V_{j_n}(0)|| \left(\frac{t^\sigma G_1}{\Gamma(\sigma+1)}\right)^n, \quad (4.15)$$

Therefore, V_{j_n} $(j = 1,2,\cdots,6)$, are uniformly bounded sequences.
In order to indirectly imply that these sequences converge to the IVP solution (4.3) with initial condition (4.2), we must show that they uniformly converge to the integral solution (4.13) on a given interval I.

Now, assume the kernels $\mathcal{F}_j (j = 1,2,\cdots,6)$ are continuous on a closed region $\mathfrak{R} = \{(t,m) : |t-t_0| \leq a,\ ||m-m_0|| \leq b\}$ with

$$\mathfrak{M} = \begin{pmatrix} S(t),\ P(t),\ E(t),\ I(t),\ R(t),\ A(t) \end{pmatrix}^T, \quad \mathfrak{M}_0 = \begin{pmatrix} S_0,\ P_0,\ E_0,\ I_0,\ R_0,\ A_0 \end{pmatrix}^T (4.16)$$

Define $K_j > 0$ such that $||\mathcal{F}_j|| < K_j$ for each $j = 1,2,\cdots,6$. Let $I = [0,h]$ where, $h = min\left\{a, \frac{b}{K}\Gamma(\sigma+1)^{\frac{1}{\sigma}}\right\}$. Obviously, we can see that

$$\mathfrak{M}_n = \mathfrak{M}_0 + \sum_{k=1}^{n}(\mathfrak{M}_k - \mathfrak{M}_{k-1}). \quad (4.17)$$

The series $\mathfrak{M}_0 + \sum_{k=1}^{n}(\mathfrak{M}_k - \mathfrak{M}_{k-1})$ need only be demonstrated to converges uniformly

on I to show that the $\mathfrak{M}_n$ sequence converges uniformly on I. Hence,

$$||\mathfrak{M}_0 + \sum_{k=1}^{n}(\mathfrak{M}_k - \mathfrak{M}_{k-1})|| \leq ||\mathfrak{M}_0|| + \sum_{k=1}^{n}||\mathfrak{M}_k - \mathfrak{M}_{k-1}||$$
$$\leq ||\mathfrak{M}_0|| + \sum_{k=1}^{n}||\mathfrak{M}_k(0)||\left(\frac{t^\sigma G_1}{\Gamma(\sigma+1)}\right)^k. \tag{4.18}$$

which converges uniformly on I provided that $\frac{t^\sigma G_1}{\Gamma(\sigma+1)} < 1$. The sequence $\mathfrak{M}_n$ converges uniformly on I, as determined by the Weierstrass M-test. The Lebesgue dominated convergence theorem may be used to show that this series converges to a limit point $\mathfrak{M}(t)$, which is the solution of the integral equation (4.13). The IVP (4.3) with initial conditions (4.2) therefore has at least one solution for each $j = 1, 2, \cdots, 6$, given that $\frac{t^\sigma G_j}{\Gamma(\sigma+1)} < 1$.

Theorem 4.3 *For each $j = 1, 2, \cdots, 6$, system (4.3), subject to the initial conditions (4.2) has a unique solution provided that*

$$1 - \frac{t^\sigma Q_j}{\Gamma(\sigma+1)} > 0.$$

Proof. Assume that $S(t)$ and $S_1(t)$ are the solutions to system (4.3) subject to its initial conditions(4.2). Then,

$$S(t) = S_0 + \frac{1}{\Gamma(\sigma)}\int_0^t (t-\tau)^{\sigma-1}\mathcal{F}_1(\tau, S(\tau))d\tau,$$
$$S_1(t) = S_0 + \frac{1}{\Gamma(\sigma)}\int_0^t (t-\tau)^{\sigma-1}\mathcal{F}_1(\tau, S_1(\tau))d\tau.$$

Subtracting the 2^{nd} equation from the 1^{st}, employing the Lipschitz condition for $\mathcal{F}_1$ and rearranging gives

$$||S(t) - S_1(t)||\left(1 - \frac{G_1 t^\sigma}{\Gamma(\sigma+1)}\right) \leq 0.$$

But, by the previous theorem $\left(1 - \frac{G_1 t^\sigma}{\Gamma(\sigma+1)}\right) > 0$. Hence, the inequality holds true only if $S(t) = S_1(t)$. The proof for the remaining state variables is similar. This completes the proof.

Solutions for epidemiological models need to be both distinct and easily accessible in order to have biological significance. Existence guarantees that the model may produce real illness dynamics, whereas uniqueness guarantees that the dynamics of the disease are steady and predictable. When taken as a whole, non-negativity, boundedness, existence, and uniqueness of solutions increase the precision of models that direct

public health programs and help understand how illnesses spread.

4.2.3 Fractional Threshold Condition and Stability Criterion

Theorem 4.4 *[Fractional Threshold Condition] Consider the Caputo fractional-order model:*

$$ {}_0^C D_t^\sigma X(t) = G(X(t)), \quad 0 < \sigma \leq 1, \tag{4.19} $$

where $X = (X_1, X_2, \cdots, X_n)^T \in \mathbb{R}_+^n$ *denotes the compartmental state vector, and* $G : \mathbb{R}^n \to \mathbb{R}^n$ *represents the nonlinear model equations with a disease-free equilibrium* $\mathcal{E}^0$.

Define the fractional basic reproduction number *as:*

$$ \mathcal{R}_0^{(\sigma)} = \rho\left(F[-\hat{V}(\sigma)]^{-1}\right), \tag{4.20} $$

with $F = \left[\frac{\partial \mathcal{F}_i}{\partial x_j}\right]_{\mathcal{E}^0}$, $V = \left[\frac{\partial \mathcal{V}_i}{\partial x_j}\right]_{\mathcal{E}^0}$, *and* $\hat{V}(\sigma) = V\Psi(\sigma)$ *where* $\Psi(\sigma) = \operatorname{diag}(\psi_1(\sigma), \ldots, \psi_m(\sigma))$, *with* $\psi_i(\sigma) = \frac{\Gamma(\sigma)}{v_i^{1-\sigma}}$, *and* m *representing the number of infected compartments. Here,* $\mathcal{F}$, $\mathcal{V}$ *are respectively matrices of new infection terms and transition terms. Then:*

(i) ***Stability Boundary:*** *The surface* $\mathcal{R}_0^{(\sigma)} = 1$ *defines the stability boundary in parameter space.*

(ii) ***Mittag-Leffler Stability:*** *If* $\mathcal{R}_0^{(\sigma)} < 1$ *and all eigenvalues* λ *of the Jacobian matrix at* $\mathcal{E}^0$ *satisfy* $|\arg(\lambda)| > \frac{\sigma\pi}{2}$, *then* $\mathcal{E}^0$ *is locally Mittag-Leffler stable.*

(iii) ***Instability:*** *If* $\mathcal{R}_0^{(\sigma)} > 1$, *then* $\mathcal{E}^0$ *is unstable.*

Lemma 4.2 *[Fractional Linear System Stability (Matignon, 1996)]*
For the Caputo fractional linear system:

$$ {}_0^C D_t^\sigma x(t) = Ax(t), \quad x(0) = x_0, \quad 0 < \sigma \leq 1, \tag{4.21} $$

the equilibrium $x = 0$ *is asymptotically stable if and only if* $|\arg(\lambda_i)| > \frac{\sigma\pi}{2}$ *for all eigenvalues* λ_i *of* A *and unstable if there exists at least one eigenvalue* λ_i *such that* $|\arg(\lambda_i)| < \frac{\sigma\pi}{2}$.

Lemma 4.3 *[Mittag-Leffler Decay (Pudlubny, 1999)]*
If $|\arg(\lambda)| > \frac{\alpha\pi}{2}$, *then there exist constants* $M, \mu > 0$ *such that:*

$$ |E_{\sigma,1}(\lambda t^\sigma)| \leq \frac{M}{1 + |\lambda| t^\sigma}, \quad \forall t \geq 0. \tag{4.22} $$

Moreover, there exists $\eta > 0$ such that:

$$\frac{1}{1+|\lambda|t^{\sigma}} \leq mE_{\sigma,1}(-\eta t^{\sigma}), \quad \forall t \geq 0, \tag{4.23}$$

for some $m > 0$.

Lemma 4.4 *[Fractional Routh–Hurwitz Conditions (Bourafa et al., 2020)] Consider a fractional system of order $\sigma \in (0,1]$ with characteristic polynomial $P(\lambda) = \lambda^n + a_{n-1}\lambda^{n-1} + \cdots + a_0$.*

i) For $0 < \sigma \leq \frac{1}{2}$, the system is asymptotically stable if and only if

$$a_i > 0, \quad \forall i, \quad \text{and} \quad \Delta_i > 0, \quad \forall i, \tag{4.24}$$

where Δ_i are the Hurwitz determinants.

ii) For $\frac{1}{2} < \sigma \leq 1$, the system is asymptotically stable if and only if

$$a_i > 0, \quad \forall i, \quad \text{and} \quad |\arg(\lambda_i)| > \frac{\sigma\pi}{2}, \quad \forall \lambda_i. \tag{4.25}$$

Lemma 4.5 *[Spectral Monotonicity] For the next-generation matrix $K(\lambda) = F(V+\lambda I)^{-1}$ with $F \geq 0$ and V an M-matrix, the spectral radius function*

$$\phi(\lambda) = \rho(K(\lambda)) \tag{4.26}$$

is strictly decreasing for $\Re(\lambda) \geq 0$.

Proof. Since V is an M-matrix, $V^{-1} \geq 0$ elementwise. For $\lambda_1 < \lambda_2$ with $\Re(\lambda_i) \geq 0$, we have $(V+\lambda_1 I)^{-1} > (V+\lambda_2 I)^{-1}$ elementwise. By the Perron–Frobenius theorem for nonnegative matrices, $\phi(\lambda_1) > \phi(\lambda_2)$.

Proof of Theorem (i). Let $x = (x_1, x_2, \cdots, x_n)^T$ denote the infected compartments. The linearized infected subsystem at the DFE $\mathcal{E}^0$ is:

$$_0^C D_t^{\sigma} x(t) = (F-V)x(t). \tag{4.27}$$

Taking Laplace transforms with zero initial conditions gives:

$$s^{\sigma}\hat{x}(s) = (F-V)\hat{x}(s) \quad \Rightarrow \quad [s^{\sigma}I - (F-V)]\hat{x}(s) = 0. \tag{4.28}$$

Hence, the characteristic equation is:

$$\det(s^{\sigma}I - (F-V)) = 0. \tag{4.29}$$

The eigenvalue problem associated with (4.29) can be expressed as:

$$Fv = \mu(V + \lambda I)v. \tag{4.30}$$

Setting $\mu = 1$ and $\lambda = s^\sigma$ gives $(F - V)v = s^\sigma v$, which leads to the reformulation:

$$\det(I - F(V + s^\sigma I)^{-1}) = 0. \tag{4.31}$$

A nontrivial solution exists when

$$\rho(F(V + s^\sigma I)^{-1}) = 1. \tag{4.32}$$

By Lemma (4.5), $\phi(s^\sigma) = \rho(F(V + s^\sigma I)^{-1})$ is strictly decreasing in $\Re(s^\sigma)$. Therefore, its minimum value on $\Re(s^\sigma) = 0$ occurs at $s^\sigma = 0$. Hence, the stability boundary satisfies:

$$\phi(0) = \rho(FV^{-1}) = \mathcal{R}_0^{(\sigma)} = 1. \tag{4.33}$$

Proof of Theorem (ii). Assume $\mathcal{R}_0^{(\sigma)} < 1$ and all eigenvalues λ of the Jacobian matrix at $\mathcal{E}^0$ satisfy $|\arg(\lambda)| > \frac{\sigma\pi}{2}$. The linearized system solution is given by:

$$x(t) = E_{\sigma,1}(At^\sigma)x(0), \quad A = F - V. \tag{4.34}$$

By Lemma (4.3), for each λ_i, there exist constants $M_i, \mu_i > 0$ such that

$$|E_{\sigma,1}(\lambda_i t^\sigma)| \leq \frac{M_i}{1 + |\lambda_i| t^\sigma}. \tag{4.35}$$

Hence, $\|x(t)\| \leq m_0 E_{\sigma,1}(-\eta t^\sigma)\|x(0)\|$ for some $m_0, \eta > 0$, implying Mittag-Leffler stability.

For the nonlinear system ${}_0^C D_t^\sigma X = G(X)$, a fractional Lyapunov function $V(x) = w^T x$ with $w > 0$ satisfying $w^T K^{(\sigma)} = \mathcal{R}_0^{(\sigma)} w^T$ yields

$${}_0^C D_t^\sigma V(x) = w^T(F - V)x + w^T \mathcal{N}(x) \leq -cV(x), \tag{4.36}$$

for some $c > 0$, proving local Mittag-Leffler stability by (Li et al., 2009).

Proof of Theorem (iii). If $\mathcal{R}_0^{(\sigma)} > 1$, then $\phi(0) = \rho(FV^{-1}) > 1$, and since $\phi(\lambda)$ is strictly decreasing and continuous, there exists $\lambda_0 > 0$ such that $\rho(F(V + \lambda_0 I)^{-1}) = 1$. This implies $(F - V)w = \lambda_0 w$ for some $w > 0$, yielding a positive real eigenvalue $\lambda_0 > 0$. Hence, $|\arg(\lambda_0)| = 0 < \frac{\sigma\pi}{2}$, implying instability by Lemma (4.2).

4.2.4 Computation of the Basic Reproduction Number

The HIV/AIDS-free equilibrium point of model (4.3), which signifies a population that is free of HIV/AIDS, is given by $\mathcal{E}^0 = \left(\frac{\Lambda(\mu+\epsilon)}{\mu(\mu+\epsilon)+\mu\eta}, \frac{\Lambda\eta}{\mu(\mu+\epsilon)+\mu\eta}, 0, 0, 0, 0\right)$. The basic reproduction number is defined as the average number of secondary cases resulting from a single infected individual in a fully susceptible population.

Considering E, I, R and A as infected classes and using the next-generation matrix approach developed in Diekmann et al. (1990), the matrices corresponding to the new infection terms (F) and the transfer terms (V) are as follows:

$$F = \begin{bmatrix} \beta(t)\rho_1\frac{S^0}{N^0} & \beta(t)\rho_2\frac{S^0}{N^0} & \beta(t)\rho_3\frac{S^0}{N^0} & \beta(t)\frac{S^0}{N^0} \\ 0 & 0 & 0 & 0 \\ 0 & 0 & 0 & 0 \\ 0 & 0 & 0 & 0 \end{bmatrix},$$

$$V = \begin{bmatrix} \mu+\delta & 0 & 0 & 0 \\ -\delta & \mu+\theta_1 & 0 & 0 \\ 0 & -\phi\gamma\theta_1 & \mu+\tau+\theta_2 & 0 \\ 0 & -(1-\phi\gamma)\theta_1 & -\theta_2 & \mu+d_A \end{bmatrix},$$

Define $d = \frac{S^0}{N^0} = \frac{\mu+\epsilon}{\mu+\epsilon+\eta}$, $a_1 = \mu+\delta$, $a_2 = \mu+\theta_1$, $a_3 = \mu+\tau+\theta_2$, $a_4 = \mu+d_A$, $a_5 = \phi\gamma\theta_1$, $a_6 = (1-\phi\gamma)\theta_1$. Then, noting that $\beta(t) = \beta_0 e^{-q(I^0+A^0)} = \beta_0$, at the HIV/AIDS free equilibrium point $\mathcal{E}^0$, we now obtain

$$F = \begin{bmatrix} \beta_0\rho_1 d & \beta_0\rho_2 d & \beta_0\rho_3 d & \beta_0 d \\ 0 & 0 & 0 & 0 \\ 0 & 0 & 0 & 0 \\ 0 & 0 & 0 & 0 \end{bmatrix}, \quad V = \begin{bmatrix} a_1 & 0 & 0 & 0 \\ -\delta & a_2 & 0 & 0 \\ 0 & -a_5 & a_3 & 0 \\ 0 & -a_6 & -\theta_2 & a_4 \end{bmatrix}.$$

Using the computer algebra system we obtain

$$V^{-1} = \begin{bmatrix} \frac{1}{a_1} & 0 & 0 & 0 \\ \frac{\delta}{a_1 a_2} & \frac{1}{a_2} & 0 & 0 \\ \frac{a_5\delta}{a_1 a_2 a_3} & \frac{a_5}{a_2 a_3} & \frac{1}{a_3} & 0 \\ \frac{\delta(a_3 a_6 + a_5\theta_2)}{a_1 a_2 a_3 a_4} & \frac{a_3 a_6 + a_5\theta_2}{a_2 a_3 a_4} & \frac{\theta_2}{a_3 a_4} & \frac{1}{a_4} \end{bmatrix}$$

Consequently, the basic reproduction number for the fractional HIV/AIDS model, which is the largest spectral radius of FV^{-1}, becomes:

$$\mathcal{R}_0^{(\sigma)} = \beta_0 d \left(\frac{a_2 a_3 a_4 \rho_1 + \delta a_3 a_4 \rho_2 + \delta a_4 a_5 \rho_3 + \delta(a_3 a_6 + a_5\theta_2)}{a_1 a_2 a_3 a_4} \right) \Psi(\sigma)$$

with $\Psi(\sigma)$ being fractional correction factor. In the above expression, the terms

$$\left(\frac{\beta_0 d\rho_1}{a_1}\right)\Psi(\sigma),\ \left(\frac{\beta_0 d\delta\rho_2}{a_1a_2}\right)\Psi(\sigma),\ \beta_0 d\left(\frac{\delta a_5\rho_3}{a_1a_2a_3}\right)\Psi(\sigma),\ \beta_0 d\left(\frac{\delta(a_3a_6+a_5\theta_2)}{a_1a_2a_3a_4}\right)\Psi(\sigma)$$

respectively signifies the number of average secondary infections caused by a single infectious persons in E, I, R and A compartments in an entirely susceptible populations.

4.2.5 Bifurcation Analysis

In this part, we discuss the two types of bifurcations in epidemic models that occur at the threshold value $\mathcal{R}_0^{(\sigma)} = 1$: forward (supercritical) and backward (subcritical) bifurcations. A forward bifurcation happens when $\mathcal{R}_0^{(\sigma)}$ increases above one, leading to the emergence of a small positive stable equilibrium while destabilizing the disease-free equilibrium. Conversely, a backward bifurcation occurs when $\mathcal{R}_0^{(\sigma)}$ is below one, resulting in an unstable equilibrium alongside stable disease-free and larger positive equilibria. This indicates that merely reducing $\mathcal{R}_0^{(\sigma)}$ below one may not suffice to eradicate the disease, highlighting potential hysteresis effects. The aim of the section is to explore the bifurcation direction using center manifold theory C. Castillo-Chavez & Song (2004), which simplifies the examination of dynamical systems near equilibrium points.

Thus, let $u = [u_1, u_2, u_3, u_4, u_5, u_6]^T = [S, P, E, I, R, A]^T$. Then, the HIV/AIDS model (4.3) can be rewritten compactly as

$$\begin{cases} {}_0^C D_t^\sigma u_1(t) = \Lambda + \epsilon u_2 - \lambda_b u_1 - b u_1 = g_1(u_1, u_2, u_3, u_4, u_5, u_6), \\ {}_0^C D_t^\sigma u_2(t) = \eta u_1 - c u_2 = g_2(u_1, u_2, u_3, u_4, u_5, u_6), \\ {}_0^C D_t^\sigma u_3(t) = \lambda_b u_1 - a_1 u_3 = g_3(u_1, u_2, u_3, u_4, u_5, u_6), \\ {}_0^C D_t^\sigma u_4(t) = \delta u_3 - a_2 u_4 = g_4(u_1, u_2, u_3, u_4, u_5, u_6), \\ {}_0^C D_t^\sigma u_5(t) = a_5 u_4 - a_3 u_5 = g_5(u_1, u_2, u_3, u_4, u_5, u_6), \\ {}_0^C D_t^\sigma u_6(t) = a_6 u_4 + \theta_2 u_5 - a_4 u_6 = g_6(u_1, u_2, u_3, u_4, u_5, u_6), \end{cases} \tag{4.37}$$

with

$$\lambda_b = \frac{\beta_0\left(\rho_1 u_3 + \rho_2 u_4 + \rho_3 u_5 + u_6\right)}{N_b},\ \ N_b = u_1+u_2+u_3+u_4+u_5+u_6,\ \ b = \mu+\eta,\ \ c = \mu+\epsilon$$

and $a_i's$ $(i = 1, 2, \cdots, 6)$ are as defined under section (4.2.4). Here, β_0 is a parameter indicating baseline transmission rate for HIV/AIDS disease.

Choosing β_0^* as a bifurcation parameter and setting $\mathcal{R}_0^{(\sigma)} = 1$ we obtain,

$$\beta_0^* = \frac{a_1 a_2 a_3 a_4}{d\left(a_2 a_3 a_4 \rho_1 + a_3 a_4 \delta \rho_2 + a_4 a_5 \delta \rho_3 + \delta(a_3 a_6 + a_5 \theta_2)\right)}$$

It's evident that $\beta_0^\star > 0$. Using $\beta_0 = \beta_0^*$ and evaluating the Jacobean of system (4.37) at $\mathcal{E}^0$, represented by $\mathcal{J}(\mathcal{E}^0,\ \beta_0^*)$ and the fractional Routh-Hurwitz criterion, we can demonstrate that $\mathcal{J}(\mathcal{E}^0, \beta_0^*)$ has a simple zero eigenvalue, and the remaining eigenvalues have negative sign, indicating that $\mathcal{E}^0$ is a non-hyperbolic equilibrium, when $\beta_0 = \beta_0^*$. Hence, based on the center manifold theory let

$$w = (w_1, w_2, w_3, w_4, w_5, w_6)^T, \quad v = (v_1, v_2, v_3, v_4, v_5, v_6)$$

be respectively the right and left eigenvectors associated to the zero eigenvalue. Then, solving $\mathcal{J}(\mathcal{E}^0, \beta_0^*).w = 0$ we get,

$$w_3 = w_3 > 0, \quad w_4 = \frac{\delta w_3}{a_2} > 0, \quad w_5 = \frac{a_5 \delta w_3}{a_2 a_3} > 0, \quad w_6 = \frac{(a_3 a_6 + \theta_2 a_5)\delta w_3}{a_2 a_3 a_4} > 0,$$

$$w_1 = \frac{\mathcal{R}_0 a_1 a_2 c w_3}{\eta\epsilon - bc} < 0, \quad w_2 = \frac{\eta w_1}{c} < 0.$$

Similarly, solving $v.\mathcal{J}(\mathcal{E}^0, \beta_0^*) = 0$ we have,

$$v_1 = v_2 = 0, \quad v_3 = v_3 > 0, \quad v_4 = \frac{[a_3 a_4 + \beta_0 d(\rho_2 a_3 a_4 + \rho_3 a_4 a_5 + \theta_2 a_5 + a_3 a_6)]v_3}{a_2 a_3 a_4} > 0,$$

$$v_5 = \frac{\beta_0 d(\rho_3 a_4 + \theta_2)v_3}{a_3 a_4} > 0, \quad v_6 = \frac{\beta_d v_3}{a_4} > 0.$$

The eigenvectors w and v satisfy the condition $v.w = 1$.

Let c, d be the coefficients of the normal form representing the dynamics of the system in the central manifold such that $\dot{y} = cy^2 + d\beta_0^* y$. Then, following C. Castillo-Chavez & Song (2004) the bifurcation coefficients c and d at the DFE, $\mathcal{E}^0$ is given by

$$c = \sum_{k,i,j=1}^{6} v_k w_i w_j \frac{\partial^2 g_k}{\partial u_i \partial u_j}(\mathcal{E}^0, \beta_0^*)\ , \quad d = \sum_{k,i=1}^{6} v_k w_i \frac{\partial^2 g_k}{\partial u_i \partial \beta_0}(\mathcal{E}^0, \beta_0^*) \tag{4.38}$$

Since $v_1 = v_2 = 0$, we compute only the second order partial derivatives of $g_3,\ g_4,\ g_5$ and g_6. Consequently, after computing these derivatives and using them in equation (4.38) we obtain

$$c = \frac{2\beta_0^* w_1 v_3[\rho_1 w_3 + \rho_2 w_4 + \rho_3 w_5 + w_6]}{N_b} < 0, \quad d = \frac{2\beta_0^* v_3[\rho_1 w_3 + \rho_2 w_4 + \rho_3 w_5 + w_6]}{N_b} > 0.$$

Therefore, the HIV/AIDS model (4.3) experiences a forward bifurcation at $\mathcal{R}_0^{(\sigma)} = 1$ since $c < 0$ and $d > 0$. The forward bifurcation phenomenon indicates that the stable HIVFEP splits into two non-negative equilibrium points: the unstable HIVFEP and the stable positive HIVEEP, as $\mathcal{R}_0^{(\sigma)}$ passes unity. This suggests, epidemiologically, that HIV cannot infiltrate the population for $\mathcal{R}_0^{(\sigma)} < 1$.

4.2.6 Stability Analysis of the HIV/AIDS Free Equilibrium Point

Theorem 4.5 *The HIV/AIDS free equilibrium $\mathcal{E}^0$ is locally asymptotically stable if $|arg(\lambda_j)| > \sigma\frac{\pi}{2}$ for all eigenvalue λ_j of K, where K is a linearized matrix obtained by computing the Jacobian of system (4.3) at $\mathcal{E}^0$ and unstable if there exists at least one eigenvalue λ_j such that $|arg(\lambda_j)| < \sigma\frac{\pi}{2}$.*

Proof. Define $b = \mu + \eta,\ c = \mu + \epsilon$ and assume that a_j $(j = 1, 2, \cdots, 6)$ and d are as defined before.
Rewrite system (4.3) as a fractional linear system

$$ {}_0^C D_t^\sigma x(t) = Kx(t), \quad x(0) = x_0, \quad 0 < \sigma \leq 1, $$

where $x = (S, P, E, I, R, A)^T$ and

$$ K = \begin{bmatrix} -b & \epsilon & -\beta_0\rho_1 d & -\beta_0\rho_2 d & -\beta_0\rho_3 d & -\beta_0 d \\ \eta & -c & 0 & 0 & 0 & 0 \\ 0 & 0 & \beta_0\rho_1 d - a_1 & \beta_0\rho_2 d & \beta_0\rho_3 d & \beta_0 d \\ 0 & 0 & \delta & -a_2 & 0 & 0 \\ 0 & 0 & 0 & a_5 & -a_3 & 0 \\ 0 & 0 & 0 & a_6 & \theta_2 & -a_4 \end{bmatrix} $$

is a linearized matrix, which is the Jacobian of model (4.3) evaluated at $\mathcal{E}^0$.
After taking simple algebraic computations using computer algebra system one can see that each eigenvalue λ_j of K satisfy $|arg(\lambda_j)| > \frac{\sigma\pi}{2}$. Therefore, by Lemma (4.2) $\mathcal{E}^0$ is locally asymptotically stable.

Remark 4.2 *From an epidemiological point of view, HIV/AIDS can be eradicated from the community when the fractional-order σ satisfy the condition $|arg(\lambda_j)| > \frac{\sigma\pi}{2}$ for each eigenvalue λ_j of the linearized matrix K, because this ultimately leads to the infection's extinction. In contrast, if $|arg(\lambda_j)| < \frac{\sigma\pi}{2}$, for at least one eigenvalue λ_j, the illness keeps spreading across the population. These findings have been validated through numerical simulations in Section (4.5).*

In the following theorem, we examine the global stability of HIV free equilibrium point.

4.2.7 Fractional-order extension of Lyapunov direct method

Consider a Caputo fractional-order system given in equation (4.19). The following definition and theorem are adopted from (Khalil & Grizzle, 2002).

Definition 4.1 *A continuous function $\psi : [0, t] \to [0, \infty]$ is said to belong to class-$\mathcal{K}$ if it is strictly increasing and $\psi(0) = 0$.*

Theorem 4.6 *Let $x = 0$ be an equilibrium point for the fractional-order system (4.19). Assume that there exists a Lyapunov function $V(t, x(t))$ and a class-$\mathcal{K}$ functions $\psi_i (i = 1, 2, 3)$ such that*

$$\psi_1(||x||) \leq V(t, x(t)) \leq \psi_2(||x||) \tag{4.39}$$

$$_0^C D_t^\beta V(t, x(t)) \leq -\psi_3(||x||) \tag{4.40}$$

where $\beta \in (0, 1)$. Then, system (4.19) is asymptotically stable.

Consider the following Lemma and Corollary (Aguila-Camacho et al., 2014).

Lemma 4.6 *Let $x(t) \in \mathbb{R}^n$ be a continuous and differentiable function. Then, for all $t \geq t_0$*

$$\frac{1}{2}\, {}_0^C D_t^\sigma x^2(t) = {}_0^C D_t^\sigma \frac{1}{2} x^2(t) \leq x(t) {}_0^C D_t^\sigma, \ \forall \sigma \in (0, 1) \tag{4.41}$$

Corollary 4.1 *For system (4.19) , where x=0 is the equilibrium point,*

i) if $x(t)g(x(t)) \leq 0, \forall x$ the origin of system (4.19) is stable.

ii) if $x(t)g(x(t)) < 0, \forall x \neq 0$ the origin of system (4.19) is asymptotically stable.

Lemma 4.7 *Let $V(\boldsymbol{y}(t)) = \frac{1}{2}\|\boldsymbol{y}(t)\|^2$. Then, for the Caputo derivative, there exists a constant $K(\alpha) > 0$ such that:*

$$_0^C D_t^\sigma V(\boldsymbol{y}(t)) \leq \sum_{i=1}^{10} y_i(t) \cdot {}_0^C D_t^\sigma y_i(t) + K(\sigma)\|\boldsymbol{y}(t)\|^2.$$

Proof. Follows from the standard results in Li et al. (2010).

Theorem 4.7 *If $\mathcal{R}_0^{(\sigma)} < 1$, the HIV/AIDS free equilibrium point $\mathcal{E}^0$ of model (4.3) is globally asymptotically stable in its biologically feasible region*

$$\mathcal{D} = \left\{ (S, P, E, I, R, A) \in \mathbb{R}_+^6 : 0 < N \leq \frac{\Lambda}{\mu} \right\}.$$

Proof. Consider the quadratic Lyapunov candidate:

$$V(\mathbf{y}) = \frac{1}{2}\|\mathbf{y}\|^2 = \frac{1}{2}\sum_{i=1}^{6} y_i^2, \quad \textit{with } \mathbf{y} = \mathbf{x} - \mathcal{E}^0, \quad \textit{where } \mathbf{x} = (S, P, E, I, R, A).$$

Due to the non-local nature of fractional derivatives, utilizing Lemma (4.7) and the systems dynamics, we compute:

$$\sum_{i=1}^{6} y_i \cdot {}_0^C D_t^\sigma y_i = y_1\Big[\Lambda + \epsilon P - (\lambda + \mu + \eta)S\Big] + y_2\Big[\eta S - (\mu + \epsilon)P\Big] + \cdots + y_6\Big[(1 - \phi\gamma)\theta_1 I + \theta_2 R - (\mu + d_A)A\Big].$$

The following hold at $\mathcal{E}^0$:

$$\Lambda + \epsilon P = (\lambda + \mu + \eta)S^0, \quad \eta S = (\mu + \epsilon)P^0, \quad \cdots, \ (1 - \phi\gamma)\theta_1 I + \theta_2 R = (\mu + d_A)A^0.$$

Substituting these into the derivative expression and simplifying yields:

$$\sum_{i=1}^{6} y_i \cdot {}_0^C D_t^\sigma y_i \leq -\sum_{i=1}^{6} c_i y_i^2.$$

Using this into Lemma (4.7) we get

$${}_0^C D_t^\sigma V(\mathbf{y}(t)) \leq -\sum_{i=1}^{6} c_i y_i^2 + \mathcal{R}(\mathbf{y}),$$

where $c_i > 0$ and $\mathcal{R}(\mathbf{y})$ denotes bounded cross terms.

Applying Young's inequality:

$$|y_i y_j| \leq \frac{\varepsilon}{2} y_i^2 + \frac{1}{2\varepsilon} y_j^2,$$

we bound $\mathcal{R}(\mathbf{y})$ and absorb it into the main negative definite term to obtain

$${}_0^C D_t^\sigma V(\mathbf{y}) \leq -c\|\mathbf{y}\|^2 < 0, \ \forall_x \neq \mathcal{E}^0, \quad \text{and for some constant } c > 0.$$

The fractional derivative of the Lyapunov function is negative semi definite. Thus, by Corollary (4.1) , $\mathcal{E}^0$ is globally asymptotically stable in its feasible region if $\mathcal{R}_0^{(\sigma)} < 1$.

4.2.8 Existence of HIV/AIDS Endemic Equilibrium Point

Theorem 4.8 *When $\mathcal{R}_0^{(\sigma)} > 1$, the HIV/AIDS model (4.3) has a unique HIV endemic equilibrium point, $\mathcal{E}^* = (S^*, P^*, E^*, I^*, R^*, A^*)$.*

Where

$$S^\star = \frac{\Lambda + \epsilon P^\star}{\lambda^\star + \mu + \eta},\ P^\star = \frac{\eta S^\star}{\mu + \epsilon},\ E^\star = \frac{\lambda^\star S^\star}{\mu + \delta},\ I^\star = \frac{\delta E^\star}{\mu + \theta_1},$$
$$R^\star = \frac{\phi\gamma\theta_1 I^\star}{\mu + \tau + \theta_2},\ A^\star = \frac{(1-\phi\gamma)\theta_1 I^\star + \theta_2 R^\star}{\mu + d_A}.$$

Proof. The HIV/AIDS endemic equilibrium is the state at which HIV/AIDS remains in the community. To obtain the above relations for $S^*, P^*, E^*, I^*, R^*, A^*$ we solve the system of equation given as

$$\Lambda + \epsilon P^\star - \lambda^\star S^\star - (\mu + \eta)S^\star = 0, \quad \eta S^\star - (\mu + \epsilon)P^\star = 0,$$
$$\lambda^\star S^\star - (\mu + \delta)E^\star = 0, \quad \delta E^\star - (\mu + \theta_1)I^\star = 0,$$
$$\phi\gamma\theta_1 I^\star - (\mu + \tau + \theta_2)R^\star = 0, \quad (1-\phi\gamma)\theta_1 I^\star + \theta_2 R^\star - (\mu + d_A)A^\star = 0,$$

The proof for the existence of the TBEEP follows the same techniques developed in Theorem (3.3) of (Khajanchi et al., 2018) and Theorem 2 of (Aldila et al., 2020).

Theorem 4.9 *The unique positive HIV/AIDS endemic equilibrium $\mathcal{E}^*$ of model (4.3) is locally asymptotically stable if $\mathcal{R}_0^{(\sigma)} > 1$.*

Proof. We linearize system (4.3) near $\mathbf{x}^* = \mathcal{E}^*$ to get:

$$_0^C D_t^\sigma \mathbf{y}(t) = J(\mathbf{x}^*)\mathbf{y}(t) + \mathbf{g}(\mathbf{y}(t)),$$

where $\mathbf{y}(t) = \mathbf{x}(t) - \mathbf{x}^*$, $\mathbf{x} = (S, P, E, I, R, A)$, $J(\mathbf{x}^*)$ denotes the Jacobian matrix at equilibrium, and $\mathbf{g}$ contains higher-order nonlinear terms.

Let λ_i be the eigenvalues of $J(\mathbf{x}^*)$. By Matignon's theorem, the linearized system is locally asymptotically stable if:

$$|\arg(\lambda_i)| > \frac{\sigma\pi}{2}, \quad \text{for all } i = 1, \ldots, 6.$$

Numerical evaluation with parameters from Table (4.2) confirms that this condition holds when $\mathcal{R}_0^{(\sigma)} > 1$.

Theorem 4.10 *The unique positive HIV/AIDS endemic equilibrium $\mathcal{E}^*$ of model (4.3) is globally asymptotically stable if $\mathcal{R}_0^{(\sigma)} > 1$.*

Proof. Similar to that of Theorem (4.7) with $\mathbf{y} = \mathbf{x} - \mathcal{E}^*$.

4.3 Estimation of Model Parameters

This section will estimate some of the biological parameters of model (4.3) using eight years (2016–2023) yearly reported real data of HIV/AIDS-infected cases in

Ethiopia that we obtained from the Ethiopian Federal Ministry of Health. The 'fminunc' OCTAVE/MATLAB Optimization Toolbox is then used to fit the data. Nonetheless, some of the model parameters are assumed, while others are estimated from the literature. The average life expectancy and total population of Ethiopians in 2023 are 67.81 and $N(0) = 126,527$ thousands, respectively (Macrotrends, 2024). Therefore, the reciprocal of the average life expectancy, $\mu = 1/67.81$, is used to determine the natural death rate of individuals. The relation $\frac{\Lambda}{\mu} = N(0)$, yields the recruitment rate of sensitive people (Λ), which is approximately 1265 thousands.

Figure (4.2) displays the estimated fits of the proposed model to the real-data for different values of the fractional order $\sigma = (0.5, 0.6, 0.7, 0.8, 0.9, 1.0)$. One can recognize from this figure that, the estimated curve approaches to the real data as the fractional order tends to decrease. Hence $\sigma = 0.5$ gives the best estimated curve to the real data than others. The values of biological parameters used in numerical simulations are summarized in Table (4.2).

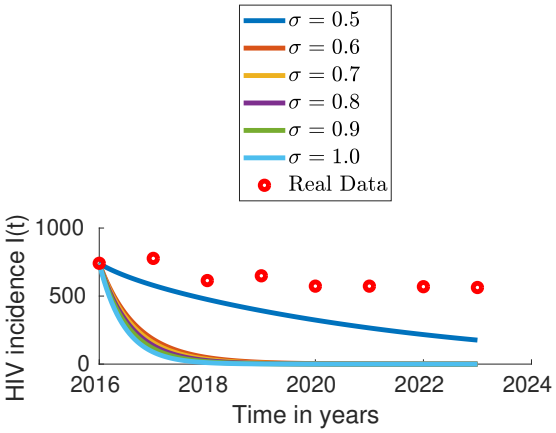

Figure 4.2: Fitting of system (4.3) with respect to Ethiopian HIV incidence data from January, 2016 to December, 2023, where the population is taken in thousands.

4.4 Sensitivity Analysis

In this section, we do sensitivity analysis to evaluate how various factors affect the dynamics of the proposed model. The sensitivity analysis of the reproduction number determines the relative importance of various parameters in reducing illness-induced morbidity and mortality, as well as the effects of parameters that contribute to the prevalence and transmission of disease (Tanvi A., 2021).

Definition 4.2 *If a parameter $\mathcal{Y}$ determines the basic reproduction number $\mathcal{R}_0$ in a differentiable way, then the normalized forward sensitivity index of $\mathcal{R}_0$ with respect to*

$\mathcal{Y}$ *is defined as (Chitnis et al., 2008):*

$$\Upsilon_{\mathcal{Y}}^{\mathcal{R}_0} = \frac{\partial \mathcal{R}_0}{\partial \mathcal{Y}} \frac{\mathcal{Y}}{\mathcal{R}_0} \tag{4.42}$$

Table 4.2: Values of biological parameters used for numerical simulation.

Parameters	Values	Source	Unit
Λ	1265	calculated	pers/yr
β_0	0.2952	fitted	1/(yr×pers)
μ	0.01	calculated	1/yr
η	0.1853	fitted	pers/yr
ϵ	0.0338	fitted	pers/yr
θ_1	9.9917	fitted	1/(yr×pers)
θ_2	1.3861	fitted	1/(yr×pers)
γ	0.12	M. A. Ullah & Raza (2024)	pers/yr
ϕ	0.7711	fitted	1/(yr×pers)
δ	0.03	M. A. Ullah & Raza (2024)	pers/yr
τ	0.02	assumed	1/yr
d_A	0.01	Olaniyi, Kareem, et al. (2024)	1/yr
q	0.5	assumed	-
ρ_1, ρ_2, ρ_3	0.25, 0.35, 0.45	assumed	-

The baseline transmission rate of $\beta_0 = 0.2952$ indicates a significant level of ongoing HIV/AIDS transmission, highlighting the need for effective intervention strategies. Meanwhile, the PrEP initiation rate of $\eta = 0.1853$ reflects a moderate uptake of pre-exposure prophylaxis among at-risk individuals, suggesting potential for improvement in prevention efforts. Together, these rates emphasize the urgency of reducing new infections through enhanced access to and awareness of PrEP, while continuous monitoring is essential to evaluate the effectiveness of public health strategies. The treatment non-adherence rate in the symptomatic infectious class ($\theta_1 = 9.9917$) indicates a significant challenges in managing these populations, with higher non-adherence rates suggesting that the virus can mutate and develop resistance, leading to the transmission of drug-resistant strain. The drug resistance development rate of $\phi = 0.7711$ emphasizes the urgent need for improved adherence strategies and regular monitoring to prevent resistance. These factors contribute to increased morbidity and mortality, complicate public health efforts, and necessitate a focus on developing new treatments and educational initiatives to enhance patient outcomes.

Table (4.3) summarizes the sensitivity indices of model parameters relative to $\mathcal{R}_0$ which are computed using formula (4.42). From this table one can understand that the parameters β_0, ϵ, θ_1, θ_2, γ, ϕ, ρ_1, ρ_2 and ρ_3 have positive indices, while the rest have negative indices. $\mathcal{R}_0$ has a direct relationship with parameters having positive indices meaning that a decrease/increase in these parameters will lead to a decrease/increase

in $\mathcal{R}_0$. On the other way round, $\mathcal{R}_0$ has an inverse relationship with those having negative indices, which means a decrease/increase in these parameters will lead to an increase/decrease in $\mathcal{R}_0$. Although the death rates $\mu,\ \tau,\ d_A$ have negative indices and are inversely proportional with $\mathcal{R}_0$, it is ethically unacceptable to increase the death rates for reducing $\mathcal{R}_0$.

The sensitivity analysis result further justifies that the increase in PrEP initiation rate and detection rate of symptomatic cases will significantly lower $\mathcal{R}_0$. Moreover, $\mathcal{R}_0$ can be reduced by lowering the baseline transmission rate, PrEP discontinuation rate, the treatment non-adherence rates, and the drug resistance development rate. Public health sectors should therefore endeavor to lower the baseline transmission rate, the PrEP discontinuation rate, the treatment non-adherence rates, drug resistance development rate and raise the PrEP initiation rate and detection rate of symptomatic cases. Lastly, by implementing proper prevention and control mechanisms such as increasing awareness about safe sexual practices, ensuring that people living with HIV/AIDS have proper adherence to ART, and providing PrEP to high-risk populations can be used to lower $\mathcal{R}_0$, ultimately decreasing the disease burden.

Table 4.3: Sensitivity indices of $\mathcal{R}_0$ to the parameters.

Parameters	Sensitivity indices	Parameters	Sensitivity indices	Parameters	Sensitivity indices
β_0	1.0000	μ	-0.6122	η	-0.6026
ϵ	0.3903	θ_1	0.0198	ϕ	0.3489
θ_2	0.0662	γ	0.3489	d_A	-0.4079
δ	-0.2400	τ	-0.0437	ρ_3	0.0085
ρ_1	0.1758	ρ_2	0.1801		

4.5 Numerical Simulations and Discussions

Here, we have performed numerical simulations of system (4.3) to support the analytical conclusions of our model using Octave/MATLAB software and the fractional PECE algorithm developed in Diethelm et al. (2004); Diethelm & Freed (1998). With the population measured in thousands, the initial conditions were assumed to be S(0) = 123, 005, P(0)=120, E(0) = 740, I(0) = 563, R(0) = 80, and A(0) = 42. With fitted value of β_0 which is 0.2952, and $\sigma = 0.5$ we see that $\mathcal{R}_0 = 2.2475 > 1$ implying that HIV/AIDS remains endemic in the community. By reducing $\beta_0 = 0.0452$, while fixing the values of other parameters as in Table (4.2), we observe that $\mathcal{R}_0 = 0.8795 < 1$. In this case, HIV/AIDS will die out of the community in the long run and the disease free equilibrium $\mathcal{E}^0 = (141.3326, 214.3358, 0, 0, 0, 0)$ will come to existence.

Figure (4.3) shows the local asymptotic stability of $\mathcal{E}^0$ for different values of $\sigma \in$

$\{0.3, 0.5, 0.8, 1.0\}$. Numerical computations confirm that for each σ, all eigenvalues $\lambda_i < 0$ for each i. The Matignon's fractional linear stability criterion has been satisfied even for $\sigma = 0.8, 1.0$ for which $\mathcal{R}_0^{(0.8)} = 1.1974$, $\mathcal{R}_0^{(1.0)} = 1.4388$ are greater than unity. For smaller σ values, we observe slow dynamics with higher convergence time. Furthermore, we see that $\mathcal{R}_0$ decreases with σ, with smaller σ (long-memory) representing sustained preventive behaviors and long-term immunity effects. These figures also show how crucial the Caputo fractional order model is for correctly describing the dynamics of HIV/AIDS transmission. Because memory effects are incorporated into the system, its long-term behavior is significantly influenced by the disease's past exposure as the order of the derivative takes smaller fractional values. The Caputo operator can well characterize the dynamics of the system because of its slow dynamics and great stability. Therefore, taking memory effects into consideration, a Caputo derivative can be used to assist in the development of efficient preventative and control methods.

More interestingly, as shown in Figures (4.4a)-(4.4d), we provide strong numerical evidence for the global asymptotic stability of equilibrium point $\mathcal{E}^0$. The phase portrait of model (4.3) is shown in Figure (4.4a), showing susceptible (S) versus asymptomatic infectious (E). In this case, S and E both converge to $\mathcal{E}^0$, the disease-free equilibrium point. Likewise, Figures (4.4b)–(4.4d) show how the vector fields of state variables converge to the corresponding components of the equilibrium point $\mathcal{E}^0$. The graphs in Figures (4.5)-(4.7) illustrate how different parameter values affect the size of different disease compartments using the values of model parameters from Table (4.2).

4.5.1 The effect of PrEP initiation rate η

This subsection looks at how increasing the initiation rates of PrEP affects the number of people in S and P compartments. The number of people in S(t), P(t) classes significantly increases as the PrEP initiation rate rises, as seen in Figures (4.5a and (4.5b) with $\sigma = 0.5$. P(t) increases from 106,800 to 380,000 and S(t) increases from 86,670 to 281,000 with a 50% increase in η.

4.5.2 The effect of PrEP discontinuation rate ϵ

The objective of this subsection is to investigate the impact of decreasing the PrEP discontinuation rate on size of S and P compartments. Figures (4.5c) and (4.5d) demonstrate that, for $\sigma = 0.5$, a considerable increase in the number of individuals in S(t), P(t) classes occurs when the PrEP discontinuation rate is decreased. Particularly, S(t) increases from 86,670 to 157,700 and P(t) increases from 106,800 to 213,100 when ϵ decreases by 50%.

The rise in the number of susceptibles is driven by several factors. First, the widespread adoption of PrEP significantly reduces the overall transmission rates of HIV among high-risk populations. This decrease in new infections allows more individuals to remain uninfected and thus susceptible to the virus. Second, individuals using PrEP may engage in riskier sexual behaviors, such as having unprotected sex, under the assumption that they are well-protected against HIV. This behavioral shift can inadvertently increase the pool of susceptibles, as these individuals may still be vulnerable to HIV or other sexually transmitted infections (Abbas et al., 2011).

Additionally, the increasing availability of PrEP often correlates with heightened public awareness and testing initiatives, leading to more individuals recognizing their susceptibility to HIV. This can result in a greater number of people being identified as at risk. Furthermore, as the general population grows and access to PrEP expands, previously untested individuals may be diagnosed as susceptible, adding to the overall count. Lastly, effective retention in care for those on PrEP ensures ongoing monitoring of their risk status, which can keep them engaged in preventive health measures. Collectively, these factors illustrate how rising PrEP initiation rates can lead to an increase in the number of susceptibles in HIV/AIDS models (Heads et al., 2024).

4.5.3 The effect of non-adherence rate of ART treatment θ_1 in symptomatic compartment

This section aims to assess the effect of reducing the non-adherence rate of ART, θ_1 for people in the symptomatic class. Figures (4.6a) and (4.6b) show that, for $\sigma = 0.5$, lowering the ART non-adherence rate results in a significant rise in the number of persons in I(t) and a decrease in the number of individuals in R(t). Specifically, when θ_1 drops by 50%, I(t) rises from 22.29 to 33.02 while R(t) falls from 13.37 to 12.71.

The ART non-adherence rate may yield to a rise in the number of people in the symptomatic infectious compartment for several reasons. When ART non-adherence rates are lower, more people are successfully lowering their viral load. But if ART doesn't completely eradicate the virus, some people can still have detectable viral levels, which over time could result in symptoms. People may live longer even if they have some residual viral activity if HIV is better managed with less non-adherence to ART. Because they may not develop the disease to its most severe stages as rapidly, this can result in a rise in the symptomatic infectious population (Baggaley et al., 2006).

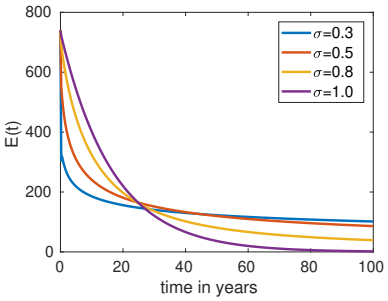

(a) Asymptomatic infectious class

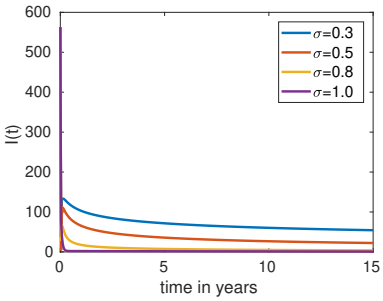

(b) Symptomatic infectious class

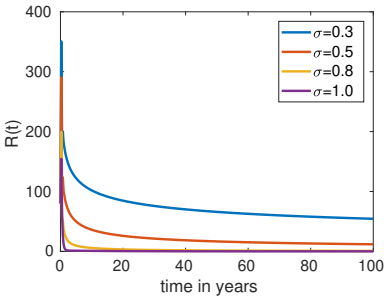

(c) Drug-resistant class

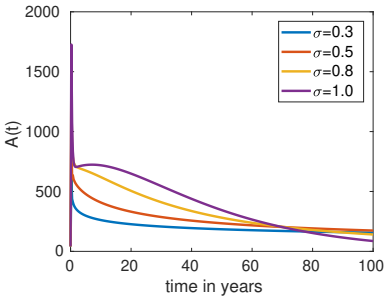

(d) AIDS class

Figure 4.3: Plots confirming local asymptotic stability of $\mathcal{E}^0$ for different values of σ.

4.5.4 The effect of ART non-adherence rate θ_2 in drug-resistant compartment

Investigating the effects of lowering the ART non-adherence rate in drug-resistant compartments is the aim of this subsection. Figures (4.7a) and (4.7b) reveal that, for $\sigma = 0.5$, lowering the ART non-adherence rate results in a significant rise in the number of persons in R(t) and a decrease in the number of individuals in A(t). More specifically, when θ_2 drops by 50%, R(t) rises from 13.37 to 17.4 while A(t) drops from 228.8 to 224.

In mathematical modeling of HIV/AIDS, particularly when considering a drug-resistant compartment, a decrease in the ART non-adherence rate can lead to an increase in the number of individuals in the drug-resistant compartment while simultaneously decreasing those in the AIDS compartment. This occurs because effective adherence to ART reduces the progression to AIDS, allowing individuals to maintain their health longer. However, if ART does not completely suppress the virus, individuals may still harbor drug-resistant strains, contributing to the drug-resistant compartment. Additionally, as individuals live longer with chronic HIV, they may remain in the drug-resistant compartment if they develop resistance due to incomplete viral suppression or poor adherence to treatment. This dynamic illustrates the complex interplay between efficacy of treatment adherence, viral resistance, and disease

progression in HIV/AIDS modeling (M. Khan et al., 2025).

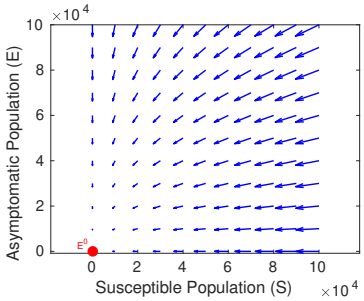

(a) Phase portrait plot considering susceptible vs asymptomatic infectious people

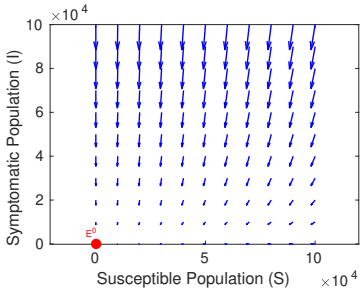

(b) Phase portrait plot considering susceptible vs symptomatic infectious population

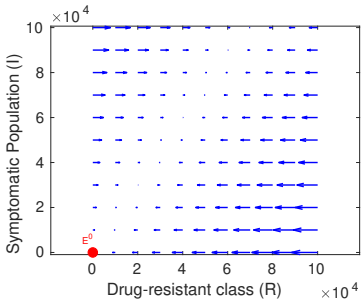

(c) Phase portrait plot considering symptomatic infectious vs drug-resistant class

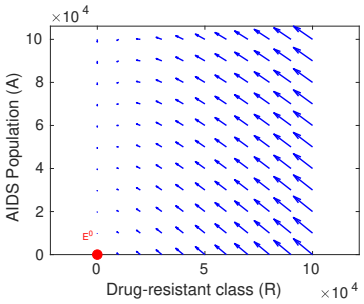

(d) Phase portrait plot considering drug-resistant vs AIDS class

Figure 4.4: Phase portrait plot displaying the global asymptomatic stability of the HIV/AIDS free equilibrium $\mathcal{E}^0$ of model (4.3) when $\sigma = 0.5$.

In this chapter, we developed and analyzed an HIV/AIDS transmission dynamics incorporating PrEP and drug-resistant compartments using a Caputo fractional-order model that takes into account the memory effects and hereditary factors inherent in the progression and treatment history of the disease. The analytical finding shows that the HIV/AIDS-free equilibrium is locally asymptotically stable if all the eigenvalues of a linearized matrix satisfy the Matignon's stability criterion. Sensitivity analysis result suggests that lowering β_0, $\epsilon, \theta_1, \theta_2, \phi$, and increasing η, δ, significantly lower the infection prevalence of HIV/AIDS disease. The simulation results also demonstrate that by taking memory effects into account, a Caputo fractional-order provides a deeper understanding of the disease and aids to implement effective management and prevention strategies.

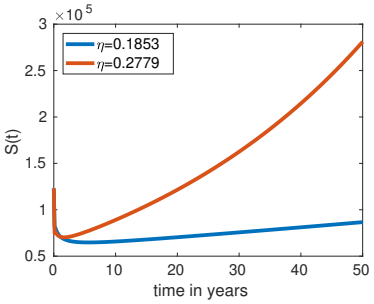

(a) Effect of varying η on $S(t)$

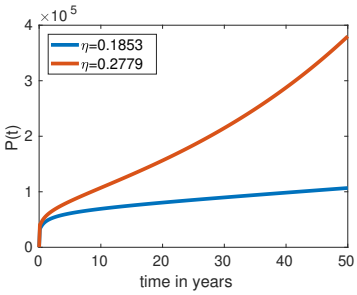

(b) Effect of varying η on $P(t)$

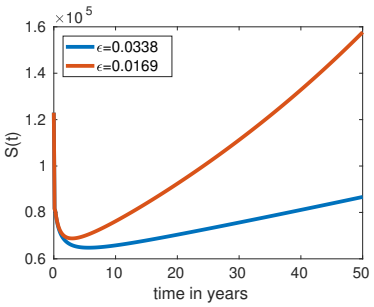

(c) Effect of varying ϵ on $S(t)$

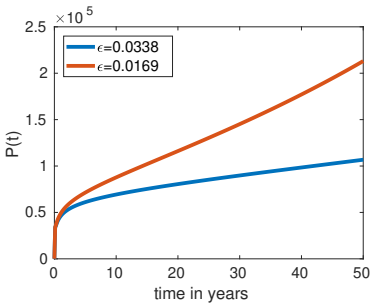

(d) Effect of varying ϵ on $P(t)$

Figure 4.5: Graphs illustrating the effect of varying η, ϵ on $S(t)$ and $P(t)$.

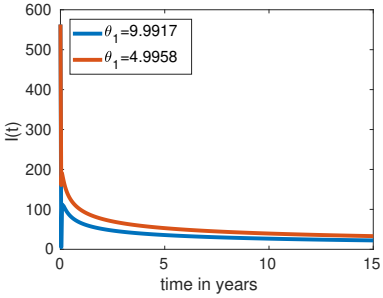

(a) Effect of varying θ_1 on $I(t)$

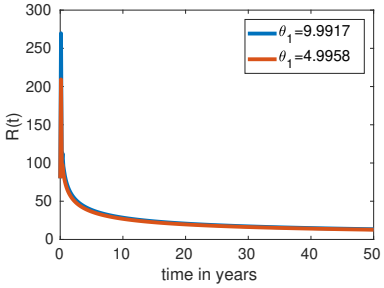

(b) Effect of varying θ_1 on $R(t)$

Figure 4.6: Graphs illustrating the effect of varying θ_1 on $I(t)$ and $R(t)$.

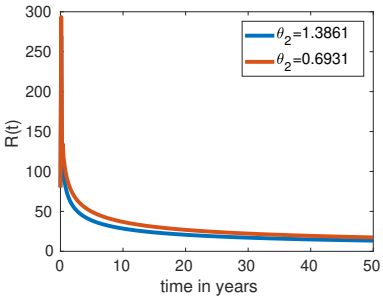

(a) Effect of varying θ_2 on $R(t)$

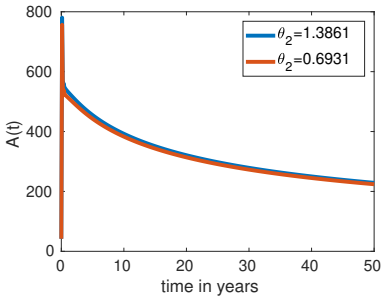

(b) Effect of varying θ_2 on $A(t)$

Figure 4.7: Graphs illustrating the effect of varying θ_2 on $R(t)$ and $A(t)$.

CHAPTER 5

FRACTIONAL-ORDER MODELING OF TB WITH VACCINATION AND DOUBLE TREATMENT MODALITIES

This chapter examines a Caputo approach mathematical model of TB transmission dynamics that considers vaccination and two lines of treatment modalities. Both mathematical and epidemiological well-posedness of the model have been verified. The stability of the model equilibria are carried out. Furthermore, the numerical simulations of the model has been performed to assist the analytical results.

5.1 Model Formulation

In order to examine the effects of vaccination and two lines of treatment modalities on the dynamics of disease transmission, this section discusses the development of a mathematical model for TB using the Caputo fractional approach. Therefore, we divide the human population under investigation into seven mutually exclusive compartments based on the epidemiological status of the disease: Susceptible people $S(t)$ are healthy now but could get TB in the future, vaccinated people $V(t)$ are people who have been vaccinated against TB infections, exposed people $E(t)$ are people who have TB but do not show any symptoms and are not infectious, active TB infected people $I(t)$ are people who have active TB infections and show all symptoms of the disease, patients receiving first-line TB treatment $X(t)$, those receiving second-line TB treatment or care for patients with multidrug-resistant strain $Y(t)$, and recovered individuals $R(t)$ who have fully recovered from the disease and have temporary immunity. Thus, the total human population at a time t is given by

$$N(t) = S(t) + V(t) + E(t) + I(t) + X(t) + Y(t) + R(t).$$

To formulate our mathematical model, we take into considerations the following basic assumptions:

i) the recruitment rate Λ into susceptible class is assumed to be by immigration or by birth.

ii) the population is not constant and it is assumed to be large. Therefore, TB incidence is determined by the law of a standard incidence.

iii) A force of infection, defined by $\lambda = \beta\left(\frac{I}{N} + \gamma_1\frac{X}{N} + \gamma_2\frac{Y}{N}\right)$, infects susceptible individuals when they come into contact with those who belong to the infectious compartments I, X, and Y. The probability of an infection resulting from an effective contact between susceptible and infectious individuals is represented by β. The modification parameters $\gamma_1, \gamma_2 \in (0, 1)$, which show an increase or reduction in the relative infectiousness of people in the X and Y compartments, respectively, in comparison to those in the I compartment, account for the assumed variability (Aggarwal et al., 2021).

iv) The infection rate among vaccinated individuals is reduced to $(1-p)\eta_1$, where $p \in (0, 1)$ indicates the vaccine efficacy and η_1 is the per capita rate of being infectious. We assume that susceptible individuals are vaccinated at a rate φ and that the TB vaccine provides partial immunity (S. Ullah, Ullah, et al., 2020). Due to the vaccine's flaws, vaccinated people may contract the disease from people in the I, X, and Y compartments when they come into contact with them with the force of infection given by $\tau = \beta(1-p)\eta_1\left(\frac{I}{N} + \gamma_1\frac{X}{N} + \gamma_2\frac{Y}{N}\right)$.

v) We also assume that some proportion of vaccinated individuals return to the susceptible compartment as their immunity wanes at a rate $p\eta_1$.

vi) Since the bacteria will remain in the body system, it is also expected that a certain fraction of people in the first-line treatment compartment will move to the exposed compartment at a rate $(1-q)\eta_2$. The remaining $q\eta_2$ will move to active TB compartment due to treatment failure. In this case, q is the treatment failure rate, and η_2 is the movement rate of patients in the first-line treatment compartment (Oshinubi et al., 2023).

vii) We assume homogeneous mixing of the population, which may affect the epidemiological or biological aspects of our model, especially in fractional-order settings.

Following the onset of TB symptoms, exposed individuals join the active TB compartment and become actively infected at a rate α. In order to get first-line treatment at

a rate θ, active TB patients enter the first-line treatment compartment. To determine whether they contracted a drug-resistant or drug-susceptible strain of tuberculosis, individuals in first-line treatment compartment will undergo screening. After successfully finishing the first-line treatment, those with drug-susceptible strains will join the recovered compartment at a rate ν_1. To get second-line treatment at a rate ω, individuals detected with drug-resistant strains are enrolled in the second-line treatment compartment. At a rate ν_2, people who have recovered from drug-resistant TB strains join the recovered compartment.

After losing immunity at rate ϕ, recovered individuals may return to the susceptible compartment. A natural death rate μ applies to all classes. However, the disease-induced death rates for patients in the active TB, first-line treatment and second-line treatment compartments becomes ξ_1, ξ_2, and ξ_3 respectively.

The flow diagram of the model is illustrated in Figure (5.1).

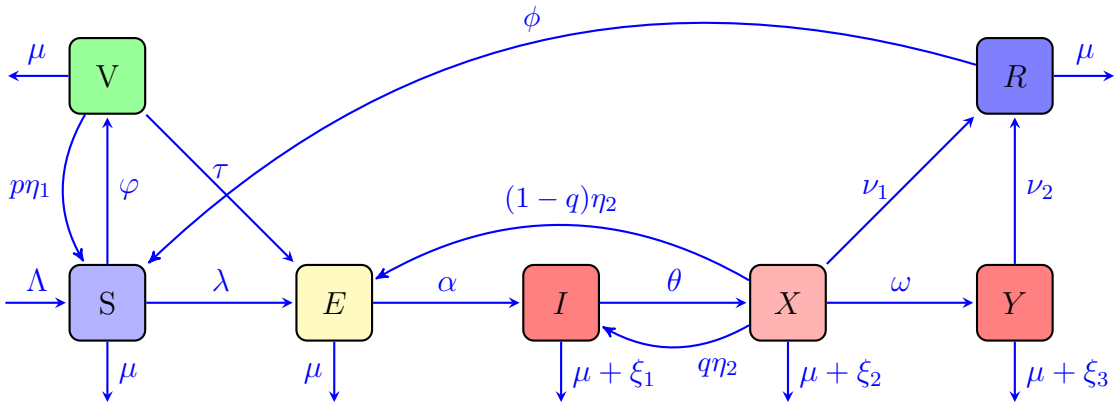

Figure 5.1: Schematic Diagram of TB Model

By taking into account the interaction between disease compartments and the above model assumptions, we formulate the governing system of nonlinear integer-order ordinary differential equations as follows:

$$
\begin{cases}
\frac{dS}{dt} = \Lambda + p\eta_1 V + \phi R - \frac{\beta(I+\gamma_1 X+\gamma_2 Y)}{N} S - (\varphi+\mu)S \ , \\
\frac{dV}{dt} = \varphi S - \frac{\beta(1-p)\eta_1(I+\gamma_1 X+\gamma_2 Y)}{N} V - (p\eta_1+\mu)V \ , \\
\frac{dE}{dt} = \frac{\beta(I+\gamma_1 X+\gamma_2 Y)}{N} S + \frac{\beta(1-p)\eta_1(I+\gamma_1 X+\gamma_2 Y)}{N} V + (1-q)\eta_2 X - (\alpha+\mu)E \ , \\
\frac{dI}{dt} = \alpha E + q\eta_2 X - (\theta+\mu+\xi_1)I \ , \\
\frac{dX}{dt} = \theta I - (\omega+\mu+\nu_1+\eta_2+\xi_2)X \ , \\
\frac{dY}{dt} = \omega X - (\mu+\nu_2+\xi_3)Y \ , \\
\frac{dR}{dt} = \nu_1 X + \nu_2 Y - (\phi+\mu)R \ , \quad 0 < \psi \leq 1,
\end{cases}
\tag{5.1}
$$

with the initial conditions given as

$$S(0) = S_0 \geq 0\ ,\ V(0) = V_0 \geq 0\ , E(0) = E_0 > 0\ ,\ I(0) = I_0 > 0\ ,$$
$$X(0) = X_0 > 0\ , Y(0) = Y_0 > 0\ \ R(0) = R_0 \geq 0. \tag{5.2}$$

A Caputo fractional-order models incorporate memory effects, capturing the long-term dependencies and non-local behaviors that are characteristic of TB transmission, particularly due to its latent period and the influence of past exposures on current dynamics. Furthermore, fractional derivatives allow for a more realistic representation of biological phenomena, as they can model hereditary effects that significantly impact disease progression and control strategies. This approach enhances the model's flexibility, making it better suited to reflect the complexities of TB transmission dynamics (Bhatter et al., 2025; Agbata et al., 2025). With this motivation, we extend an integer-order TB model (5.1) to a Caputo fractional-order system

$$\begin{cases} {}_0^C D_t^{\psi} S(t) = \Lambda + p\eta_1 V + \phi R - \frac{\beta(I+\gamma_1 X+\gamma_2 Y)}{N} S - (\varphi+\mu)S\ , \\ {}_0^C D_t^{\psi} V(t) = \varphi S - \frac{\beta(1-p)\eta_1(I+\gamma_1 X+\gamma_2 Y)}{N} V - (p\eta_1+\mu)V\ , \\ {}_0^C D_t^{\psi} E(t) = \frac{\beta(I+\gamma_1 X+\gamma_2 Y)}{N} S + \frac{\beta(1-p)\eta_1(I+\gamma_1 X+\gamma_2 Y)}{N} V + (1-q)\eta_2 X - (\alpha+\mu)E\ , \\ {}_0^C D_t^{\psi} I(t) = \alpha E + q\eta_2 X - (\theta+\mu+\xi_1)I\ , \\ {}_0^C D_t^{\psi} X(t) = \theta I - (\omega+\mu+\nu_1+\eta_2+\xi_2)X\ , \\ {}_0^C D_t^{\psi} Y(t) = \omega X - (\mu+\nu_2+\xi_3)Y\ , \\ {}_0^C D_t^{\psi} R(t) = \nu_1 X + \nu_2 Y - (\phi+\mu)R\ , \quad 0 < \psi \leq 1, \end{cases} \tag{5.3}$$

with its initial conditions given as in (5.2).

Remark 5.1 *System (5.3) has an appropriate time dimensions since both its left and right hand sides have time dimension of $t^{-\psi}$. Each model parameters are assumed to be non-negative and they depend on ψ (Dokoumetzidis et al., 2010; Almeida, 2018).*

Table 5.1: Description of model parameters

Parameters	Descriptions
Λ	constant recruitment rate
β	effective contact rate
μ	natural death rate
ξ_1	disease induced death rate of individuals in I class
ξ_2	disease induced death rate of individuals in X class
ξ_3	disease induced death rate of individuals in Y class
φ	vaccination rate
p	efficacy of vaccine
ϕ	rate of losing immunity
q	treatment failure rate
ν_1	recovery rate of individuals in X class
ν_2	recovery rate of individuals in Y class
α	progression rate of individuals from L class to I class
θ	treatment adherence rate for X class
ω	treatment adherence rate for Y class
η_1	per capita rate of being infectious
η_2	movement rate of individuals in X class
γ_1, γ_2	modification parameters

5.2 Model Analysis

The fundamental properties of model (5.3) including its boundedness and non-negativity, existence and uniqueness of the solutions, equilibrium points, the basic reproduction number, and both local and global stabilities of the disease-free equilibrium point will be examined in this section.

5.2.1 Non-negativity and Boundedness of the Solution

Theorem 5.1 *For all $t \geq 0$, all the solution components $S(t), V(t), E(t), I(t), X(t), Y(t)$ and $R(t)$ of system (5.3) are non-negative and bounded. Furthermore, the closed region*

$$\Theta = \left\{ (S, V, E, I, X, Y, R) \in \mathbb{R}_+^7 : 0 < N \leq \frac{\Lambda}{\mu} \right\}$$

is positively invariant.

Proof. Applying the same approaches used in subsection (4.2.1) we observe that;

$$ {}_0^C D_t^{\psi} S(t)|_{S=0} = \Lambda + p\eta_1 V + \phi R \geq 0, \quad {}_0^C D_t^{\psi} V(t)|_{V=0} = \varphi S \geq 0 \ , $$

$${}_0^C D_t^{\psi} E(t)|_{E=0} = \lambda S + \tau V + (1-q)\eta_2 X \geq 0 \ , \quad {}_0^C D_t^{\psi} I(t)|_{I=0} = \alpha E + q\eta_2 X \geq 0 \ ,$$

$${}_0^C D_t^{\psi} X(t)|_{X=0} = \theta I \geq 0 \ , \quad {}_0^C D_t^{\psi} Y(t)|_{Y=0} = \omega X \geq 0 \ , \quad {}_0^C D_t^{\psi} R(t)|_{R=0} = \nu_1 X + \nu_2 Y \geq 0.$$

Consequently, on each hyperplane, the vector field $\mathcal{X} = (S(t), V(t), E(t), I(t), X(t), Y(t), R(t))^T$ points into $\mathbb{R}_+^7$. We therefore deduce that all of the solution components of system (5.3) are non-negative based on this fact and the fact that all of the initial conditions in (5.2) are non-negative.

Hence, every solution that starts in $\mathbb{R}_+^7$ remains in $\mathbb{R}_+^7$ and based on this we conclude that the closed region

$$\Theta = \left\{ (S, V, E, I, X, Y, R) \in \mathbb{R}_+^7 : 0 < N \leq \frac{\Lambda}{\mu} \right\}$$

is positively invariant.

Now, to show the boundedness we add all the equations in (5.3) to get:

$${}_0^C D_t^{\psi} N(t) + \mu N(t) \leq \Lambda. \tag{5.4}$$

Applying the Laplace transform on both sides of the inequality (5.4) we have,

$$\mathcal{L}\{{}_0^C D_t^{\psi} N(t)\} + \mu \mathcal{L}\{N(t)\} \leq \Lambda \mathcal{L}\{1\} \ ,$$

$$s^{\psi} N(s) - \sum_{k=0}^{n-1} s^{\psi-k-1} N^{(k)}(0) + \mu N(s) \leq \Lambda \frac{1}{s}. \tag{5.5}$$

Since $0 < \psi \leq 1$, we have $n = 1$ and inequality (5.5) becomes $s^{\psi} N(s) - s^{\psi-1} N(0) + \mu N(s) \leq \Lambda \frac{1}{s}$, implying that $(s^{\psi} + \mu) N(s) \leq \Lambda s^{-1} + N_0 s^{\psi-1}$, and this gives us

$$N(s) \leq \Lambda \frac{s^{-1}}{s^{\psi} + \mu} + N_0 \frac{s^{\psi-1}}{s^{\psi} + \mu}. \tag{5.6}$$

Now, taking the inverse Laplace transform on both sides the inequality (5.6) we get;

$$N(t) \leq \Lambda \mathcal{L}^{-1}\{\frac{s^{-1}}{s^{\psi} + \mu}\} + N_0 \mathcal{L}^{-1}\{\frac{s^{\psi-1}}{s^{\psi} + \mu}\}. \tag{5.7}$$

Using the relation,

$$\mathcal{L}^{-1}\{\frac{s^{\alpha-\beta}}{s^{\alpha} - \lambda}\} = t^{\beta-1} E_{\alpha,\beta}(\lambda t^{\alpha})$$

and comparing its exponents with that of inequality (5.7) we get $\beta = \alpha + 1$ for the first term, $\beta = 1, \alpha = \psi$ for the second term and $\lambda = -\mu$.

Accordingly we have,

$$\begin{aligned} N(t) &\leq \Lambda t^{\psi+1-1} E_{\psi,\psi+1}(-\mu t^{\psi}) + N_0 t^{1-1} E_{\psi,1}(-\mu t^{\psi}) \ , \\ &= \Lambda t^{\psi} E_{\psi,\psi+1}(-\mu t^{\psi}) + N_0 E_{\psi,1}(-\mu t^{\psi}). \end{aligned} \tag{5.8}$$

From the properties of Mittag-Leffler function,

$$\begin{aligned} E_{c,d}(z) &= z E_{c,c+d}(z) + \frac{1}{\Gamma(d)} \ , \\ E_{c,c+d}(z) &= \frac{1}{z}\left(E_{c,d}(z) - \frac{1}{\Gamma(d)} \right) \ , \end{aligned} \tag{5.9}$$

substituting $c = \psi$, $d = 1$ and $z = -\mu t^{\psi}$ in equation (5.9) we get,

$$\begin{aligned} E_{\psi,\psi+1}(-\mu t^{\psi}) &= \frac{1}{-\mu t^{\psi}} \left(E_{\psi,1}(-\mu t^{\psi}) - \frac{1}{\Gamma(1)} \right) \\ &= \frac{1}{-\mu t^{\psi}} \left(E_{\psi,1}(-\mu t^{\psi}) - 1 \right) \ , \ \Gamma(1) = 1 \end{aligned} \tag{5.10}$$

Using (5.10) in (5.8) we get,

$$\begin{aligned} N(t) &\leq \Lambda t^{\psi} E_{\psi,\psi+1}(-\mu t^{\psi}) + N_0 E_{\psi,1}(-\mu t^{\psi}) \\ = \left(\Lambda t^{\psi}\right) &\left(\frac{1}{-\mu t^{\psi}} \right) \left(E_{\psi,1}(-\mu t^{\psi}) - 1 \right) + N_0 E_{\psi,1}(-\mu t^{\psi}) \\ &= N_0 E_{\psi,1}(-\mu t^{\psi}) - \frac{\Lambda}{\mu} E_{\psi,1}(-\mu t^{\psi}) + \frac{\Lambda}{\mu} \\ &= \left(N_0 - \frac{\Lambda}{\mu} \right) E_{\psi,1}(-\mu t^{\psi}) + \frac{\Lambda}{\mu}. \end{aligned} \tag{5.11}$$

Thus, if $N_0 \leq \frac{\Lambda}{\mu}$, then

$$\limsup_{t \to \infty} (N(t)) \leq \frac{\Lambda}{\mu}.$$

Therefore, $N(t)$ is bounded from above by $\frac{\Lambda}{\mu}$ and this in turn implies the boundedness of all solution components.

By guaranteeing that human populations cannot contain negative individuals, non-negativity in a model solution accurately captures the dynamics of disease dissemination. Model parameters are easier to understand when the solutions are non-negative. Boundedness enables more realistic long-term forecasts but may also misrepresent outcomes like extinction or stable endemic states, when the model admits infinite growth or decay.

5.2.2 Existence and Uniqueness of the Solution

Under this subsection we establish the existence and uniqueness of the solution of the dynamical system (5.3). Hence, let us rewrite model (5.3) as

$$\begin{cases} {}_0^C D_t^{\psi} S(t) = \mathcal{H}_1(t,S) \ , \quad {}_0^C D_t^{\psi} V(t) = \mathcal{H}_2(t,V) \ , \\ {}_0^C D_t^{\psi} E(t) = \mathcal{H}_3(t,E) \ , \quad {}_0^C D_t^{\psi} I(t) = \mathcal{H}_4(t,I) \ , \\ {}_0^C D_t^{\psi} X(t) = \mathcal{H}_5(t,X) \ , \quad {}_0^C D_t^{\psi} Y(t) = \mathcal{H}_6(t,Y), \\ {}_0^C D_t^{\psi} R(t) = \mathcal{H}_7(t,R), \end{cases} \tag{5.12}$$

with the initial conditions given as in (5.2).
Where;

$$\begin{aligned} \mathcal{H}_1(t,S) &= \Lambda + p\eta_1 V + \phi R - \frac{\beta\left(I+\gamma_1 X+\gamma_2 Y\right)}{N} S - (\varphi+\mu)S \ , \\ \mathcal{H}_2(t,V) &= \varphi S - \frac{\beta(1-p)\eta_1\left(I+\gamma_1 X+\gamma_2 Y\right)}{N} V - (p\eta_1+\mu)V \ , \\ \mathcal{H}_3(t,E) &= \frac{\beta\left(I+\gamma_1 X+\gamma_2 Y\right)}{N} S + \frac{\beta(1-p)\eta_1\left(I+\gamma_1 X+\gamma_2 Y\right)}{N} V \\ &+ (1-q)\eta_2 X - (\alpha+\mu)E \ , \\ \mathcal{H}_4(t,I) &= \alpha E + q\eta_2 X - (\theta+\mu+\xi_1)I \ , \\ \mathcal{H}_5(t,X) &= \theta I - (\omega+\mu+\nu_1+\eta_2+\xi_2)X \ , \\ \mathcal{H}_6(t,Y) &= \omega X - (\mu+\nu_2+\xi_3)Y \ , \\ \mathcal{H}_7(t,R) &= \nu_1 X + \nu_2 Y - (\phi+\mu)R. \end{aligned} \tag{5.13}$$

Taking integral transform on both sides of equation (5.12) we have

$$\begin{aligned} S(t) &= S_0 + \frac{1}{\Gamma(\psi)}\int_0^t (t-\tau)^{\psi-1}\mathcal{H}_1(\tau,S(\tau))d\tau, \\ V(t) &= V_0 + \frac{1}{\Gamma(\psi)}\int_0^t (t-\tau)^{\psi-1}\mathcal{H}_2(\tau,V(\tau))d\tau, \\ E(t) &= E_0 + \frac{1}{\Gamma(\psi)}\int_0^t (t-\tau)^{\psi-1}\mathcal{H}_3(\tau,E(\tau))d\tau, \\ I(t) &= I_0 + \frac{1}{\Gamma(\psi)}\int_0^t (t-\tau)^{\psi-1}\mathcal{H}_4(\tau,I(\tau))d\tau, \\ X(t) &= X_0 + \frac{1}{\Gamma(\psi)}\int_0^t (t-\tau)^{\psi-1}\mathcal{H}_5(\tau,X(\tau))d\tau, \\ Y(t) &= Y_0 + \frac{1}{\Gamma(\psi)}\int_0^t (t-\tau)^{\psi-1}\mathcal{H}_6(\tau,Y(\tau))d\tau, \\ R(t) &= R_0 + \frac{1}{\Gamma(\psi)}\int_0^t (t-\tau)^{\psi-1}\mathcal{H}_7(\tau,R(\tau))d\tau. \end{aligned} \tag{5.14}$$

Lemma 5.1 *For each $j = 1, 2, \cdots, 7$, the kernels $\mathcal{H}_j$ are lipschitz with corresponding lipschitz constants K_j and they are contractions provided that $0 < K_j < 1$; where, $K_1 = b_1 + \varphi + \mu$, $K_2 = b_2 + p\eta_1 + \mu$, $K_3 = \alpha + \mu$, $K_4 = \theta + \mu + \xi_1$, $K_5 = \omega + \mu + \nu_1 + \eta_2 + \xi_2$, $K_6 = \mu + \xi_3 + \nu_2$, $K_7 = \phi + \mu$, and $\lambda(t) \leq b_1$, $\tau(t) \leq b_2$ are bounded functions.*

Proof. In similar way to Lemma (4.1), for S and S_1, we have $||\mathcal{H}_1(t, S) - \mathcal{H}_1(t, S_1)|| = || - (\lambda(t) + \varphi + \mu)(S - S_1)|| \leq (||\lambda(t)|| + \varphi + \mu)||S - S_1||$ $= K_1||S - S_1||$, with $K_1 = b_1 + \varphi + \mu$. Thus, the kernel $\mathcal{H}_1$ is Lipschitz with a Lipschitz constant K_1 and it is contraction provided that $0 < K_1 < 1$. Similarly for V and V_1, $||\mathcal{H}_2(t, V) - \mathcal{H}_2(t, V_1)|| = || - (\tau(t) + p\eta_1 + \mu)(V - V_1)|| \leq (||\tau(t)|| + p\eta_1 + \mu)||V - V_1||$ $= K_2||V - V_1||$, with $K_2 = b_2 + p\eta_1 + \mu$. Hence, the kernel $\mathcal{H}_2$ is Lipschitz with a Lipschitz constant K_2 and it is contraction provided that $0 < K_2 < 1$. With the same techniques we can show that the kernels $\mathcal{H}_3$, $\mathcal{H}_4$, $\mathcal{H}_5$, $\mathcal{H}_6$, and $\mathcal{H}_7$ are lipschtiz and contraction.

Theorem 5.2 *System (5.3) subject to the initial conditions (5.2) has at least one solution provided that $\frac{t^\psi K_w}{\Gamma(\psi+1)} < 1$ for each $w = 1, 2, \cdots, 7$.*

Proof. Similar to Theorem (4.2), let us define the following recursive patterns:

$$\begin{aligned}
\Psi_{1n}(t) = S_n(t) - S_{n-1}(t) &= \frac{1}{\Gamma(\psi)} \int_0^t (\mathcal{H}_1(\tau, S_{n-1}) - \mathcal{H}_1(\tau, S_{n-2}))(t-\tau)^{\psi-1} d\tau \ , \\
\Psi_{2n}(t) = V_n(t) - V_{n-1}(t) &= \frac{1}{\Gamma(\psi)} \int_0^t (\mathcal{H}_2(\tau, V_{n-1}) - \mathcal{H}_2(\tau, V_{n-2}))(t-\tau)^{\psi-1} d\tau \ , \\
\Psi_{3n}(t) = E_n(t) - E_{n-1}(t) &= \frac{1}{\Gamma(\psi)} \int_0^t (\mathcal{H}_3(\tau, E_{n-1}) - \mathcal{H}_3(\tau, E_{n-2}))(t-\tau)^{\psi-1} d\tau \ , \\
\Psi_{4n}(t) = I_n(t) - I_{n-1}(t) &= \frac{1}{\Gamma(\psi)} \int_0^t (\mathcal{H}_4(\tau, I_{n-1}) - \mathcal{H}_4(\tau, I_{n-2}))(t-\tau)^{\psi-1} d\tau \ , \\
\Psi_{5n}(t) = X_n(t) - X_{n-1}(t) &= \frac{1}{\Gamma(\psi)} \int_0^t (\mathcal{H}_5(\tau, X_{n-1}) - \mathcal{H}_5(\tau, X_{n-2}))(t-\tau)^{\psi-1} d\tau \ , \\
\Psi_{6n}(t) = Y_n(t) - Y_{n-1}(t) &= \frac{1}{\Gamma(\psi)} \int_0^t (\mathcal{H}_6(\tau, Y_{n-1}) - \mathcal{H}_6(\tau, Y_{n-2}))(t-\tau)^{\psi-1} d\tau \ , \\
\Psi_{7n}(t) = R_n(t) - R_{n-1}(t) &= \frac{1}{\Gamma(\psi)} \int_0^t (\mathcal{H}_7(\tau, R_{n-1}) - \mathcal{H}_7(\tau, R_{n-2}))(t-\tau)^{\psi-1} d\tau \ ,
\end{aligned} \tag{5.15}$$

with the initial conditions as in equation (5.2). Now, applying the lipschitz condition from Lemma (5.1) and after some algebraic manipulations we have,

$$\begin{aligned}
||S_n(t) - S_{n-1}(t))|| &\leq ||S_n(0)|| \left(\frac{t^\psi K_1}{\Gamma(\psi)}\right)^n, \\
||V_n(t) - V_{n-1}(t))|| &\leq ||V_n(0)|| \left(\frac{t^\psi K_2}{\Gamma(\psi+1)}\right)^n, \\
||E_n(t) - E_{n-1}(t))|| &\leq ||E_n(0)|| \left(\frac{t^\psi K_3}{\Gamma(\psi+1)}\right)^n, \\
||I_n(t) - I_{n-1}(t))|| &\leq ||I_n(0)|| \left(\frac{t^\psi K_4}{\Gamma(\psi+1)}\right)^n, \\
||X_n(t) - X_{n-1}(t))|| &\leq ||X_n(0)|| \left(\frac{t^\psi K_5}{\Gamma(\psi+1)}\right)^n, \\
||Y_n(t) - Y_{n-1}(t))|| &\leq ||Y_n(0)|| \left(\frac{t^\psi K_6}{\Gamma(\psi+1)}\right)^n, \\
||R_n(t) - R_{n-1}(t))|| &\leq ||R_n(0)|| \left(\frac{t^\psi K_7}{\Gamma(\psi+1)}\right)^n.
\end{aligned} \tag{5.16}$$

Thus, $S_n,\ V_n,\ E_n,\ I_n,\ X_n,\ Y_n$, and R_n are sequences with uniform bounds.
The next step is to demonstrate that these sequences uniformly converge to the integral solution (5.14) on a specified interval I. This implies that they converge to the IVP solution (5.3) with initial condition (5.2).
Now, suppose the kernels $\mathcal{H}_j (j = 1, 2, \cdots, 7)$ are continuous on a closed region $\mathfrak{R} = \{(t, x) : |t - t_0| \leq a,\ ||x - x_0|| \leq b\}$ with

$$\begin{aligned}
\mathcal{X} &= \Big(\ S(t),\ V(t),\ E(t),\ I(t),\ X(t),\ Y(t),\ R(t)\ \Big)^T, \\
\mathcal{X}_0 &= \Big(\ S_0,\ V_0,\ E_0,\ I_0,\ X_0,\ Y_0,\ R_0\ \Big)^T.
\end{aligned} \tag{5.17}$$

Let $M_j > 0$ such that $||\mathcal{H}_j|| < M_j$ for each $j = 1, 2, \cdots, 7$.
Define $I = [0, h]$ where, $h = min\left\{a, \frac{b}{M}\Gamma(\psi+1)^{\frac{1}{\psi}}\right\}$. It is clear to see that,

$$\mathcal{X}_n = \mathcal{X}_0 + \sum_{k=1}^{n} (\mathcal{X}_k - \mathcal{X}_{k-1}). \tag{5.18}$$

To show that the sequence $\mathcal{X}_n$ uniformly converges on I, it is enough to show that the series $\mathcal{X}_0 + \sum_{k=1}^{n} (\mathcal{X}_k - \mathcal{X}_{k-1})$ converges uniformly on I.

Hence,

$$||\mathcal{X}_0 + \sum_{k=1}^{n}(\mathcal{X}_k - \mathcal{X}_{k-1})|| \leq ||\mathcal{X}_0|| + \sum_{k=1}^{n} ||\mathcal{X}_k - \mathcal{X}_{k-1}||$$
$$\leq ||\mathcal{X}_0|| + \sum_{k=1}^{n} ||\mathcal{X}_k(0)|| \left(\frac{t^{\psi} K_1}{\Gamma(\psi+1)}\right)^k . \tag{5.19}$$

which converges uniformly on I provided that $\frac{t^{\psi} K_1}{\Gamma(\psi+1)} < 1$. Accordingly, the sequence $\mathcal{X}_n$ uniformly converges on I according to the Weierstrass M-test. Thus, using the Lebesgue dominated convergence theorem, it can be demonstrated that this sequence converges to a limit point $\mathcal{X}(t)$, which is the solution of the integral equation (5.14). Hence, for each $w = 1, 2, \cdots, 7$, the IVP (5.3) with initial conditions (5.2) has at least one solution provided that $\frac{t^{\psi} K_w}{\Gamma(\psi+1)} < 1$.

Theorem 5.3 *System (5.3) subject to the initial conditions (5.2) has a unique solution if the inequality* $1 - \frac{t^{\psi} K_j}{\Gamma(\psi+1)} > 0$ *is satisfied for each* $j = 1, 2, \cdots, 7$.

Proof. The proof can be sketched similar to that of Theorem (4.3).

The existence and uniqueness of solutions are crucial for ensuring the biological significance of epidemiological models. Existence guarantees that the model can produce real illness dynamics, whereas uniqueness guarantees that the dynamics of the disease are steady and predictable.

When taken as a whole, the non-negativity, boundedness, existence, and uniqueness of solutions enhance the precision of models used to understand the transmission of disease and they direct public health policies.

5.2.3 TB Free Equilibrium Point (TBFEP)

Define $m_1 = \varphi + \mu$, $m_2 = p\eta_1 + \mu$, $m_3 = \alpha + \mu$, $m_4 = \theta + \mu + \xi_1$, $m_5 = \omega + \mu + \nu_1 + \eta_2 + \xi_2$, $m_6 = \mu + \xi_3 + \nu_2$, and $m_7 = \phi + \mu$.
Then system (4.3) can be rewritten as:

$$\begin{cases} {}_0^C D_t^{\psi} S(t) = \Lambda + p\eta_1 V + \phi R - \lambda S - m_1 S \ , \\ {}_0^C D_t^{\psi} V(t) = \varphi S - \tau V - m_2 V \ , \\ {}_0^C D_t^{\psi} E(t) = \lambda S + \tau V + (1-q)\eta_2 X - m_3 E \ , \\ {}_0^C D_t^{\psi} I(t) = \alpha E + q\eta_2 X - m_4 I \ , \\ {}_0^C D_t^{\psi} X(t) = \theta I - m_5 X \ , \\ {}_0^C D_t^{\psi} Y(t) = \omega X - m_6 Y \ , \\ {}_0^C D_t^{\psi} R(t) = \nu_1 X + \nu_2 Y - m_7 R \ , \quad 0 < \psi \leq 1 \ , \end{cases} \tag{5.20}$$

with initial conditions in (5.2).

TBFEP is a steady-state solution in which there is no TB infection. Consequently, setting $E(t) = I(t) = X(t) = Y(t) = 0$ and equating all of the model's equations of (5.3) to zero, the TBFEP is given by

$$\begin{aligned} \mathcal{E}^0 &= (S^0,\ V^0,\ E^0,\ I^0,\ X^0,\ Y^0,\ R^0) \\ &= \left(\frac{\Lambda(\mu + p\eta_1)}{\mu(\mu + \varphi + p\eta_1)}\ ,\ \frac{\Lambda\varphi}{\mu(\mu + \varphi + p\eta_1)}\ ,0\ ,0\ ,0\ ,0\ ,0 \right) \end{aligned} \tag{5.21}$$

5.2.4 Basic Reproduction Number

We utilize the next-generation matrix-approach employed in Zhu et al. (2020) to calculate the basic reproduction number of model (5.3). Thus, taking into account the compartments E, I, X, and Y as infected classes and treating the relapse term $(1-q)\eta_2 X$ as new infection, the matrix of new infection terms $\mathcal{F}$ and the matrix of progression terms $\mathcal{V}$ are respectively expressed as follows

$$\mathcal{F} = \begin{bmatrix} \mathcal{F}_1 \\ \mathcal{F}_2 \\ \mathcal{F}_3 \\ \mathcal{F}_4 \end{bmatrix} = \begin{bmatrix} \frac{\beta(I+\gamma_1 X+\gamma_2 Y)}{N} S + \frac{\beta(1-p)\eta_1(I+\gamma_1 X+\gamma_2 Y)}{N} V + (1-q)\eta_2 X \\ 0 \\ 0 \\ 0 \end{bmatrix}$$

and

$$\mathcal{V} = \begin{bmatrix} \mathcal{V}_1 \\ \mathcal{V}_2 \\ \mathcal{V}_3 \\ \mathcal{V}_4 \end{bmatrix} = \begin{bmatrix} m_3 E \\ -\alpha E - q\eta_2 X + m_4 I \\ -\theta I + m_5 X \\ -\omega X + m_6 Y \end{bmatrix}$$

Let F and V be the jacobian of $\mathcal{F}$ and $\mathcal{V}$ evaluated at $\mathcal{E}^0$ respectively. Then we have

$$F = \begin{bmatrix} 0 & \beta\mathcal{D} & \beta\gamma_1\mathcal{D} + (1-q)\eta_2 & \beta\gamma_2\mathcal{D} \\ 0 & 0 & 0 & 0 \\ 0 & 0 & 0 & 0 \\ 0 & 0 & 0 & 0 \end{bmatrix},\ V = \begin{bmatrix} m_3 & 0 & 0 & 0 \\ -\alpha & m_4 & -q\eta_2 & 0 \\ 0 & -\theta & m_5 & 0 \\ 0 & 0 & -\omega & m_6 \end{bmatrix},$$

with

$$\mathcal{D} = \left(\frac{S^0 + (1-p)\eta_1 V^0}{N^0} \right) = \left(\frac{\mu + p\eta_1 + (1-p)\eta_1\varphi}{\mu + p\eta_1 + \varphi} \right).$$

Thus, the maximum spectral radius of FV^{-1} is the basic reproduction number of the model, which is the average number of secondary cases generated by a single infected

individual and is determined by:

$$\mathcal{R}_0^{(\psi)} = \left(\frac{\beta\alpha\mathcal{D}}{\alpha+\mu}\right)\left(\frac{(\omega+\mu+\nu_1+\eta_2+\xi_2)(\mu+\xi_3+\nu_2)+\gamma_1\theta(\mu+\xi_3+\nu_2)+\gamma_2\omega\theta}{(\theta+\mu+\xi_1)(\omega+\mu+\nu_1+\eta_2+\xi_2)(\mu+\xi_3+\nu_2)-(\mu+\xi_3+\nu_2)q\eta_2\theta}\right)\Psi(\psi),$$

where $\Psi(\psi)$ is a fractional corrector factor which arises due to the dependence of each parameter on ψ.

In this notation, the terms

$$\frac{\beta\alpha\mathcal{D}(\omega+\mu+\nu_1+\eta_2+\xi_2)(\mu+\xi_3+\nu_2)}{(\alpha+\mu)(\theta+\mu+\xi_1)(\omega+\mu+\nu_1+\eta_2+\xi_2)(\mu+\xi_3+\nu_2)-(\alpha+\mu)(\mu+\xi_3+\nu_2)q\eta_2\theta}\Psi(\psi),$$

$$\frac{\beta\alpha\mathcal{D}\gamma_1\theta(\mu+\xi_3+\nu_2)}{(\alpha+\mu)(\theta+\mu+\xi_1)(\omega+\mu+\nu_1+\eta_2+\xi_2)(\mu+\xi_3+\nu_2)-(\alpha+\mu)(\mu+\xi_3+\nu_2)q\eta_2\theta}\Psi(\psi),$$

$$\frac{\beta\alpha\mathcal{D}\gamma_2\omega\theta}{(\alpha+\mu)(\theta+\mu+\xi_1)(\omega+\mu+\nu_1+\eta_2+\xi_2)(\mu+\xi_3+\nu_2)-(\alpha+\mu)(\mu+\xi_3+\nu_2)q\eta_2\theta}\Psi(\psi)$$

indicate the average number of secondary infections caused by a single person actively infected with TB, the average number of secondary infections caused by a single person receiving first line TB treatment, and the average number of secondary infections caused by a single person receiving second line TB treatment during their infectious period in a population that is completely susceptible. The terms

$$\frac{1}{\theta+\mu+\xi_1}, \quad \frac{1}{\omega+\mu+\nu_1+\eta_2+\xi_2}, \quad \frac{1}{\mu+\xi_3+\nu_2}$$

denotes the fractional average infectious period of those who are actively infected, those undergoing first-line treatment, and those undergoing second-line treatment, respectively.

5.2.5 Local and Global Stability of TB Free Equilibrium Point

Theorem 5.4 *The TBFEP $\mathcal{E}^0$ is locally asymptotically stable if $|arg(\lambda_i)| > \psi\frac{\pi}{2}$ for all eigenvalue λ_i of A, where A is a linearized matrix obtained by computing the Jacobian of system (5.3) at $\mathcal{E}^0$ and unstable if there exists atleast one eigenvalue λ_i such that $|arg(\lambda_i)| < \psi\frac{\pi}{2}$.*

Proof. Assume that λ, τ, $m_i(i = 1, 2, \cdots, 7)$ are as defined under subsection (5.2.3). Rewrite system (5.3) as a fractional linear system

$${}_0^C D_t^{\psi} x(t) = Ax(t), \quad x(0) = x_0, \quad 0 < \psi \leq 1, where\ x = (S, V, E, I, X, Y, R)^T \quad (5.22)$$

where,

$$A = \begin{bmatrix} -m_1 & p\eta_1 & 0 & -\frac{\beta S^0}{N^0} & -\frac{\beta\gamma_1 S^0}{N^0} & -\frac{\beta\gamma_2 S^0}{N^0} & \phi \\ \varphi & -m_2 & 0 & -\frac{\beta(1-p)\eta_1 V^0}{N^0} & -\frac{\beta(1-p)\eta_1\gamma_1 V^0}{N^0} & -\frac{\beta(1-p)\eta_1\gamma_2 V^0}{N^0} & 0 \\ 0 & 0 & -m_3 & w_1^0 & w_2^0 & w_3^0 & 0 \\ 0 & 0 & \alpha & -m_4 & q\eta_2 & 0 & 0 \\ 0 & 0 & 0 & \theta & -m_5 & 0 & 0 \\ 0 & 0 & 0 & 0 & \omega & -m_6 & 0 \\ 0 & 0 & 0 & 0 & \nu_1 & \nu_2 & -m_7 \end{bmatrix} \tag{5.23}$$

with

$$w_1^0 = \frac{\beta}{N^0}(S^0 + (1-p)\eta_1 V^0), \quad w_2^0 = \frac{\beta\gamma_1}{N^0}(S^0 + (1-p)\eta_1 V^0) + (1-q)\eta_2,$$

$$w_3^0 = \frac{\beta\gamma_2}{N^0}(S^0 + (1-p)\eta_1 V^0)$$

is a linearized matrix , obtained by computing the Jacobean of system (5.3) evaluated at $\mathcal{E}^0$. Using computer algebra system, it can be proved that all eigenvalues λ_i $(i = 1, 2, \cdots, 7)$ of A satisfy the condition $|arg(\lambda_i)| > \frac{\psi\pi}{2}$. Therefore, by Lemma (4.2) $\mathcal{E}^0$ is locally asymptotically stable.

Remark 5.2 *Epidemiologically speaking, TB can be eliminated from a population when the fractional-order ψ satisfy the condition $|arg(\lambda_i)| > \frac{\psi\pi}{2}$ for each eigenvalue λ_i of the linearized matrix A, because this ultimately leads to the infection's extinction. In contrast, if $|arg(\lambda_i)| < \frac{\psi\pi}{2}$, for at least one eigenvalue λ_i, the illness keeps spreading across the population. Numerical simulations in Section (5.3) have corroborated these results.*

Theorem 5.5 *The TB free equilibrium $\mathcal{E}^0$ of model (5.3) is globally asymptotically stable in its feasible region if $\mathcal{R}_0^{(\psi)} < 1$.*

Proof. Consider the quadratic Lyapunov candidate:

$$V(\mathbf{z}) = \frac{1}{2}\|\mathbf{z}\|^2 = \frac{1}{2}\sum_{i=1}^{7} z_i^2, \quad \textit{with } \mathbf{z} = \mathbf{x} - \mathcal{E}^0, \quad \textit{where } \mathbf{x} = (S, V, E, I, X, Y, R).$$

Let

$$\Theta = \left\{(S, V, E, I, X, Y, R) \in \mathbb{R}_+^7 : 0 < N \leq \frac{\Lambda}{\mu}\right\}$$

be a biologically feasible region.

Due to the non-local nature of fractional derivatives, utilizing Lemma (4.7) and the

systems dynamics, we compute:

$$\sum_{i=1}^{7} z_i \cdot {}_0^C D_t^{\psi} z_i = z_1\Big[\Lambda + p\eta_1 V + \phi R - (\lambda + \varphi + \mu)S\Big] + z_2\Big[\varphi S - (\tau + p\eta_1 + \mu)V\Big] + z_3\Big[\lambda S + \tau V + (1-q)\eta_2 X - (\alpha + \mu)E\Big] \cdots + z_7\Big[\nu_1 X + \nu_2 Y - (\phi + \mu)R\Big].$$

At $\mathcal{E}^0$, the following hold:

$$\Lambda + p\eta_1 V + \phi R = (\lambda + \varphi + \mu)S^0, \quad \varphi S = (\tau + p\eta_1 + \mu)V^0, \quad \cdots, \ \nu_1 X + \nu_2 Y = (\phi + \mu)R^0.$$

Substituting these into the derivative expression and simplifying yields:

$$\sum_{i=1}^{7} z_i \cdot {}_0^C D_t^{\psi} z_i \leq -\sum_{i=1}^{7} c_i z_i^2$$

Using this into Lemma (4.7) we get

$${}_0^C D_t^{\psi} V(\mathbf{y}(t)) \leq -\sum_{i=1}^{7} c_i z_i^2 + \mathcal{R}(\mathbf{y}),$$

where $c_i > 0$ and $\mathcal{R}(\mathbf{z})$ denotes bounded cross terms. Applying Young's inequality:

$$|z_i z_j| \leq \frac{\varepsilon}{2} z_i^2 + \frac{1}{2\varepsilon} z_j^2,$$

we bound $\mathcal{R}(\mathbf{z})$ and absorb it into the main negative definite term to get

$${}_0^C D_t^{\psi} V(\mathbf{z}) \leq -c\|\mathbf{z}\|^2 < 0, \ \forall_x \neq \mathcal{E}^0, \quad \text{and for some constant } c > 0.$$

The fractional derivative of the Lyapunov function is negative semi definite. Thus, by Corollary (4.1) , $\mathcal{E}^0$ is globally asymptotically stable in its feasible region if $\mathcal{R}_0^{(\psi)} < 1$.

5.2.6 Existence of TB Endemic Equilibrium Point (TBEEP)

Theorem 5.6 *When $\mathcal{R}_0^{(\psi)} > 1$, the TB model (5.3) has a unique TB endemic equilibrium point, $\mathcal{E}^* = (S^*, V^*, E^*, I^*, X^*, Y^*, R^*)$.*

Proof. The TBEEP is the steady state at which TB disease is present in the community. Hence, following Theorem 2 of Aldila et al. (2020) and Theorem (3.3) of

Khajanchi et al. (2018), we need to solve the system

$$\begin{cases} \Lambda + p\eta_1 V^* + \phi R^* - \lambda^* S^* - m_1 S^* = 0 \ , \\ \varphi S^* - \tau^* V^* - m_2 V^* = 0 \ , \\ \lambda^* S^* + \tau^* V^* + (1-q)\eta_2 X^* - m_3 E^* = 0 \ , \\ \alpha E^* + q\eta_2 X^* - m_4 I^* = 0 \ , \\ \theta I^* - m_5 X^* = 0 \ , \\ \omega X^* - m_6 Y^* = 0 \ , \\ \nu_1 X^* + \nu_2 Y^* - m_7 R^* = 0, \end{cases} \tag{5.24}$$

with

$$\lambda^* = \frac{\beta(I^* + \gamma_1 X^* + \gamma_2 Y^*)}{N^*}, \quad \tau^* = \frac{\beta(1-p)\eta_1(I^* + \gamma_1 X^* + \gamma_2 Y^*)}{N^*},$$

$$N^* = S^* + V^* + E^* + I^* + X^* + Y^* + R^*,$$

where $m_1,\ m_2,\ m_3,\ m_4,\ m_5,\ m_6$ and m_7 are as defined before.
Now after solving system (5.24) we obtain,

$$S^* = \frac{(\Lambda + \phi R^*)(\tau^* + m_2)}{(\tau^* + m_2)(\lambda^* + m_1) - p\eta_1\varphi} \ , \ V^* = \frac{\varphi S^*}{\tau^* + m_2}, \quad E^* = \frac{\lambda^* S^* + \tau^* V^* + (1-q)X^*}{m_3},$$

$$I^* = \frac{\alpha E^* + q\eta_2 X^*}{m_4}, \quad X^* = \frac{\theta I^*}{m_5}, \quad Y^* = \frac{\omega\theta I^*}{m_5 m_6}, \quad R^* = \left(\frac{\theta\nu_1}{m_5 m_7} + \frac{\omega\theta\nu_2}{m_5 m_6 m_7}\right) I^*$$

5.2.7 Bifurcation Analysis

There can be a chance for two different bifurcations in a given epidemic models: forward (supercritical) and backward (subcritical) at $\mathcal{R}_0^{(\psi)} = 1$. When $\mathcal{R}_0^{(\psi)}$ crosses unity from below, a forward bifurcation takes place. In this case, a little positive asymptotically stable equilibrium emerges throughout this period, and the disease-free equilibrium becomes unstable. On the other hand, when $\mathcal{R}_0^{(\psi)}$ is smaller than unity, a backward bifurcation takes place. In this instance, the disease-free equilibrium and a larger positive equilibrium are locally asymptotically stable, but a small positive unstable equilibrium emerges. Epidemiologically speaking, a backward bifurcation phenomena imply that a disease cannot be eradicated by lowering the basic reproduction number below unity alone. Hysteresis may occur when $\mathcal{R}_0^{(\psi)}$ passes unity. Thus, our primary goal in this section is to examine the direction of bifurcation using the center manifold theory established in (C. Castillo-Chavez & Song, 2004).

Bifurcation analysis relies heavily on center manifold theory. It detects the modes that are neither strongly stable nor unstable and makes studying dynamical systems

close to equilibrium points easier. These modes are in charge of the system's bifurcation and long-term behavior. While other approaches, such as normal form theory and direct numerical analysis, may provide distinct benefits, center manifold theory is still a potent tool that may be applied to a variety of bifurcations.

Thus, consider $u = [u_1, u_2, u_3, u_4, u_5, u_6, u_7]^T = [S, V, E, I, X, , Y, R]^T$. Then, the TB model (5.3) can be written compactly in the form of

$$\begin{cases} {}_0^C D_t^{\psi} u_1(t) = \Lambda + p\eta_1 u_2 + \phi u_7 - \lambda u_1 - m_1 u_1 = f_1(u_1,\ u_2,\ u_3,\ u_4,\ u_5,\ u_6,\ u_7)\ , \\ {}_0^C D_t^{\psi} u_2(t) = \varphi u_1 - \tau u_2 - m_2 u_2 = f_2(u_1,\ u_2,\ u_3,\ u_4,\ u_5,\ u_6,\ u_7)\ , \\ {}_0^C D_t^{\psi} u_3(t) = \lambda u_1 + \tau u_2 + (1-q)\eta_2 u_5 - m_3 u_3 = f_3(u_1,\ u_2,\ u_3,\ u_4,\ u_5,\ u_6,\ u_7)\ , \\ {}_0^C D_t^{\psi} u_4(t) = \alpha u_3 + q\eta_2 u_5 - m_4 u_4 = f_4(u_1,\ u_2,\ u_3,\ u_4,\ u_5,\ u_6,\ u_7)\ , \\ {}_0^C D_t^{\psi} u_5(t) = \theta u_4 - m_5 u_5 = f_5(u_1,\ u_2,\ u_3,\ u_4,\ u_5,\ u_6,\ u_7)\ , \\ {}_0^C D_t^{\psi} u_6(t) = \omega u_5 - m_6 u_6 = f_6(u_1,\ u_2,\ u_3,\ u_4,\ u_5,\ u_6,\ u_7)\ , \\ {}_0^C D_t^{\psi} u_7(t) = \nu_1 u_5 + \nu_2 u_6 - m_7 u_7 = f_7(u_1,\ u_2,\ u_3,\ u_4,\ u_5,\ u_6,\ u_7)\ ,\quad 0 < \psi \leq 1\ , \end{cases} \tag{5.25}$$

with

$$\lambda = \frac{\beta(u_4 + \gamma_1 u_5 + \gamma_2 u_6)}{N}, \quad \tau = \frac{\beta(1-p)\eta_1(u_4 + \gamma_1 u_5 + \gamma_2 u_6)}{N},$$
$$N = u_1 + u_2 + u_3 + u_4 + u_5 + u_6 + u_7$$

and $m_1, m_2, m_3, m_4, m_5, m_6$ and m_7 are as defined under subsection (5.2.3).

Choosing β^* as a bifurcation parameter and setting $\mathcal{R}_0^{(\psi)} = 1$ we obtain,

$$\beta^* = \frac{[m_3 m_4 m_5 m_6 - (m_3 + m_6 + m_3 m_6)q\eta_2\theta - m_6(1-q)\eta_2\alpha\theta]\,[\mu + p\eta_1\varphi]}{\alpha\,[m_5 + m_6 + m_5 m_6 + \gamma_1\theta m_6 + \gamma_2\theta\omega]\,[\mu + p\eta_1 + (1-p)\eta_1\varphi]}.$$

Clearly, we can see that $\beta^\star > 0$. Now, setting $\beta = \beta^*$ and evaluating the Jacobean of system (5.25) at $\mathcal{E}^0$ denoted by $\mathcal{J}(\mathcal{E}^0,\ \beta^*)$ and applying the fractional Routh-Hurwitz criterion, we can show that $\mathcal{J}(\mathcal{E}^0, \beta^*)$ has a simple zero eigenvalue and the remaining eigenvalues have negative sign indicating that $\mathcal{E}^0$ is a non-hyperbolic equilibrium. Thus, following the center manifold theory let

$$w = (w_1, w_2, w_3, w_4, w_5, w_6, w_7)^T, \quad v = (v_1, v_2, v_3, v_4, v_5, v_6, v_7)$$

be respectively the right and left eigenvectors associated to the zero eigenvalue. Then, solving $\mathcal{J}(\mathcal{E}^0, \beta^*).w = 0$ we get,

$$w_1 = \left[\frac{\beta^*}{m_1}\left(p\eta_1(\tilde{a} - \tilde{b}) - \tilde{c}\right) + \frac{\phi\tilde{d}}{m_1}\right] w_4, \quad w_2 = \beta^*(\tilde{a} - \tilde{b})w_4,$$

$$w_3 = \beta^* \tilde{e} w_4 > 0, \;\; w_4 = w_4 > 0, \;\; w_5 = \frac{\theta}{m_5} w_4 > 0, \;\; w_6 = \frac{\omega\theta}{m_5 m_6} w_4 > 0, \;\; w_7 = \beta^* \tilde{d} w_4 \; > 0,$$

where;

$$\tilde{a} = \frac{\left(1 + \frac{\gamma_1\theta}{m_5} + \frac{\gamma_2\omega\theta}{m_5 m_6}\right)\left(\varphi \frac{u_1^0}{N^0} + m_1(1-p)\eta_1 \frac{u_2^0}{N^0}\right)}{p\eta_1\varphi - m_1 m_2}, \quad \tilde{b} = \frac{\varphi\phi\left(\frac{\theta\nu_1}{m_5 m_7} + \frac{\theta\omega\nu_2}{m_5 m_6 m_7}\right)}{p\eta_1\varphi - m_1 m_2},$$

$$\tilde{c} = \left(1 + \frac{\gamma_1\theta}{m_5} + \frac{\gamma_2\omega\theta}{m_5 m_6}\right)\frac{u_1^0}{N^0}, \quad \tilde{d} = \frac{\theta\nu_1}{m_5 m_7} + \frac{\theta\omega\nu_2}{m_5 m_6 m_7},$$

$$\tilde{e} = \left(1 + \frac{\gamma_1\theta}{m_5} + \frac{\gamma_2\omega\theta}{m_5 m_6}\right)\left(\frac{u_1^0 + (1-p)\eta_1 u_2^0}{N^0}\right).$$

After taking some simple algebraic manipulations, and using the numerical values of model parameters depicted in Table (5.2) one can show that $w_1 < 0$ and $w_2 < 0$. Similarly, solving $v.\mathcal{J}(\mathcal{E}^0, \beta^*) = 0$ we have,

$$v_1 = v_2 = v_7 = 0, \quad v_3 = \frac{\alpha}{m_3} v_4 > 0, \quad v_4 = v_4 > 0,$$

$$v_5 = \left(\frac{\beta^*\omega\tilde{f}}{m_5} + \frac{q\eta_2}{m_5} + \frac{\alpha\tilde{g}}{m_3 m_5}\right) v_4 > 0, v_6 = \beta^*\tilde{f} v_4 > 0 \;,$$

where;

$$\tilde{f} = \left(\frac{\alpha\gamma_2}{m_3 m_6}\right)\left(\frac{u_1^0 + (1-p)\eta_1 u_2^0}{N^0}\right), \quad \tilde{g} = \beta^*\gamma_1\left[\frac{u_1^0 + (1-p)\eta_1 u_2^0}{N^0}\right] + (1-q)\eta_2.$$

The eigenvectors w and v should satisfy the requirement $v.w = 1$.

To find the direction of the bifurcation, as it was done in C. Castillo-Chavez & Song (2004), let a and b be the coefficients of the normal form representing the dynamics of the system in the central manifold such that $\dot{z} = az^2 + b\beta^* z$, where the bifurcation coefficients a and b at the DFE, $\mathcal{E}^0$ is given by

$$a = \sum_{k,i,j=1}^{6} v_k w_i w_j \frac{\partial^2 f_k}{\partial x_i \partial x_j}(\mathcal{E}^0, \beta^*) \;, \quad b = \sum_{k,i=1}^{6} v_k w_i \frac{\partial^2 f_k}{\partial x_i \partial \beta}(\mathcal{E}^0, \beta^*) \tag{5.26}$$

Computing the second order partial derivatives of $f_i (i = 1, 2, \cdots, 7)$, and using these values in equation (5.26) we can show that

$$a = v_3\left(2w_1 w_4 \frac{\beta^*}{N^0} + 2w_1 w_5 \frac{\beta^*\gamma_1}{N^0} + 2w_1 w_6 \frac{\beta^*\gamma_2}{N^0}\right) = 2\frac{\beta^*}{N^0} v_3 w_1 \left[w_4 + \gamma_1 w_5 + \gamma_2 w_6\right] < 0$$

and

$$b = v_3 \left[w_4 + \gamma_1 w_5 + \gamma_2 w_6 \right] \left[\frac{u_1^0 + (1-p)\eta_1 u_2^0}{N^0} \right] > 0.$$

Since $a < 0$ and $b > 0$, the TB model (5.3) undergoes a phenomenon of forward bifurcation at $\mathcal{R}_0^{(\psi)} = 1$. Hence, we have the following result.

Corollary 5.1 *The unique positive TB endemic equilibrium $\mathcal{E}^*$ of TB model (5.3) is locally asymptotically stable if $\mathcal{R}_0^{(\psi)} > 1$.*

Proof. We linearize system (5.3) near $\mathbf{x}^* = \mathcal{E}^*$ to get:

$$_0^C D_t^{\psi} \mathbf{y}(t) = J(\mathbf{x}^*)\mathbf{y}(t) + \mathbf{f}(\mathbf{y}(t)),$$

where $\mathbf{y}(t) = \mathbf{x}(t) - \mathbf{x}^*$, $\mathbf{x} = (S, V, E, I, X, Y, R)$, $J(\mathbf{x}^*)$ denotes the Jacobian matrix at equilibrium, and $\mathbf{f}$ contains higher-order nonlinear terms.

Let λ_i be the eigenvalues of $J(\mathbf{x}^*)$. By Matignon's theorem, the linearized system is locally asymptotically stable if:

$$|\arg(\lambda_i)| > \frac{\psi\pi}{2}, \quad \text{for all } i = 1, \ldots, 7.$$

Numerical evaluation with parameters from Table (5.2) confirms that this condition holds when $\mathcal{R}_0^{(\psi)} > 1$.

The forward bifurcation phenomenon indicates that the stable TBFEP splits into two non-negative equilibrium points: the unstable TBFEP and the stable positive TBEEP, as $\mathcal{R}_0^{\psi}$ passes unity. In terms of epidemiology, this means that for $\mathcal{R}_0^{(\psi)} < 1$, TB disease cannot spread throughout the population.

Corollary 5.2 *The unique positive TB endemic equilibrium $\mathcal{E}^*$ of TB model (5.3) is globally asymptotically stable if $\mathcal{R}_0^{(\psi)} > 1$.*

Proof. The proof follows the same procedure to that of Theorem (5.5) with $\mathbf{z} = \mathbf{x} - \mathcal{E}^*$.

While we have estimated the value of five model parameters using a real data on TB obtained from the Ethiopian Federal Ministry of Health, some of them are taken from the existing literature and the others are assumed. The best fit to our model with these real data is depicted in Figure (5.2). The parameters Λ and μ are computed with the same technique under section (4.3).

Table (5.2) shows values of biological parameters used for the numerical simulation of system (5.3). Using formula (4.42) and the values of model parameters from Table (5.2), the sensitivity indices of model parameters relative to $\mathcal{R}_0$ are computed and are summarized in Table (5.3). It can be seen from Table (5.3) that the parameters μ, ξ_1, ξ_2, ξ_3, φ, θ, ω, ν_1, ν_2 have negative sensitivity indices and are inversely

Table 5.2: Values of model parameters used in numerical simulations.

Parameters	Values	Source
Λ	1265 persons/year	calculated
β	0.2597/(year×persons)	fitted
μ	0.016/year	calculated
ξ_1	0.0111/year	fitted
ξ_2	4.6308/year	fitted
ξ_3	2.6963/year	fitted
φ	0.2634/year	fitted
p	0.8/(year×persons)	assumed
ϕ	0.01/(year×persons)	assumed
q	0.2959/(year×persons)	(S. Ullah, Ullah, et al., 2020)
ν_1	0.8/year	assumed
ν_2	0.7/year	assumed
α	0.2351/(year×persons)	(S. Ullah, Ullah, et al., 2020)
θ	0.0013/(year×persons)	fitted
ω	0.7027/(year×persons)	assumed
η_1	0.1/(year×persons)	assumed
η_2	0.1/(year×persons)	assumed
γ_1, γ_2	0.1, 0.1	assumed

proportional to $\mathcal{R}_0$. The remaining parameters have direct relationship with $\mathcal{R}_0$ since they have positive sensitivity index. Furthermore, β, η_1, φ and θ are highly sensitive parameters influencing $\mathcal{R}_0$. Thus, $\mathcal{R}_0$ will decrease if we increase vaccination rate and the adherence rates to treatments. Similarly, lowering the effective contact rate and the per capita rate of being infectious will reduce basic reproduction number.

The more people receive vaccinations, the stronger the population's immune system will be, which lowers the number of people who are at risk of contracting tuberculosis, thereby lowering the disease's spread across the community. The chance of minimizing the spread of the disease will increase as we assist more patients to adhere to both first- and second-line therapies. The worst stage of tuberculosis will occur as the effective contact rate and the per capita infectiousness rate rise.

Therefore, it should be the responsibility of public health sectors to ensure that TB vaccine is widely distributed, lowering the infectiousness rate, and promote adherence to both first-line and second-line TB therapies as this can successfully minimize the spread of the disease. Lastly, we can lower the incidence and prevalence of TB disease by lowering $\mathcal{R}_0$.

5.3 Numerical Simulations and Discussion

The aim of this section is to numerically support the analytical results of the previous sections using a PECE algorithm implemented in Diethelm et al. (2004); Diethelm

Table 5.3: Sensitivity indices of $\mathcal{R}_0$ to the parameters.

Parameters	Sensitivity indices	Parameters	Sensitivity indices	Parameters	Sensitivity indices
β	+1.0000	q	0.0054	p	0.0163
μ	-0.5224	α	0.2069	ν_1	-0.0018
ξ_1	-0.3954	θ	-0.1265	ν_2	-0.0002
ξ_2	-0.0044	ω	-0.0008	γ_1, γ_2	0.0026, 0.0008
ξ_3	-0.0005	η_1	0.3968		
φ	-0.7416	η_2	0.0047		

& Freed (1998) via GNU Octave/MATLAB software. For this purpose we have assumed the initial data as $S(0) = 123005,\ V(0) = 1,800,\ E(0) = 141,\ I(0) = 135,$ $X(0) = 8,\ Y(0) = 5,\ R(0) = 118.$

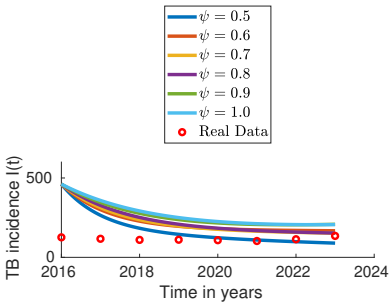

Figure 5.2: Fitting of system (5.3) with respect to Ethiopian TB incidence data from January, 2016 to December, 2023, where the population is in thousands.

Utilizing the values of model parameters from Table (5.2), we can see that $\mathcal{E}^0$ is locally asymptotically stable only for $\psi = 0.5$ according to the Matignons' stability criterion since $\mathcal{R}_0^{(\alpha)} < 1,\ \lambda_i < 0,\ \forall_i$, and $|arg(\lambda_i)| > \psi\frac{\pi}{2}$ in this case, where λ_i is an eigenvalue of the linearized matrix $\mathcal{A}$ in equation (5.23). On the other hand, for each $\psi \in \{0.7, 0.9, 1.0\}$, $\mathcal{E}^0$ is unstable as $\mathcal{R}_0^{(\alpha)} > 1$ and there exists λ_i, such that $|arg(\lambda_i)| < \psi\frac{\pi}{2}$. This shows that small fractional orders have an ability to expand the stability region of the disease-free equilibrium due to the fact that they retain a long-term history of the disease. However, if we reduce β to 0.1073 while keeping the values of the remaining model parameters, we observe that the condition $|arg(\lambda_i)| > \psi\frac{\pi}{2}$ is satisfied for each eigenvalue λ_i and for each $\psi \in \{0.5, 0.7, 0.9, 1.0\}$. Additionally, $\mathcal{R}_0^{(\alpha)} < 1,\ \forall_\alpha$. Hence, $\mathcal{E}^0$ is locally asymptotically stable as demonstrated by Table (5.4) and Figures (5.3a)–(5.3g). Additionally, the graphical results of Figures (5.3a)–(5.3g) support the convergence of the solution trajectories toward $\mathcal{E}^0 = (2727.8, 7484.5, 0, 0, 0, 0, 0)$.

A Caputo fractional order model is effective in predicting long-term behavior in infectious diseases, particularly TB, due to its ability to incorporate the past and the current history of the disease and it accounts for memory effects. This model is especially valuable for TB, which has a long latency period influenced by past infection

histories. Unlike traditional integer-order models, it offers greater accuracy in analyzing TB transmission dynamics by allowing for smoother transitions between compartments, such as latent and active TB. Integer-order models may yield inaccurate predictions because they do not account for the past exposures and history of the disease(Podlubny, 1998; Saeedian et al., 2017).

With the optimal $\psi = 0.5$, Figures (5.4a)-(5.4d) show how varying the model parameters β, η_1, φ and θ affects the basic reproduction number $\mathcal{R}_0$. Consequently, as illustrated in Figures (5.4a), (5.4b) a 50% decrease in β and η_1 results in respectively 29.3% and 12.8% decrease in $\mathcal{R}_0$. On the other hand Figures (5.4c), (5.4d) depict that imposing a 50% increase in φ, θ respectively yields to an approximately 10.3% and 3% decrease in $\mathcal{R}_0$. This significant reduction in $\mathcal{R}_0$ indirectly yields to a substantial decrease in TB prevalence.

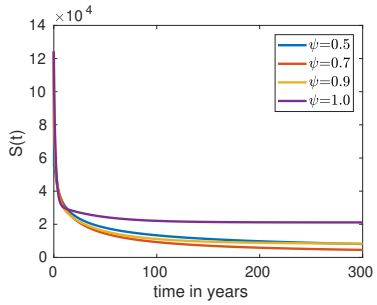

(a) Susceptible population for $\psi = (0.5, 0.7, 0.9, 1.0)$.

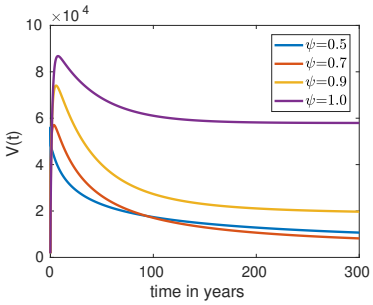

(b) Vaccenated population for $\psi = (0.5, 0.7, 0.9, 1.0)$.

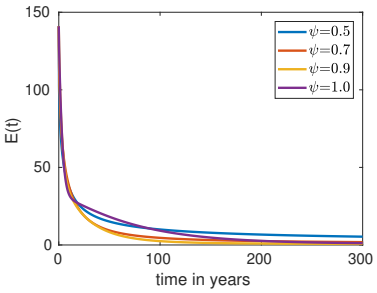

(c) Exposed population for $\psi = (0.5, 0.7, 0.9, 1.0)$.

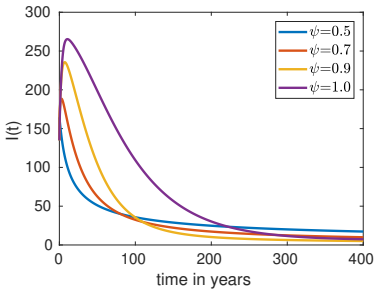

(d) Active TB infected for $\psi = (0.5, 0.7, 0.9, 1.0)$.

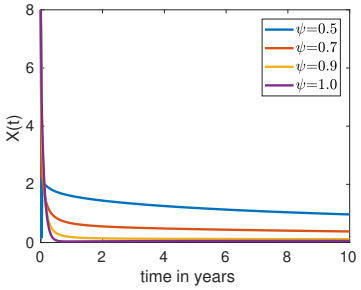

(e) First line treatment for $\psi = (0.5, 0.7, 0.9, 1.0)$.

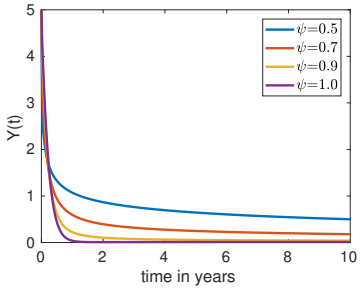

(f) Second line treatment for $\psi = (0.5, 0.7, 0.9, 1.0)$.

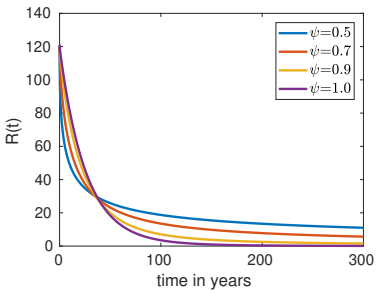

(g) Recoverd population for $\psi = (0.5, 0.7, 0.9, 1.0)$.

Figure 5.3: Plots showing local asymptotic stability of TBFEP $\mathcal{E}^0$.

Table 5.4: Stability test using the fractional Matignon's stability criterion and stability zone for different values of fractional-order ψ with $\lambda_i < 0$, $|arg(\lambda_i)| = 180^0$ for all i and $\beta = 0.1073$.

ψ	critical angle $(\psi\frac{\pi}{2})$	Matignon criterion $(\lvert arg(\lambda_i)\rvert > \psi\frac{\pi}{2})$	$\mathcal{R}_0$	stability condition
0.5	45^0	satisfied	0.4523	stable
0.7	63^0	satisfied	0.6489	stable
0.9	81^0	satisfied	0.8744	stable
1.0	90^0	satisfied	0.9970	stable

Table 5.5: Stability conditions and their epidemiological implications.

Fractional Order ψ	Critical Angle	Epidemiological Interpretation
$\alpha = 0.5$	45°	**Strong memory effects**: System retains long-term disease history. Enhanced stability allows elimination even with moderately positive growth rates. Represents populations with lasting behavioral adaptations. Slow rates of convergence due to their high decay time.
$\alpha = 0.7$	63°	**Moderate memory**: Intermediate stability region. Captures partial retention of past epidemic experiences and control measures. Intermediate rates of convergence.
$\alpha = 0.9$	81°	**Low memory**: Small stability region. Captures extremely low retention of past epidemic experiences and control measures.
$\alpha = 1.0$	90°	**Classical memoryless system**: Standard $R_0 < 1$ condition. No historical dependence - represents instantaneous response without behavioral memory. Quick rates of convergence due to their low decay time.

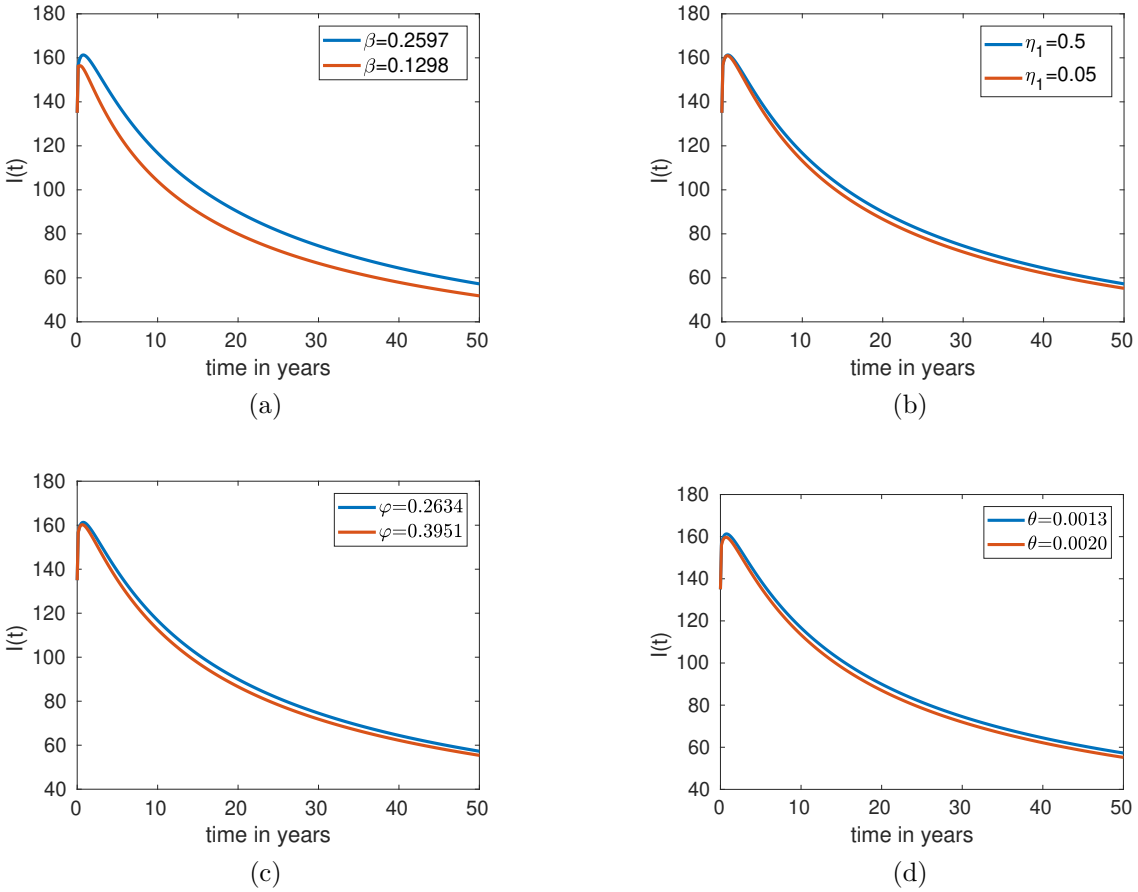

Figure 5.4: Graphs demonstrating the impact of varying a) β on I(t) b) η_1 on I(t) c) φ on I(t) and d) θ on I(t).

5.4 TB Model with Controls

The aim of this section is to investigate the transmission dynamics of TB epidemic by extending model (5.3) into a fractional optimal control problem (5.27). Three control variables, $u_1(.)$, $u_2(.)$ and $u_3(.)$ are introduced. The first control u_1 represents preventive actions such as wearing masks, maintaining physical distance, and properly disposing of tissues and sputum. These actions help reduce the transmission of pathogens by minimizing close contact and limiting the spread of respiratory droplets. The second control u_2 is vaccination. Vaccination is a critical public health strategy that helps build immunity against specific infectious diseases. It protects not only the individuals who are vaccinated but also contributes to herd immunity, reducing overall disease prevalence in the community. The third control u_3 is a treatment control which involves providing medical care to infected individuals to manage their symptoms and prevent complications. Effective treatment can also reduce the infectious period, thereby lowering the risk of transmission to others (Guo & Zhang, 2023; Oshinubi et

al., 2023; WHO, 2025a).

Let $E(t) = L(t)$, $X(t) = F_L(t)$ and $Y(t) = S_L(t)$. Then, the extended Caputo fractional optimal control for system (5.3) is then given by

$$\begin{cases} {}_0^C D_t^{\psi} S(t) = \Lambda + p\eta_1 V + \phi R - [1-u_1(t)]\lambda S - (\varphi + u_2(t) + \mu)S \ , \\ {}_0^C D_t^{\psi} V(t) = [\varphi + u_2(t)]S - [1-u_1(t)]\tau V - (p\eta_1 + \mu)V \ , \\ {}_0^C D_t^{\psi} L(t) = [1-u_1(t)]\lambda S + [1-u_1(t)]\tau V + (1-q)\eta_2 F_L - (\alpha + \mu)L \ , \\ {}_0^C D_t^{\psi} I(t) = \alpha L + q\eta_2 F_L - (\theta + u_3(t) + \mu + \xi_1)I \ , \\ {}_0^C D_t^{\psi} F_L(t) = (\theta + u_3(t))I - (\omega + \mu + \nu_1 + \eta_2 + \xi_2)F_L \ , \\ {}_0^C D_t^{\psi} S_L(t) = \omega F_L - (\mu + \nu_2 + \xi_3)S_L \ , \\ {}_0^C D_t^{\psi} R(t) = \nu_1 F_L + \nu_2 S_L - (\phi + \mu)R \ , \quad 0 < \psi \leq 1, \end{cases} \tag{5.27}$$

with initial conditions given as in equation (5.2). The control system (5.27) involves seven state variables as before with their description given as in section (5.2).

5.4.1 Basic Reproduction Number of the Extended Model

In the following theorem, we use the next-generation matrix approach presented in Zhu et al. (2020) to determine the basic reproduction number $\mathcal{R}_c$ of the control system (5.27).

Theorem 5.7 *The basic reproduction number $\mathcal{R}_c$ for the control system (5.27) is given by*

$$\mathcal{R}_c(u_1, u_2, u_3) = \frac{\beta\alpha(1-u_1)\mathcal{D}_c}{d_1 d_6(d_2 d_5 - d_3 d_4)}(d_5 d_6 + \gamma_1 d_4 d_6 + \gamma_2 \omega d_4) + \frac{(1-q)\eta_2 \alpha d_4}{d_1(d_2 d_5 - d_3 d_4)}, \tag{5.28}$$

where,

$$d_1 = \alpha + \mu, \ d_2 = \theta + u_3 + \mu + \xi_1, \ d_3 = q\eta_2, \ d_4 = \theta + u_3, \ d_5 = \omega + \mu + \nu_1 + \eta_2 + \xi_2,$$

$$d_6 = \mu + \nu_2 + \xi_3 \quad \textit{and} \quad \mathcal{D}_c = \frac{\mu + p\eta_1 + \eta_1(1-p)(\varphi + u_2)}{\mu + p\eta_1 + \varphi + u_2}.$$

Proof. With $L(t) = I(t) = F_L(t) = S_L(t) = 0$, the disease free equilibrium for the controlled system (5.27) is obtained as

$$\mathcal{E}_c^0 = \left(\frac{\Lambda(\mu + p\eta_1)}{\mu(\mu + \varphi + u_2 + p\eta_1)}, \frac{\Lambda(\varphi + u_2)}{\mu(\mu + \varphi + u_2 + p\eta_1)}, 0, 0, 0, 0, 0 \right)$$

and its stability can be shown by following similar techniques as in (F. Z. . H. W. Castillo-Chavez C., 2002).

Following the next-generation matrix method outlined in Zhu et al. (2020), we compute the basic reproduction number for model (5.27). Consequently, by taking into account the compartments L, I, F_L, and S_L as infected classes and the relapse term $(1-q)\eta_2 F_L$ as new infection, the matrix of new infection terms $\mathcal{F}$ and the matrix of progression terms $\mathcal{V}$ are expressed as

$$\mathcal{F} = \begin{bmatrix} \frac{\beta(1-u_1)(I+\gamma_1 F_L+\gamma_2 S_L)}{N} S + \frac{\beta\eta_1(1-p)(1-u_1)(I+\gamma_1 F_L+\gamma_2 S_L)}{N} V + (1-q)\eta_2 F_L \\ 0 \\ 0 \\ 0 \end{bmatrix},$$

$$\mathcal{V} = \begin{bmatrix} d_1 L \\ -\alpha L - q\eta_2 F_L + d_2 I \\ -(\theta+u_3) I + d_5 F_L \\ -\omega F_L + d_6 S_L \end{bmatrix}.$$

Define F and V as the jacobian of $\mathcal{F}$ and $\mathcal{V}$ evaluated at $\mathcal{E}_c^0$ respectively. Then we have

$$F = \begin{bmatrix} 0 & \beta(1-u_1)\mathcal{D}_c & \beta\gamma_1(1-u_1)\mathcal{D}_c + (1-q)\eta_2 & \beta\gamma_2(1-u_1)\mathcal{D}_c \\ 0 & 0 & 0 & 0 \\ 0 & 0 & 0 & 0 \\ 0 & 0 & 0 & 0 \end{bmatrix},$$

$$V = \begin{bmatrix} d_1 & 0 & 0 & 0 \\ -\alpha & d_2 & -d_3 & 0 \\ 0 & -d_4 & d_5 & 0 \\ 0 & 0 & -\omega & d_6 \end{bmatrix},$$

with $d_1, d_2, d_3, d_4, d_5, d_6$ and $\mathcal{D}_c$ as defined in (5.28). Therefore, the basic reproduction number of model (5.27) which is the largest spectral radius of FV^{-1} is given as in (5.28).

Remark 5.3 *$\mathcal{R}_c > 0$ since $d_2 d_5 - d_3 d_4 = (\omega+\mu+\nu_1+\xi_2+(1-q)\eta_2)d_4 + (\mu+\xi_1)d_5 > 0$*

Let $\tilde{\beta} = \beta\alpha(u_1 - 1)$. Then, using formula (4.42) and the computer algebra system, the sensitivity indices of model parameters relative to $\mathcal{R}_c$ are computed as follows and are summarized in Table (5.6).

$$\Upsilon_{\beta}^{\mathcal{R}_c} = \frac{\tilde{\beta} e_3 e_1}{\left[\frac{e_4}{d_1 e_5} + \frac{\tilde{\beta} e_3 e_1}{d_1 d_6 e_5 e_2}\right] d_1 d_6 e_5 e_2} > 0$$

with $e_1 = (\mu + \eta_1 p + \eta_1(u_2 + \varphi)(1-p)) > 0,\ e_2 = (\mu + u_2 + \varphi + \eta_1 p) > 0,$
$e_3 = d_5 d_6 + \gamma_2 \omega d_4 + \gamma_1 d_4 d_6 > 0,\ \ e_4 = \eta_2 \alpha d_4 (q-1) < 0$ and $e_5 = d_2 d_5 - d_3 d_4 > 0.$

With $e_6 = (d_5 + d_6 + \gamma_1 d_4) > 0$, we have

$$\Upsilon_{\mu}^{\mathcal{R}_c} = \frac{-\mu\left[\frac{e_4}{d_1^2 e_5} + \frac{e_4(d_2+d_5)}{d_1 e_5^2} - \frac{\tilde{\beta} e_3}{d_1 e_5 d_6 e_2} - \frac{\tilde{\beta} e_1 e_6}{d_1 e_5 d_6 e_2} + \frac{\tilde{\beta} e_3 e_1}{d_1 e_5 d_6 e_2^2} + \frac{\tilde{\beta} e_3 e_1}{d_1 e_5 d_6^2 e_2} + \frac{\tilde{\beta} e_3 e_1}{d_1^2 e_5 d_6 e_2}\right]}{\frac{e_4}{d_1 e_5} + \frac{\tilde{\beta} e_3 e_1}{d_1 e_5 d_6 e_2}}$$

$$< 0.$$

$$\Upsilon_{u_1}^{\mathcal{R}_c} = -\frac{\beta\alpha\left(d_5 d_6 + \gamma_2 \omega d_4 + \gamma_1 d_4 d_6\right) e_1}{d_1 e_5 d_6 e_2} < 0.$$

$$\Upsilon_{u_2}^{\mathcal{R}_c} == \frac{\tilde{\beta}\left(d_5 d_6 + \gamma_2 \omega d_4 + \gamma_1 d_4 d_6\right)\left[\frac{(\mu+\eta_1)(1+\eta_1 p - \eta_1)}{e_2}\right]}{d_1 e_5 d_6 e_2} < 0.$$

$$\Upsilon_{u_3}^{\mathcal{R}_c} = \frac{e_4\left(d_5 - d_3\right)}{d_1 e_5^2} - \frac{\eta_2 \alpha (q-1)}{d_1 e_5} - \frac{\tilde{\beta} e_1\left(\gamma_2 \omega + \gamma_1 d_6\right)}{d_1 e_5 d_6 e_2}$$

$$+\frac{\tilde{\beta} e_1\left(d_5 d_6 + \gamma_2 \omega d_4 + \gamma_1 d_4 d_6\right)\left(d_5 - d_3\right)}{d_1 e_5^2 d_6 e_2} < 0$$

The computations of sensitivity indices for the remaining parameters follows the same fashion. Table (5.6) shows that the parameters $\beta,\ \alpha,\ \eta_1,\ \eta_2,\ \gamma_1$, and γ_2 have a

Table 5.6: Sensitivity indices (S.I) of $\mathcal{R}_c$ to the parameters.

Parameters	S.I	Parameters	S.I	Parameters	S.I
β	0.6134	q	-0.4326	p	-0.2175
μ	-0.2637	α	0.2069	ν_1	-0.0920
ξ_1	-0.1411	θ	-0.0183	ν_2	-0.0024
ξ_2	-0.2215	ω	-0.0789	γ_1, γ_2	0.0228, 0.0074
ξ_3	-0.0046	η_1	0.3408	u_1, u_2, u_3	-2.4537, -0.2472, -0.2543
φ	-0.1606	η_2	0.3826		

positive sign, indicating that $\mathcal{R}_c$ falls in the same way as the parameters does. For the remaining parameters, $\mathcal{R}_c$ decreases, following their increase since they have a negative indices. Additionally, this suggests that if parameter v is increased (or decreased) by $\mathcal{Y}\%$, the basic reproduction number will also be decreased (or increased) by $\mathcal{Y}\%$. Since it is unethical to raise the human mortality rate in order to control a disease pandemic, we did not take this into account.

Furthermore, according to the sensitivity result, increasing vaccination rate, along with improved treatment adherence rates and preventing contact between susceptible and infected individuals will significantly lower the basic reproduction number, which will indirectly lower the disease's prevalence.

5.4.2 The Fractional Optimal Control Problem (FOCP)

This subsection examines an optimal control issue that describes endemic tuberculosis mitigation. The goal is to minimize the objective functional and determine the ideal values $\tilde{u} = (\tilde{u_1}, \tilde{u_2}, \tilde{u_3})$ of the controls $u = (u_1, u_2, u_3)$ such that the associated state trajectories $S,\ V,\ L,\ I,\ F_L,\ S_L$, and R are solutions of the system (5.27) in the intervention time interval $[0, t_f]$ with initial conditions as stated (5.2). The control function u_1 plays the role of preventive measures including: using a face mask, avoiding social gatherings, and properly disposing of used tissues and sputum that help to reduce contact rate with health individuals. The control u_2 indicates vaccination control which can contribute to herd immunity, reducing the transmission of TB within communities while the control function u_3 measures extensive medical care for all the confirmed cases to raise recover rate of infected persons.

The range of the controls is 0 to 1. When the controls disappear, it indicates that no additional steps are being taken to lower the sickness. Since the intervention is not 100% properly executed when the controls take the maximum value of 1, we assumed that $u_k \leq 1 - \sigma,\ k = 1, 2, 3$, where $\sigma << 1$ indicates a positive real number.

Our cost functional takes into account the number of exposed people (L), the number of infected people (I), the number of patients receiving first-line treatment (F_L), the number of patients receiving second-line treatment (S_L) and the cost of putting control-related initiatives into practice. Thus, the objective functional which is the total cost due to TB infection is more precisely defined by

$$\mathcal{J}(u_1, u_2, u_3) = \int_0^{t_f} \left(A_1 L(t) + A_2 I(t) + A_3 F_L(t) + A_4 S_L(t) + \frac{1}{2} \sum_{k=1}^{3} B_k u_k^2 \right) dt \to min \tag{5.29}$$

The positive coefficients A_1, A_2, A_3, and A_4, respectively, stand for the weight constants for latent TB infection, active TB infection, infections associated to patients receiving first-line TB treatment , and to those receiving second-line TB treatment. The parameters B_1, B_2 and B_3, respectively, reflect the weight constants that measure the relative costs of the treatments associated with the controls u_1, u_2 and u_3. The cost of implementing the treatment increases as the values of B_1, B_2 and B_3 rise. The fixed constant t_f indicates the ultimate intervention time. The costs associated with latent TB infection, active TB infection, patients receiving first-line TB treatment , and to those receiving second-line TB treatment are also indicated by the terms $A_1 L(t),\ A_2 I(t),\ A_3 F_L(t)$, and $A_4 S_L(t)$, respectively.

The collection of acceptable control functions is given by

$$\mathcal{U} = \{u = (u_1, u_2, u_3) \text{ are measurable and } 0 \leq u_j(t) \leq 1, j = 1, 2, 3, \forall_t \in [0, t_f]\} \tag{5.30}$$

Theorem 5.8 *There exists an optimal control triple* $\tilde{u} = (\tilde{u_1}, \tilde{u_2}, \tilde{u_3}) \in \mathcal{U}$ *and a corresponding solution vector* $\tilde{Z} = (\tilde{S},\ \tilde{V},\ \tilde{L},\ \tilde{I},\ \tilde{F_L},\ \tilde{S_L},\ \tilde{R})$ *to the control system (5.27) subject to the non-negative initial conditions (5.2) such that*

$$\mathcal{J}(\tilde{u}) = min(\mathcal{J}(u(.)) : u \in \mathcal{U}) \tag{5.31}$$

Proof. We aim to identify the optimal control $\tilde{u} = (\tilde{u_1}, \tilde{u_2}, \tilde{u_3})$ of the control functions $u(t) = (u_1(t), u_2(t), u_3(t))$ such that the associated state trajectories minimize the cost functional given in (5.29) and represent the solution of system (5.27) during the intervention time period $[0, t_f]$. Specifically,

$$\mathcal{J}(u^*(t)) = min(\mathcal{J}(u) : u \in \mathcal{U})$$

subject to system (5.27), where,

$$\mathcal{U} = \{u = (u_1, u_2, u_3) \text{ are measurable and } 0 \leq u_j(t) \leq 1, j = 1, 2, 3, \forall_t \in [0, t_f]\}$$

With the help of the fractional Pontryagin's Minimum Principle presented in Bergounioux & Bourdin (2020); Mahata et al. (2022), problems (5.27), (5.29), and (5.30) may be reduced to a problem of minimizing the Hamiltonian $\mathcal{H}$, with

$$\mathcal{H} = A_1 L(t) + A_2 I(t) + A_3 F_L(t) + A_4 S_L(t) + \frac{1}{2}\sum_{k=1}^{3} B_k u_k^2 + \sum_{j=1}^{7} p_j(t) f_j(t, Z), \tag{5.32}$$

where $f_j^{'}s$ represents the right-hand side of the functions given in equation (5.27) above, $Z = (S,\ V,\ L,\ I,\ F_L,\ S_L,\ R)$ and $p : [0, t_f] \to \mathbb{R}^7$ given by $p = (p_1(t),\ p_2(t), \cdots,\ p_7(t))$ is a nontrivial absolutely continuous adjoint vector.

Thus, based on Baba & Bilgehan (2021), we need to show that

a) The integrand of $\mathcal{J}$ is convex with respect to controls u_1, u_2 and u_3.

b) The set $\mathcal{U}$ is convex and closed.

c) The state solutions of system (5.27) are Lipschitz with respect to the state variables.

The integrand of $\mathcal{J}$ is a linear combinations of convex functions

$$A_1L(t),\ A_2I(t),\ A_3F_L(t),\ A_4S_L(t),\ \frac{1}{2}B_1u_1^2(t),\ \frac{1}{2}B_2u_2^2(t)\ and\ \frac{1}{2}B_3u_3^2(t).$$

Hence, it is convex. Thus, condition (a) is proved.
To prove (b), assume $\mathcal{U} = \{u \in \mathbb{R}^3 : ||u|| \leq 1 - \epsilon\}$. Let $u_1, u_2, u_3 \in \mathcal{U}$ such that $||u_1|| \leq 1 - \epsilon,\ ||u_2|| \leq 1 - \epsilon, ||u_3|| \leq 1 - \epsilon$. Then, for any $k \in [0, 1]$,

$$||ku_1 + (1 - k)u_2|| \leq k||u_1|| + (1 - k)||u_2|| \leq 1 - \epsilon.$$

This implies that $\mathcal{U}$ is convex and closed.
Each state variables $S,\ V,\ L,\ I,\ F_L,\ S_L,\ R$ are continuously differentiable and the total human population is defined by

$$N = S(t) + V(t) + L(t) + I(t) + F_L(t) + S_L(t) + R(t).$$

Adding all equations in (5.27) we get ${}_0^C D_t^{\psi} N(t) + \mu N(t) \leq \Lambda$, which after some algebraic manipulations gives

$$N(t) \leq \left(N_0 - \frac{\Lambda}{\mu}\right) E_{\psi,1}(-\mu t^{\psi}) + \frac{\Lambda}{\mu},$$

implying that

$$\limsup_{t\to\infty}(N(t)) \leq \frac{\Lambda}{\mu}.$$

provided that $N_0 \leq \frac{\Lambda}{\mu}$. This implies that for each admissible control function $\mathcal{U}$, the state system's solutions are bounded and continuous. Furthermore, with regard to state variables, the right hand side functions of model (5.27) satisfy the Lipschitz condition. As a result, the control system (5.27) subject to the initial conditions (5.2) has a unique solution corresponding to any admissible control function $u \in \mathcal{U}$. Condition (c) is therefore proven.

Theorem 5.9 *Under the same conditions as in Theorem (5.8), if the cost functional $\mathcal{J}(u)$ is strictly convex in u, then the optimal control $\tilde{u}$ that minimizes $\mathcal{J}(u)$ is unique.*

Proof. The proof follows from Baba & Bilgehan (2021); Bahaa (2017).

Remark 5.4 *By verifying $\frac{\partial^2 \mathcal{H}}{\partial u^2} > 0$, one can observe that the pair $(\tilde{x}, \tilde{u})$ is a candidate for minimizer.*

Theorem 5.10 *Let $u \in [0, 1]$ be a measurable control function on $[0, t_f]$. Then an optimal control $\tilde{u}$ minimizing the objective function $\mathcal{J}(u)$ of (5.29) is*

$$\tilde{u} = min\left\{max\left\{0, u^*\right\}, 1\right\},$$

with

$$u^* = (u_1^*, u_2^*, u_3^*)$$

$$= \left(\frac{\beta\left(I + \gamma_1 F_L + \gamma_2 S_L\right) I_T}{B_1 N} \left[(p_3 - p_1)S + \eta_1(1-p)(p_3 - p_2)V\right], \frac{(p_1 - p_2)\, S}{B_2}, \frac{(p_4 - p_5)\, I}{B_3} \right).$$

Furthermore, from the boundedness of $\tilde{u_k}(t)$ *on* $(0,1)$ *and the minimality condition, we have:*

$$\tilde{u_1} = \begin{cases} 0, & if \quad \frac{\partial \mathcal{H}}{\partial u_1} > 0, \\ \frac{\beta(I+\gamma_1 F_L+\gamma_2 S_L) I_T}{B_1 N} \left[(p_3 - p_1)S + \eta_1(1-p)(p_3 - p_2)V\right], & if \quad \frac{\partial \mathcal{H}}{\partial u_1} = 0, \\ 1, & if \quad \frac{\partial \mathcal{H}}{\partial u_1} < 0. \end{cases}$$

$$\tilde{u_2} = \begin{cases} 0, & if \quad \frac{\partial \mathcal{H}}{\partial u_2} > 0, \\ \frac{(p_1-p_2)S}{B_2}, & if \quad \frac{\partial \mathcal{H}}{\partial u_2} = 0, \\ 1, & if \quad \frac{\partial \mathcal{H}}{\partial u_2} < 0. \end{cases} \quad \tilde{u_3} = \begin{cases} 0, & if \quad \frac{\partial \mathcal{H}}{\partial u_2} > 0, \\ \frac{(p_4-p_5)I}{B_3}, & if \quad \frac{\partial \mathcal{H}}{\partial u_2} = 0, \\ 1, & if \quad \frac{\partial \mathcal{H}}{\partial u_2} < 0. \end{cases}$$

Proof. The minimality condition of PMP verifies that the optimal controls are achieved by solving $\frac{\partial \mathcal{H}}{\partial u_k} = 0$, using the same methods as in Mahata et al. (2022); Rosa & Torres (2023). Thus, these controls are provided as

$$\begin{cases} u_1(t) = \frac{\beta(I+\gamma_1 F_L+\gamma_2 S_L) I_T}{B_1 N} \left[(p_3 - p_1)S + \eta_1(1-p)(p_3 - p_2)V\right], \\ u_2(t) = \frac{(p_1-p_2)S}{B_2}, \\ u_3(t) = \frac{(p_4-p_5)I}{B_3}, \end{cases} \tag{5.33}$$

Theorem 5.11 *Let* $\tilde{u} = (\tilde{u_1}, \tilde{u_2}, \tilde{u_3})$ *be the optimal control and* $[\tilde{S}(.),\ \tilde{V}(.),\ \tilde{L}(.),\ \tilde{I}(.),\ \tilde{F_L}(.),\ \tilde{S_L}(.),\ \tilde{R}(.)]$ *be the corresponding unique optimal solutions of the optimal control problem (5.27), (5.29)–(5.31) with fixed final time* t_f*. Then there exists adjoint function* $\tilde{p}_j(\mathring{u}),\ j = 1, 2, \cdots, 7$ *satisfying the following equations:*

$$\begin{cases} {}_0^C D_t^{\psi} p_1(t) = \frac{\beta(1-u_1)(I+\gamma_1 F_L+\gamma_2 S_L)(p_1-p_3)}{N} + (\varphi + u_2 + \mu)p_1 - (\varphi + u_2)p_2, \\ {}_0^C D_t^{\psi} p_2(t) = -p\eta_1 p_1 + \frac{\beta\eta_1(1-p)(1-u_1)(I+\gamma_1 F_L+\gamma_2 S_L)(p_2-p_3)}{N} + (p\eta_1 + \mu)p_2, \\ {}_0^C D_t^{\psi} p_3(t) = -A_1 + d_1 p_3 - \alpha p_4, \\ {}_0^C D_t^{\psi} p_4(t) = -A_2 + \frac{\beta S(1-u_1)(p_1-p_3)}{N} + \frac{\beta\eta_1 V(1-p)(1-u_1)(p_2-p_3)}{N} + d_2 p_4 - d_4 p_5, \\ {}_0^C D_t^{\psi} p_5(t) = -A_3 + \frac{\beta\gamma_1 S(1-u_1)(p_1-p_3)}{N} + \frac{\beta\eta_1\gamma_1 V(1-p)(1-u_1)(p_2-p_3)}{N} - (1-q)\eta_2 p_3 \\ \qquad\qquad -q\eta_2 p_4 + d_5 p_5 - \omega p_6 - \nu_1 p_7, \\ {}_0^C D_t^{\psi} p_6(t) = -A_4 + \frac{\beta\gamma_2 S(1-u_1)(p_1-p_3)}{N} + \frac{\beta\eta_1\gamma_2 V(1-p)(1-u_1)(p_2-p_3)}{N} + d_6 p_6 - \nu_2 p_7, \\ {}_0^C D_t^{\psi} p_7(t) = -\phi p_1 + (\phi + \mu)p_7. \end{cases} \tag{5.34}$$

with initial conditions

$$p_j(t)|_{t=0} = 0,\ j = 1, 2, \cdots, 7. \tag{5.35}$$

Proof. The following relations can be used to obtain the adjoint system, which is a fractional system of right Riemann-Liouville derivatives.

$$ {}_tD^{\psi}_{t_f} p_1(t) = \frac{-\partial \mathcal{H}}{\partial S}, \quad {}_tD^{\psi}_{t_f} p_2(t) = \frac{-\partial \mathcal{H}}{\partial V}, \quad {}_tD^{\psi}_{t_f} p_3(t) = \frac{-\partial \mathcal{H}}{\partial L}, \quad {}_tD^{\psi}_{t_f} p_4(t) = \frac{-\partial \mathcal{H}}{\partial I}, $$

$$ {}_tD^{\psi}_{t_f} p_5(t) = \frac{-\partial \mathcal{H}}{\partial F_L}, \quad {}_tD^{\psi}_{t_f} p_6(t) = \frac{-\partial \mathcal{H}}{\partial S_L}, \quad {}_tD^{\psi}_{t_f} p_7(t) = \frac{-\partial \mathcal{H}}{\partial R} $$

More specifically this can be explained as

$$ \begin{cases} {}_tD^{\psi}_{t_f} p_1(t) = \frac{\beta(1-u_1)(I+\gamma_1 F_L+\gamma_2 S_L)(p_1-p_3)}{N} + (\varphi+u_2+\mu)p_1 - (\varphi+u_2)p_2, \\ {}_tD^{\psi}_{t_f} p_2(t) = -p\eta_1 p_1 + \frac{\beta\eta_1(1-p)(1-u_1)(I+\gamma_1 F_L+\gamma_2 S_L)(p_2-p_3)}{N} + (p\eta_1+\mu)p_2, \\ {}_tD^{\psi}_{t_f} p_3(t) = -A_1 + d_1 p_3 - \alpha p_4, \\ {}_tD^{\psi}_{t_f} p_4(t) = -A_2 + \frac{\beta S(1-u_1)(p_1-p_3)}{N} + \frac{\beta\eta_1 V(1-p)(1-u_1)(p_2-p_3)}{N} + d_2 p_4 - d_4 p_5, \\ {}_tD^{\psi}_{t_f} p_5(t) = -A_3 + \frac{\beta\gamma_1 S(1-u_1)(p_1-p_3)}{N} + \frac{\beta\eta_1\gamma_1 V(1-p)(1-u_1)(p_2-p_3)}{N} - (1-q)\eta_2 p_3 \\ \qquad -q\eta_2 p_4 + d_5 p_5 - \omega p_6 - \nu_1 p_7, \\ {}_tD^{\psi}_{t_f} p_6(t) = -A_4 + \frac{\beta\gamma_2 S(1-u_1)(p_1-p_3)}{N} + \frac{\beta\eta_1\gamma_2 V(1-p)(1-u_1)(p_2-p_3)}{N} + d_6 p_6 - \nu_2 p_7, \\ {}_tD^{\psi}_{t_f} p_7(t) = -\phi p_1 + (\phi+\mu)p_7. \end{cases} \tag{5.36} $$

With the transversality conditions

$$ {}_tD^{\psi-1}_{t_f} p_j(t)|_{t_f} = 0 \;\Leftrightarrow\; {}_tI^{1-\psi}_{t_f} p_j(t)|_{t_f} = p_j(t_f) = 0, \; j = 1, 2, \cdots, 7, \tag{5.37} $$

holds true where, ${}_tI^{1-\psi}_{t_f}$ is the right Riemann–Liouville fractional integral of order $1-\psi$.

Applying the change of variable $t' = t_f - t$, to equation (5.36) and to the transversality conditions (5.37), we obtain the following left Riemann–Liouville fractional initial value problem (Rosa & Torres, 2023):

$$ \begin{cases} {}_0D^{\psi}_{t'} p_1(t') = -[\frac{\beta(1-u_1)(I+\gamma_1 F_L+\gamma_2 S_L)(p_1-p_3)}{N} + (\varphi+u_2+\mu)p_1 - (\varphi+u_2)p_2], \\ {}_0D^{\psi}_{t'} p_2(t') = -[-p\eta_1 p_1 + \frac{\beta\eta_1(1-p)(1-u_1)(I+\gamma_1 F_L+\gamma_2 S_L)(p_2-p_3)}{N} + (p\eta_1+\mu)p_2], \\ {}_0D^{\psi}_{t'} p_3(t') = -[-A_1 + d_1 p_3 - \alpha p_4], \\ {}_0D^{\psi}_{t'} p_4(t') = -[-A_2 + \frac{\beta S(1-u_1)(p_1-p_3)}{N} + \frac{\beta\eta_1 V(1-p)(1-u_1)(p_2-p_3)}{N} + d_2 p_4 - d_4 p_5], \\ {}_0D^{\psi}_{t'} p_5(t') = -[-A_3 + \frac{\beta\gamma_1 S(1-u_1)(p_1-p_3)}{N} + \frac{\beta\eta_1\gamma_1 V(1-p)(1-u_1)(p_2-p_3)}{N} - (1-q)\eta_2 p_3 \\ \qquad -q\eta_2 p_4 + d_5 p_5 - \omega p_6 - \nu_1 p_7], \\ {}_0D^{\psi}_{t'} p_6(t') = -[-A_4 + \frac{\beta\gamma_2 S(1-u_1)(p_1-p_3)}{N} + \frac{\beta\eta_1\gamma_2 V(1-p)(1-u_1)(p_2-p_3)}{N} + d_6 p_6 - \nu_2 p_7], \\ {}_0D^{\psi}_{t'} p_7(t') = -[-\phi p_1 + (\phi+\mu)p_7], \end{cases} \tag{5.38} $$

with initial conditions

$$ p_j(t')|_{t'=0} = 0, \; j = 1, 2, \cdots, 7. \tag{5.39} $$

The initial conditions (5.39) imply that the adjoint system (5.38) can be considered as

a system of left Caputo fractional differential equations (5.34)-(5.35). This completes the proof.

5.4.3 Simulations of the FOCP

In this subsection, we examine the influence of control techniques on the spread of the TB epidemic and numerically explore the solution to the optimal control problem put forward in Section (5.4). The same algorithm we used so far under section (5.3) has been utilized again for this purpose.

To put it succinctly, we start by solving the control system using an initial estimate for the control variables. The present solution of state variables is then used to solve the adjoint system. After that, the controls are updated using a convex combination of the values calculated during the characterization procedure and the earlier controls. The state and adjoint system solutions are then repeated using the modified controls. Until a predetermined convergence threshold was satisfied, the iteration continued. We used the same TB epidemic initial conditions given under section (5.3) to demonstrate the numerical results. First, we show how the memory effects of the Caputo fractional operator affect the infected compartments in the dynamics of controlled tuberculosis transmission.

The values for $A_1,\ A_2,\ A_3,\ A_4,\ B_1, B_2$ and B_3 are selected in accordance with WHO recommendations (WHO, 2023b; Wolfe et al., 2024; WHO, 2023a, 2025a, 2024a). The significance of treating latent tuberculosis is represented by A_1. This course is essential for stopping the development of active tuberculosis. Given that this class directly contributes to transmission, A_2 indicates the necessity of treating active TB. The success of these treatments is essential for managing the condition, and A_3 denotes the efficacy of first-line therapy. The resource intensity of second-line treatments is represented by A_4; these treatments are usually less successful and require more resources than first-line treatments. B_1 denotes the significance of preventive measures in lowering the disease's incidence, B_2 denotes the efficiency of immunization control in preventing severe forms of TB, and B_3 denotes the pressing need for intensive treatment, which includes strict adherence to treatment guidelines and drug resistance monitoring for active TB cases. The WHO advises selecting A_1 from 0.5 to 1.0, A_2 from 1.0 to 1.5, A_3 from 0.8 to 1.2, A_4 from 0.5 to 0.8, B_1 from 1.0 to 1.5, B_2 from 0.5 to 1.0, and B_3 from 1.0 to 1.5.

Thus for simulation purpose we choose these values as $A_1 = 0.75, A_2 = 1.25, A_3 = 1, A_4 = 0.65, B_1 = 1.25, B_2 = 0.75$ and $B_3 = 1.25$. The ultimate intervention time $t_f = 5$ years are taken into consideration. Additionally, we limit the maximum values of the control variables by using $\sigma = 0.05$.

Remark 5.5 *The values of co-state functions are zero at the final time $t_f = 5$ years and as a result, all the control variables vanish at this time.*

We present a comparative analysis of the effects of control techniques on disease transmission under the following intervention strategies:

Strategy A: prevention alone $(u_1 \neq 0, u_2 = 0, u_3 = 0.)$

Strategy B: vaccination alone $(u_1 = 0, u_2 \neq 0, u_3 = 0.)$

Strategy C: treatment alone $(u_1 = 0, u_2 = 0, u_3 \neq 0.)$

Strategy D: prevention and vaccination $(u_1 \neq 0, u_2 \neq 0, u_3 = 0.)$

Strategy E: prevention and treatment $(u_1 \neq 0, u_2 = 0, u_3 \neq 0.)$

Strategy F: vaccination and treatment $(u_1 = 0, u_2 \neq 0, u_3 \neq 0.)$

Strategy G: all the three controls simultaneously $(u_1 \neq 0, u_2 \neq 0, u_3 \neq 0.)$

In the optimal control study of tuberculosis, Figures (5.5a)–(5.5d) show how the Caputo fractional order model is relevant in appropriately capturing the extended latency periods, the impacts of vaccination inefficacy, and delayed treatment effects. It is shown that the fractional order derivative plays an important role in the dynamics of controlled TB transmission. The simulation findings show that by taking memory effects into account, a Caputo fractional order derivative can be used to assist in the development of efficient preventative and control measures.

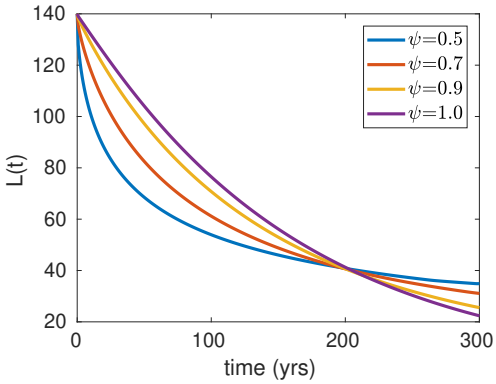

(a) Latent TB infected population for $\psi = (0.5, 0.7, 0.9, 1.0)$.

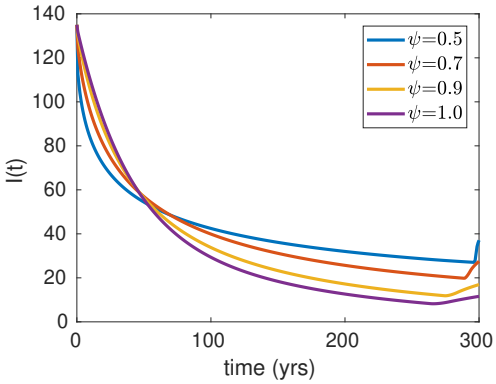

(b) Active TB infected population for $\psi = (0.5, 0.7, 0.9, 1.0)$.

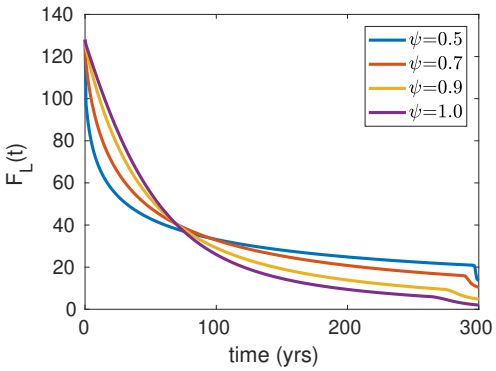

(c) Individuals receiving first-line TB treatment for $\alpha = (0.5, 0.7, 0.9, 1.0)$.

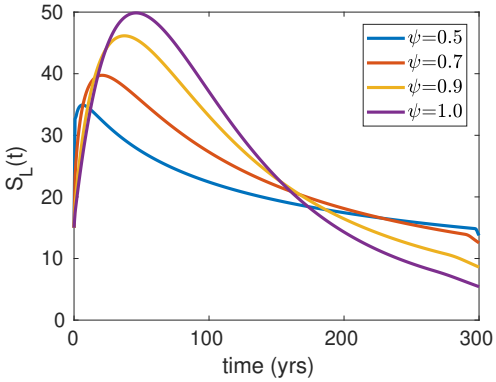

(d) Individuals receiving second-line TB treatment for $\alpha = (0.5, 0.7, 0.9, 1.0)$.

Figure 5.5: Graphs illustrating the memory effects of the Caputo fractional operator on the FOCP (5.27).

Efficiency Analysis of the Intervention Strategies

The effectiveness of an intervention strategy in epidemiological modeling is evaluated by the number of infection cases prevented during the intervention's implementation. The most effective strategy is the one with the highest efficiency index (Olaniyi, Abimbade, et al., 2024). According to Olaniyi et al. (2023), the efficiency index of an intervention strategy $\mathcal{X}$ is defined by

$$E.I(\mathcal{X}) = \frac{Total\ infection\ cases\ adverted\ by\ strategy\ \mathcal{X}}{Total\ infection\ cases\ in\ the\ absence\ of\ intervention\ strategies}, \quad (5.40)$$

where total infection cases adverted by strategy $\mathcal{X}$ is obtained by subtracting total number of infection cases in the presence of strategy $\mathcal{X}$ from total infection cases in the absence of strategy $\mathcal{X}$.

Consequently, the E.I of each intervention strategy is assessed using (5.40), and

the results are shown in Table (5.7). The study indicates that strategies F and G prevent the most infection cases with an E.I of 50.17%, whereas strategy A averts the least number of infection cases with an E.I of 28.27%. Therefore, out of the seven approaches that were studied, strategies F and G are the most effective intervention strategies. Strategies C and E are the second most effective intervention strategies.

Cost-Effectiveness Analysis of the Intervention Strategies

Although an intervention strategy might prevent the greatest number of infection cases in the community, its execution might not be cost-effective, particularly in situations where resources are scarce. Therefore, this study used the average cost-effectiveness ratio (ACER) approach to assess the cost-effectiveness of the seven intervention strategies. The ratio of the overall cost of implementing an intervention, which we obtain using formula (5.41) to the total number of infection cases prevented by the same intervention is known as the ACER of that intervention (Okosun et al., 2013). That is,

$$ACER(\mathcal{X}) = \frac{Total\ cost\ incured\ by\ intervention\ strategy\ \mathcal{X}}{Total\ infection\ cases\ averted\ by\ intervention\ strategy\ \mathcal{X}} \tag{5.41}$$

According to the ACER technique of cost analysis, the most cost-effective intervention is the one with the lowest ACER. Out of the seven intervention techniques, strategy B is the most cost-effective, as indicated by Table (5.7), which also has the lowest ACER of 0.0265. Strategy C is the next most cost-effective approach after strategy B, whereas strategy D, the combination of prevention and vaccination controls, which has an ACER of 0.0706, is the least cost-effective intervention plan. Figures (5.6a)

Table 5.7: Efficiency indices and ACER of the intervention strategies .

Strategy	Total infection averted	E.I	Total cost(in $)	ACER
A : $u_1(t)$ alone	56.4	28.27%	2.8203	0.0500
B : $u_2(t)$ alone	63.9	32.03%	1.6922	0.0265
C : $u_3(t)$ alone	97.3	48.77%	2.8203	0.0290
D : $u_1(t)u_2(t)$	63.9	32.03%	4.5125	0.0706
E : $u_1(t)u_3(t)$	97.3	48.77%	5.6406	0.0580
F : $u_2(t)u_3(t)$	100.09	50.17%	4.5125	0.0451
G : $u_1(t)u_2(t)u_3(t)$	100.09	50.17%	6.9662	0.0696

- (5.6d) examines how the control mechanisms mentioned above affect the dynamics of the fractional-order TB model when $\psi = 0.5$. It is readily apparent from Figure (5.6a) that with the application of strategy A, the total number of people in infected compartments has been reduced to 143.1. As it can be seen from Figure (5.6b), with the

implementation of strategies B and D, the total number of infected people fall to 135.6 whereas, utilizing strategies C and E forces the total number of infected individuals to drop to 102.2 which is depicted in Figure (5.6c). Additionally as demonstrate by Figure (5.6d), imposing strategies F and G reduce the total number of patients in infected compartments to 99.41.

The properties of the control functions $u_1(t)$, $u_2(t)$, and $u_3(t)$ are displayed in Figure (5.6e). The profile of the control function $u_1(t)$, shows that the control has been declined and set to zero value throughout the intervention period. A comeback in pathogen transmission and illness rates could result from this decline, which signifies a total loss of preventative effectiveness. For the first few years of the intervention period, a control function $u_2(t)$ remained constant before decaying exponentially to zero. On the other hand, $u_3(t)$ naturally declines to zero after continuing at a steady rate for many years of intervention time.

This chapter, develops and analyzes a Caputo fractional model with optimal control for TB transmission dynamics that incorporates vaccination and two lines of treatment modalities. Mathematical analysis shows that the TB-free equilibrium is locally asymptotically stable if all the eigenvalues of a linearized matrix satisfy the Matignon's stability criterion. The finding of sensitivity analysis indicates that lowering β, η_1, and increasing $\varphi, \theta, \omega, \nu_1, \nu_2$, significantly lower the infection prevalence of TB disease. The optimal control and cost-effectiveness analysis on the other hand shows that among the seven identified strategies, vaccination alone is the most cost-effective strategy to mitigate the disease. Furthermore, simulation results also demonstrate that by taking memory effects inherent in the transmission and treatment history of the disease into account, a Caputo fractional-order provides a more accurate understanding of the disease and assists to identify the most efficient and cost-effective mitigation strategy of TB disease.

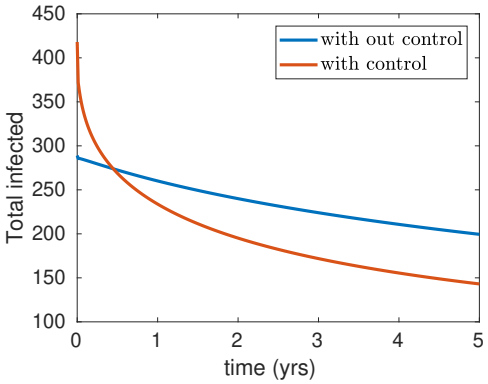

(a) Effect of strategy A on infected compartments.

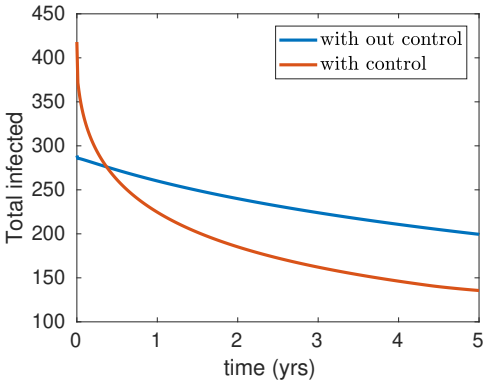

(b) Effects of strategies B and D on infected compartments.

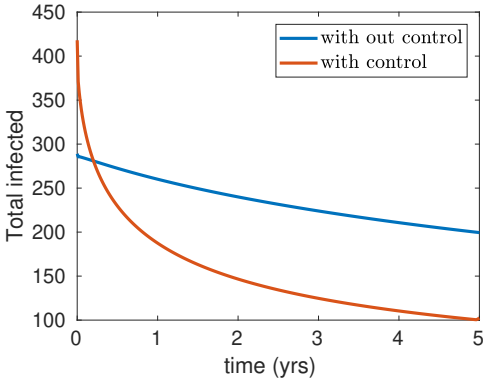

(c) Effects of strategies C and E on infected compartments.

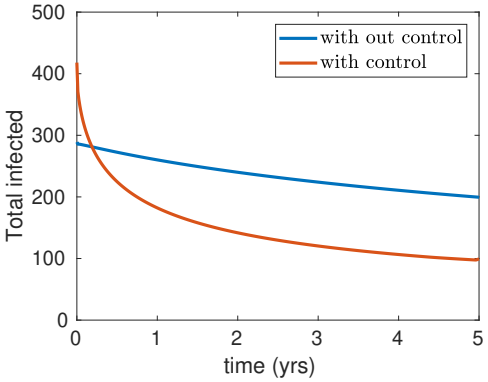

(d) Effects of strategies F and G on infected compartments.

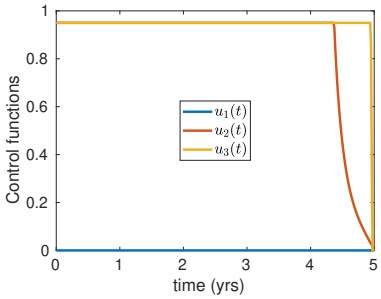

(e) Profiles of control functions

Figure 5.6: Effects of different strategies on fractional-order optimal control TB model and profiles of control functions $u_1(t),\ u_2(t)$ & $u_3(t)$ with $\psi = 0.8$.

CHAPTER 6

FRACTIONAL-ORDER MODELING OF HIV/AIDS-TB CO-INFECTION WITH VACCINATION AND TREATMENT

This chapter examines a Caputo approach mathematical model of HIV/AIDS and TB co-infection dynamics that considers vaccination for TB and treatment therapies for both. In addition to qualitative analysis of the model we have verified both mathematical and epidemiological well-posedness. The stability of the model equilibria are carried out. Furthermore, the numerical simulations of the model has been performed to assist the analytical results.

6.1 Model Formulation and Assumptions

This section examines a mathematical model for the dynamics of HIV/AIDS and TB co-infection using the Caputo fractional approach, which accounts for TB vaccination and treatment therapies for both diseases to examine their effects on the transmission dynamics of the disease. Therefore, we divided the human population under investigation into ten mutually exclusive compartments that represent different epidemiological states based on the epidemiological status of the diseases. People who are currently healthy but at risk of contracting HIV or TB are included in the Susceptible $S(t)$ compartment, highlighting the population that prevention measures should focus on. Despite not completely preventing the infection, the TB immunization that the Vaccinated class $V(t)$ have received lowers their risk of contracting active TB. The TB-Exposed class $E_T(t)$ denotes people with latent TB infections who do not exhibit any symptoms and are not infectious. The Active TB $I_T(t)$ compartment includes both infectious and symptomatic TB. Those who have recovered from TB but may eventually lose their immunity and revert to the susceptible condition are included in

the Recovered TB $R_T(t)$ compartment.

The HIV-Infected $I_H(t)$ class, which is essential for determining the spread of HIV, includes people who are infected with the virus but are not on ART. People who are co-infected with latent TB and HIV are denoted as $E_C(t)$, highlighting the necessity of coordinated treatment. People co-infected with active TB and HIV are grouped under $I_C(t)$ compartments, reflecting the increased mortality and transmission risks linked to co-infection. Those on ART are represented by the HIV-Treated $T_H(t)$ compartment, which is essential for assessing how well therapy lowers viral load and boosts immunity. Lastly, people with significant immune suppression and advanced HIV infection are included in the AIDS $A(t)$ compartment, which offers information on the course of the disease and long-term treatment results. The total population at a time t is given by:

$$N(t) = S(t) + V(t) + E_T(t) + I_T(t) + R_T(t) + I_H(t) + E_C(t) + I_C(t) + T_H(t) + A(t).$$

To formulate our model, the following basic assumptions are taken into considerations.

i) The model assumes a continuous recruitment rate Λ into the susceptible population through immigration or birth. We do, however, presume that there are no infectious immigrants or vertical transmission.

ii) The population size is not constant and it is assumed to be large. Therefore, the HIV and TB incidences are determined by the law of a standard incidence.

iii) Susceptible individuals gain TB with TB force of infection defined by $\lambda_{S_T} = \beta_T \left(\frac{I_T}{N} + \sigma \frac{I_C}{N}\right)$, where $\sigma \in (0, 1)$ indicates a change in the relative infectiousness of TB for individuals in the I_C class compared to those in the I_T class, and β_T is the effective contact rate for TB (Aggarwal et al., 2021).

iv) Individuals in $V(t)$ class are vaccinated at a rate ξ, and it is believed that the TB vaccination offers partial protection, reducing the infection rate among recipients to $\beta_T(1-\epsilon)$, where the efficiency of the vaccine is indicated by $\epsilon \in (0, 1)$ (Oshinubi et al., 2023). Because of the vaccine's shortcomings, vaccinated individuals may get infected with TB through a force of infection provided by $\lambda_{V_T} = \beta_T(1 - \epsilon)\left(\frac{I_T}{N} + \sigma \frac{I_C}{N}\right)$. Additionally, we assume that a specific proportion of vaccinated individuals return to the susceptible compartment as immunity deteriorates at a pace $\delta \in (0, 1)$.

v) We also suppose that susceptible persons can contract HIV with force of infection given as $\lambda_{S_H} = \beta_H \left(\frac{I_H}{N} + \rho_1 \frac{E_C}{N} + \rho_2 \frac{I_C}{N} + \rho_3 \frac{T_H}{N} + \rho_4 \frac{A}{N}\right)$. People in the E_T class

may get HIV infected and then join the E_C class with related force of infection $\lambda_{E_H} = \beta_H \left(\frac{I_H}{N} + \rho_2 \frac{I_C}{N} + \rho_3 \frac{T_H}{N} + \rho_4 \frac{A}{N} \right)$. Additionally, individuals in I_T class may contract HIV with a force of $\lambda_{I_H} = \beta_H \left(\frac{I_H}{N} + \rho_1 \frac{E_C}{N} + \rho_3 \frac{T_H}{N} + \rho_4 \frac{A}{N} \right)$ and join the I_C class. The effective contact rate for HIV is β_H, and the modification parameters $\rho_1, \rho_2, \rho_3, \rho_4 \in (0, 1)$ account for a decrease in the relative infectiousness of HIV for those in the E_C, I_C, T_H, and A classes relative to those in the I_H class. With the assumption that smaller value contributes to smaller reduction, and higher value accounts for higher decrease in the relative infectiousness of HIV, we adjust the values of modification parameters as $\rho_1 < \rho_2 < \rho_4 < \rho_3$ (Escombe et al., 2008; Windels et al., 2024).

vi) The population is considered to be homogeneous with regard to all epidemiological and biological factors, which may be considered as a drawback in fractional-order settings.

vii) Active TB-HIV co-infected individuals can contribute to the transmission of both diseases, but each transmission event involves only one pathogen at a time. In reality simultaneous or near-simultaneous infections occur in high burden settings. We exclude simultaneous dual infection events, as they are epidemiologically rare and introduce unnecessary complexity in model structure (Aggarwal et al., 2021; Ayele et al., 2024).

viii) HIV-positive people enroll in the T_H class in order to receive ART treatment at a rate η. It is assumed that individuals in the co-infected classes begin HIV and TB therapy at the same time. After being recovered from TB, people in the E_C, I_C classes transfer to the T_H class at the rates $(\eta + \theta_1)$, $(\eta + \theta_2)$ respectively. We assume that η is not constant and may not universally available, as it varies based on WHO guidelines. The WHO recommends that all individuals with HIV initiate ART as soon as possible after diagnosis, irrespective of CD4 cell counts, and emphasizes rapid ART initiation, ideally within one week or on the same day if ready. Adapting these guidelines to local contexts may result in variations in η based on resource availability, adherence levels, and historical practices . Thus, modeling η as a time-varying parameter is essential for accurately reflecting real-world conditions in HIV-TB co-infection dynamics (WHO, 2025).

Although latently TB infected persons are not infectious, they may contract active TB and become infectious when their immune system weakens. After successfully completing TPT, a certain percentage of people in the E_T class go on to the R_T class at a rate θ_1, while the remaining individuals move on to the I_T class at a rate κ_1, after exhibiting TB symptoms and being actively infected.

After successfully completing TB treatment, active TB patients enter the R_T class at a rate of θ_2. After losing their innate immunity, these individuals may return to the susceptible class at a rate ϕ. The rate at which members of the E_C class advance to the I_C class is κ_2. At a rate κ_3, those in the T_H class who do not adhere to effective HIV therapy move up to the A class. We assume that people in I_T have a μ_T TB-related death rate, people in I_H and E_C have a μ_H HIV-related death rate, people in A class have a μ_A AIDS-related death rate, and people in I_C class have a μ_C co-infection-related death rate. There is also a natural death rate μ for all classes. People move between compartments based on infection rates, vaccine effectiveness, treatment outcomes, and rates of natural or disease-related mortality.

The flow diagram of the model is illustrated in Figure (6.1).

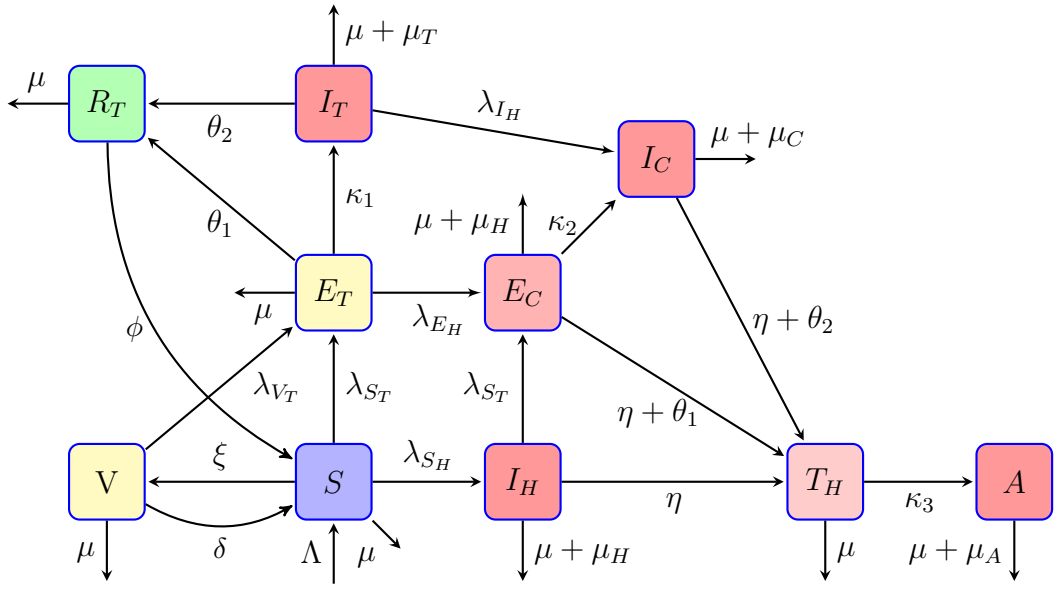

Figure 6.1: Schematic Diagram of HIV-TB Co-infection with Vaccination and Treatment

The governing integer- order non-linear systems of differential equations corresponding to Figure (6.1) can be written as

$$\begin{cases} \frac{dS}{dt} = \Lambda + \delta V + \phi R_T - (\lambda_{S_T} + \lambda_{S_H})S - (\mu + \xi)S, \\ \frac{dV}{dt} = \xi S - \lambda_{V_T} V - (\mu + \delta)V, \\ \frac{dE_T}{dt} = \lambda_{S_T} S + \lambda_{V_T} V - \lambda_{E_H} E_T - (\mu + \theta_1 + \kappa_1)E_T, \\ \frac{dI_T}{dt} = \kappa_1 E_T - \lambda_{I_H} I_T - (\theta_2 + \mu + \mu_T)I_T, \\ \frac{dR_T}{dt} = \theta_1 E_T + \theta_2 I_T - (\mu + \phi)R_T, \\ \frac{dI_H}{dt} = \lambda_{S_H} S - \lambda_{S_T} I_H - (\eta + \mu + \mu_H)I_H, \\ \frac{dE_C}{dt} = \lambda_{S_T} I_H + \lambda_{E_H} E_T - (\eta + \theta_1 + \kappa_2 + \mu + \mu_H)E_C, \\ \frac{dI_C}{dt} = \kappa_2 E_C + \lambda_{I_H} I_T - (\eta + \theta_2 + \mu + \mu_C)I_C, \\ \frac{dT_H}{dt} = \eta I_H + (\eta + \theta_1)E_C + (\eta + \theta_2)I_C - (\mu + \kappa_3)T_H, \\ \frac{dA}{dt} = \kappa_3 T_H - (\mu + \mu_A)A, \end{cases} \tag{6.1}$$

where $t > 0$ with initial conditions

$$\begin{aligned} S(0) = S_0 \geq 0,\ V(0) = V_0 \geq 0,\ E_T(0) = E_{T_0} > 0, \\ I_T(0) = I_{T_0} > 0,\ R_T(0) = R_{T_0} \geq 0,\ I_H(0) = I_{H_0} > 0, \\ E_C(0) = E_{C_0} > 0,\ I_C(0) = I_{C_0} > 0,\ T_H(0) = T_{H_0} \geq 0,\ A(0) = A_0 > 0, \end{aligned} \tag{6.2}$$

Caputo fractional-order models provide a deeper understanding of natural phenomena by accounting for memory effects and inherited features of the dynamical systems. The memory of past interactions between HIV and TB is well captured by fractional-order models, which also reflect the ongoing effects of prior infections and therapies on present health. They work well for simulating the intricate, nonlinear relationships between the two illnesses, particularly how the immune system changes over time. By adjusting the order of the fractional derivative, these models can simulate varying levels of responsiveness in biological systems, leading to more accurate representations of co-infection dynamics. They also take the nonlocal effects into consideration, showing how variations in one infection might affect another over time Podlubny (1998); Saeedian et al. (2017). Thus, motivated by this, we formulate a system of nonlinear Caputo

frational-oder differential equations associated to model (6.1) as

$$\begin{cases} {}_0^C D_t^\alpha S(t) = \Lambda + \delta V + \phi R_T - (\lambda_{S_T} + \lambda_{S_H})S - (\mu + \xi)S, \\ {}_0^C D_t^\alpha V(t) = \xi S - \lambda_{V_T} V - (\mu + \delta)V, \\ {}_0^C D_t^\alpha E_T(t) = \lambda_{S_T} S + \lambda_{V_T} V - \lambda_{E_H} E_T - (\mu + \theta_1 + \kappa_1)E_T, \\ {}_0^C D_t^\alpha I_T(t) = \kappa_1 E_T - \lambda_{I_H} I_T - (\theta_2 + \mu + \mu_T)I_T, \\ {}_0^C D_t^\alpha R_T(t) = \theta_1 E_T + \theta_2 I_T - (\mu + \phi)R_T, \\ {}_0^C D_t^\alpha I_H(t) = \lambda_{S_H} S - \lambda_{S_T} I_H - (\eta + \mu + \mu_H)I_H, \\ {}_0^C D_t^\alpha E_C(t) = \lambda_{S_T} I_H + \lambda_{E_H} E_T - (\eta + \theta_1 + \kappa_2 + \mu + \mu_H)E_C, \\ {}_0^C D_t^\alpha I_C(t) = \kappa_2 E_C + \lambda_{I_H} I_T - (\eta + \theta_2 + \mu + \mu_C)I_C, \\ {}_0^C D_t^\alpha T_H(t) = \eta I_H + (\eta + \theta_1)E_C + (\eta + \theta_2)I_C - (\mu + \kappa_3)T_H, \\ {}_0^C D_t^\alpha A(t) = \kappa_3 T_H - (\mu + \mu_A)A, \end{cases} \tag{6.3}$$

with initial conditions given as in (6.2), where $0 < \alpha \leq 1$ and ${}_0^C D_t^\alpha$ is the Caputo derivative.

Remark 6.1 *System (6.3) has an appropriate time dimensions since both its left and right hand sides have time dimension of $t^{-\alpha}$. Each model parameters are assumed to be non-negative and they depend on α (Dokoumetzidis et al., 2010; Almeida, 2018).*

6.2 Mathematical Analysis

6.2.1 Non-negativity and Boundedness of the Solution

Theorem 6.1 *For all $t \geq 0$, all the solution components $S(t)$, $V(t)$, $E_T(t)$, $I_T(t)$, $R_T(t)$, $I_H(t)$, $E_C(t)$, $I_C(t)$, $T_H(t)$ and $A(t)$ of the system (6.3) are non-negative and bounded. Furthermore, the closed region*

$$\Delta = \left\{ (S, V, E_T, I_T, R_T, I_H, E_C, I_C, T_H, A) \in \mathbb{R}_+^{10} : 0 < N \leq \frac{\Lambda}{\mu} \right\}$$

is positively invariant.

Proof. Using similar techniques in subsection (4.2.1) we obtain;

$${}_0^C D_t^\alpha S(t)|_{S=0} = \Lambda + \delta V + \phi R_T \geq 0 \ , \ {}_0^C D_t^\alpha V(t)|_{V=0} = \xi S \geq 0 \ ,$$

$${}_0^C D_t^\alpha E_T(t)|_{E_T=0} = \lambda_{S_T} S + \lambda_{V_T} V \geq 0 \ , \ {}_0^C D_t^\alpha I_T(t)|_{I_T=0} = \kappa_1 E_T \geq 0 \ ,$$

$${}_0^C D_t^\alpha R_T(t)|_{R_T=0} = \theta_1 E_T + \theta_2 I_T \geq 0 \ , \ {}_0^C D_t^\alpha I_H(t)|_{I_H=0} = \frac{\beta_H(\rho_1 E_C + \rho_2 I_C + \rho_3 T_H + \rho_4 A)S}{N} \geq 0 \ ,$$

Table 6.1: Description of biological model parameters.

Parameters	Descriptions
Λ	constant recruitment rate
β_T	effective contact rate for TB
β_H	effective contact rate for HIV
μ	natural death rate
μ_T	disease induced death rate for TB infectives
μ_H	disease induced death rate for HIV infectives
μ_A	disease induced death rate for AIDS
μ_C	disease induced death rate for HIV/AIDS-TB co-infectives
ξ	vaccination rate for TB
ϵ	vaccine efficacy
δ	vaccine wane rate
ϕ	rate of loss of natural immunity
θ_1	TPT treatment adherence rate for TB exposed people
θ_2	recovery rate of individuals from active TB infection
η	ART treatment adherence rate for HIV/AIDS infected individuals
κ_1	progression rate from E_T class to I_T class
κ_2	progression rate from E_C class to I_C class
κ_3	progression rate of individuals from T_H class to A class
σ	modification parameter for the relative infectiousness of TB for I_C class
$\rho_1, \rho_2,$	modification parameters for the relative infectiousness of HIV for E_C, I_C classes
ρ_3, ρ_4	modification parameters for the relative infectiousness of HIV for T_H, A classes

$${}_0^C D_t^\alpha E_C(t)|_{E_C=0} = \lambda_{S_T} I_H + \lambda_{E_H} E_T \geq 0 \ , \ {}_0^C D_t^\alpha I_C(t)|_{I_C=0} = \kappa_2 E_C + \lambda_{I_H} I_T \geq 0 \ ,$$

$${}_0^C D_t^\alpha T_H(t)|_{T_H=0} = \eta I_H + (\eta+\theta_1) E_C + (\eta+\theta_2) I_C \geq 0 \ , \ {}_0^C D_t^\alpha A(t)|_{A=0} = \kappa_3 T_H \geq 0 \, , \quad 0 < \alpha \leq 1.$$

Thus, on each hyperplane enclosing the non-negative area, the vector field $X = (S, V, E_T, I_T, R_T, I_H, E_C, I_C, T_H, A)^T$ points into $\mathbb{R}^{10}_+$. We therefore conclude that all of the solution components of system (6.3) are non-negative based on this fact and the fact that all of the initial conditions in (6.2) are non-negative.

Hence, the closed domain

$$\Delta = \left\{ (S, V, E_T, I_T, R_T, I_H, E_C, I_C, T_H, A) \in \mathbb{R}^{10}_+ : 0 < N \leq \frac{\Lambda}{\mu} \right\}$$

is positively invariant as any solution that starts in $\mathbb{R}^{10}_+$ remains in it.

Now, to show the boundedness we add all the equations in (6.3) to get:

$${}_0^C D_t^\alpha N(t) + \mu N(t) \leq \Lambda \tag{6.4}$$

After applying the Laplace transform on both sides of the inequality (6.4) we have,

$$\mathcal{L}\{{}_0^C D_t^\alpha N(t)\} + \mu \mathcal{L}\{N(t)\} \leq \Lambda \mathcal{L}\{1\},$$

and this yields to

$$s^\alpha N(s) - \sum_{k=0}^{n-1} s^{\alpha-k-1} N^{(k)}(0) + \mu N(s) \leq \Lambda \frac{1}{s} \tag{6.5}$$

From $0 < \alpha \leq 1$, we have $n = 1$ and obtain:

$$s^\alpha N(s) - s^{\alpha-1} N(0) + \mu N(s) \leq \Lambda \frac{1}{s}, \quad (s^\alpha + \mu) N(s) \leq \Lambda s^{-1} + N_0 s^{\alpha-1},$$

$$N(s) \leq \Lambda \frac{s^{-1}}{s^\alpha + \mu} + N_0 \frac{s^{\alpha-1}}{s^\alpha + \mu} \tag{6.6}$$

Now, applying the inverse Laplace transform on both sides the inequality (6.6) we have;

$$N(t) \leq \Lambda \mathcal{L}^{-1}\{\frac{s^{-1}}{s^\alpha + \mu}\} + N_0 \mathcal{L}^{-1}\{\frac{s^{\alpha-1}}{s^\alpha + \mu}\} \tag{6.7}$$

From the relation

$$\mathcal{L}^{-1}\{\frac{s^{\psi-\beta}}{s^\psi - \lambda}\} = t^{\beta-1} E_{\psi,\beta}(\lambda t^\psi)$$

and comparing its exponents with that of inequality (6.6) we get $\beta = \psi + 1$ for the first

term, $\beta = 1, \psi = \alpha$ for the second term and $\lambda = -\mu$. Thus, we have

$$\begin{aligned} N(t) &\leq \Lambda t^{\alpha+1-1} E_{\alpha,\alpha+1}(-\mu t^{\alpha}) + N_0 t^{1-1} E_{\alpha,1}(-\mu t^{\alpha}) \\ &= \Lambda t^{\alpha} E_{\alpha,\alpha+1}(-\mu t^{\alpha}) + N_0 E_{\alpha,1}(-\mu t^{\alpha}) \end{aligned} \tag{6.8}$$

Using the properties of Mittag-Leffler function we have,

$$E_{c,d}(z) = z E_{c,c+d}(z) + \frac{1}{\Gamma(d)},$$

and

$$E_{c,c+d}(z) = \frac{1}{z}\left(E_{c,d}(z) - \frac{1}{\Gamma(d)}\right) \tag{6.9}$$

Substituting $c = \alpha\ , d = 1$ and $z = -\mu t^{\alpha}$ in equation (6.9) we get

$$\begin{aligned} E_{\alpha,\alpha+1}(-\mu t^{\alpha}) &= \frac{1}{-\mu t^{\alpha}}\left(E_{\alpha,1}(-\mu t^{\alpha}) - \frac{1}{\Gamma(1)}\right) \\ &= \frac{1}{-\mu t^{\alpha}}\left(E_{\alpha,1}(-\mu t^{\alpha}) - 1\right)\ ,\ \Gamma(1) = 1 \end{aligned} \tag{6.10}$$

Using (6.10) in (6.8) we get

$$\begin{aligned} N(t) &\leq \Lambda t^{\alpha} E_{\alpha,\alpha+1}(-\mu t^{\alpha}) + N_0 E_{\alpha,1}(-\mu t^{\alpha}) \\ = (\Lambda t^{\alpha})\left(\frac{1}{-\mu t^{\alpha}}\right)\left(E_{\alpha,1}(-\mu t^{\alpha}) - 1\right) &+ N_0 E_{\alpha,1}(-\mu t^{\alpha}) \\ &= N_0 E_{\alpha,1}(-\mu t^{\alpha}) - \frac{\Lambda}{\mu} E_{\alpha,1}(-\mu t^{\alpha}) + \frac{\Lambda}{\mu} \\ &= \left(N_0 - \frac{\Lambda}{\mu}\right) E_{\alpha,1}(-\mu t^{\alpha}) + \frac{\Lambda}{\mu} \end{aligned} \tag{6.11}$$

Thus, if $N_0 \leq \frac{\Lambda}{\mu}$, then

$$\limsup_{t\to\infty}(N(t)) \leq \frac{\Lambda}{\mu}$$

Consequently, $\frac{\Lambda}{\mu}$ bounded $N(t)$ from above, indicating that every component of the solution is bounded. Boundedness and non-negativity are essential for ensuring that epidemiological models yield accurate and biologically meaningful predictions. Non-negativity reflects realistic population dynamics, while boundedness maintains reasonable limits on these dynamics. Together, these characteristics enhance the model's reliability, aiding in effective disease transmission analysis and public health planning.

6.2.2 Existence and Uniqueness of the Solution

Here, our goal is to prove that the solution to system (6.3) exists and is unique. Thus, rewrite equation (6.3) as

$$\begin{cases} {}_0^C D_t^\alpha S(t) = \mathcal{H}_1(t,S)\ , \quad {}_0^C D_t^\alpha V(t) = \mathcal{H}_2(t,V)\ , \\ {}_0^C D_t^\alpha E_T(t) = \mathcal{H}_3(t,E_T)\ , \quad {}_0^C D_t^\alpha I_T(t) = \mathcal{H}_4(t,I_T)\ , \\ {}_0^C D_t^\alpha R_T(t) = \mathcal{H}_5(t,R_T)\ , \quad {}_0^C D_t^\alpha I_H(t) = \mathcal{H}_6(t,I_H), \\ {}_0^C D_t^\alpha E_C(t) = \mathcal{H}_7(t,E_C), \quad {}_0^C D_t^\alpha I_C(t) = \mathcal{H}_8(t,I_C), \\ {}_0^C D_t^\alpha T_H(t) = \mathcal{H}_9(t,T_H), \quad {}_0^C D_t^\alpha A(t) = \mathcal{H}_{10}(t,A) \end{cases} \tag{6.12}$$

with the initial conditions given as in (6.2).
Where;

$$\begin{aligned} \mathcal{H}_1(t,S) &= \Lambda + \delta V + \phi R_T - (\lambda_{S_T} + \lambda_{S_H})S - (\mu + \xi)S, \\ \mathcal{H}_2(t,V) &= \xi S - \lambda_{V_T} V - (\mu + \delta)V, \\ \mathcal{H}_3(t,E_T) &= \lambda_{S_T} S + \lambda_{V_T} V - \lambda_{E_H} E_T - (\mu + \theta_1 + \kappa_1)E_T, \\ \mathcal{H}_4(t,I_T) &= \kappa_1 E_T - \lambda_{I_H} I_T - (\theta_2 + \mu + \mu_T)I_T, \\ \mathcal{H}_5(t,R_T) &= \theta_1 E_T + \theta_2 I_T - (\mu + \phi)R_T, \\ \mathcal{H}_6(t,I_H) &= \lambda_{S_H} S - \lambda_{S_T} I_H - (\eta + \mu + \mu_H)I_H, \\ \mathcal{H}_7(t,E_C) &= \lambda_{S_T} I_H + \lambda_{E_H} E_T - (\eta + \theta_1 + \kappa_2 + \mu + \mu_H)E_C, \\ \mathcal{H}_8(t,I_C) &= \kappa_2 E_C + \lambda_{I_H} I_T - (\eta + \theta_2 + \mu + \mu_C)I_C, \\ \mathcal{H}_9(t,T_H) &= \eta I_H + (\eta + \theta_1)E_C + (\eta + \theta_2)I_C - (\mu + \kappa_3)T_H, \\ \mathcal{H}_{10}(t,A) &= \kappa_3 T_H - (\mu + \mu_A)A. \end{aligned} \tag{6.13}$$

Taking integral transform on both sides of equation (6.12) we have

$$
\begin{aligned}
S(t) &= S_0 + \frac{1}{\Gamma(\alpha)}\int_0^t (t-\tau)^{\alpha-1}\mathcal{H}_1(\tau, S(\tau))d\tau,\\
V(t) &= V_0 + \frac{1}{\Gamma(\alpha)}\int_0^t (t-\tau)^{\alpha-1}\mathcal{H}_2(\tau, V(\tau))d\tau,\\
E_T(t) &= E_{T_0} + \frac{1}{\Gamma(\alpha)}\int_0^t (t-\tau)^{\alpha-1}\mathcal{H}_3(\tau, E_T(\tau))d\tau,\\
I_T(t) &= I_{T_0} + \frac{1}{\Gamma(\alpha)}\int_0^t (t-\tau)^{\alpha-1}\mathcal{H}_4(\tau, I_T(\tau))d\tau,\\
R_T(t) &= R_{T_0} + \frac{1}{\Gamma(\alpha)}\int_0^t (t-\tau)^{\alpha-1}\mathcal{H}_5(\tau, R_T(\tau))d\tau,\\
I_H(t) &= I_{H_0} + \frac{1}{\Gamma(\alpha)}\int_0^t (t-\tau)^{\alpha-1}\mathcal{H}_6(\tau, I_H(\tau))d\tau,\\
E_C(t) &= E_{C_0} + \frac{1}{\Gamma(\alpha)}\int_0^t (t-\tau)^{\alpha-1}\mathcal{H}_7(\tau, E_C(\tau))d\tau,\\
I_C(t) &= I_{C_0} + \frac{1}{\Gamma(\alpha)}\int_0^t (t-\tau)^{\alpha-1}\mathcal{H}_8(\tau, I_C(\tau))d\tau,\\
T_H(t) &= T_{H_0} + \frac{1}{\Gamma(\alpha)}\int_0^t (t-\tau)^{\alpha-1}\mathcal{H}_9(\tau, T_H(\tau))d\tau,\\
A(t) &= A_0 + \frac{1}{\Gamma(\alpha)}\int_0^t (t-\tau)^{\alpha-1}\mathcal{H}_{10}(\tau, A(\tau))d\tau.
\end{aligned}
\tag{6.14}
$$

Lemma 6.1 *For each $k = 1, 2, 3, \cdots, 10$, the kernels $\mathcal{H}_k$ are Lipschitz with corresponding Lipschitz constants Q_k and they are contractions provided that $0 < Q_k < 1$; where, $Q_1 = d_1 + d_3 + \mu + \xi$, $Q_2 = d_2 + \mu + \delta$, $Q_3 = d_4 + \mu + \theta_1 + \kappa_1$, $Q_4 = d_5 + \mu + \theta_2 + \mu_T$, $Q_5 = \mu + \phi$, $Q_6 = d_1 + \eta + \mu + \mu_H$, $Q_7 = \eta + \theta_1 + \kappa_2 + \mu + \mu_H$, $Q_8 = \eta + \theta_2 + \mu + \mu_C$, $Q_9 = \mu + \kappa_3$, $Q_{10} = \mu + \mu_A$ and $\lambda_{S_T}(t) \leq d_1$, $\lambda_{V_T}(t) \leq d_2$, $\lambda_{S_H}(t) \leq d_3$, $\lambda_{E_H}(t) \leq d_4$, $\lambda_{I_H}(t) \leq d_5$ are bounded functions.*

Proof. Following the same approach in Lemma (4.1), for S and S_1, we have $||\mathcal{H}_1(t, S) - \mathcal{H}_1(t, S_1)|| = ||-(\lambda_{S_T}(t) + \lambda_{S_H}(t) + \mu + \xi)(S - S_1)|| \leq (||\lambda_{S_T}(t)|| + ||\lambda_{S_H}(t)|| + \mu + \xi)||S - S_1|| = Q_1||S - S_1||$, with $Q_1 = d_1 + d_3 + \mu + \xi$. Hence, the kernel $\mathcal{H}_1$ is Lipschitz with a Lipschitz constant Q_1 and contraction provided that $0 < Q_1 < 1$.
Likewise, for V and V_1,
$||\mathcal{H}_2(t, V) - \mathcal{H}_2(t, V_1)|| = ||-(\lambda_{V_T}(t) + \mu + \delta)(V - V_1)|| \leq (||\lambda_{V_T}(t)|| + \mu + \delta)||V - V_1||$
$= Q_2||V - V_1||$, with $Q_2 = d_2 + \mu + \delta$. With a Lipschitz constant Q_2 , the kernel $\mathcal{H}_2$ is Lipschitz and contraction, given that $0 < Q_2 < 1$. The kernels $\mathcal{H}_j$ for $j = 3, 4, \cdots, 10$ can also be demonstrated to be Lipschitz and contraction with a Lipschitz constant Q_j as long as $0 < Q_j < 1$.

Theorem 6.2 *There exist at least one solution to the system (6.3) subject to the initial condition (6.2) provided that*

$$\frac{t^{\alpha}Q_k}{\Gamma(\alpha+1)} < 1$$

for each $k = 1, 2, \cdots, 10$.

Proof. Define the following recursive patterns using the same methods as in Theorem (5.2):

$$\Omega_{1n}(t) = S_n(t) - S_{n-1}(t) = \frac{1}{\Gamma(\alpha)}\int_0^t (\mathcal{H}_1(\tau, S_{n-1}) - \mathcal{H}_1(\tau, S_{n-2}))(t-\tau)^{\alpha-1}d\tau \ ,$$

$$\Omega_{2n}(t) = V_n(t) - V_{n-1}(t) = \frac{1}{\Gamma(\alpha)}\int_0^t (\mathcal{H}_2(\tau, V_{n-1}) - \mathcal{H}_2(\tau, V_{n-2}))(t-\tau)^{\alpha-1}d\tau \ ,$$

$$\Omega_{3n}(t) = E_{T_n}(t) - E_{T_{n-1}}(t) = \frac{1}{\Gamma(\alpha)}\int_0^t (\mathcal{H}_3(\tau, E_{T_{n-1}}) - \mathcal{H}_3(\tau, E_{T_{n-2}}))(t-\tau)^{\alpha-1}d\tau \ ,$$

$$\Omega_{4n}(t) = I_{T_n}(t) - I_{T_{n-1}}(t) = \frac{1}{\Gamma(\alpha)}\int_0^t (\mathcal{H}_4(\tau, I_{T_{n-1}}) - \mathcal{H}_4(\tau, I_{T_{n-2}}))(t-\tau)^{\alpha-1}d\tau \ ,$$

$$\Omega_{5n}(t) = R_{T_n}(t) - R_{T_{n-1}}(t) = \frac{1}{\Gamma(\alpha)}\int_0^t (\mathcal{H}_5(\tau, R_{T_{n-1}}) - \mathcal{H}_5(\tau, R_{T_{n-2}}))(t-\tau)^{\alpha-1}d\tau \ ,$$

$$\Omega_{6n}(t) = I_{H_n}(t) - I_{H_{n-1}}(t) = \frac{1}{\Gamma(\alpha)}\int_0^t (\mathcal{H}_6(\tau, I_{H_{n-1}}) - \mathcal{H}_6(\tau, I_{H_{n-2}}))(t-\tau)^{\alpha-1}d\tau \quad (6.15)$$

$$\Omega_{7n}(t) = E_{C_n}(t) - E_{C_{n-1}}(t) = \frac{1}{\Gamma(\alpha)}\int_0^t (\mathcal{H}_7(\tau, E_{C_{n-1}}) - \mathcal{H}_7(\tau, E_{C_{n-2}}))(t-\tau)^{\alpha-1}d\tau \ ,$$

$$\Omega_{8n}(t) = I_{C_n}(t) - I_{C_{n-1}}(t) = \frac{1}{\Gamma(\alpha)}\int_0^t (\mathcal{H}_8(\tau, I_{C_{n-1}}) - \mathcal{H}_8(\tau, I_{C_{n-2}}))(t-\tau)^{\alpha-1}d\tau \ ,$$

$$\Omega_{9n}(t) = T_{H_n}(t) - T_{H_{n-1}}(t) = \frac{1}{\Gamma(\alpha)}\int_0^t (\mathcal{H}_9(\tau, T_{H_{n-1}}) - \mathcal{H}_9(\tau, T_{H_{n-2}}))(t-\tau)^{\alpha-1}d\tau \ ,$$

$$\Omega_{10_n}(t) = A_n(t) - A_{n-1}(t) = \frac{1}{\Gamma(\alpha)}\int_0^t (\mathcal{H}_{10}(\tau, A_{n-1}) - \mathcal{H}_{10}(\tau, A_{n-2}))(t-\tau)^{\alpha-1}d\tau \ ,$$

with the initial conditions as in equation (6.2). Following additional algebraic adjustments and the application of the lipschitz condition from Lemma (6.1), we now

obtain

$$
\begin{aligned}
||S_n(t) - S_{n-1}(t)|| &\leq ||S_n(0)|| \left(\frac{t^\alpha Q_1}{\Gamma(\alpha+1)} \right)^n, \\
||V_n(t) - V_{n-1}(t)|| &\leq ||V_n(0)|| \left(\frac{t^\alpha Q_2}{\Gamma(\alpha+1)} \right)^n, \\
||E_{T_n}(t) - E_{T_{n-1}}(t)|| &\leq ||E_{T_n}(0)|| \left(\frac{t^\alpha Q_3}{\Gamma(\alpha+1)} \right)^n, \\
||I_{T_n}(t) - I_{T_{n-1}}(t)|| &\leq ||I_{T_n}(0)|| \left(\frac{t^\alpha Q_4}{\Gamma(\alpha+1)} \right)^n, \\
||R_{T_n}(t) - R_{T_{n-1}}(t)|| &\leq ||R_{T_n}(0)|| \left(\frac{t^\alpha Q_5}{\Gamma(\alpha+1)} \right)^n, \\
||I_{H_n}(t) - I_{H_{n-1}}(t)|| &\leq ||I_{H_n}(0)|| \left(\frac{t^\alpha Q_6}{\Gamma(\alpha+1)} \right)^n, \\
||E_{C_n}(t) - E_{C_{n-1}}(t)|| &\leq ||E_{C_n}(0)|| \left(\frac{t^\alpha Q_7}{\Gamma(\alpha+1)} \right)^n, \\
||I_{C_n}(t) - I_{C_{n-1}}(t)|| &\leq ||I_{C_n}(0)|| \left(\frac{t^\alpha Q_8}{\Gamma(\alpha+1)} \right)^n, \\
||T_{H_n}(t) - T_{H_{n-1}}(t)|| &\leq ||T_{H_n}(0)|| \left(\frac{t^\alpha Q_9}{\Gamma(\alpha+1)} \right)^n, \\
||A_n(t) - A_{n-1}(t)|| &\leq ||A_n(0)|| \left(\frac{t^\alpha Q_{10}}{\Gamma(\alpha+1)} \right)^n.
\end{aligned} \tag{6.16}
$$

The sequences $S_n,\ V_n,\ E_{T_n},\ I_{T_n},\ R_{T_n},\ I_{H_n},\ E_{C_n},\ I_{C_n},\ T_{H_n}$, and A_n are thus uniformly bounded. The next step is to show that these sequences uniformly converge to the integral solution (6.14) on a given interval I. This implies that they converge to the IVP solution (6.3) with initial condition (6.2).

Now, suppose the kernels $\mathcal{H}_j (j = 1, 2, \cdots, 10)$ are continuous on a closed region $\mathfrak{D} = \{(t, z) : |t - t_0| \leq a,\ ||z - z_0|| \leq b\}$ with

$$
\begin{aligned}
\mathcal{Z} &= \Big(\ S(t),\ V(t),\ E_T(t),\ I_T(t),\ R_T(t),\ I_H(t),\ E_C(t),\ I_C(t),\ T_H(t),\ A(t)\ \Big)^T, \\
\mathcal{Z}_0 &= \Big(\ S_0,\ V_0,\ E_{T_0},\ I_{T_0},\ R_{T_0},\ I_{H_0},\ E_{C_0},\ I_{C_0},\ T_{H_0},\ A_0\ \Big)^T.
\end{aligned} \tag{6.17}
$$

Define $M_j > 0$ such that $||\mathcal{H}_j|| < M_j$ for each $j = 1, 2, \cdots, 10$.

Let $I = [0, h]$ where, $h = min\left\{a, \frac{b}{M}\Gamma(\alpha+1)^{\frac{1}{\alpha}}\right\}$. Clearly, we can see that

$$
\mathcal{Z}_n = \mathcal{Z}_0 + \sum_{k=1}^{n} (\mathcal{Z}_k - \mathcal{Z}_{k-1}). \tag{6.18}
$$

It suffices to show that the series $\mathcal{Z}_0 + \sum_{k=1}^{n} (\mathcal{Z}_k - \mathcal{Z}_{k-1})$ converges uniformly on I in order to demonstrate that the sequence $\mathcal{Z}_n$ uniformly converges on I.

Thus,

$$||\mathcal{Z}_0 + \sum_{k=1}^{n}(\mathcal{Z}_k - \mathcal{Z}_{k-1})|| \leq ||\mathcal{Z}_0|| + \sum_{k=1}^{n} ||\mathcal{Z}_k - \mathcal{Z}_{k-1}||$$
$$\leq ||\mathcal{Z}_0|| + \sum_{k=1}^{n} ||\mathcal{Z}_k(0)|| \left(\frac{t^\alpha K_1}{\Gamma(\alpha+1)}\right)^k. \tag{6.19}$$

which converges uniformly on I provided that $\frac{t^\alpha K_1}{\Gamma(\alpha+1)} < 1$. A uniform convergence of the sequence $\mathcal{Z}_n$ on I is indicated by the Weierstrass M-test. The Lebesgue dominated convergence theorem may be used to show that this series converges to a limit point $\mathcal{Z}(t)$, which is the solution of the integral equation (6.14).
Hence, for each $k = 1, 2, \cdots, 10$, the system (6.3) subject to initial conditions (6.2) has at least one solution provided that $\frac{t^\alpha Q_k}{\Gamma(\alpha+1)} < 1$.

Theorem 6.3 *For each $j = 1, 2, \cdots, 10$, system (6.3), subject to the initial conditions (6.2) has a unique solution provided that*

$$1 - \frac{t^\alpha Q_j}{\Gamma(\alpha+1)} > 0.$$

Proof. The proof can be outlined in the same way we did for Theorem (4.3).

Epidemiological models require unique and existent solutions to ensure biological significance, with uniqueness providing stability and predictability in disease dynamics. Combined with non-negativity and boundedness, these properties enhance the accuracy of models, facilitating effective public health initiatives and a better understanding of disease transmission.

6.2.3 HIV/AIDS Sub-model

In this section, we examine the fundamental characteristics of model (6.3) on the assumption that there is no TB in the population. Therefore, the HIV/AIDS sub-model is established by setting all of the state variables and model parameters related to TB to zero and is given by

$$\begin{cases} {}_0^C D_t^\alpha S(t) = \Lambda - \beta_H \left(\frac{I_H + \rho_3 T_H + \rho_4 A}{N}\right) S - \mu S, \\ {}_0^C D_t^\alpha I_H(t) = \beta_H \left(\frac{I_H + \rho_3 T_H + \rho_4 A}{N}\right) S - (\eta + \mu + \mu_H) I_H, \\ {}_0^C D_t^\alpha T_H(t) = \eta I_H - (\mu + \kappa_3) T_H, \\ {}_0^C D_t^\alpha A(t) = \kappa_3 T_H - (\mu + \mu_A) A, \qquad 0 < \alpha \leq 1, \end{cases} \tag{6.20}$$

with initial conditions given as

$$S(0) = S_0 \geq 0,\ I_H(0) = I_{H_0} > 0,\ T_H(0) = T_{H_0} \geq 0,\ A(0) = A_0 > 0. \tag{6.21}$$

Basic Reproduction Number for HIV/AIDS Sub-model

Here, $\mathcal{E}^0_{H_A} = (\frac{\Lambda}{\mu}, 0, 0, 0)$ is the HIV/AIDS free equilibrium point (HIVAFEP) of the sub-model (6.20), which denotes the state in which the population is HIV/AIDS-free. The average number of secondary cases caused by a single infected person in a community that is completely susceptible is known as the basic reproduction number. The matrices corresponding to the new infection terms (F) and the transfer terms (V) are provided using the next-generation matrix-approach created in Zhu et al. (2020). Thus, we obtain

$$F = \begin{bmatrix} \beta_H & \rho_3\beta_H & \rho_4\beta_H \\ 0 & 0 & 0 \\ 0 & 0 & 0 \end{bmatrix},\quad V = \begin{bmatrix} \eta+\mu+\mu_H & 0 & 0 \\ -\eta & \mu+\kappa_3 & 0 \\ 0 & -\kappa_3 & \mu+\mu_A \end{bmatrix}.$$

Therefore, the basic reproduction number for HIV/AIDS which is the largest spectral radius of FV^{-1} becomes

$$\mathcal{R}^{(\alpha)}_{H_A} = \frac{\beta_H}{\eta+\mu+\mu_H}\left(1 + \frac{\eta\rho_3}{\kappa_3+\mu} + \frac{\eta\kappa_3\rho_4}{(\kappa_3+\mu)(\mu+\mu_A)}\right)\Psi(\alpha) \quad with\ \Psi(\alpha) > 0,$$

being a fractional correction factor.

In the expressions for $\mathcal{R}^{\alpha}_{H_A}$, the term $\frac{\beta_H}{\eta+\mu+\mu_H}\Psi(\alpha)$ indicates the average number of secondary infections that one HIV-positive individual usually causes, the term $\frac{\eta\rho_3\beta_H}{(\kappa_3+\mu)(\eta+\mu+\mu_H)}\Psi(\alpha)$ indicates a typical number of secondary cases caused by a single ART recipient, and the term $\frac{\eta\kappa_3\rho_4\beta_H}{(\kappa_3+\mu)(\mu+\mu_A)(\eta+\mu+\mu_H)}\Psi(\alpha)$ indicates the average number of additional infections that one AIDS patient produces. Additionally, the terms $\frac{1}{\eta+\mu+\mu_H}$, $\frac{1}{\mu+\kappa_3}$, and $\frac{1}{\mu+\mu_A}$, respectively, represent the average infectious periods of people with HIV, individuals receiving ART, and AIDS.

Stability Analysis of the HIV/AIDS Free Equilbrium Point

Theorem 6.4 *The HIV/AIDS free equilibrium point (HIVAFEP), $\mathcal{E}^0_{H_A}$ is locally asymptotically stable if $|arg(\lambda_i)| > \alpha\frac{\pi}{2}$ for all eigenvalue λ_i of $\mathcal{K}$, where $\mathcal{K}$ is a linearized matrix obtained by computing the Jacobian of system (6.20) at $\mathcal{E}^0_{H_A}$ and unstable if there exists at least one eigenvalue λ_i such that $|arg(\lambda_i)| < \alpha\frac{\pi}{2}$.*

Proof. The Jacobian of sub-model (6.20) evaluated at $\mathcal{E}^0_{H_A}$ is a linearized matrix

$$\mathcal{K} = \begin{bmatrix} -\mu & -\beta_H & -\beta_H\rho_3 & -\beta_H\rho_4 \\ 0 & \beta_H - (\eta+\mu+\mu_H) & \beta_H\rho_3 & \beta_H\rho_4 \\ 0 & \eta & -(\mu+\kappa_3) & 0 \\ 0 & 0 & \kappa_3 & -(\mu+\mu_A) \end{bmatrix}$$

After some algebraic simplifications, it can be shown that each eigenvalue λ_i $(i = 1, 2, 3, 4)$ of $\mathcal{K}$ satisfy the condition $|arg(\lambda_i)| > \frac{\alpha\pi}{2}$. Thus by Lemma (4.2), $\mathcal{E}^0_{H_A}$ is locally asymptotically stable.

Remark 6.2 *Epidemiologically speaking, HIV/AIDS can be eliminated from a population when the fractional-order α satisfy the condition $|arg(\lambda_i)| > \frac{\alpha\pi}{2}$ for each eigenvalue λ_i of the linearized matrix $\mathcal{K}$, because this ultimately leads to the infection's extinction. In contrast, if $|arg(\lambda_i)| < \frac{\alpha\pi}{2}$, for at least one eigenvalue λ_i, the illness keeps spreading across the population. We examine the global stability of the HIV/AIDS free equilibrium point in the following theorem.*

Theorem 6.5 *If $\mathcal{R}^{(\alpha)}_{H_A} < 1$, the HIV/AIDS free equilibrium point $\mathcal{E}^0_{H_A}$ of model (6.20) is globally asymptotically stable in its biologically feasible region*

$$\triangle_{\mathcal{H}} = \left\{ (S, I_H, T_H, A) \in \mathbb{R}^4_+ : 0 < N \leq \frac{\Lambda}{\mu} \right\}.$$

Proof. Consider a Lyapunov function:

$$V(\mathbf{y}) = \frac{1}{2}\|\mathbf{y}\|^2 = \frac{1}{2}\sum_{i=1}^{4} y_i^2, \quad with\ \mathbf{y} = \mathbf{X}_H - \mathcal{E}^0_H, \quad where\ \mathbf{X}_H = (S, I_H, T_H, A).$$

Employing the non-local nature of fractional derivatives, Lemma (4.7) and the systems dynamics, we compute:

$$\begin{aligned} \sum_{i=1}^{4} y_i \cdot {}^{C}_{0}D^{\alpha}_{t} y_i = {} & y_1\Big[\Lambda - \beta_H\left(\frac{I_H + \rho_3 T_H + \rho_4 A}{N}\right) S - \mu S\Big] \\ & + y_2\Big[\beta_H\left(\frac{I_H + \rho_3 T_H + \rho_4 A}{N}\right) S - (\eta+\mu+\mu_H) I_H\Big] \\ & + y_3\Big[\eta I_H - (\mu+\kappa_3) T_H\Big] + y_4\Big[\kappa_3 T_H - (\mu+\mu_A) A\Big]. \end{aligned}$$

The following hold at $\mathcal{E}^0$:

$$\Lambda = \Big[\beta_H\left(\frac{I_H + \rho_3 T_H + \rho_4 A}{N}\right) + \mu\Big] S^0, \quad \beta_H\left(\frac{I_H + \rho_3 T_H + \rho_4 A}{N}\right) S = (\eta+\mu+\mu_H)\, I^0_H,$$

$$\eta I_H = (\mu + \kappa_3)T_H^0, \quad \kappa_3 T_H = (\mu + \mu_A)A^0.$$

Substituting these into the derivative expression and simplifying yields:

$$\sum_{i=1}^{4} y_i \cdot {}_0^C D_t^\alpha y_i \leq -\sum_{i=1}^{4} c_i y_i^2$$

Using this into Lemma (4.7) we get

$${}_0^C D_t^\alpha V(\mathbf{y}(t)) \leq -\sum_{i=1}^{4} c_i y_i^2 + \mathcal{R}(\mathbf{y}),$$

where $c_i > 0$ and $\mathcal{R}(\mathbf{y})$ denotes bounded cross terms. Applying Young's inequality:

$$|y_i y_j| \leq \frac{\varepsilon}{2} y_i^2 + \frac{1}{2\varepsilon} y_j^2,$$

we bound $\mathcal{R}(\mathbf{y})$ and absorb it into the main negative definite term to get

$${}_0^C D_t^\alpha V(\mathbf{y}) \leq -c\|\mathbf{y}\|^2 < 0, \ \forall_x \neq \mathcal{E}^0, \quad \text{and for some constant } c > 0.$$

The fractional derivative of the Lyapunov function is negative semi definite. Thus, by Corollary (4.1) , $\mathcal{E}^0$ is globally asymptotically stable in its feasible region if $\mathcal{R}_{H_A}^{(\alpha)} < 1$.

The HIV/AIDS Endemic Equilibrium Point

Theorem 6.6 *If $\mathcal{R}_{H_A}^{(\alpha)} > 1$, the sub-model (6.20) has a unique positive HIV/AIDS endemic equilibrium point, $\mathcal{E}_{H_A}^* = (S^*, I_H^*, T_H^*, A^*)$.*

Proof. The HIV/AIDS endemic equilibrium point is the state at which the disease persists in the community. Thus, following the same approaches in Theorem 2 of Aldila et al. (2020) and Theorem (3.3) of Khajanchi et al. (2018), we solve the system

$$\begin{cases} \Lambda - \beta_H \left(\frac{I_H^* + \rho_3 T_H^* + \rho_4 A^*}{N^*}\right) S^* - \mu S^* = 0, \\ \beta_H \left(\frac{I_H^* + \rho_3 T_H^* + \rho_4 A^*}{N^*}\right) S^* - (\eta + \mu + \mu_H) I_H^* = 0, \\ \eta I_H^* - (\mu + \kappa_3) T_H^* = 0, \\ \kappa_3 T_H^* - (\mu + \mu_A) A^* = 0. \end{cases} \tag{6.22}$$

Thus, after solving for S^*, I_H^*, T_H^* and A^* implicitly from (6.22) we obtain

$$S^* = \frac{\Lambda N^*}{(\eta + \mu + \mu_H)\mathcal{R}_{H_A} I_H^* + \mu N^*}, \ I_H^* = \frac{\beta_H}{\eta + \mu + \mu_H} \left(\frac{I_H^* + \rho_3 T_H^* + \rho_4 A^*}{N^*}\right) S^*,$$

$$T_H^* = \frac{\eta I_H^*}{\mu + \kappa_3}, \ A^* = \frac{\eta \kappa_3 I_H^*}{(\mu + \kappa_3)(\mu + \mu_A)}.$$

This completes the proof.

To determine the condition under which the HIVAEEP, $\mathcal{E}^*_{H_A}$ is locally asymptotically stable, we compute the Jacobian of (6.20) and evaluate it at $\mathcal{E}^*_{H_A}$ to obtain a linearized matrix

$$\mathcal{C} = \begin{bmatrix} -a-\mu & -b & -b\rho_3 & -b\rho_4 \\ a & b-e & b\rho_3 & b\rho_4 \\ 0 & \eta & -c & 0 \\ 0 & 0 & \kappa_3 & -d \end{bmatrix}$$

where $a = \beta_H \left(\frac{I^*_H+\rho_3 T^*_H+\rho_4 A^*}{N^*}\right)$, $b = \beta_H \frac{S^*}{N^*}$, $c = \mu+\kappa_3$, $d = \mu+\mu_A$ and $e = \eta+\mu+\mu_H$. A corresponding characteristic polynomial of matrix $\mathcal{C}$ is

$$\mathcal{P}(\lambda) = \lambda^4 + m_1\lambda^3 + m_2\lambda^2 + m_3\lambda + m_4 \tag{6.23}$$

where $m_1 = a-b+c+d+e+\mu$, $m_2 = (a+\mu)e-\mu b+(c+d)(a-b+e+\mu)+cd-b\eta\rho_3$,
$m_3 = (c+d)(ae+\mu e-\mu b)+cd(a-b+e+\mu)-(a+d+\mu)b\eta\rho_3-b\eta\rho_4\kappa_3$,
$m_4 = cd(ae+\mu e-\mu b)-b\eta(a+\mu)(d\rho_3+\kappa_3\rho_4)+b\eta\kappa_3\rho_4$.
In the following theorem we state the condition under which the HIVAEEP, $\mathcal{E}^*_{H_A}$ is locally asymptotically stable.

Theorem 6.7 *(Bourafa et al., 2020)*

i) If the discriminant of the above polynomial is negative, $m_i > 0$ for all $i = 1, 2, 3, 4$ then $\mathcal{E}^*_{H_A}$ is locally asymptotically stable for all $\alpha \in [0, \frac{1}{2}]$.

ii) If the discriminant of the above polynomial is negative, $m_i > 0$ for all $i = 1, 2, 3, 4$ and
$m_2 = \frac{m_1 m_4}{m_3} + \frac{m_3}{m_1}$, then $\mathcal{E}^*_{H_A}$ is locally asymptotically stable for all $\alpha \in [0, 1]$.

Theorem 6.8 *When $\mathcal{R}^{(\alpha)}_{H_A} > 1$, the unique positive HIV/AIDS endemic equilibrium $\mathcal{E}^*_{H_A}$ of the HIV/AIDS sub-model (6.20) is globally asymptotically stable in its biologically feasible region*

$$\triangle_{\mathcal{H}} = \left\{ (S, I_H, T_H, A) \in \mathbb{R}^4_+ : 0 < N \leq \frac{\Lambda}{\mu} \right\}.$$

Proof. As we did under Theorem (6.5) let us define a Lyapunov function

$$V(\mathbf{y}) = \frac{1}{2}\|\mathbf{y}\|^2 = \frac{1}{2}\sum_{i=1}^{4} y_i^2, \quad \textit{with } \mathbf{y} = \mathbf{X}_H - \mathcal{E}^*_H, \quad \textit{where } \mathbf{X}_H = (S, I_H, T_H, A).$$

From the non-local nature of fractional derivatives, and using Lemma (4.7) we have:

$$\begin{aligned}\sum_{i=1}^{4} y_i \cdot {}_0^C D_t^\alpha y_i = y_1\Big[\Lambda - \beta_H\left(\frac{I_H + \rho_3 T_H + \rho_4 A}{N}\right) S - \mu S\Big] \\ + y_2\Big[\beta_H\left(\frac{I_H + \rho_3 T_H + \rho_4 A}{N}\right) S - (\eta + \mu + \mu_H) I_H\Big] \\ + y_3\Big[\eta I_H - (\mu + \kappa_3) T_H\Big] + y_4\Big[\kappa_3 T_H - (\mu + \mu_A) A\Big].\end{aligned}$$

At $\mathcal{E}^*$ we get

$$\Lambda = \Big[\beta_H\left(\frac{I_H^* + \rho_3 T_H^* + \rho_4 A^*}{N^*}\right) + \mu\Big] S^*, \quad \beta_H\left(\frac{\rho_3 T_H^* + \rho_4 A^*}{N^*}\right) S^* = \left(\frac{\beta_H}{N^*} + \eta + \mu + \mu_H\right) I_H^*,$$

$$\eta I_H^* = (\mu + \kappa_3) T_H^*, \ \kappa_3 T_H^* = (\mu + \mu_A) A^*.$$

Substituting these into the derivative expression and simplifying yields:

$$\sum_{i=1}^{4} y_i \cdot {}_0^C D_t^\alpha y_i \leq -\sum_{i=1}^{4} c_i y_i^2$$

Using this into Lemma (4.7) we get

$${}_0^C D_t^\alpha V(\mathbf{y}(t)) \leq -\sum_{i=1}^{4} c_i y_i^2 + \mathcal{R}(\mathbf{y}),$$

where $c_i > 0$ and $\mathcal{R}(\mathbf{y})$ denotes bounded cross terms. Applying Young's inequality:

$$|y_i y_j| \leq \frac{\varepsilon}{2} y_i^2 + \frac{1}{2\varepsilon} y_j^2,$$

we bound $\mathcal{R}(\mathbf{y})$ and absorb it into the main negative definite term to get

$${}_0^C D_t^\alpha V(\mathbf{y}) \leq -c\|\mathbf{y}\|^2 < 0, \ \forall_x \neq \mathcal{E}^*, \quad \text{and for some constant } c > 0.$$

The fractional derivative of the Lyapunov function is negative semi definite. Thus, by Corollary (4.1), $\mathcal{E}^*$ is globally asymptotically stable in its feasible region. Epidemiologically, this finding implies that, while $\mathcal{R}_{H_A}^{(\alpha)} > 1$, it will be difficult to eradicate HIV/AIDS from the population in the long run.

6.2.4 The TB Sub-model

Assuming that there is no HIV/AIDS in the population, we examine the fundamental characteristics of model (6.3) in this section. When all of the state variables

I_H, E_C, I_C, T_H, and A are set to zero, the TB sub-model thus becomes

$$\begin{cases} {}_0^C D_t^\alpha S(t) = \Lambda + \delta V + \phi R_T - \beta_T \frac{I_T}{N} S - (\mu + \xi) S, \\ {}_0^C D_t^\alpha V(t) = \xi S - \beta_T (1-\epsilon) \frac{I_T}{N} V - (\mu + \delta) V, \\ {}_0^C D_t^\alpha E_T(t) = \beta_T \frac{I_T}{N} S + \beta_T (1-\epsilon) \frac{I_T}{N} V - (\mu + \theta_1 + \kappa_1) E_T, \\ {}_0^C D_t^\alpha I_T(t) = \kappa_1 E_T - (\theta_2 + \mu + \mu_T) I_T, \\ {}_0^C D_t^\alpha R_T(t) = \theta_1 E_T + \theta_2 I_T - (\mu + \phi) R_T, \qquad 0 < \alpha \leq 1, \end{cases} \tag{6.24}$$

with the initial conditions given as

$$\begin{aligned} S(0) = S_0 \geq 0,\ V(0) = V_0 \geq 0,\ E_T(0) = E_{T_0} > 0, \\ I_T(0) = I_{T_0} > 0,\ R_T(0) = R_{T_0} \geq 0. \end{aligned} \tag{6.25}$$

Basic Reproduction Number for TB Sub-model

The TB free equilibrium point (TBFEP) of the sub-model (6.24) which refers to the condition in which the population is free from TB is computed as

$$\mathcal{E}_T^0 = \left(\frac{\Lambda(\mu + \delta)}{\mu(\mu + \xi + \delta)}, \frac{\Lambda \xi}{\mu(\mu + \xi + \delta)}, 0, 0, 0 \right).$$

To compute basic reproduction number corresponding to TB, we follow the next-generation matrix-approach developed in Zhu et al. (2020). Thus, the matrices corresponding to the new infection terms (F) and the transfer terms (V) are given as

$$F = \begin{bmatrix} 0 & \beta_T \left(\frac{S^0 + (1-\epsilon) V^0}{N^0} \right) \\ 0 & 0 \end{bmatrix} = \begin{bmatrix} 0 & \beta_T \left(1 - \frac{\epsilon \xi}{\mu + \delta + \xi} \right) \\ 0 & 0 \end{bmatrix},\ V = \begin{bmatrix} \mu + \theta_1 + \kappa_1 & 0 \\ -\kappa_1 & (\theta_2 + \mu + \mu_T) \end{bmatrix},$$

$$FV^{-1} = \begin{bmatrix} 0 & \beta_T \left(1 - \frac{\epsilon \xi}{\mu + \delta + \xi} \right) \\ 0 & 0 \end{bmatrix} \begin{bmatrix} \frac{1}{\mu + \theta_1 + \kappa_1} & 0 \\ \frac{\kappa_1}{(\mu + \theta_1 + \kappa_1)(\theta_2 + \mu + \mu_T)} & \frac{1}{\theta_2 + \mu + \mu_T} \end{bmatrix}$$

$$= \begin{bmatrix} \frac{\beta_T \kappa_1 \left(1 - \frac{\epsilon \xi}{\mu + \delta + \xi} \right)}{(\mu + \theta_1 + \kappa_1)(\theta_2 + \mu + \mu_T)} & \frac{\beta_T \left(1 - \frac{\epsilon \xi}{\mu + \delta + \xi} \right)}{\theta_2 + \mu + \mu_T} \\ 0 & 0 \end{bmatrix}$$

Therefore, the basic reproduction number is the largest spectral radius of FV^{-1} and is given as

$$\mathcal{R}_T^{(\alpha)} = \frac{\beta_T \kappa_1 \left(\mu + \delta + (1-\epsilon) \xi \right)}{(\mu + \theta_1 + \kappa_1)(\theta_2 + \mu + \mu_T)(\mu + \delta + \xi)} \Psi_T(\alpha),$$

with $\Psi_T(\alpha)$ being a fractional correction factor.

Bifurcation Analysis of the TB Sub-model

Let

$$x = [x_1, x_2, x_3, x_4, x_5]^T = [S, V, E_T, I_T, R_T]^T$$

Then, the TB sub-model (6.24) can be written compactly in the form of

$$\begin{cases} {}_0^C D_t^\alpha x_1(t) = \Lambda + \delta x_2 + \phi x_5 - \beta_T \frac{x_4}{N} x_1 - g_1 x_1 = f_1(x_1, x_2, x_3, x_4, x_5), \\ {}_0^C D_t^\alpha x_2(t) = \xi x_1 - \beta_T (1-\epsilon) \frac{x_4}{N} x_2 - g_2 x_2 = f_2(x_1, x_2, x_3, x_4, x_5), \\ {}_0^C D_t^\alpha x_3(t) = \beta_T \frac{x_4}{N} x_1 + \beta_T (1-\epsilon) \frac{x_4}{N} x_2 - g_3 x_3 = f_3(x_1, x_2, x_3, x_4, x_5), \\ {}_0^C D_t^\alpha x_4(t) = \kappa_1 x_3 - g_4 x_4 = f_4(x_1, x_2, x_3, x_4, x_5), \\ {}_0^C D_t^\alpha x_5(t) = \theta_1 x_3 + \theta_2 x_4 - g_5 x_5 = f_5(x_1, x_2, x_3, x_4, x_5), \end{cases} \tag{6.26}$$

with $g_1 = \mu + \xi$, $g_2 = \mu + \delta$, $g_3 = \mu + \theta_1 + \kappa_1$, $g_4 = \mu + \theta_2 + \mu_T$, $g_5 = \mu + \phi$ and $N = x_1 + x_2 + x_3 + x_4 + x_5$.

Choosing $\delta = \delta^*$ as a bifurcation parameter and evaluating the Jacobean of system (6.24) at $(\mathcal{E}_T^0, \delta^*)$ we obtain

$$\mathcal{J} = \begin{bmatrix} -g_1 & \delta^* & 0 & -q_1 & \phi \\ \xi & -g_2 & 0 & -q_2 & 0 \\ 0 & 0 & -g_3 & c & 0 \\ 0 & 0 & \kappa_1 & -g_4 & 0 \\ 0 & 0 & 0 & \theta_2 & -g_5 \end{bmatrix}.$$

where, $q_1 = \beta_T \frac{S^0}{N^0}$, $q_2 = \beta_T \frac{(1-\epsilon)V^0}{N^0}$ and $c = q_1 + q_2$.

Using a computer algebra system, we can show that $\mathcal{J}$ has a simple zero eigenvalue, while the other eigenvalues are either negative or have negative real parts. The equilibrium $\mathcal{E}_T^0$ is hence non-hyperbolic. To get the bifurcation point, we set $\mathcal{R}_T^{(\alpha)} = 1$ and solve for $\delta = \delta^* = -(\mu + \xi)$.

Let $u = (u_1, u_2, u_3, u_4, u_5)^T$ and $v = (v_1, v_2, v_3, v_4, v_5)$ be respectively the right and left eigenvectors associated to the zero eigenvalue. Then, solving $\mathcal{J}(\mathcal{E}_T^0, \beta_T^*).u = 0$ we get,

$$\begin{bmatrix} -g_1 & \delta & 0 & -q_1 & \phi \\ \xi & -g_2 & 0 & -q_2 & 0 \\ 0 & 0 & -g_3 & c & 0 \\ 0 & 0 & \kappa_1 & -g_4 & 0 \\ 0 & 0 & 0 & \theta_2 & -g_5 \end{bmatrix} . \begin{bmatrix} u_1 \\ u_2 \\ u_3 \\ u_4 \\ u_5 \end{bmatrix} = 0,$$

which has a trivial solutions $u_i = 0$, for all $i = 1, 2, \cdots, 5$. Similarly, solving

$$v.\mathcal{J}(\mathcal{E}_T^0, \beta_T^*) = \begin{bmatrix} v_1 & v_2 & v_3 & v_4 & v_5 \end{bmatrix} . \begin{bmatrix} -g_1 & \delta & 0 & -q_1 & \phi \\ \xi & -g_2 & 0 & -q_2 & 0 \\ 0 & 0 & -g_3 & c & 0 \\ 0 & 0 & \kappa_1 & -g_4 & 0 \\ 0 & 0 & 0 & \theta_2 & -g_5 \end{bmatrix} = 0$$

will give us a trivial solution $v_i = 0$, for all $i = 1, 2, \cdots, 5$.

We observe that the eigenvectors u and v cannot satisfy the requirement $u.v = 1$ and the bifurcation coefficients a, b defined by

$$a = \sum_{k,i,j=1}^{5} v_k u_i u_j \frac{\partial^2 f_k}{\partial x_i \partial x_j} |(\mathcal{E}_T^0, \beta_T^*), \; b = \sum_{k,i=1}^{5} v_k u_i \frac{\partial^2 f_k}{\partial x_i \partial \beta_T} |(\mathcal{E}_T^0, \beta_T^*)$$

are both zero. Thus, with the center manifold theory it may be difficult to determine the direction of the bifurcation.

When both bifurcation coefficients are zero, the analysis of nonlinear dynamical systems becomes complex, indicating non-hyperbolic behavior and the potential for backward bifurcations. This condition suggests that linearization alone cannot determine stability or bifurcation direction, necessitating further exploration of higher-order terms. The equilibrium point then requires additional investigation into the dynamics through nonlinear methods. Such a degenerate bifurcation can lead to phenomena like pitchfork or transcritical bifurcations, where stability properties may change without clear transitions from linear terms (C. Castillo-Chavez & Song, 2004; Gómez-Acevedo & Li, 2005; Chinviriyasit et al., 2018).

Stability Analysis of the TB Free Equilibrium Point

Theorem 6.9 *The TB free equilibrium point (TBFEP), $\mathcal{E}_T^0$ is locally asymptotically stable if $|arg(\lambda_i)| > \alpha\frac{\pi}{2}$ for all eigenvalue λ_i of $\mathcal{M}$, where $\mathcal{M}$ is a linearized matrix obtained by computing the Jacobian of system (6.24) at $\mathcal{E}_T^0$ and unstable if there exists at least one eigenvalue λ_i such that $|arg(\lambda_i)| < \alpha\frac{\pi}{2}$.*

Proof. The Jacobian of sub-model (6.24) evaluated at $\mathcal{E}_T^0$ is a linearized matrix

$$\mathcal{M} = \begin{bmatrix} -p_1 & \delta & 0 & -q_1 & \phi \\ \xi & -p_2 & 0 & -q_2 & 0 \\ 0 & 0 & -p_3 & c & 0 \\ 0 & 0 & \kappa_1 & -p_4 & 0 \\ 0 & 0 & 0 & \theta_2 & -p_5 \end{bmatrix},$$

where $p_1 = \mu+\xi,\ p_2 = \mu+\delta,\ p_3 = \mu+\theta_1+\kappa_1,\ p_4 = \theta_2+\mu+\mu_T,\ p_5 = \mu+\phi,\ q_1 = \beta_T\frac{S^0}{N^0}$, $q_2 = \beta_T\frac{(1-\epsilon)V^0}{N^0}$ and $c = q_1 + q_2 = \beta_T\left[\frac{S^0+(1-\epsilon)V^0}{N^0}\right] = \beta_T\left(\frac{\mu+\delta+\xi-\epsilon\xi}{\mu+\delta+\xi}\right)$.

Numerical computations confirm that the eigenvalues of $\mathcal{M}$ satisfy the condition $|arg(\lambda_i)| > \frac{\alpha\pi}{2}$ for each $i = 1, 2, \cdots, 5$, and $\alpha \in (0, 1)$. Thus, by Lemma (4.2) $\mathcal{E}_T^0$ is locally asymptotically stable. This implies that TB can eventually be eradicated from a community. The following theorem examines the global stability of TBFEP.

Theorem 6.10 *If $\mathcal{R}_T^{(\alpha)} < 1$, the TB free equilibrium point $\mathcal{E}_T^0$ of model (6.24) is globally asymptotically stable in its biologically feasible region*

$$\triangle_{\mathcal{T}} = \left\{(S, V, E_T, I_T, R_T) \in \mathbb{R}_+^5 : 0 < N \leq \frac{\Lambda}{\mu}\right\}.$$

Proof. Consider a Lyapunov function:

$$V(\mathbf{y}) = \frac{1}{2}\|\mathbf{y}\|^2 = \frac{1}{2}\sum_{i=1}^{5} y_i^2, \quad with\ \mathbf{y} = \mathbf{X}_T - \mathcal{E}_T^0, \quad where\ \mathbf{X}_T = (S, V, E_T, I_T, R_T).$$

Employing the non-local nature of fractional derivatives, Lemma (4.7) and the systems dynamics, we compute:

$$\begin{aligned} \sum_{i=1}^{5} y_i \cdot {}_0^C D_t^{\alpha} y_i = {} & y_1\Big[\Lambda + \delta V + \phi R_T - \beta_T\frac{I_T}{N}S - (\mu+\xi)S\Big] \\ & + y_2\Big[\xi S - \beta_T(1-\epsilon)\frac{I_T}{N}V - (\mu+\delta)V\Big] \\ & + y_3\Big[\beta_T\frac{I_T}{N}S + \beta_T(1-\epsilon)\frac{I_T}{N}V - (\mu+\theta_1+\kappa_1)E_T\Big] \\ & + y_4\Big[\kappa_1 E_T - (\theta_2+\mu+\mu_T)I_T\Big] + y_5\Big[\theta_1 E_T + \theta_2 I_T - (\mu+\phi)R_T\Big]. \end{aligned}$$

The following hold at $\mathcal{E}^0$:

$$\Lambda + \delta V + \phi R_T = \left(\beta_T\frac{I_T}{N} + \mu + \xi\right)S^0, \quad \xi S = \left(\beta_T(1-\epsilon)\frac{I_T}{N} + \mu + \delta\right)V^0,$$

$$\beta_T\frac{I_T}{N}S + \beta_T(1-\epsilon)\frac{I_T}{N}V = (\mu+\theta_1+\kappa_1)E_T^0,\ \ \kappa_1 E_T = (\theta_2+\mu+\mu_T)I_T^0,\ \ \theta_1 E_T + \theta_2 I_T = (\mu+\phi)R_T^0$$

Substituting these into the derivative expression and simplifying yields:

$$\sum_{i=1}^{5} y_i \cdot {}_0^C D_t^\alpha y_i \leq -\sum_{i=1}^{5} c_i y_i^2$$

Using this into Lemma (4.7) we get

$${}_0^C D_t^\alpha V(\mathbf{y}(t)) \leq -\sum_{i=1}^{5} c_i y_i^2 + \mathcal{R}(\mathbf{y}),$$

where $c_i > 0$ and $\mathcal{R}(\mathbf{y})$ denotes bounded cross terms. Applying Young's inequality:

$$|y_i y_j| \leq \frac{\varepsilon}{2} y_i^2 + \frac{1}{2\varepsilon} y_j^2,$$

we bound $\mathcal{R}(\mathbf{y})$ and absorb it into the main negative definite term to get

$${}_0^C D_t^\alpha V(\mathbf{y}) \leq -c\|\mathbf{y}\|^2 < 0, \ \forall_x \neq \mathcal{E}^0, \quad \text{and for some constant } c > 0.$$

The fractional derivative of the Lyapunov function is negative semi definite. Thus, by Corollary (4.1) , $\mathcal{E}^0$ is globally asymptotically stable in its feasible region. This finding implies that, while $\mathcal{R}_T^{(\alpha)} < 1$, we will finally be able to eradicate TB from the population.

Existence of TB Endemic Equilibrium Point

Theorem 6.11 *If $\mathcal{R}_T^{(\alpha)} > 1$, system (6.24) has a unique positive TB endemic equilibrium point given by, $\mathcal{E}_T^* = (S^*, V^*, E_T^*, I_T^*, R_T^*)$, where*

$$S^* = \frac{\Lambda + \delta V^* + \phi R_T^*}{\frac{\beta_T I_T^*}{N^*} + p_1}, \ V^* = \frac{\xi S^*}{\frac{\beta_T(1-\epsilon) I_T^*}{N^*} + p_2}, \ E_T^* = \frac{\beta_T[S^* + (1-\epsilon)V^*]I_T^*}{p_3 N^*},$$

$$I_T^* = \frac{\kappa_1 E_t^*}{p_4}, \ R_T^* = \left(\frac{\beta_T \theta_1 [S^* + (1-\epsilon)V^*]}{p_3 N^*} + \theta_2\right)\frac{I_T^*}{p_5}.$$

Proof. The TB endemic equilibrium point is the state at which TB persists in the community. Thus, following the same approaches in Theorem 2 of Aldila et al. (2020) and Theorem (3.3) of Khajanchi et al. (2018), and solving the system

$$\begin{cases} \Lambda + \delta V^* + \phi R_T^* - \beta_T \frac{I_T^*}{N^*} S^* - (\mu + \xi) S^* = 0, \\ \xi S^* - \beta_T (1-\epsilon)\frac{I_T^*}{N^*} V^* - (\mu + \delta) V^* = 0, \\ \beta_T \frac{I_T^*}{N^*} S^* + \beta_T (1-\epsilon)\frac{I_T^*}{N^*} V^* - (\mu + \theta_1 + \kappa_1) E_T^* = 0, \\ \kappa_1 E_T^* - (\theta_2 + \mu + \mu_T) I_T^* = 0, \\ \theta_1 E_T^* + \theta_2 I_T^* - (\mu + \phi) R_T^* = 0. \end{cases} \tag{6.27}$$

implicitly for S^*, V^*, E_T^*, I_T^* and R_T^* completes the proof.

Theorem 6.12 *The unique positive TB endemic equilibrium point, $\mathcal{E}_T^*$ of the sub-model (6.24) is locally asymptotically stable if $\mathcal{R}_T^{(\alpha)} > 1$.*

Proof. The Jacobian of sub-model (6.24) evaluated at $\mathcal{E}_T^*$ is a linearized matrix

$$\mathcal{J} = \begin{bmatrix} -f_1 & \delta & 0 & -g_1 & \phi \\ \xi & -f_2 & 0 & -g_2 & 0 \\ g_3 & g_4 & -f_3 & h & 0 \\ 0 & 0 & \kappa_1 & -f_4 & 0 \\ 0 & 0 & 0 & \theta_2 & -f_5 \end{bmatrix},$$

where

$$f_1 = \frac{\beta_T I_T^*}{N^*} + (\mu + \xi), \quad f_2 = \beta_T(1-\epsilon)\frac{I_T^*}{N^*} + (\mu + \delta), \quad f_3 = \mu + \theta_1 + \kappa_1, \quad f_4 = \theta_2 + \mu + \mu_T,$$

$$f_5 = \mu + \phi, \quad g_1 = \frac{\beta_T S^*}{N^*}, \quad g_2 = \beta_T(1-\epsilon)\frac{V^*}{N^*}, \quad g_3 = \frac{\beta_T I_T^*}{N^*}, \quad g_4 = \beta_T(1-\epsilon)\frac{I_T^*}{N^*}, \quad h = g_1 + g_2.$$

Numerical computation using parameter values from Table (6.2) ensures that the eigenvalues of $\mathcal{J}$ satisfy the condition $|arg(\lambda_i)| > \frac{\alpha\pi}{2}$ for every $i = 1, 2, \cdots, 5$ and $\alpha \in (0, 1]$. Therefore, by the fractional Routh-Huwirtz stability criterion (Naik et al., 2020), $\mathcal{E}_T^*$ is locally asymptotically stable when $\mathcal{R}_T^{(\alpha)} > 1$.

Theorem 6.13 *The unique positive TB endemic equilibrium point, $\mathcal{E}_T^*$ of the TB sub-model (6.24) is globally asymptotically stable if $\mathcal{R}_T^{(\alpha)} > 1$.*

Proof. The proof can be sketched in the same manner we did under Theorem (6.8). Epidemiologically, this finding implies that, while $\mathcal{R}_T^{(\alpha)} > 1$, it will be difficult to eradicate TB from the population in the long run and the disease persist in community.

6.2.5 Analysis of HIV/AIDS - TB Co-infection Model

In this section we will examine the existence and stability of equilibrium points for the HIV/AIDS-TB co-infection model (6.3).

Basic Reproduction Number

The basic reproduction number of the HIV/AIDS-TB co-infection model, $\mathcal{R}_0^{(\alpha)}$ which is the number of secondary cases produced by a single individual with the dominant disease in a fully susceptible population, is obtained using the formula

$$\mathcal{R}_0^{(\alpha)} = max\{\mathcal{R}_{H_A}^{(\alpha)}, \mathcal{R}_T^{(\alpha)}\}, \tag{6.28}$$

, where $\mathcal{R}_{H_A}^{(\alpha)}$ and $\mathcal{R}_T^{(\alpha)}$ are the reproduction numbers corresponding to HIV/AIDS and TB, respectively, and are calculated under sections (6.2.3) and (6.2.4). The illness with the higher basic reproduction number dominates the dynamics of the co-infection model.

Stability of the Disease free Equilibrium (DFE)

The DFE of HIV/AIDS-TB co-infection model (6.3) is the point at which the population is free from both HIV/AIDS and TB. It is given as

$$\mathcal{E}^0 = \left(\frac{\Lambda(\mu+\delta)}{\mu(\mu+\xi+\delta)}, \frac{\Lambda\xi}{\mu(\mu+\xi+\delta)}, 0, 0, 0, 0, 0, 0, 0, 0 \right).$$

Theorem 6.14 *The DFE, $\mathcal{E}^0$ of HIV/AIDS-TB co-infection model (6.3) is locally asymptotically stable if $|arg(\lambda_i)| > \alpha\frac{\pi}{2}$ for all eigenvalue λ_i of $\mathcal{L}$, where $\mathcal{L}$ is a linearized matrix obtained by computing the Jacobian of system (6.3) at $\mathcal{E}^0$ and unstable if there exists at least one eigenvalue λ_i such that $|arg(\lambda_i)| < \alpha\frac{\pi}{2}$.*

Proof. The jacobian of system (6.3) evaluated at $\mathcal{E}^0$ is a linearized matrix

$$\mathcal{L} = \begin{pmatrix}
-q_1 & \delta & 0 & -\xi_1 & -\phi & -\xi_2 & -\rho_1\xi_1 & -(\sigma\xi_1+\rho_2\xi_2) & -\rho_3\rho_2 & -\rho_4\xi_2 \\
\xi & -q_2 & 0 & -\xi_3 & 0 & 0 & 0 & -\sigma\xi_3 & 0 & 0 \\
0 & 0 & -q_3 & \xi_1+\xi_3 & 0 & 0 & 0 & 0 & 0 & 0 \\
0 & 0 & \kappa_1 & -q_4 & 0 & 0 & 0 & 0 & 0 & 0 \\
0 & 0 & \theta_1 & \theta_2 & -q_5 & 0 & 0 & 0 & 0 & 0 \\
0 & 0 & 0 & 0 & 0 & -q_6 & \rho_1\xi_2 & \rho_2\xi_2 & \rho_3\xi_2 & \rho_4\xi_2 \\
0 & 0 & 0 & 0 & 0 & 0 & -q_7 & 0 & 0 & 0 \\
0 & 0 & 0 & 0 & 0 & 0 & \kappa_2 & -q_8 & 0 & 0 \\
0 & 0 & 0 & 0 & 0 & \eta & \eta+\theta_1 & \eta+\theta_2 & -q_9 & 0 \\
0 & 0 & 0 & 0 & 0 & 0 & 0 & 0 & \kappa_3 & -q_{10}
\end{pmatrix},$$

where

$$q_1 = \mu+\xi,\ q_2 = \mu+\delta,\ q_3 = \mu+\theta_1+\kappa_1,\ q_4 = \theta_2+\mu+\mu_T,\ q_5 = \mu+\phi,\ q_6 = \eta+\mu+\mu_H,$$

$$q_7 = \theta_1+\kappa_2+q_6, q_8 = \eta+\theta_2+\mu+\mu_C,\ q_9 = \mu+\kappa_3,\ q_{10} = \mu+\mu_A,$$

$$\xi_1 = \beta_T\frac{S^0}{N^0},\ \xi_2 = \beta_H\frac{S^0}{N^0},\ \xi_3 = \frac{\beta_T(1-\epsilon)V^0}{N^0}.$$

After evaluating the eigenvalues of $\mathcal{L}$ using the computer algebra system, we can see

that the condition $|arg(\lambda_i)| > \frac{\alpha\pi}{2}$ holds true for each $i = 1, 2, \cdots, 10$ and $\alpha \in (0, 1)$. Thus, by Lemma (4.2) $\mathcal{E}^0$ is locally asymptotically stable.

Theorem 6.15 *When $\mathcal{R}_0 < 1$, the DFE, $\mathcal{E}^0$ of HIV/AIDS-TB co-infection model (6.3) is globally asymptotically stable in its biologically feasible region*

$$\triangle = \left\{ (S, V, E_T, I_T, R_T, I_H, E_C, I_C, T_H, A) \in \mathbb{R}_+^{10} : 0 < N \leq \frac{\Lambda}{\mu} \right\}.$$

Proof. The proof follows in similar way to Theorems (6.5) and (6.10).

Existence of the endemic steady states

Biologically, there exists three endemic equlibria for the HIV/AIDS-TB co-infection model. These are:

a) The HIV/AIDS Endemic Equilibrium
It describes the situation where the only endemic disease in the community is HIV/AIDS. It is given as

$$\hat{\mathcal{E}_{H_A}} = (S^*, 0, 0, 0, 0, I_H^*, 0, 0, T_H^*, A^*),$$

where the non-zero components of $\hat{\mathcal{E}_{H_A}}$ are derived from theorem (6.6).

b) The TB Endemic Equilibrium
This describes the condition in which the only endemic disease in the population is TB. It becomes

$$\hat{\mathcal{E}_T} = (S^*, V^*, \ E_T^*, \ I_T^*, \ R_T^*, 0, 0, 0, 0),$$

where the non-zero components of $\hat{\mathcal{E}_T}$ are derived from theorem (6.11).

c) The interior HIV/AIDS-TB co-endemic Equilibrium
When HIV/AIDS and TB are endemic in a population, we get an interior co-endemic equilibrium

$$\mathcal{E}_{H_T}^\star = (S^\star, V^\star, E_T^\star, I_T^\star, R_T^\star, I_H^\star, E_C^\star, I_C^\star, A^*, T_H^\star),$$

where the components of $\mathcal{E}_{H_T}^\star$ are obtained by solving the non-linear systems of

equations

$$\begin{cases} \Lambda + \delta V^* + \phi R_T^* - (\lambda_{S_T}^* + \lambda_{S_H}^*)S^* - (\mu + \xi)S^* = 0, \\ \xi S^* - \lambda_{V_T}^* V^* - (\mu + \delta)V^* = 0, \\ \lambda_{S_T}^* S^* + \lambda_{V_T}^* V^* - \lambda_{E_H}^* E_T^* - (\mu + \theta_1 + \kappa_1)E_T^* = 0, \\ \kappa_1 E_T^* - \lambda_{I_H}^* I_T^* - (\theta_2 + \mu + \mu_T)I_T^* = 0, \\ \theta_1 E_T^* + \theta_2 I_T^* - (\mu + \phi)R_T^* = 0, \\ \lambda_{S_H}^* S^* - \lambda_{S_T}^* I_H^* - (\eta + \mu + \mu_H)I_H^* = 0, \\ \lambda_{S_T}^* I_H^* + \lambda_{E_H}^* E_T^* - (\eta + \theta_1 + \kappa_2 + \mu + \mu_H)E_C^* = 0, \\ \kappa_2 E_C^* + \lambda_{I_H}^* I_T^* - (\eta + \theta_2 + \mu + \mu_C)I_C^* = 0, \\ \eta I_H^* + (\eta + \theta_1)E_C^* + (\eta + \theta_2)I_C^* - (\mu + \kappa_3)T_H^* = 0, \\ \kappa_3 T_H^* - (\mu + \mu_A)A^* = 0, \end{cases} \tag{6.29}$$

with

$$\lambda_{S_T}^* = \frac{\beta_T(I_T^* + \sigma I_C^*)}{N^*}, \ \lambda_{V_T}^* = \frac{\beta_T(1-\epsilon)(I_T^* + \sigma I_C^*)}{N^*},$$

$$\lambda_{S_H}^* = \frac{\beta_H(I_H^* + \rho_1 E_C^* + \rho_2 I_C^* + \rho_3 T_H^* + \rho_4 A^*)}{N},$$

$$\lambda_{E_H}^* = \frac{\beta_H(I_H^* + \rho_2 I_C^* + \rho_3 T_H^* + \rho_4 A^*)}{N^*}, \ \lambda_{I_H}^* = \frac{\beta_H(I_H^* + \rho_1 E_C^* + \rho_3 T_H^* + \rho_4 A^*)}{N^*}.$$

Theorem 6.16 *If the basic reproduction number $\mathcal{R}_0^{(\alpha)} > 1$, then the unique endemic equilibrium $\mathcal{E}^* = (S^*, V^*, E_T^*, I_T^*, R_T^*, I_H^*, E_C^*, I_C^*, T_H^*, A^*)$ is locally asymptotically stable in the biologically feasible region Δ.*

Proof. We linearize system (6.3) near $\mathbf{x}^* = \mathcal{E}^*$ to get:

$$_0^C D_t^\alpha \mathbf{y}(t) = J(\mathbf{x}^*)\mathbf{y}(t) + \mathbf{g}(\mathbf{y}(t)),$$

where $\mathbf{y}(t) = \mathbf{x}(t) - \mathbf{x}^*$, $\mathbf{x} = (S, V, E_T, I_T, R_T, I_H, E_C, I_C, T_H, A)$, $J(\mathbf{x}^*)$ denotes the Jacobian matrix at equilibrium, and $\mathbf{g}$ contains higher-order nonlinear terms.

Let λ_i be the eigenvalues of $J(\mathbf{x}^*)$. By Matignon's theorem, the linearized system is locally asymptotically stable if:

$$|\arg(\lambda_i)| > \frac{\alpha\pi}{2}, \quad \text{for all } i = 1, \ldots, 10.$$

Numerical evaluation with parameters from Table (6.2) confirms that this condition holds when $\mathcal{R}_0^{(\alpha)} > 1$.

Theorem 6.17 *If the basic reproduction number $\mathcal{R}_0^{(\alpha)} > 1$, then the unique endemic*

equilibrium $\mathcal{E}^* = (S^*, V^*, E_T^*, I_T^*, R_T^*, I_H^*, E_C^*, I_C^*, T_H^*, A^*)$ *is globally asymptotically stable in the biologically feasible region* Δ.

Proof. Consider the quadratic Lyapunov candidate:

$$V(\mathbf{y}) = \frac{1}{2}\|\mathbf{y}\|^2 = \frac{1}{2}\sum_{i=1}^{10} y_i^2.$$

Due to the non-local nature of fractional derivatives, we invoke Lemma (4.7).

Using the system dynamics, we compute:

$$\sum_{i=1}^{10} y_i \cdot {}_0^C D_t^\alpha y_i = y_1\Big[\Lambda + \delta V + \phi R_T - (\lambda_{S_T} + \lambda_{S_H} + \mu + \xi)S\Big] + y_2\Big[\xi S - (\lambda_{V_T} + \mu + \delta)V\Big] + \cdots + y_{10}\Big[\kappa_3 T_H - (\mu + \mu_A)A\Big].$$

At $\mathcal{E}^*$, the following hold:

$$\Lambda+\delta V+\phi R_T = (\lambda_{S_T}+\lambda_{S_H}+\mu+\xi)S^*, \quad \xi S = (\lambda_{V_T}+\mu+\delta)V^*, \quad \cdots, \quad \kappa_3 T_H = (\mu+\mu_A)A^*.$$

Substituting these into the derivative expression and simplifying yields:

$$\sum_{i=1}^{10} y_i \cdot {}_0^C D_t^\alpha y_i \leq -\sum_{i=1}^{10} c_i y_i^2.$$

Using this in Lemma (4.7) we get

$${}_0^C D_t^\alpha V(\mathbf{y}(t)) \leq \sum_{i=1}^{10} y_i \cdot {}_0^C D_t^\alpha y_i \leq -\sum_{i=1}^{10} c_i y_i^2 + \mathcal{R}(\mathbf{y}),$$

where $c_i > 0$ and $\mathcal{R}(\mathbf{y})$ denotes bounded cross terms.

Applying Young's inequality:

$$|y_i y_j| \leq \frac{\varepsilon}{2} y_i^2 + \frac{1}{2\varepsilon} y_j^2,$$

we bound $\mathcal{R}(\mathbf{y})$ and absorb it into the main negative definite term to get

$${}_0^C D_t^\alpha V(\mathbf{y}) \leq -c\|\mathbf{y}\|^2, \quad \text{for some constant } c > 0.$$

The fractional derivative of the Lyapunov function is negative semi definite. Thus, by Corollary (4.1) , $\mathcal{E}^*$ is globally asymptotically stable in its feasible region if $\mathcal{R}_0^{(\alpha)} > 1$.

6.3 Parameter Estimation

Based on eight years data on TB and HIV gathered from the Ethiopian Ministry of Health, we have estimated some of the model parameters of system (6.3). The PYTHON Optimization Toolbox is used to fit these data. Nonetheless, some of the model parameters are assumed, while others are borrowed from the literature. The average life expectancy and total population of Ethiopians in 2023 are 67.81 and $N(0) = 126,527,060$, respectively (Macrotrends, 2024). Therefore, the reciprocal of the average life expectancy, $\mu = 1/67.81$, is used to determine the natural death rate of individuals. The relation $\frac{\Lambda}{\mu} = N(0)$, yields the constant recruitment rate (Λ), which now becomes 1, 265,270.

Figure (6.2) shows the best fit of our model to the annually reported confirmed TB and HIV cases. Table (6.2) summarizes the values of model parameters utilized in numerical simulations.

Ethiopia faces a significant risk of continuous TB transmission, particularly in densely populated areas, with an effective contact rate of 1.525 indicating that each infectious individual can spread the disease to more than one person. This situation necessitates robust contact tracing and enhanced screening to identify and treat hidden cases, thus breaking transmission chains. Public health policies should focus on increasing community awareness of TB, funding active case discovery, and training health extension personnel for thorough investigations. Vulnerable groups, such as children under five and immunocompromised individuals, require targeted interventions for timely treatment and prevention. Additionally, long-term strategies should aim to improve healthcare access, living conditions, and integrate TB control efforts within broader public health initiatives to effectively address the high contact rate (Seid et al., 2024; Arja et al., 2023).

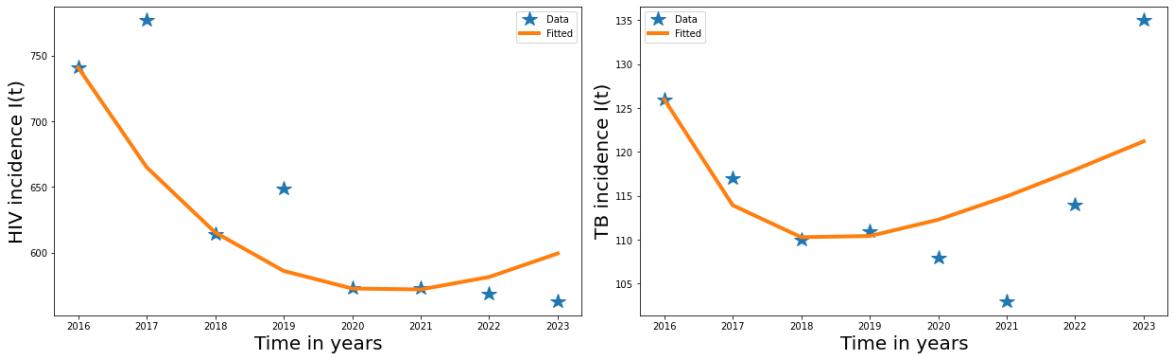

(a) Fitting of HIV/AIDS sub-model (b) Fitting of TB sub-model

Figure 6.2: Fitting of systems (6.20) and (6.24) with respect to Ethiopian HIV and TB incidence data from January, 2016 to December, 2023, where the population is in thousands.

Table 6.2: Parameter values used in numerical simulations.

Parameters	Values	Source
Λ	1265 $pers/yr$	calculated
β_T	$1.525/(pers \times yr)$	fitted
β_H	$0.1855/(pers \times yr)$	fitted
μ	$0.01/year$	calculated
μ_T	$0.0767/year$	(Adeyemo et al., 2023)
μ_H	$0.0154/year$	(Adeyemo et al., 2023)
μ_A	$0.0256/year$	assumed
μ_C	$0.2096/year$	(Adeyemo et al., 2023)
ξ	$0.1/(pers \times yr)$	(Ojo et al., 2023)
ϵ	$0.70/(pers \times yr)$	assumed
δ	$1.525/(pers \times yr)$	fitted
ϕ	$0.01/(pers \times yr)$	assumed
θ_1	$0.2959/(pers \times yr)$	assumed
θ_2	$0.2506/(pers \times yr)$	fitted
η	$0.33/(pers \times yr)$	(Kumar & Jain, 2018)
κ_1	$0.1142/(pers \times yr)$	fitted
κ_2	$0.0017/(pers \times yr)$	(Tanvi A., 2021)
κ_3	$0.35/(pers \times yr)$	fitted
σ	0.1	assumed
$\rho_1, \rho_2, \rho_3, \rho_4$	0.2, 0.3, 0.45, 0.4	assumed

The TB vaccine's waning rate of 1.525 indicates that immunity diminishes rapidly after vaccination, heightening vulnerability to TB, especially in high-burden regions of Ethiopia. This quick loss of immunity may complicate disease control efforts, leading to increased active TB cases and posing challenges to reaching international elimination goals. To maintain protective immunity, high-risk groups should receive booster shots. Public health policies need to adapt by regularly assessing vaccine efficacy and creating targeted campaigns for susceptible populations. The declining immunity could

strain existing TB control initiatives, resulting in higher healthcare costs and resource allocation challenges. Consequently, further research into novel vaccines or alternative strategies that provide longer-lasting protection against TB is essential for effective long-term disease management (WHO, 2025c).

The values of model parameters are summarized in Table (6.2). The sensitivity indices of model parameters with respect to $\mathcal{R}_T$ and $\mathcal{R}_{H_A}$ are therefore calculated according to formula (4.42) and are provided in Table (6.3). There is a direct correlation

Table 6.3: Sensitivity indices of $\mathcal{R}_T$ and $\mathcal{R}_{H_A}$ to the parameters.

Parameters	Sensitivity index($\mathcal{R}_T$)	Parameters	Sensitivity index($\mathcal{R}_{H_A}$)
β_T	+1.0000	β_H	+1.0000
μ	0.0183	μ	-0.2522
μ_T	0.2274	μ_H	-0.0433
κ_1	0.7282	η	-0.1278
θ_1	-0.7044	μ_A	-0.5167
θ_2	0.7430	κ_3	-0.0600
ξ	0.0803	ρ_3	0.0822
ϵ	-0.0447	ρ_4	0.7185
δ	1.9072		

between the reproduction number and the model parameters with positive sensitivity indices. Basic reproduction numbers rise or fall in response to changes in these parameters. However, there is an inverse association between the parameters with negative sensitivity indices and their corresponding basic reproduction number. Basic reproduction numbers drop/ rise in response to rise/drop in these parameters.

6.4 Numerical Simulations and Discussions

We provide a numerical simulation of the suggested model to bolster the findings of our mathematical analysis. Using Octave/MATLAB software, we utilize the fractional Adams–Bashforth–Moulton, or PECE algorithm, which has been developed in Diethelm et al. (2004); Diethelm & Freed (1998). Since global and local truncation errors are crucial for non-local fractional derivatives, they are the primary focus of error analysis in this algorithm. Because it can handle non-local behavior, adapt to different fractional orders, and enhance accuracy through an iterative refining process, the PECE technique is particularly helpful for fractional equations (Rosa & Torres, 2023).

We have used the initial data $S(0) = 123,005$, $E_T(0) = 205$, $I_T(0) = 126$, $I_H(0) = 741$, $T_H(0) = 394$ from Ethiopian real data on TB and HIV whereas, $V(0) = 1800$, $R_T(0) = 117$, $E_C(0) = 60$, $I_C(0) = 37$, and $A(0) = 42$ are taken by assumption. In all cases, the population is assumed to be in thousands.

The basic reproductive values $\mathcal{R}_T = 0.8992$ and $\mathcal{R}_{H_A} = 2.2398$ are derived using the parameter values from Table (6.2), with $\alpha = 0.85$ demonstrating that HIV/AIDS is an endemic disease in the community. $\mathcal{R}_0 = max\{\mathcal{R}_T, \mathcal{R}_H\} = 2.2398$ is the basic reproduction number of the HIV/AIDS-TB co-infection model. HIV/AIDS disease thus dominates the dynamics of HIV/AIDS-TB co-infection, which is endemic in the population.

If we use $\beta_H = 0.0455$, with $\alpha = 0.85$ while maintaining the values of the other model parameters as shown in Table (6.2), the reproduction number corresponding to HIV/AIDS becomes $\mathcal{R}_{H_A} = 0.6783$, which illustrates the dominance of TB disease over HIV/AIDS for the suggested co-infection model. However, in this instance, since $\mathcal{R}_0 < 1$, both diseases and their co-infection can be eliminated from the society over time.

The simulations of biological model parameters affecting the fundamental reproduction numbers related to TB and HIV/AIDS are shown in Figures (6.3a) and (6.3b). It can be shown that $\delta, \beta_T, \kappa_1, \theta_1$, and ϵ have a significant impact on $\mathcal{R}_T$. In contrast, the most important parameters influencing $\mathcal{R}_{H_A}$ are β_H and η.

Numerical computation show that for $\alpha = 0.5$, $\lambda_{5,6}$ have negative real parts and $|arg(\lambda_{5,6})| = 176.93^0$. For each $i \neq 5, 6$, $\lambda_i < 0$ and $|arg(\lambda_{5,6})| = 180^0$. For the remaining values of $\alpha = \{0.7, 0.9, 1.0\}$, $\lambda_i < 0$, $\forall_i$ and $|arg(\lambda_i)| = 180^0$ where, λ_i is an eigenvalue of the a linearized matrix $\mathcal{L}$, obtained by computing the Jacobian of system (6.3) at $\mathcal{E}^0$. Figures (6.4a)- (6.4d) demonstrate local asymptomatic stability of the diseases free equilibrium $\mathcal{E}^0$ using the fractional Matignon's stability criterion. As it can be seen from Figure (6.4d), $\mathcal{E}^0$ is stable, even though $\alpha = 1.0$ and $\mathcal{R}_0 > 1$. This confirms the ability of fractional-order modeling to expand the stability region of a given dynamical system.

Figures (6.5a)–(6.5d) illustrate the applicability of the Caputo fractional order model in precisely representing the extended latency periods and postponed treatment impacts in the transmission dynamics of TB and HIV/AIDS. It is shown that the fractional order derivative influences the transmission dynamics of HIV/AIDS-TB co-infection. The simulation findings show that by taking memory effects into account, a Caputo fractional order derivative can be used to assist in the development of efficient preventative and control strategies.

If a system can return to its equilibrium state from any initial condition, not just nearby ones, it is said to be globally asymptotically stable. Particularly for disease models like TB or HIV/AIDS where the dynamics of infection rely on previous states, fractional-order models are frequently more globally stable than their integer-order counterparts. The global asymptotic stability of the HIV/AIDS-TB free equilibrium

point $\mathcal{E}^0 = (50199, 4885, 0, 0, 0, 0, 0, 0, 0, 0)$ is displayed using $\alpha = 0.85$, in Figures (6.6a)–(6.6f).

In Figure (6.7), the global stability of endemic equilibrium for the Caputo fractional-order HIV/AIDS-TB co-infection model has been verified through extensive numerical simulations. The computational experiments were designed to test convergence from diverse initial conditions across the entire biologically feasible region, providing robust empirical evidence for the analytical stability claims. All trajectories from diverse initial conditions in Δ converge to $\mathcal{E}^*$. The Lyapunov function $V(\mathbf{y}(t))$ decreases monotonically. Sensitivity analysis confirms stability for all $\alpha \in (0, 1]$ and under parameter variations.

The global stability of the endemic equilibrium when $\mathcal{R}_0^{(\alpha)} = 17.34 > 1$ indicates that once HIV/AIDS and TB become established in a population, they will persist endemically regardless of initial conditions. This mathematical finding aligns with empirical observations in high-burden regions where elimination has proven challenging despite intensive control efforts.

The convergence behavior observed across all initial conditions suggests that: Short-term interventions that temporarily reduce prevalence will not achieve eradication if $\mathcal{R}_0^{(\alpha)} > 1$. Sustained control measures are necessary to maintain disease incidence at manageable levels. Combination therapies (ART, TB preventive therapy, vaccination) work synergistically to reduce the effective reproduction number.

The 100% convergence rate across diverse initial conditions, combined with the mathematical rigor of the Caputo fractional framework, establishes a solid foundation for predicting long-term disease dynamics and designing effective control strategies. The numerical results demonstrate that the system satisfies the conditions for global stability:

$$ {}^{C}D_t^{\alpha} V(\mathbf{y}(t)) \leq -c\|\mathbf{y}\|^2 \quad \text{for some } c > 0 \tag{6.30}$$

across the entire biologically feasible region Δ, confirming the endemic equilibrium $\mathcal{E}^*$ as a global attractor when $\mathcal{R}_0^{(\alpha)} > 1$. This numerical evidence, combined with the analytical arguments, provides comprehensive support for the global stability of the endemic equilibrium when $\mathcal{R}_0^{(\alpha)} > 1$.

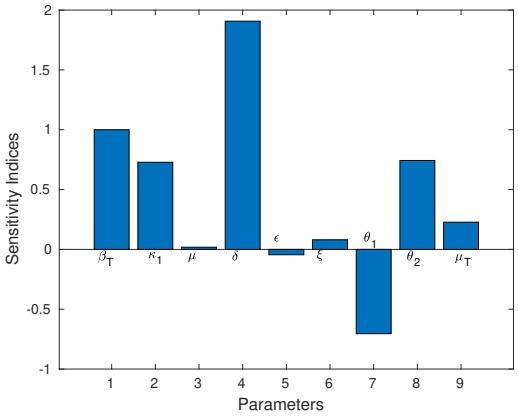

(a) Sensitivity indices of $\mathcal{R}_T$

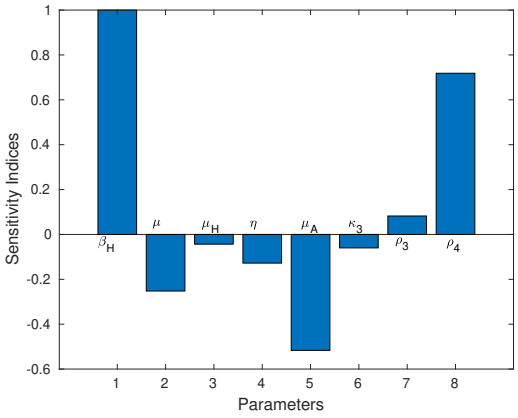

(b) Sensitivity indices of $\mathcal{R}_{H_A}$

Figure 6.3: Simulations of the sensitivity indices of parameters relative to basic reproductive numbers.

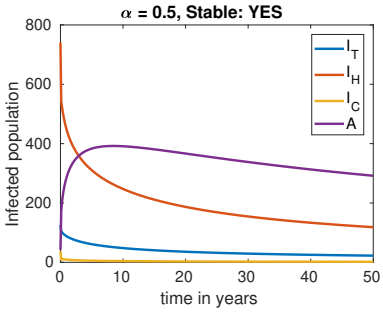

(a) $\lambda_{5,6} = -0.8067 \pm 0.0432i$, $|arg(\lambda_{5,6})| = 176.93^0$, $for\ i \neq 5,6\ \lambda_i < 0$, $|arg(\lambda_i)| = 180^0$, $\mathcal{R}_0 = 0.7352$.

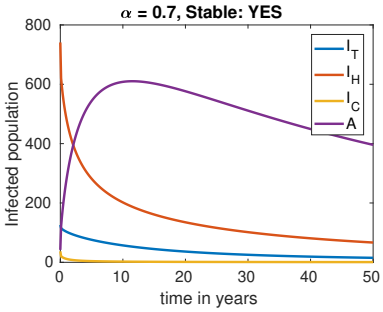

(b) $\lambda_i < 0$, $|arg(\lambda_i)| = 180^0, \forall_i$, $\mathcal{R}_0 = 0.7108$.

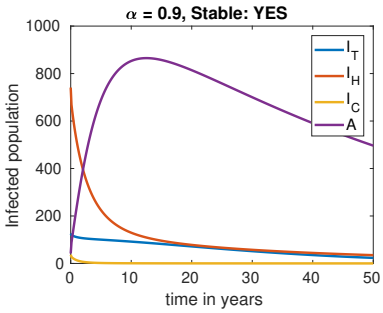

(c) $\lambda_i < 0$, $|arg(\lambda_i)| = 180^0, \forall_i$, $\mathcal{R}_0 = 0.9871$.

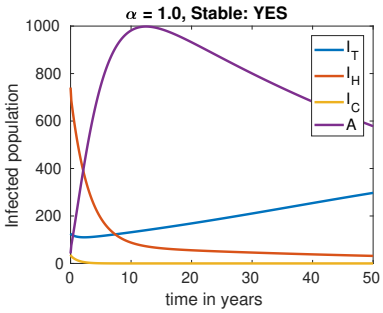

(d) $\lambda_i < 0$, $|arg(\lambda_i)| = 180^0, \forall_i$, $\mathcal{R}_0 = 1.1764$.

Figure 6.4: Graphs demonstrating the stability of $\mathcal{E}^0$ using the Matignon's fractional stability criterion.

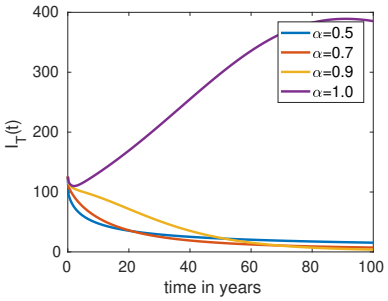

(a) Active TB infected population for $\alpha = (0.5, 0.7, 0.9, 1.0)$.

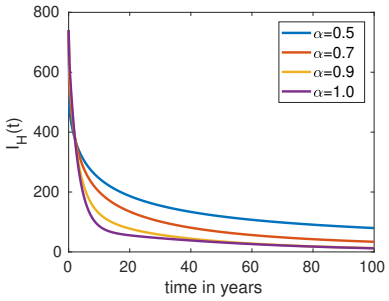

(b) HIV infected population for $\alpha = (0.5, 0.7, 0.9, 1.0)$.

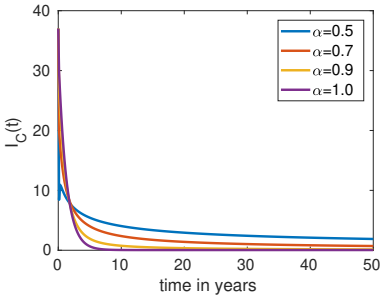

(c) Active TB and HIV infected population for $\alpha = (0.5, 0.7, 0.9, 1.0)$.

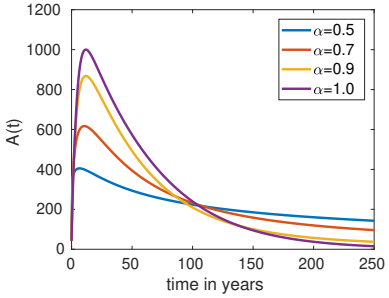

(d) AIDS infected population for $\alpha = (0.5, 0.7, 0.9, 1.0)$.

Figure 6.5: Graphs demonstrating the memory effects of the Caputo fractional operator for different value of α.

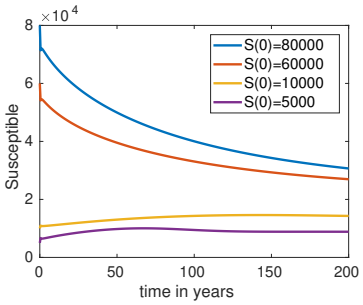

(a) Susceptible population

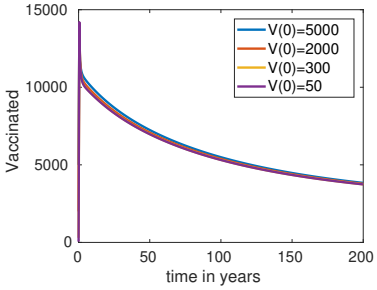

(b) Vaccenated population

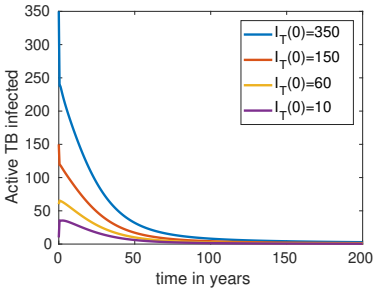

(c) Active TB infected population

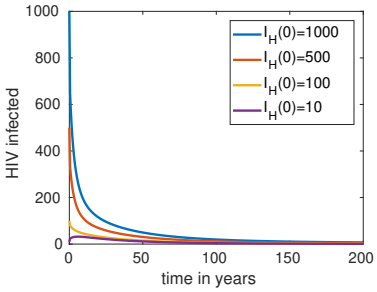

(d) HIV infected population

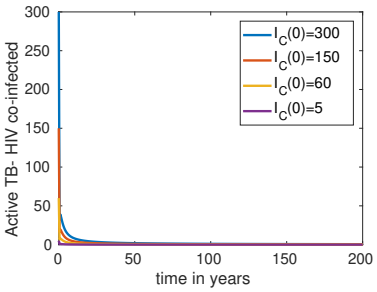

(e) HIV-Active TB co-infected population

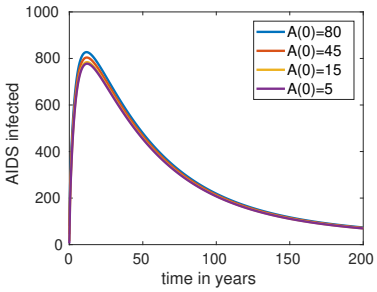

(f) AIDS infected population

Figure 6.6: Graphs showing global asymptotic stability of the disease free equilibrium point $\mathcal{E}^0 = (50199, 4885, 0, 0, 0, 0, 0, 0, 0, 0)$ with $\alpha = 0.85$.

6.4.1 The effects of η and θ_1 on disease compartments

This section aims to evaluate the impact of increasing the rates of ART and TPT on the number of people in the compartments of the proposed model. The parameters η, θ_1 have negative sensitivity indices, according to the results of sensitivity analysis, and they have an inverse relationship with the basic reproduction numbers, $\mathcal{R}_{H_A}, \mathcal{R}_T$. Figures (6.8a) and (6.8b) illustrate the impact of varying the adherence rate to ART, η on the number of AIDS-infected individuals $A(t)$ and HIV-TB co-infected individuals $I_C(t)$. The simulations show that increasing η by 30% causes $\mathcal{R}_{H_A}$, to decrease by about 2.7%, showing a considerable decrease in the number of infected individuals. On the other hand, Figures (6.8c) and (6.8d) illustrate the effects of changing adherence

rate to TPT, θ_1 on the number of people who are exposed to TB and those who are actively infected with TB, $E_T(t)$ and $I_T(t)$, respectively. The simulations show that a 30% increase in θ_1 at t=30 years leads to a significant drop in the number of exposed people from 78.28 to 43.98 and in the number of people with active TB from 35.54 to 22.26.

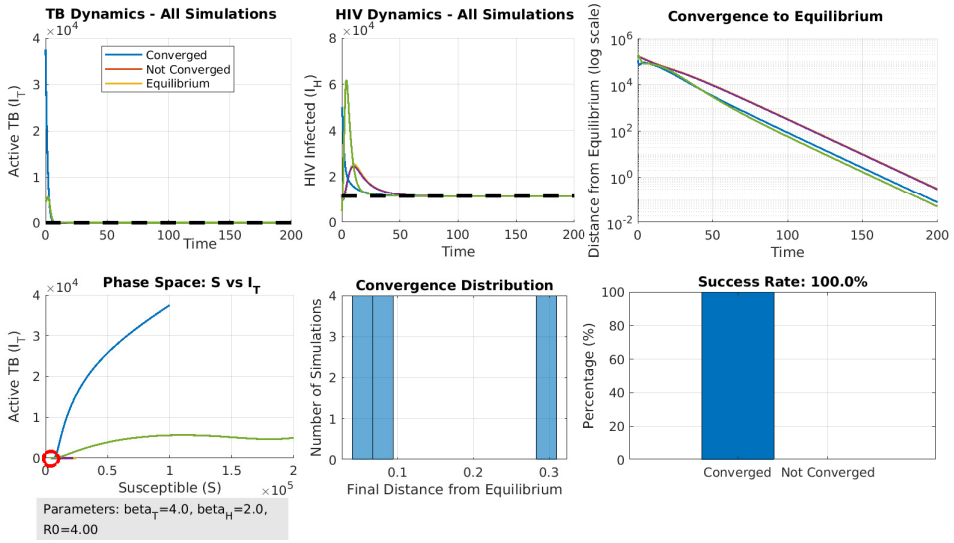

Figure 6.7: Graphs illustrating global asymptotic stability of endemic equilibrium point $\mathcal{E}^*$ *with* $\alpha = 0.85$. Global stability analysis-success rate:100.0%.

6.4.2 The effect of β_H and β_T on disease compartments

In this part, we tried to assess how effective contact rates for TB and HIV affect the dynamics of the proposed model. The sensitivity analysis indicates that the parameters β_H and β_T are directly proportional to the basic reproduction numbers that relate to them. Changing the HIV effective contact rate β_H has an impact on the number of HIV-infected individuals $I_H(t)$ and active TB-HIV co-infected individuals $I_C(t)$, as shown in Figures (6.9a) and (6.9b). Figures (6.9c) and (6.9d) illustrate the impact of altering the TB effective contact rate β_T on the number of individuals with active TB infection $I_T(t)$ and HIV-Active TB co-infection $I_C(t)$. The simulations show a considerable decrease in the number of people in the infected compartments, with a 50% decline in β_H, β_T respectively leading to a roughly 44.5% drop in $\mathcal{R}_{H_A}, \mathcal{R}_T$.

6.4.3 The effect of vaccine wane rate δ

This section aims to evaluate the impact of vaccine fading rate on the dynamics of the suggested model. The results obtained from the sensitivity analysis show that δ and $\mathcal{R}_T$ are directly proportional. The effects of altering a vaccination wane rate δ on the number of susceptible and vaccinated individuals $S(t)$ and $V(t)$, respectively, are

depicted in Figures (6.10a) and (6.10b). The simulations show that at a time t=100, a 50% decrease in δ leads to a significant decrease of susceptible individuals from 55,040 to 51,490 and a significant increase in vaccinated individuals from 5,383 to 9,008.

In this chapter, we developed and analyzed an HIV/AIDS-TB co-infection dynamics that considers vaccination for TB and treatment for HIV/AIDS employing a Caputo fractional-order model that takes into account the memory effects inherent in the progression and treatment history of the disease, and complex interaction between the disease. The model analysis reveals that $\mathcal{E}^0_{H_A}$, $\mathcal{E}^0_T$, $\mathcal{E}^0$ satisfy local asymptotic stability if $|arg(\lambda_i)| > \alpha\frac{\pi}{2}$, for all eigenvalue λ_i of the corresponding linearized matrices and global asymptotic stability if $\mathcal{R}^{(\alpha)}_{H_A}$, $\mathcal{R}^{(\alpha)}_T$, $R^{(\alpha)}_0 < 1$. Sensitivity analysis reveals that $\delta, \beta_T, \kappa_1, \theta_1$, and ϵ have a significant impact on $\mathcal{R}^{(\alpha)}_T$, whereas the most important parameters influencing $\mathcal{R}^{(\alpha)}_{H_A}$ are β_H and η. Moreover, simulation results suggest that by taking memory effects into account, a Caputo fractional-order provides a more accurate understanding of the complex interaction between the two diseases and aids in designing effective management and prevention strategies.

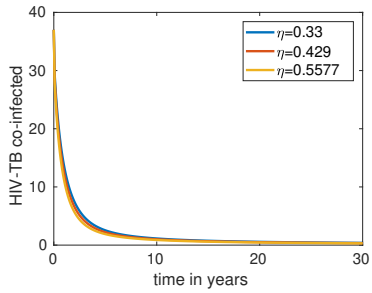

(a) Effect of varying η on $I_C(t)$

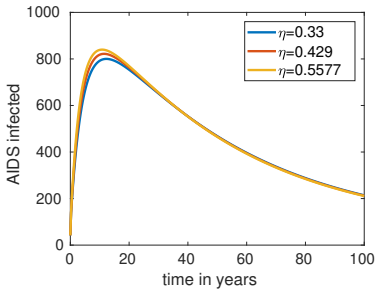

(b) Effect of varying η on $A(t)$

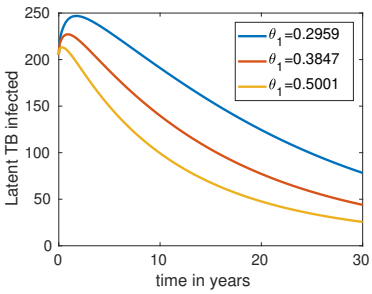

(c) Effect of varying θ_1 on $E_T(t)$

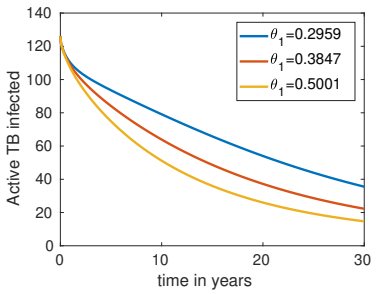

(d) Effect of varying θ_1 on $I_T(t)$

Figure 6.8: The effect of varying the rates η, θ_1 on disease compartments with $\alpha = 0.85$.

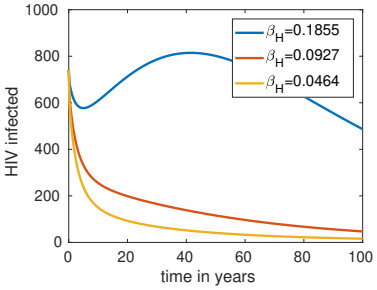

(a) Effect of varying β_H on $I_H(t)$

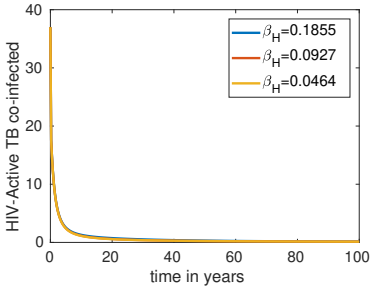

(b) Effect of varying β_H on $I_C(t)$

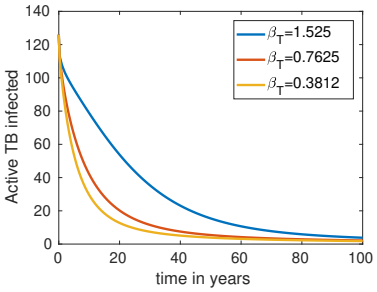

(c) Effect of varying β_T on $I_T(t)$

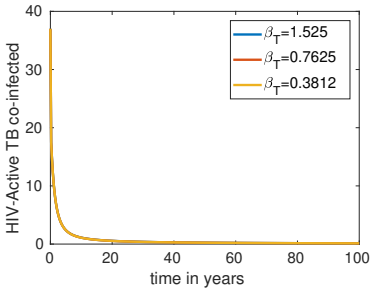

(d) Effect of varying β_T on $I_C(t)$

Figure 6.9: The effect of varying β_H, β_T on disease compartments with $\alpha = 0.85$.

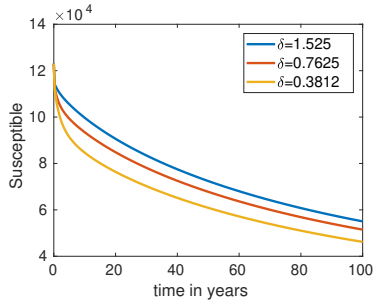

(a) Effect of varying δ on $S(t)$

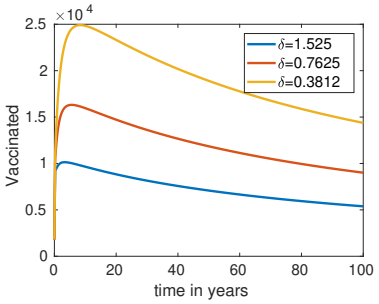

(b) Effect of varying δ on $V(t)$

Figure 6.10: The effect of varying δ on $S(t)$ and $V(t)$ compartments when $\alpha = 0.85$.

CHAPTER 7

FRACTIONAL-ORDER MODELING OF HIV-TB CO-INFECTION: OPTIMAL CONTROL AND COST-EFFECTIVENESS OF TREATMENT STRATEGIES

This chapter overlooks a mathematical model of HIV-TB co-infection with optimal control and the cost-effectiveness of its treatment strategies using the Caputo fractional derivatives. Both mathematical and epidemiological well-posedness of the model has been verified. We have performed the qualitative aspects like stability and bifurcation analyses. we have also conducted the quantitative analysis to support the analytical results of our model.

7.1 Model Formulation and its Assumptions

Based on the disease status individuals are classified into nine distinct categories. These are the susceptible class (S), which are in good health condition, but could get both HIV and TB in the future, a class of individuals latently infected only with tuberculosis (L_T), which are asymptomatic and not infectious yet, but can develop active TB when their immune system gets weak and can eventually be infectious, individuals actively infected with tuberculosis only (I_T), which are symptomatic and infectious, a class of individuals infected only with active TB which are under treatment (T_T), a class of individuals infected only with active TB who are now recovered from it after treatment (R_T), HIV only infected class (I_H), a class of individuals co-infected with HIV and latent TB (L_C), HIV and active TB co-infected class (I_C), a class

of individuals who were previously co-infected with active TB and HIV, which are now recovered from TB and under treatment of HIV (T_H) such that the total human population at a time t is

$$N(t) = S(t) + L_T(t) + I_T(t) + T_T(t) + R_T(t) + I_H(t) + L_C(t) + \ I_C(t) + T_H(t).$$

While we formulate the model, we take the following assumptions into account:

a) the population is drawn into the susceptible class at a steady rate Λ. It is assumed that all recruitment's are births without diseases and there is no infective immigrant,

b) active TB-HIV co-infected individuals can contribute to the transmission of both diseases, but each transmission event involves only one pathogen at a time. In reality simultaneous or near-simultaneous infections occur in high burden settings. We exclude simultaneous dual infection events, as they are epidemiologically rare and introduce unnecessary complexity in model structure (Aggarwal et al., 2021; Ayele et al., 2024),

c) individuals in I_T, I_C and T_T classes may pass on TB to susceptible people with a TB-associated force of infection defined by $\lambda_T = \beta_T \left(\frac{I_T}{N} + \rho_1 \frac{I_C}{N} + \rho_2 \frac{T_T}{N}\right)$ where $\rho_1, \rho_2 \in (0, 1)$ with $\rho_1 > \rho_2$ respectively show a relate infectiousness for people in the I_C and T_T classes compared to those in the active TB class, β_T is effective contact rate for TB,

d) although HIV transmission mechanisms are biologically identical, we make the assumption that susceptible, latently TB only infected, and actively TB only infected patients contract HIV through three distinct forces of infection. Therefore, susceptible persons contract HIV with the corresponding force of infection defined by $\lambda_H = \beta_H \left(\frac{I_H}{N} + \xi_1 \frac{L_C}{N} + \xi_2 \frac{I_C}{N} + \xi_3 \frac{T_H}{N}\right)$. People in the L_T class contract HIV with a force of infection given by $\lambda_{L_H} = \beta_H \left(\frac{I_H}{N} + \xi_2 \frac{I_C}{N} + \xi_3 \frac{T_H}{N}\right)$, and then they join the L_C class. Additionally, those in the I_T class acquire HIV with a force of infection defined by $\lambda_{I_H} = \beta_H \left(\frac{I_H}{N} + \xi_1 \frac{L_C}{N} + \xi_3 \frac{T_H}{N}\right)$, and progress to the I_C class. The modification parameter $\xi_1, \xi_2, \xi_3 \in (0, 1)$ with $\xi_1 > \xi_2 > \xi_3$ respectively accounts for the relative contagiousness of HIV for individuals in the L_C, I_C and T_H classes in comparison to those in the I_H class, β_H is the effective contact rate for HIV, and α is as defined above.

The exclusion of ξ_1 from λ_{L_H} and ξ_2 from λ_{I_H} in the model for HIV-TB co-infection is justified by the biological states of individuals in these respective compartments. Individuals in the latent TB class L_T do not exhibit active TB symptoms and are not yet

co-infected, meaning the infectiousness of the L_C class does not influence their acquisition of HIV. Likewise, for individuals in the actively TB-infected class I_T, the force of infection λ_{I_H} reflects their risk of acquiring HIV before they become co-infected, relying solely on the infectiousness of those already HIV-positive. This sequential acquisition approach aligns with co-infection modeling literature, which often emphasizes the dynamics of sequential, rather than simultaneous, infections. Thus, the model accurately captures the pathogen transmission based on the disease stage at the time of infection (Aggarwal et al., 2021; Ayele et al., 2024).

Furthermore, we also assume that individuals in L_T class join the I_T class after developing the symptom of TB and become actively infected at a rate $(\kappa_1+\varphi\lambda_T)$, where the terms κ_1 and $\varphi\lambda_T$ respectively represent progression coefficient and exogenous re-infection resulting from the new exposure of latent TB infectives to TB. Active TB individuals join T_T class to get treatment at a rate ω. Individuals in T_T class who recovered from infection join R_T class at a rate γ_1.

We again assume that some fractions of people who receive TB treatment will shift to the latent TB group with a rate $(1-\theta)\sigma$ because the pathogens will stay in the human immune system, and the remaining $\theta\sigma$ will shift to the active TB group as a result of treatment failure (Oshinubi et al., 2023). Here, $\theta \in (0,1)$ represents the TB treatment failure rate, and σ denotes the mobility rate of people in the T_T group.

We further suppose that after shedding their inherent immunity at a rate τ, recovered people may go back to the vulnerable class. Individuals in L_C class progress to the I_C class at a rate κ_2, where the term κ_2 represents progression coefficient. HIV infected individuals join T_H class at a rate η_1 . Individuals in I_C class simultaneously start both TB and HIV treatment and move to T_H class at a rate $(\eta_2+\gamma_2)$, after being recovered from TB. Each class has a natural mortality rate μ. However, the rates of disease-related fatalities for people in the I_T, I_H, and I_C classes are μ_T, μ_H, and μ_C, respectively.

We assume the condition where $\kappa_1 > \kappa_2$, which can occur under specific circumstances. Early initiation of ART in newly diagnosed HIV-infected individuals can significantly reduce the risk of progression to active TB, thereby lowering κ_2 compared to κ_1 in HIV-negative individuals. Furthermore, the atypical presentation of TB in HIV-positive persons often leads to lower rates of cavitary pulmonary disease and increased occurrences of extrapulmonary TB. Consequently, these factors contribute to a reduced transmissibility of TB among those co-infected with HIV. Studies indicate that individuals with HIV may generate fewer secondary TB cases than their HIV-negative counterparts, providing a biological basis for the reduced infectiousness in this group (Datiko et al., 2008; Windels et al., 2024).

The population is assumed to be homogeneous with regard to all epidemiological and biological factors, which may be acknowledged as a limitation for fractional-order setting. The flow diagram of the model is depicted in Figure (7.1).

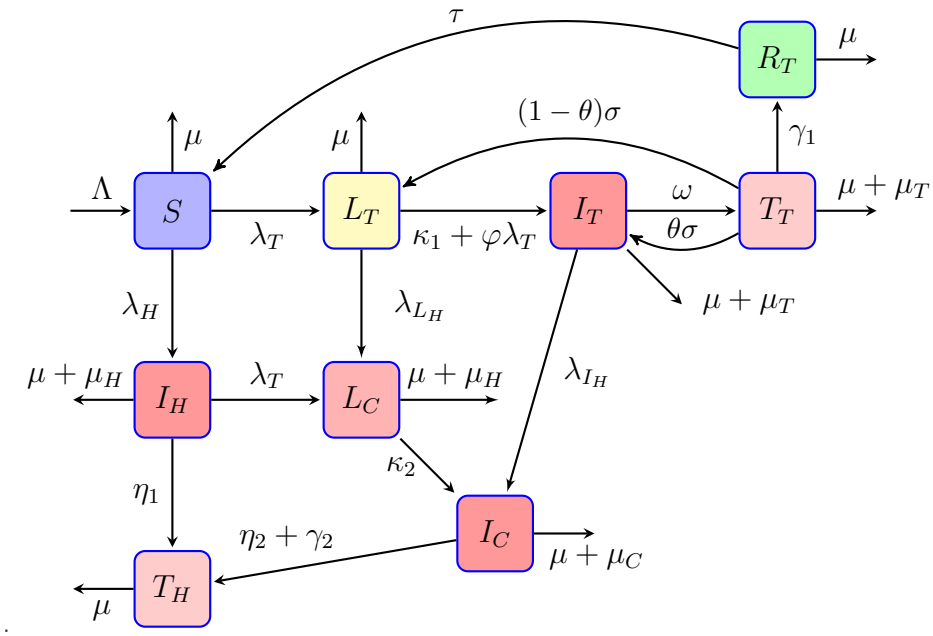

Figure 7.1: Diagram illustrating the Co-infection of HIV and TB

The governing integer-order non-linear systems of differential equations corresponding to Figure (7.1) can be written as

$$\begin{cases} \frac{dS}{dt} = \Lambda + \tau R_T - (\lambda_T + \lambda_H)S - \mu S, \\ \frac{dL_T}{dt} = \lambda_T S + (1-\theta)\sigma T_T - \lambda_{L_H} L_T - \varphi\lambda_T L_T - (\mu + \kappa_1)L_T, \\ \frac{dI_T}{dt} = \kappa_1 L_T + \varphi\lambda_T L_T + \theta\sigma T_T - \lambda_{I_H} I_T - (\omega + \mu + \mu_T)I_T, \\ \frac{dT_T}{dt} = \omega I_T - (\sigma + \gamma_1 + \mu + \mu_T)T_T, \\ \frac{dR_T}{dt} = \gamma_1 T_T - (\mu + \tau)R_T, \\ \frac{dI_H}{dt} = \lambda_H S - \lambda_T I_H - (\eta_1 + \mu + \mu_H)I_H, \\ \frac{dL_C}{dt} = \lambda_T I_H + \lambda_{L_H} L_T - (\kappa_2 + \mu + \mu_H)L_C, \\ \frac{dI_C}{dt} = \lambda_{I_H} I_T + \kappa_2 L_C - (\eta_2 + \gamma_2 + \mu + \mu_C)I_C, \\ \frac{dT_H}{dt} = \eta_1 I_H + (\eta_2 + \gamma_2)I_C - \mu T_H, \end{cases} \tag{7.1}$$

with the initial conditions given as

$$\begin{aligned} S(0) = S_0 \geq 0,\ L_T(0) = L_{T_0} > 0,\ I_T(0) = I_{T_0} > 0,\ T_T(0) = T_{T_0} \geq 0,\ R_T(0) = R_{T_0} \geq 0, \\ I_H(0) = I_{H_0} > 0,\ L_C(0) = L_{C_0} > 0,\ I_C(0) = I_{C_0} > 0,\ T_H(0) = T_{H_0} \geq 0 \end{aligned} \tag{7.2}$$

The Caputo fractional-order derivative for system (7.1) is given by a deterministic

system of nonlinear differential equations:

$$\begin{cases} {}_0^C D_t^\alpha S(t) = \Lambda + \tau R_T - (\lambda_T + \lambda_H)S - \mu S, \\ {}_0^C D_t^\alpha L_T(t) = \lambda_T S + (1-\theta)\sigma T_T - \lambda_{L_H} L_T - \varphi\lambda_T L_T - (\mu + \kappa_1)L_T, \\ {}_0^C D_t^\alpha I_T(t) = \kappa_1 L_T + \varphi\lambda_T L_T + \theta\sigma T_T - \lambda_{I_H} I_T - (\omega + \mu + \mu_T)I_T, \\ {}_0^C D_t^\alpha T_T(t) = \omega I_T - (\sigma + \gamma_1 + \mu + \mu_T)T_T, \\ {}_0^C D_t^\alpha R_T(t) = \gamma_1 T_T - (\mu + \tau)R_T, \\ {}_0^C D_t^\alpha I_H(t) = \lambda_H S - \lambda_T I_H - (\eta_1 + \mu + \mu_H)I_H, \\ {}_0^C D_t^\alpha L_C(t) = \lambda_T I_H + \lambda_{L_H} L_T - (\kappa_2 + \mu + \mu_H)L_C, \\ {}_0^C D_t^\alpha I_C(t) = \lambda_{I_H} I_T + \kappa_2 L_C - (\eta_2 + \gamma_2 + \mu + \mu_C)I_C, \\ {}_0^C D_t^\alpha T_H(t) = \eta_1 I_H + (\eta_2 + \gamma_2)I_C - \mu T_H, \qquad 0 < \alpha \leq 1, \end{cases} \tag{7.3}$$

with the initial conditions given as in (7.2).

Remark 7.1 *All of the parameters used in the model are presumed to be non-negative and they depend on* α.

Table 7.1: Description of model parameters.

Parameters	Descriptions
Λ	constant recruitment rate
β_T	effective contact rate for TB
β_H	effective contact rate for HIV
μ	natural death rate
μ_T	disease induced death rate for TB infectives
μ_H	disease induced death rate for HIV infectives
μ_C	disease induced death rate for HIV-TB co-infectives
τ	rate of loss of natural immunity
θ	treatment failure rate for TB
σ	movement rate of individuals in TB treated class
η_1	infectiousness rate for individuals in I_H class
η_2	ART adherence rate for individuals in I_C class
ω	treatment adherence rate for active TB individuals
γ_1	recovery rate of TB for individuals in T_T class
γ_2	recovery rate of TB for individuals in I_C class
κ_1	per-capita rate of being infectious for individuals in L_T class
κ_2	per-capita rate of being infectious for individuals in L_C class
ρ_1, ρ_2	modification parameters for the relative infectiousness of TB
ξ_1, ξ_2, ξ_3	modification parameters for the relative infectiousness of HIV
φ	exogenous re-infection rate

7.2 Model Analysis

Our aim in this section is to proof the epidemiological and mathematical well-posedness of system (7.3) by showing the non-negativity, boundedness, existence and uniqueness of its solution.

7.2.1 Boundedness and Non-Negativity of the Solution

Theorem 7.1 *For every $t \geq 0$, each solution trajectory of system (7.3) is bounded and non-negative. Moreover, the closed area*

$$\mathfrak{O} = \left\{ (S, L_T, I_T, T_T, R_T, I_H, L_C, I_C, T_H) \in \mathbb{R}_+^9 : 0 < N \leq \frac{\Lambda}{\mu} \right\}$$

is positively invariant region.

Proof. Performing the same computations as in Tanvi A. (2021); Mahata et al. (2022); Oshinubi et al. (2023) we have;

$$ {}_0^C D_t^\alpha S(t)|_{(S=0)} = \Lambda + \tau R_T \geq 0, \quad {}_0^C D_t^\alpha L_T(t)|_{(L_T=0)} = \lambda_T S + (1-\theta)\sigma T_T \geq 0,$$

$$ {}_0^C D_t^\alpha I_T(t)|_{(I_T=0)} = \kappa_1 L_T + \varphi L_T \frac{\beta_T}{N}(\rho_1 I_C + \rho_2 T_T) + \theta\sigma T_T \geq 0,$$

$$ {}_0^C D_t^\alpha T_T(t)|_{(T_T=0)} = \omega I_T \geq 0, \quad {}_0^C D_t^\alpha R_T(t)|(R_T = 0) = \gamma_1 T_T \geq 0,$$

$$ {}_0^C D_t^\alpha I_H(t)|_{(I_H=0)} = \frac{\beta_H S}{N}(\xi_1 L_C + \xi_2 I_C + \xi_3 T_H) \geq 0, \quad {}_0^C D_t^\alpha L_C(t)|_{(L_C=0)} = \lambda_T I_H + \lambda_{L_H} L_T,$$

$$ {}_0^C D_t^\alpha I_C(t)|_{(I_C=0)} = \lambda_{I_H} I_T + \kappa_2 L_C \geq 0, \quad {}_0^C D_t^\alpha T_H(t)|_{(T_H=0)} = \eta_1 I_H + (\eta_2 + \gamma_2) I_C \geq 0.$$

Thus, the vector field $\mathcal{V} = (S, L_T, I_T, T_T, R_T, I_H, L_C, I_C, T_H)^T$ points into $\mathbb{R}_+^9$ on each hyperplane bounding the non-negative region. Therefore, we deduce that all of the solution components of system (7.3) are non-negative based on this fact and the fact that all of the initial conditions in (7.2) are non-negative. Therefore, the closed region

$$\mathfrak{O} = \left\{ (S, L_T, I_T, T_T, R_T, I_H, L_C, I_C, T_H) \in \mathbb{R}_+^9 : 0 < N \leq \frac{\Lambda}{\mu} \right\}$$

is positively invariant, since every solution that begins in $\mathbb{R}_+^9$ stays in $\mathbb{R}_+^9$.
To demonstrate boundedness, let us take a sum of each single equations in system (7.3) so that we obtain

$$ {}_0^C D_t^\alpha N(t) + \mu N(t) \leq \Lambda. \tag{7.4}$$

Imposing the Laplace transform to (7.4) yields to,

$$\mathcal{L}\{{}_0^C D_t^\alpha N(t)\} + \mu\mathcal{L}\{N(t)\} \leq \Lambda\mathcal{L}\{1\},$$

which gives

$$s^\alpha N(s) - \sum_{m=0}^{n-1} s^{\alpha-m-1} N^{(m)}(0) + \mu N(s) \leq \Lambda\frac{1}{s} \tag{7.5}$$

From $0 < \alpha \leq 1$, we have $n = 1$ and obtain:

$$s^\alpha N(s) - s^{\alpha-1}N(0) + \mu N(s) \leq \Lambda\frac{1}{s}, \quad (s^\alpha + \mu)N(s) \leq \Lambda s^{-1} + N_0 s^{\alpha-1},$$

$$N(s) \leq \Lambda\frac{s^{-1}}{s^\alpha + \mu} + N_0\frac{s^{\alpha-1}}{s^\alpha + \mu} \tag{7.6}$$

Carrying out the inverse Laplace transform on (7.6) gives;

$$N(t) \leq \Lambda\mathcal{L}^{-1}\{\frac{s^{-1}}{s^\alpha + \mu}\} + N_0\mathcal{L}^{-1}\{\frac{s^{\alpha-1}}{s^\alpha + \mu}\} \tag{7.7}$$

Considering the relation

$$\mathcal{L}^{-1}\{\frac{s^{\psi-\beta}}{s^\psi - \lambda}\} = t^{\beta-1}E_{\psi,\beta}(\lambda t^\psi)$$

when we compare its exponents with (7.6), we obtain $\beta = \psi + 1$ for preceding term, $\beta = 1,\ \psi = \alpha$ for the next term and $\lambda = -\mu$. Thus, this leads to

$$\begin{aligned} N(t) &\leq \Lambda t^{\alpha+1-1}E_{\alpha,\alpha+1}(-\mu t^\alpha) + N_0 t^{1-1}E_{\alpha,1}(-\mu t^\alpha) \\ &= \Lambda t^\alpha E_{\alpha,\alpha+1}(-\mu t^\alpha) + N_0 E_{\alpha,1}(-\mu t^\alpha) \end{aligned} \tag{7.8}$$

Applying the properties of Mittag-Leffler function we have,

$$E_{a,b}(y) = yE_{a,a+b}(y) + \frac{1}{\Gamma(b)},$$

and

$$E_{a,a+b}(y) = \frac{1}{y}\left(E_{a,b}(y) - \frac{1}{\Gamma(b)}\right) \tag{7.9}$$

Replacing $a = \alpha\ , b = 1$ and $y = -\mu t^\alpha$ in equation (7.9) we get

$$\begin{aligned} E_{\alpha,\alpha+1}(-\mu t^\alpha) &= \frac{1}{-\mu t^\alpha}\left(E_{\alpha,1}(-\mu t^\alpha) - \frac{1}{\Gamma(1)}\right) \\ &= \frac{1}{-\mu t^\alpha}\left(E_{\alpha,1}(-\mu t^\alpha) - 1\right)\ ,\ \Gamma(1) = 1 \end{aligned} \tag{7.10}$$

Using (7.10) in (7.8) we have

$$\begin{aligned} N(t) &\leq \Lambda t^{\alpha} E_{\alpha,\alpha+1}(-\mu t^{\alpha}) + N_0 E_{\alpha,1}(-\mu t^{\alpha}) \\ &= (\Lambda t^{\alpha}) \left(\frac{1}{-\mu t^{\alpha}} \right) (E_{\alpha,1}(-\mu t^{\alpha}) - 1) + N_0 E_{\alpha,1}(-\mu t^{\alpha}) \\ &= N_0 E_{\alpha,1}(-\mu t^{\alpha}) - \frac{\Lambda}{\mu} E_{\alpha,1}(-\mu t^{\alpha}) + \frac{\Lambda}{\mu} \\ &= \left(N_0 - \frac{\Lambda}{\mu} \right) E_{\alpha,1}(-\mu t^{\alpha}) + \frac{\Lambda}{\mu} \end{aligned} \tag{7.11}$$

Thus, if $N_0 \leq \frac{\Lambda}{\mu}$, $\limsup_{t\to\infty}(N(t)) \leq \frac{\Lambda}{\mu}$.

Consequently, $\frac{\Lambda}{\mu}$ bounded $N(t)$ from above, which indicates that all solution trajectories are bounded. Boundedness and non-negativity are both necessary to guarantee that epidemiological models produce accurate and biologically meaningful predictions. Since the human population cannot have a negative value, non-negativity ensures that the model accurately depicts population dynamics, while boundedness keeps the dynamics within reasonable bounds, enabling insightful analyses of disease transmission and management tactics. When combined, these characteristics improve the models' dependability for public health response and planning.

7.2.2 Existence and Uniqueness of the Solution

The existence and uniqueness of solutions are crucial points for ensuring the scientific relevance of epidemiological models. Existence guarantees that the model can produce real illness dynamics, whereas uniqueness guarantees that this illness's processes is steady and foreseeable. The aim of this particular section is to show that the solution to the problem (7.3) exists and is unique.
Thus, rewrite equation (7.3) as

$$\begin{cases} {}_0^C D_t^{\alpha} S(t) = \mathcal{H}_1(t,S) \ , \ {}_0^C D_t^{\alpha} L_T(t) = \mathcal{H}_2(t,L_T) \ , \ {}_0^C D_t^{\alpha} I_T(t) = \mathcal{H}_3(t,I_T) \ , \\ {}_0^C D_t^{\alpha} T_T(t) = \mathcal{H}_4(t,T_T) \ , \ {}_0^C D_t^{\alpha} R_T(t) = \mathcal{H}_5(t,R_T) \ , \ {}_0^C D_t^{\alpha} I_H(t) = \mathcal{H}_6(t,I_H), \\ {}_0^C D_t^{\alpha} L_C(t) = \mathcal{H}_7(t,L_C), \ {}_0^C D_t^{\alpha} I_C(t) = \mathcal{H}_8(t,I_C), \ {}_0^C D_t^{\alpha} T_H(t) = \mathcal{H}_9(t,T_H), \end{cases} \tag{7.12}$$

with the same initial values in (7.2).
Where;

$$\begin{aligned}
\mathcal{H}_1(t,S) &= \Lambda + \tau R_T - (\lambda_T + \lambda_H)S - \mu S,\\
\mathcal{H}_2(t,L_T) &= \lambda_T S + (1-\theta)\sigma T_T - \lambda_{L_H} L_T - \varphi\lambda_T L_T - (\mu+\kappa_1)L_T,\\
\mathcal{H}_3(t,I_T) &= \kappa_1 L_T + \varphi\lambda_T L_T + \theta\sigma T_T - \lambda_{I_H} I_T - (\omega+\mu+\mu_T)I_T,\\
\mathcal{H}_4(t,T_T) &= \omega I_T - (\sigma+\gamma_1+\mu+\mu_T)T_T,\\
\mathcal{H}_5(t,R_T) &= \gamma_1 T_T - (\mu+\tau)R_T,\\
\mathcal{H}_6(t,I_H) &= \lambda_H S - \lambda_T I_H - (\eta_1+\mu+\mu_H)I_H,\\
\mathcal{H}_7(t,L_C) &= \lambda_T I_H + \lambda_{L_H} L_T - (\kappa_2+\mu+\mu_H)L_C,\\
\mathcal{H}_8(t,I_C) &= \lambda_{I_H} I_T + \kappa_2 L_C - (\eta_2+\gamma_2+\mu+\mu_C)I_C,\\
\mathcal{H}_9(t,T_H) &= \eta_1 I_H + (\eta_2+\gamma_2)I_C - \mu T_H.
\end{aligned} \tag{7.13}$$

Carrying out integral transformations on both sides of equation (7.12) we have

$$\begin{aligned}
S(t) &= S_0 + \frac{1}{\Gamma(\alpha)}\int_0^t (t-\tau)^{\alpha-1}\mathcal{H}_1(\tau,S(\tau))d\tau,\\
L_T(t) &= L_{T_0} + \frac{1}{\Gamma(\alpha)}\int_0^t (t-\tau)^{\alpha-1}\mathcal{H}_2(\tau,L_T(\tau))d\tau,\\
I_T(t) &= I_{T_0} + \frac{1}{\Gamma(\alpha)}\int_0^t (t-\tau)^{\alpha-1}\mathcal{H}_3(\tau,I_T(\tau))d\tau,\\
T_T(t) &= T_{T_0} + \frac{1}{\Gamma(\alpha)}\int_0^t (t-\tau)^{\alpha-1}\mathcal{H}_4(\tau,T_T(\tau))d\tau,\\
R_T(t) &= R_{T_0} + \frac{1}{\Gamma(\alpha)}\int_0^t (t-\tau)^{\alpha-1}\mathcal{H}_5(\tau,R_T(\tau))d\tau,\\
I_H(t) &= I_{H_0} + \frac{1}{\Gamma(\alpha)}\int_0^t (t-\tau)^{\alpha-1}\mathcal{H}_6(\tau,I_H(\tau))d\tau,\\
L_C(t) &= L_{C_0} + \frac{1}{\Gamma(\alpha)}\int_0^t (t-\tau)^{\alpha-1}\mathcal{H}_7(\tau,L_C(\tau))d\tau,\\
I_C(t) &= I_{C_0} + \frac{1}{\Gamma(\alpha)}\int_0^t (t-\tau)^{\alpha-1}\mathcal{H}_8(\tau,I_C(\tau))d\tau,\\
T_H(t) &= T_{H_0} + \frac{1}{\Gamma(\alpha)}\int_0^t (t-\tau)^{\alpha-1}\mathcal{H}_9(\tau,T_H(\tau))d\tau,.
\end{aligned} \tag{7.14}$$

Lemma 7.1 *With associated Lipschitz constants G_k, the kernels $\mathcal{H}_k$ are Lipschitz for each $k = 1,2,3,\cdots,9$, and are contractions as long as $0 < G_k < 1$; where,*
$G_1 = e_1+e_2+\mu$, $G_2 = e_3+\varphi e_1+\mu+\kappa_1$, $G_3 = e_4+\omega+\mu+\mu_T$, $G_4 = \sigma+\gamma_1+\mu+\mu_T$, $G_5 = \mu+\tau$, $G_6 = e_1+\eta_1+\mu+\mu_H$, $G_7 = \kappa_2+\mu+\mu_H$, $G_8 = \eta_2+\gamma_2+\mu+\mu_C$, $G_9 = \mu$, *and* $\lambda_T(t) \le e_1$, $\lambda_H(t) \le e_2$, $\lambda_{L_H}(t) \le e_3$, $\lambda_{I_H}(t) \le e_4$ *are bounded functions.*

Proof. Following the same approach in Mahata et al. (2022), for S and $S^\star$, we have $||\mathcal{H}_1(t,S) - \mathcal{H}_1(t,S^\star)|| = || - (\lambda_T(t) + \lambda_H(t) + \mu)(S - S^\star)|| \leq (||\lambda_T(t)|| + ||\lambda_H(t)|| + \mu)||S - S^\star|| = G_1||S - S^\star||$, with $G_1 = e_1 + e_2 + \mu$. Consequently, with a Lipschitz constant G_1, the kernel $\mathcal{H}_1$ is Lipschitz and contraction provided that $0 < G_1 < 1$.
In the same way, for L_T and $L_T^\star$,
$||\mathcal{H}_2(t,L_T) - \mathcal{H}_2(t,L_T^\star)|| = || - (\lambda_{L_H}(t) + \varphi\lambda_T(t) + \mu + \kappa_1)(L_T - L_T^\star)|| \leq (||\lambda_{L_H}(t)|| + \varphi||\lambda_T(t)|| + \mu + \kappa_1)||L_T - L_T^\star|| = G_2||L_T - L_T^\star||$, with $G_2 = e_3 + \varphi e_1 + \mu + \kappa_1$. Hence, the kernel $\mathcal{H}_2$ is Lipschitz with a Lipschitz constant G_2 and contraction provided that $0 < G_2 < 1$. Finally, with the same method we can demonstrate that for $j = 3, 4, \cdots, 9$ with a Lipschitz constant G_j, the kernels $\mathcal{H}_j$ are Lipschitz and contraction given that $0 < G_j < 1$.

Theorem 7.2 *There exist at least one solution to system (7.3) subject to the initial conditions (7.2) provided that*

$$\frac{t^\alpha G_k}{\Gamma(\alpha+1)} < 1$$

for each $k = 1, 2, \cdots, 9$.

Proof. Consider the following recursive patterns (Mahata et al., 2022; Oshinubi et al., 2023):

$$\begin{aligned}
\Omega_{1n}(t) = S_n(t) - S_{n-1}(t) &= \frac{1}{\Gamma(\alpha)}\int_0^t (\mathcal{H}_1(\tau, S_{n-1}) - \mathcal{H}_1(\tau, S_{n-2}))(t-\tau)^{\alpha-1}d\tau \ , \\
\Omega_{2n}(t) = L_{T_n}(t) - L_{T_{n-1}}(t) &= \frac{1}{\Gamma(\alpha)}\int_0^t (\mathcal{H}_2(\tau, L_{T_{n-1}}) - \mathcal{H}_2(\tau, L_{T_{n-2}}))(t-\tau)^{\alpha-1}d\tau \ , \\
\Omega_{3n}(t) = I_{T_n}(t) - I_{T_{n-1}}(t) &= \frac{1}{\Gamma(\alpha)}\int_0^t (\mathcal{H}_3(\tau, I_{T_{n-1}}) - \mathcal{H}_3(\tau, I_{T_{n-2}}))(t-\tau)^{\alpha-1}d\tau \ , \\
\Omega_{4n}(t) = T_{T_n}(t) - T_{T_{n-1}}(t) &= \frac{1}{\Gamma(\alpha)}\int_0^t (\mathcal{H}_4(\tau, T_{T_{n-1}}) - \mathcal{H}_4(\tau, T_{T_{n-2}}))(t-\tau)^{\alpha-1}d\tau \ , \\
\Omega_{5n}(t) = R_{T_n}(t) - R_{T_{n-1}}(t) &= \frac{1}{\Gamma(\alpha)}\int_0^t (\mathcal{H}_5(\tau, R_{T_{n-1}}) - \mathcal{H}_5(\tau, R_{T_{n-2}}))(t-\tau)^{\alpha-1}d\tau \quad (7.15) \\
\Omega_{6n}(t) = I_{H_n}(t) - I_{H_{n-1}}(t) &= \frac{1}{\Gamma(\alpha)}\int_0^t (\mathcal{H}_6(\tau, I_{H_{n-1}}) - \mathcal{H}_6(\tau, I_{H_{n-2}}))(t-\tau)^{\alpha-1}d\tau \ , \\
\Omega_{7n}(t) = L_{C_n}(t) - L_{C_{n-1}}(t) &= \frac{1}{\Gamma(\alpha)}\int_0^t (\mathcal{H}_7(\tau, L_{C_{n-1}}) - \mathcal{H}_7(\tau, L_{C_{n-2}}))(t-\tau)^{\alpha-1}d\tau \ , \\
\Omega_{8n}(t) = I_{C_n}(t) - I_{C_{n-1}}(t) &= \frac{1}{\Gamma(\alpha)}\int_0^t (\mathcal{H}_8(\tau, I_{C_{n-1}}) - \mathcal{H}_8(\tau, I_{C_{n-2}}))(t-\tau)^{\alpha-1}d\tau \ , \\
\Omega_{9n}(t) = T_{H_n}(t) - T_{H_{n-1}}(t) &= \frac{1}{\Gamma(\alpha)}\int_0^t (\mathcal{H}_9(\tau, T_{H_{n-1}}) - \mathcal{H}_9(\tau, T_{H_{n-2}}))(t-\tau)^{\alpha-1}d\tau,
\end{aligned}$$

with the initial conditions as in equation (7.2).
Performing additional algebraic computations and applying the lipschitz condition from

Lemma (7.1), we have

$$
\begin{aligned}
||S_n(t) - S_{n-1}(t)|| &\leq ||S_n(0)|| \left(\frac{t^\alpha G_1}{\Gamma(\alpha+1)} \right)^n, \\
||L_{T_n}(t) - L_{T_{n-1}}(t)|| &\leq ||L_{T_n}(0)|| \left(\frac{t^\alpha G_2}{\Gamma(\alpha+1)} \right)^n, \\
||I_{T_n}(t) - I_{T_{n-1}}(t)|| &\leq ||I_{T_n}(0)|| \left(\frac{t^\alpha G_3}{\Gamma(\alpha+1)} \right)^n, \\
||T_{T_n}(t) - T_{T_{n-1}}(t)|| &\leq ||T_{T_n}(0)|| \left(\frac{t^\alpha G_4}{\Gamma(\alpha+1)} \right)^n, \\
||R_{T_n}(t) - R_{T_{n-1}}(t)|| &\leq ||R_{T_n}(0)|| \left(\frac{t^\alpha G_5}{\Gamma(\alpha+1)} \right)^n, \\
||I_{H_n}(t) - I_{H_{n-1}}(t)|| &\leq ||I_{H_n}(0)|| \left(\frac{t^\alpha G_6}{\Gamma(\alpha+1)} \right)^n, \\
||L_{C_n}(t) - L_{C_{n-1}}(t)|| &\leq ||L_{C_n}(0)|| \left(\frac{t^\alpha G_7}{\Gamma(\alpha+1)} \right)^n, \\
||I_{C_n}(t) - I_{C_{n-1}}(t)|| &\leq ||I_{C_n}(0)|| \left(\frac{t^\alpha G_8}{\Gamma(\alpha+1)} \right)^n, \\
||T_{H_n}(t) - T_{H_{n-1}}(t)|| &\leq ||T_{H_n}(0)|| \left(\frac{t^\alpha G_9}{\Gamma(\alpha+1)} \right)^n.
\end{aligned} \tag{7.16}
$$

Hence, this justify that the sequences $S_n,\ L_{T_n},\ I_{T_n},\ T_{T_n},\ R_{T_n},\ I_{H_n},\ L_{C_n},\ I_{C_n},\ T_{H_n}$ are bounded uniformly.

We now aim to prove that they converge uniformly to (7.14) upon a specified interval I, by showing indirectly that they converge to system (7.3) subject to initial conditions (7.2). Now, suppose the kernels $\mathcal{H}_j (j = 1, 2, \cdots, 9)$ are continuous on a closed area $\mathfrak{R} = \{(t, y) : |t - t_0| \leq a,\ ||y - y_0|| \leq b\}$ with

$$
\begin{aligned}
\mathcal{Y} &= \left(\ S(t),\ L_T(t),\ I_T(t),\ T_T(t),\ R_T(t),\ I_H(t),\ L_C(t),\ I_C(t),\ T_H(t) \ \right)^T, \\
\mathcal{Y}_0 &= \left(\ S_0,\ L_{T_0},\ I_{T_0},\ T_{T_0},\ R_{T_0},\ I_{H_0},\ L_{C_0},\ I_{C_0},\ T_{H_0} \ \right)^T.
\end{aligned} \tag{7.17}
$$

Define $K_j > 0$ such that $||\mathcal{H}_j|| < K_j$ for each $j = 1, 2, \cdots, 9$.
Let $I = [0, w]$ where, $w = min\left\{a, \frac{b}{K}\Gamma(\alpha+1)^{\frac{1}{\alpha}}\right\}$. Clearly, we observe see that

$$
\mathcal{Y}_n = \mathcal{Y}_0 + \sum_{m=1}^{n} (\mathcal{Y}_k - \mathcal{Y}_{m-1}). \tag{7.18}
$$

The sequence $\mathcal{Y}_n$ uniformly converges on I if it can be demonstrated that the series $\mathcal{Y}_0 + \sum_{k=1}^{n}(\mathcal{Y}_k - \mathcal{Y}_{k-1})$ converges uniformly on I.

Thus,

$$||\mathcal{Y}_0 + \sum_{k=1}^{n}(\mathcal{Y}_k - \mathcal{Y}_{k-1})|| \leq ||\mathcal{Y}_0|| + \sum_{k=1}^{n} ||\mathcal{Y}_k - \mathcal{Y}_{k-1}||$$
$$\leq ||\mathcal{Y}_0|| + \sum_{k=1}^{n} ||\mathcal{Y}_k(0)|| \left(\frac{t^\alpha G_1}{\Gamma(\alpha+1)}\right)^k. \tag{7.19}$$

This serious uniformly converges on I if $\frac{t^\alpha G_1}{\Gamma(\alpha+1)} < 1$. From the Weierstrass M-test theorem, we then deduce that $\mathcal{Y}_n$ uniformly converges on I. As can be shown by the Lebesgue dominated convergence theorem, this series converges to a limit point $\mathcal{Y}(t)$, which is the solution of the integral equation (7.14). Hence, for each $k = 1, 2, \cdots, 9$, the IVP (7.3) with the initial solutions (7.2) possess at least one solution provided that $\frac{t^\alpha G_k}{\Gamma(\alpha+1)} < 1$.

Theorem 7.3 *For each $j = 1, 2, \cdots, 9$, system (7.3), with the initial values (7.2) possess a unique solution provided that*

$$1 - \frac{t^\alpha G_j}{\Gamma(\alpha+1)} > 0.$$

Proof. The proof can be sketched similar to that of Theorem (4.3).

Understanding the dynamics of co-infection from a biological, epidemiological, and mathematical standpoint requires a distinct analysis of the HIV and TB sub-models. The biological mechanisms and treatment approaches of HIV and TB are different. While TB is caused by Mycobacterium tuberculosis and mostly affects the lungs, HIV targets CD4+ T cells, weakening the immune system. Making this distinction is essential for improving treatment plans that take side effects and medication interactions into account. The mechanics of HIV and TB transmission are very different. While TB is mostly spread through the air, HIV is spread through sexual contact and blood. By examining these models independently, it becomes clearer how each disease spreads and enables the development of focused public health interventions according to the unique risk factors linked to each disease. By separating the models, the intricacy of co-infection dynamics is reduced, allowing for more precise parameter estimation and understandable stability evaluations. This method makes it easier to identify crucial cutoff points for successful intervention techniques. After all, a separate study of HIV and TB sub-models enhances our understanding of their interplay and guides better public health strategies for handling each disease in co-infected populations (Raza et al., 2025; Awoke & Semu, 2018).

7.2.3 The HIV Sub-model

Here, we need to analyze the basic properties of system (7.3) assuming that the population is free from TB. Hence, equating all the state variables L_T, I_T, T_T, R_T, L_C and I_C to zero, the HIV sub-model becomes

$$\begin{cases} {}_0^C D_t^\alpha S(t) = \Lambda - \frac{\beta_H}{N}(I_H + \xi_3 T_H)S - \mu S, \\ {}_0^C D_t^\alpha I_H(t) = \frac{\beta_H}{N}(I_H + \xi_3 T_H)S - (\eta_1 + \mu + \mu_H)I_H, \\ {}_0^C D_t^\alpha T_H(t) = \eta_1 I_H - \mu T_H, \ 0 < \alpha \leq 1, \end{cases} \tag{7.20}$$

subject to the initial values

$$S(0) = S_0 \geq 0, \quad I_H(0) = I_{H_0} > 0, \quad T_H(0) = T_{H_0} \geq 0. \tag{7.21}$$

Basic Reproduction Number for HIV Sub-model

The HIV free equilibrium point (HIVFEP) of the sub-model (7.20) which refers to the situation in which the population is free from HIV is given as $\mathcal{E}_H^0 = (\frac{\Lambda}{\mu}, 0, 0)$. Using the next generation matrix approach, the basic reproduction number corresponding to HIV which is the average number of secondary cases produced by a single infected individual is computed as

$$\mathcal{R}_H^{(\alpha)} = \frac{\beta_H}{\eta_1 + \mu + \mu_H}\left(1 + \frac{\xi_3 \eta_1}{\mu}\right)\Psi(\alpha),$$

with $\Psi(\alpha)$ being a fractional correction factor.

In the above expressions, the term $\frac{\beta_H}{\eta_1+\mu+\mu_H}$ represents the typical quantity of subsequent infections resulting from a single individual infected by HIV, whereas the term $\frac{\beta_H \xi_3 \eta_1}{\mu(\eta_1+\mu+\mu_H)}$ symbolizes the typical quantity of additional infections that a single ART recipient causes. Furthermore, $\frac{1}{\eta_1+\mu+\mu_H}$ and $\frac{1}{\mu}$, respectively, represent the median contagious duration for HIV-positive people and those undergoing HIV therapy.

Local and Global Stability of the HIV Free Equilbrium Point(HIVFEP)

Theorem 7.4 *The HIV free equilibrium point, $\mathcal{E}_H^0$ is locally asymptotically stable if $|arg(\lambda_i)| > \alpha\frac{\pi}{2}$ for all eigenvalue λ_i of $\mathcal{A}$, where $\mathcal{A}$ is a linearized matrix obtained by computing the Jacobian of system (7.20) at $\mathcal{E}_H^0$ and unstable if there exists atleast one eigenvalue λ_i such that $|arg(\lambda_i)| < \alpha\frac{\pi}{2}$.*

Proof. The Jacobian of sub-model (7.20) evaluated at $\mathcal{E}_H^0$ is a linearized matrix

$$\mathcal{A} = \begin{bmatrix} -\mu & -\beta_H & -\xi_3\beta_H \\ 0 & \beta_H - (\eta_1 + \mu + \mu_H) & \xi_3\beta_H \\ 0 & \eta_1 & -\mu \end{bmatrix}$$

The eigenvalues of $\mathcal{A}$ are the solutions of the characteristic equation

$$\begin{vmatrix} -\mu - \lambda & -\beta_H & -\xi_3\beta_H \\ 0 & \beta_H - (\eta_1 + \mu + \mu_H) - \lambda & \xi_3\beta_H \\ 0 & \eta_1 & -\mu - \lambda \end{vmatrix} = 0.$$

After some algebraic simplification, it can be shown that the eigenvalues of $\mathcal{A}$ satisfy the condition $|arg(\lambda_i)| > \frac{\alpha\pi}{2}$ for each $i = 1, 2, 3$ and $\alpha \in (0, 1)$. Accordingly, by Lemma (4.2) $\mathcal{E}_H^0$ is locally asymptotically stable.

The following theorem examines the global level stability of HIVFEP.

Theorem 7.5 *The HIVFEP $\mathcal{E}_H^0$ of model (7.20) is globally asymptotically stable throughout its feasible region if $\mathcal{R}_H^{(\alpha)} < 1$.*

Proof. The proof can be established in similar way to that of Theorem (6.5).

Existence of HIV Endemic Equilibrium Point (HIVEEP)

Theorem 7.6 *When $\mathcal{R}_H^{(\alpha)} > 1$, the HIV sub-model (7.20) has a unique positive HIVEEP $\mathcal{E}_H^* = (S^*, I_H^*, T_H^*)$, where*

$$S^* = \frac{\Lambda N^*}{\beta_H(I_H^* + \xi_3 T_H^*) + \mu N^*}, \; I_H^* = \frac{\beta_H \xi_3 T_H^* S^*}{(\eta_1 + \mu + \mu_H)N^* - \beta_H S^*}, \; T_H^* = \frac{\eta_1}{\mu} I_H^*.$$

Proof. The point where HIV illness is prevalent in the population is known as the HIVEEP. Consider the system of non-linear equations,

$$\begin{cases} \Lambda - \frac{\beta_H}{N^*}(I_H^* + \xi_3 T_H^*)S^* - \mu S^* = 0 \\ \frac{\beta_H}{N^*}(I_H^* + \xi_3 T_H^*)S^* - (\eta_1 + \mu + \mu_H)I_H^* = 0 \\ \eta_1 I_H^* - \mu T_H^* = 0 \end{cases} \tag{7.22}$$

Thus, by solving system (7.22) we obtain the above expressions for S^*, I_H^* and T_H^*. The proof for the existence of the HIVEEP follows the same techniques developed in Theorem (3.3) of (Khajanchi et al., 2018) and Theorem 2 of (Aldila et al., 2020).

To determine the condition under which the HIVEEP, $\mathcal{E}_H^*$ is locally asymptotically stable, we compute the Jacobian of (7.20) and evaluate it at $\mathcal{E}_H^*$ to obtain a linearized

matrix

$$\mathcal{B} = \begin{bmatrix} -b_3 - \mu & -b_1 & -b_2 \\ b_3 & b_1 - (\eta_1 + \mu + \mu_H) & b_2 \\ 0 & \eta_1 & -\mu \end{bmatrix}$$

where $b_1 = \beta_H \frac{S^*}{N^*}$, $b_2 = \beta_H \xi_3 \frac{S^*}{N^*}$ and $b_3 = b_1 + b_2$. The corresponding characteristic equation of matrix $\mathcal{B}$ is given by

$$\lambda^3 + c_2\lambda^2 + c_1\lambda + c_0 = 0 \tag{7.23}$$

where $c_2 = \eta_1 + 3\mu + \mu_H + b_2$, $c_1 = (2\mu + b_3)(\eta_1 + \mu + \mu_H - b_1) + \mu(\mu + b_3) + \eta_1 b_2 - b_1 b_3$, $c_0 = \mu(\mu + b_3)(\eta_1 + \mu + \mu_H - b_1) + \mu(\eta_1 b_2 - b_1 b_3)$.
The discriminant of the polynomial

$$\mathcal{P}(\lambda) = \lambda^3 + c_2\lambda^2 + c_1\lambda + c_0 \tag{7.24}$$

can be written as

$$D(\mathcal{P}) = 18c_0c_1c_2 + (c_2c_1)^2 - 4(c_0c_2^3 + c_1^3) - 27c_0^2$$

Hence, in the following theorem we state the condition under which the HIVEEP, $\mathcal{E}_H^*$ is locally asymptotically stable (Bourafa et al., 2020; Özalp & Demirci, 2011).

Theorem 7.7 *For $\alpha \in (0, 1]$ all the roots of equation (7.23) satisfy $|arg(\lambda_i)| > \frac{\alpha\pi}{2}$, for each $i = 1, 2, 3$ if the following conditions hold true.*

i) $D(\mathcal{P}) > 0,\ c_0 > 0,\ c_2 > 0$ *and* $c_1c_2 > c_0$

ii) $D(\mathcal{P}) < 0, c_1 \geq 0,\ c_2 \geq 0,\ c_0 > 0,\ c_1c_2 < c_0$ *and* $\alpha < \frac{2}{3}$

iii) $D(\mathcal{P}) < 0, c_1 > 0,\ c_2 > 0$ *and* $c_1c_2 = c_0$

Theorem 7.8 *The HIVEEP, $\mathcal{E}_H^*$ is locally asymptotically stable if any one of the requirements listed in Theorem (7.7) is met.*

Theorem 7.9 *The HIV sub-model (7.20) has a unique positive HIV endemic equilibrium $\mathcal{E}_H^*$ that is globally asymptotically stable whenever $\mathcal{R}_H(\alpha) > 1$.*

Proof. We follow the same approach developed under Theorem (6.8). In the context of epidemiology, this finding implies that as long as $\mathcal{R}_H^{(\alpha)} > 1$, one can not be able to avoid HIV from the society in the long run.

7.2.4 The TB Sub-model

In this section, we analyze the basic properties of model (7.3) assuming that the population is free from HIV. Hence, equating all the state variables I_H, L_C, I_C and T_H to zero, the TB sub-model becomes

$$\begin{cases} {}_0^C D_t^\alpha S(t) = \Lambda + \tau R_T - \frac{\beta_T}{N}(I_T + \rho_2 T_T)S - \mu S, \\ {}_0^C D_t^\alpha L_T(t) = \frac{\beta_T}{N}(I_T + \rho_2 T_T)S + (1-\theta)\sigma T_T - \frac{\varphi\beta_T}{N}(I_T + \rho_2 T_T)L_T - (\mu + \kappa_1)L_T, \\ {}_0^C D_t^\alpha I_T(t) = \frac{\varphi\beta_T}{N}(I_T + \rho_2 T_T)L_T + \kappa_1 L_T + \theta\sigma T_T - (\omega + \mu + \mu_T)I_T, \\ {}_0^C D_t^\alpha T_T(t) = \omega I_T - (\sigma + \gamma_1 + \mu + \mu_T)T_T, \\ {}_0^C D_t^\alpha R_T(t) = \gamma_1 T_T - (\mu + \tau)R_T, \quad 0 < \alpha \leq 1. \end{cases} \tag{7.25}$$

subject to initial values

$$\begin{aligned} S(0) = S_0 \geq 0,\ L_T(0) = L_{T_0} > 0,\ I_T(0) = I_{T_0} > 0, \\ T_T(0) = T_{T_0} \geq 0,\ R_T(0) = R_{T_0} \geq 0. \end{aligned} \tag{7.26}$$

Basic Reproduction Number for TB Sub-model

The TB free equilibrium point (TBFEP) of the sub-model (7.25), which describes the state in which there is no TB in the population is, $\mathcal{E}_T^0 = (\frac{\Lambda}{\mu}, 0, 0, 0, 0)$. Using the next-generation matrix technique established in Zhu et al. (2020), we now calculate the basic reproduction number of our TB sub-model. As a result, the matrices for the transfer terms (V) and the new infection terms (F) are provided as

$$F = \begin{bmatrix} 0 & \beta_T & \beta_T\rho_2 \\ 0 & 0 & 0 \\ 0 & 0 & 0 \end{bmatrix}, \quad V = \begin{bmatrix} q_1 & 0 & -q_2 \\ -\kappa_1 & q_3 & -q_5 \\ 0 & -\omega & q_4 \end{bmatrix},$$

where, $q_1 = \mu + \kappa_1$, $q_2 = (1-\theta)\sigma$, $q_3 = \omega + \mu + \mu_T$, $q_4 = \sigma + \gamma_1 + \mu + \mu_T$ and $q_5 = \theta\sigma$. Consequently, the largest spectral radius of FV^{-1} is the basic reproduction number of the TB sub-model and it is expressed as

$$\mathcal{R}_T^{(\alpha)} = -\frac{\beta_T\kappa_1}{D}\left[q_4 + \rho_2\omega\right]\Psi(\alpha)$$

where $D = \kappa_1 q_2\omega - q_1 q_3 q_4 + q_1 q_5\omega < 0$, with $\Psi(\alpha)$ being a fractional corrector factor.

In the above expressions for $\mathcal{R}_T$, the term $-\frac{\beta_T\kappa_1 q_4}{D}\Psi(\alpha)$ corresponds to the mean quantity of subsequent infections caused by a single, actively infected person with TB, whereas $-\frac{\beta_T\kappa_1\rho_2\omega}{D}\Psi(\alpha)$ shows how many additional infections a single person receiving

TB treatment typically causes. Additionally, the terms $\frac{1}{q_3}$ and $\frac{1}{q_4}$ represents, respectively, the typical communicable duration of those who are actively infected and those undergoing treatment.

Bifurcation Analysis of the TB Sub-model

By applying the center manifold theory developed in C. Castillo-Chavez & Song (2004), we now investigate the direction of the bifurcation.
Let

$$x = [x_1, x_2, x_3, x_4, x_5]^T = [S, L_T, I_T, T_T, R_T]^T$$

Then, the TB sub-model (7.25) can be written compactly in the form of

$$\begin{cases} {}_0^C D_t^\alpha x_1(t) = \Lambda + \tau x_5 - \frac{\beta_T}{N}(x_3 + \rho_2 x_4)x_1 - \mu x_1, \\ {}_0^C D_t^\alpha x_2(t) = \frac{\beta_T}{N}(x_3 + \rho_2 x_4)x_1 + (1-\theta)\sigma x_4 - \frac{\varphi\beta_T}{N}(x_3 + \rho_2 x_4)x_2 - h_1 x_2, \\ {}_0^C D_t^\alpha x_3(t) = \frac{\varphi\beta_T}{N}(x_3 + \rho_2 x_4)x_2 + \kappa_1 x_2 + \theta\sigma x_4 - h_2 x_3, \\ {}_0^C D_t^\alpha x_4(t) = \omega x_3 - h_3 x_4, \\ {}_0^C D_t^\alpha x_5(t) = \gamma_1 x_4 - h_4 x_5 \end{cases} \tag{7.27}$$

with $h_1 = \mu + \kappa_1$, $h_2 = \omega + \mu + \mu_T$, $h_3 = \sigma + \gamma_1 + \mu + \mu_T$, $h_4 = \mu + \tau$ and $N = x_1 + x_2 + x_3 + x_4 + x_5$.

Choosing β_T^* as a bifurcation parameter and solving for it at $\mathcal{R}_T^{(\alpha)} = 1$

we get $\beta_T^* = \frac{h_1 h_2 h_3 - \omega\sigma(\mu\theta + \kappa_1)}{\kappa_1 \rho_2 \omega}$. Hence, $\beta^\star > 0$ is evident. It is possible to demonstrate that $\mathcal{J}(\mathcal{E}_T^0, \beta_T^*)$ has a simple zero eigenvalue and that the other eigenvalues are either negative or have negative real parts by setting $\beta_T = \beta_T^*$ and calculating the Jacobean model (7.25) at $\mathcal{E}_T^0$. The equilibrium $\mathcal{E}_T^0$ is hence non-hyperbolic. For the zero eigenvalue, let $u = (u_1, u_2, u_3, u_4, u_5)^T$ be the right eigenvector and $v = (v_1, v_2, v_3, v_4, v_5)$ be the left eigenvector. When $\mathcal{J}(\mathcal{E}_T^0, \beta_T^*).u$ is solved then we obtain

$$u_1 = \left(\frac{\tau\gamma_1\omega}{\mu h_3 h_4} - \frac{\beta_T^*}{\mu} - \frac{\rho_2\omega}{\mu h_3}\right)u_3,\ u_2 = \left[\frac{\beta_T^*}{h_1} + \frac{\omega}{h_1 h_3}(\beta_T^*\rho_2 + (1-\theta)\sigma)\right]u_3 > 0,$$

$$u_3 = u_3 > 0,\ u_4 = \frac{\omega}{h_3}u_3 > 0, u_5 = \frac{\gamma_1\omega}{h_3 h_4}u_3 > 0.$$

Similarly, solving $v.\mathcal{J}(\mathcal{E}_T^0, \beta_T^*) = 0$ we obtain

$$v_1 = v_5 = 0,\ v_3 = v_3 > 0, v_2 = \frac{\kappa_1}{h_1}v_3 > 0,\ v_4 = \left[\frac{\kappa_1}{h_1 h_3}(\beta_T^*\rho_2 + (1-\theta)\sigma) + \frac{\theta\sigma}{h_3}\right]v_3 > 0.$$

The criteria $u.v = 1$ should be met by the eigenvectors u and v. To determine which

way the bifurcation is going, let

$$a = \sum_{k,i,j=1}^{5} v_k u_i u_j \frac{\partial^2 f_k}{\partial x_i \partial x_j}|(\mathcal{E}_T^0, \beta_T^*),\ b = \sum_{k,i=1}^{5} v_k u_i \frac{\partial^2 f_k}{\partial x_i \partial \beta_T}|(\mathcal{E}_T^0, \beta_T^*)$$

be the bifurcation coefficients illustrating the system's behavior in the center manifold. Since $v_1 = v_5 = 0$, only the second order partial derivatives of f_2, f_3, and f_4 need to be calculated.

Finally we arrive at,

$$a = \frac{2v_2\beta_T^*}{N}(u_1u_3 + \rho_2 u_1 u_4) + \frac{2\varphi\beta_T^*}{N}(u_2u_3 + \rho_2 u_2 u_4)(v_3 - v_2), \quad b = v_2(u_3 + \rho_2 u_4) > 0.$$

We see that $a > 0$ if

$$\varphi > \varphi^* = \frac{-\kappa_1(u_1u_3 + \rho_2 u_1 u_4)}{\mu(u_2u_3 + \rho_2 u_2 u_4)} = \frac{-\kappa_1 u_1}{\mu u_2}.$$

Thus, we summarize this section with the following theorem.

Theorem 7.10 *At $\mathcal{R}_T^{(\alpha)} = 1$, the TB sub-model (7.25) runs through*

i) a forward bifurcation if $\varphi < \frac{-\kappa_1 u_1}{\mu u_2}$ and

ii) a backward bifurcation if $\varphi > \frac{-\kappa_1 u_1}{\mu u_2}$.

The forward bifurcation phenomenon indicates that the stable TBFEP splits into two non-negative equilibrium points: the unstable TBFEP and the stable positive TBEEP, as $\mathcal{R}_T^{(\alpha)}$ passes unity. According to epidemiology, this means that TB cannot spread throughout the population for $\mathcal{R}_T^{(\alpha)} < 1$.

Furthermore, the phenomena of backward bifurcation reveals that two positive TBEEP (the smaller unstable and the larger stable) co-exist with a locally asymptotically stable TBFEP when $\mathcal{R}_T^{(\alpha)} < 1$. This means that a disease cannot be eradicated from the population by lowering the basic reproduction number below unity alone.

Local and Global Stability of the TB Free Equilbrium Point

Theorem 7.11 *The TB free equilibrium point, $\mathcal{E}_T^0$ is locally asymptotically stable if $|arg(\lambda_i)| > \alpha\frac{\pi}{2}$ for all eigenvalue λ_i of $\mathcal{M}$, where $\mathcal{M}$ is a linearized matrix obtained by computing the Jacobian of system (7.25) at $\mathcal{E}_T^0$ and unstable if there exists at least one eigenvalue λ_i such that $|arg(\lambda_i)| < \alpha\frac{\pi}{2}$.*

Proof. The Jacobian of sub-model (7.25) evaluated at $\mathcal{E}_T^0$ is a linearized matrix

$$\mathcal{M} = \begin{bmatrix} -\mu & 0 & -\beta_T & -\beta_T\rho_2 & \tau \\ 0 & -h_1 & \beta_T & \beta_T\rho_2 + (1-\theta)\sigma & 0 \\ 0 & \kappa_1 & -h_2 & \theta\sigma & 0 \\ 0 & 0 & \omega & -h_3 & 0 \\ 0 & 0 & 0 & \gamma_1 & -h_4 \end{bmatrix}$$

with $h_1,\ h_2,\ h_3$ and h_4 as defined under equation (7.27). Numerical evaluation using parameter values from Table (7.2) shows that the condition $|arg(\lambda_i)| > \frac{\alpha\pi}{2}$ holds true for $\forall\lambda_i$ and $\alpha \in (0, 1]$. Accordingly, Lemma (4.2) validates that $\mathcal{E}_T^0$ is locally asymptotically stable. We examine the global stability of TBFEP in the following theorem.

Theorem 7.12 *If the exogenous re-infection rate $\varphi < \frac{-\kappa_1 u_1}{\mu u_2}$, the TB free equilibrium $\mathcal{E}_T^0$ of sub-model (7.25) is globally asymptotically stable in its biologically feasible region for $\mathcal{R}_T^{(\alpha)} < 1$.*

Proof. To complete the proof, by assuming that $\varphi < \frac{-\kappa_1 u_1}{\mu u_2}$, we construct and analyze an appropriate Lyapunov function as we did for Theorem (6.10). Based on an epidemiological perspective, this result suggests that we will eventually be able to wipe out tuberculosis from the community when $\mathcal{R}_T^{(\alpha)} < 1$.

The presence of endemic equilibrium point for TB (TBEEP)

Theorem 7.13 *When $\mathcal{R}_T^{(\alpha)} > 1$, the TB sub-model (7.25) has a unique positive TBEEP given by, $\mathcal{E}_T^* = (S^*, L_T^*, I_T^*, T_T^*, R_T^*)$, where,*

$$S^* = \frac{N^*[\Lambda h_3(\mu+\tau) + \tau\gamma_1\omega I_T^*]}{(\mu+\tau)[\beta_T I_T^*(h_3+\rho_2\omega) + \mu h_3 N^*]},\ L_T^* = \frac{\beta_T S^* I_T^*(h_3+\rho_2\omega+(1-\theta)\omega\sigma)}{\varphi\beta_T I_T^*(h_3+\rho_2\omega) + h_1 h_3 N^*},$$

$$I_T^* = \frac{\kappa_1 h_3 L_T^* N^*}{h_2 h_3 N^* - (\varphi\beta_T h_3 L_T^* + \omega\varphi\beta_T\rho_2 L_T^* + \omega\theta\sigma N^*)},\ T_T^* = \frac{\omega}{h_3} I_T^*,\ R_T^* = \frac{\gamma_1\omega}{h_3(\mu+\tau)} I_T^*,$$

h_1, h_2 and h_3 are as defined before.

Proof. The TB endemic equilibrium is the state at which TB persists in the community. To obtain the above expressions for $S^*, L_T^*, I_T^*, T_T^*, R_T^*$ we solve the system of

equation given as

$$\begin{cases} \Lambda + \tau R_T^* - \frac{\beta_T}{N^*}(I_T^* + \rho_2 T_T^*)S^* - \mu S^* = 0, \\ \frac{\beta_T}{N^*}(I_T^* + \rho_2 T_T^*)S^* + (1-\theta)\sigma T_T^* - \frac{\varphi\beta_T}{N^*}(I_T^* + \rho_2 T_T^*)L_T^* - (\mu + \kappa_1)L_T^* = 0, \\ \frac{\varphi\beta_T}{N^*}(I_T^* + \rho_2 T_T^*)L_T^* + \kappa_1 L_T^* + \theta\sigma T_T^* - (\omega + \mu + \mu_T)I_T^* = 0, \\ \omega I_T^* - (\sigma + \gamma_1 + \mu + \mu_T)T_T^* = 0, \\ \gamma_1 T_T^* - (\mu + \tau)R_T^* = 0, \end{cases} \tag{7.28}$$

The proof for the existence of the TBEEP follows the same techniques developed in Theorem (3.3) of (Khajanchi et al., 2018) and Theorem 2 of (Aldila et al., 2020).

Theorem 7.14 *The TBEEP, $\mathcal{E}_T^*$ of the TB sub-model (7.25) is locally asymptotically stable for $\mathcal{R}_T^{(\alpha)} > 1$ provided that $\varphi < \frac{-\kappa_1 u_1}{\mu u_2}$.*

Proof. We linearize system (7.25) at $\mathcal{E}_T^*$ to obtain a linearize matrix $\mathcal{B}$. Employing the computer algebra system with parameter values from Table (7.2) we confirm that $|arg(\lambda_i)| > \alpha\frac{\pi}{2}$ for all eigenvalues λ_i of $\mathcal{B}$. Thus, by Lemma (4.2) we conclude that $\mathcal{E}_T^*$ is locally asymptotically stable for $\mathcal{R}_T^{(\alpha)} > 1$.

Theorem 7.15 *If $\mathcal{R}_T^{(\alpha)} > 1$, the TBEEP $\mathcal{E}_T^*$ of sub-model (7.25) is globally asymptotically stable.*

From an epidemiological perspective, this result suggests that we will not be able to completely eliminate tuberculosis from the community whenever $\mathcal{R}_T^{(\alpha)} > 1$.

7.2.5 Analysis of the HIV-TB Co-infection Model

In this section we analyze the HIV-TB co-infection model (7.3).

Basic Reproduction Number

The number of subsequent infections resulting from a single person with dominant disease in the fully susceptible population is known as the basic reproduction number, or $\mathcal{R}_0$, in the whole HIV-TB model. It is defined as

$$\mathcal{R}_0^{(\alpha)} = max\{\mathcal{R}_H^{(\alpha)}, \mathcal{R}_T^{(\alpha)}\},$$

where $\mathcal{R}_H^{(\alpha)}$ and $\mathcal{R}_T^{(\alpha)}$ are the reproduction numbers corresponding to HIV and TB respectively which are computed under sections (7.2.3) and (7.2.4). Thus, the dynamics of the HIV-TB co-infection model is dominated by the disease with the highest basic reproduction number.

Stability of the Disease Free Equilibrium (DFE)

In the entire HIV-TB model (7.3), the point at which the community is free of both HIV and TB is known as the disease free equilibrium (DFE). It is given as

$$\mathcal{E}^0 = \left(\frac{\Lambda}{\mu}, 0, 0, 0, 0, 0, 0, 0, 0\right).$$

Theorem 7.16 *The DFE, $\mathcal{E}^0$ of HIV-TB co-infection model (7.3) is locally asymptotically stable if $|arg(\lambda_i)| > \alpha\frac{\pi}{2}$ for all eigenvalue λ_i of $\mathcal{C}$, where $\mathcal{C}$ is a linearized matrix obtained by computing the Jacobian of system (7.3) at $\mathcal{E}^0$ and unstable if there exists at least one eigenvalue λ_i such that $|arg(\lambda_i)| < \alpha\frac{\pi}{2}$.*

Proof. The jacobian of system (7.3) evaluated at $\mathcal{E}^0$ is a linearized matrix

$$\mathcal{C} = \begin{pmatrix} -\mu & 0 & -\beta_T & -\beta_T\rho_2 & \tau & -\beta_H & -\beta_H\xi_1 & -\beta_T\rho_1 - \beta_H\xi_1 & -\beta_H\xi_3 \\ 0 & -g_1 & \beta_T & \beta_T\rho_2 + (1-\theta)\sigma & 0 & 0 & 0 & \beta_T\rho_1 & 0 \\ 0 & \kappa_1 & -g_2 & \theta\sigma & 0 & 0 & 0 & 0 & 0 \\ 0 & 0 & \omega & -g_3 & 0 & 0 & 0 & 0 & 0 \\ 0 & 0 & 0 & \gamma_1 & -g_4 & 0 & 0 & 0 & 0 \\ 0 & 0 & 0 & 0 & 0 & \beta_H - g_5 & \beta_H\xi_1 & \beta_H\xi_2 & \beta_H\xi_3 \\ 0 & 0 & 0 & 0 & 0 & 0 & -g_6 & 0 & 0 \\ 0 & 0 & 0 & 0 & 0 & 0 & \kappa_2 & -g_7 & 0 \\ 0 & 0 & 0 & 0 & 0 & \eta_1 & 0 & \eta_2 + \gamma_2 & -\mu \end{pmatrix},$$

where $g_1 = \mu + \kappa_1$, $g_2 = \omega + \mu + \mu_T$, $g_3 = \sigma + \gamma_1 + \mu + \mu_T$, $g_4 = \mu + \tau$, $g_5 = \eta_1 + \mu + \mu_H$, $g_6 = \kappa_2 + \mu + \mu_H$ and $g_7 = \eta_2 + \gamma_2 + \mu + \mu_C$.

Numerical evaluation using parameter values from Table (7.2) shows that each eigenvalues of $\mathcal{C}$ satisfy the Matignon's stability criterion. Therefore, $\mathcal{E}^0$ is locally asymptotically stable.

Existence of the Endemic Steady States

Biologically, there exists three endemic steady states for the HIV-TB co-infection model (Aggarwal et al., 2021). These are:

a) The HIV endemic steady state

It describes the situation where the sole endemic disease in the community is HIV. It is given as

$$\hat{\mathcal{E}_H} = (S^*, 0, 0, 0, 0, I_H^*, 0, 0, T_H^*),$$

where the non zero components of $\hat{\mathcal{E}_H}$ are obtained from theorem (7.6).

b) The TB endemic steady state

It refers to the state at which only TB is endemic in the population. It is given as

$$\hat{\mathcal{E}_T} = (S^*, L_T^*, I_T^*, T_T^*, R_T^*, 0, 0, 0, 0),$$

where the non zero components of $\hat{\mathcal{E}_T}$ are obtained from theorem (7.13).

c) The interior HIV-TB co-endemic steady state

This refers to the state at which both HIV and TB are endemic in the population and is given as

$$\mathcal{E}^\star = (S^\star, L_T^\star, I_T^\star, T_T^\star, R_T^\star, I_H^\star, L_C^\star, I_C^\star, T_H^\star),$$

where each components of $\mathcal{E}^\star$ are positive and computed by setting the right hand sides of equation (7.3) to zero.

Theorem 7.17 *The DFE , $\mathcal{E}^0$ of HIV-TB co-infection model (7.3) is globally asymptotically stable in its biologically feasible region $\mathcal{D}$ if $\mathcal{R}_T^{(\alpha)} < 1$.*

Proof. It can be outlined similar to that of Theorem (6.15).

Theorem 7.18 *The unique positive endemic equilibrium , $\mathcal{E}^*$ of HIV-TB co-infection model (7.3) is both locally and globally asymptotically stable in its biologically feasible region $\mathcal{D}$ if $\mathcal{R}_T^{(\alpha)} > 1$.*

Proof. We can sketch the proof similar to the way we did in Theorems (6.16) and (6.17). Table (7.2) provides a summary of the model parameter values. While some of these model parameters are assumed, others are taken from the literature. The sensitivity indices of model parameters with respect to $\mathcal{R}_T$ and $\mathcal{R}_H$ are therefore calculated using formula (4.42) and are provided in Table (7.3). According to the sensitivity analysis's findings, the parameters $\beta_T, \kappa_1, \theta, \sigma, \rho_2, \beta_H, \eta_1$, and ξ_3 have positive indices, whereas the others have negative ones. A positive index indicates a direct association between the model parameters and the associated fundamental reproductive number, while an index that is negative indicates inverse relationship. As a result, $\mathcal{R}_T$ will decrease as the active TB treatment rate rises and the TB effective contact rate, per-capita rates of being infectious for individuals in L_T class falls. Likewise, lowering the HIV effective contact rate and the infectiousness rate of individuals in I_H class results in a drop in $\mathcal{R}_H$. Biologically, this means that the likelihood of the diseases spreading will be reduced if interactions between diseased and non-infected individuals are reduced.

Table 7.2: Parameter values used in numerical simulations.

Parameters	Values	Source
Λ	1265 $pers/yr$	calculated
β_T	$1.525/(pers \times yr)$	Table (6.2)
β_H	$0.1855/(pers \times yr)$	Table (6.2)
μ	$0.01/year$	calculated
μ_T	$0.0767/year$	assumed
μ_H	$0.0154/year$	(Adeyemo et al., 2023)
μ_C	$0.2096/year$	(Adeyemo et al., 2023)
τ	$0.01/(pers \times yr)$	assumed
θ	$0.0866/(pers \times yr)$	assumed
σ	$0.01/(pers \times yr)$	assumed
η_1	$0.46/(pers \times yr)$	assumed
η_2	$0.1/(pers \times yr)$	(Aggarwal et al., 2021)
ω	$0.2506/(pers \times yr)$	assumed
γ_1	$0.0686/year$	assumed
γ_2	$0.0097/year$	assumed
κ_1	$0.1142/(pers \times yr)$	Table (6.2)
κ_2	$0.0017/(pers \times yr)$	(Aggarwal et al., 2021)
ρ_1, ρ_2	0.1, 0.01	assumed
ξ_1, ξ_2, ξ_3	0.2, 0.15, 0.1	assumed
φ	$0.71/(pers \times yr)$	(Aggarwal et al., 2021)

Table 7.3: Sensitivity indices of $\mathcal{R}_T$ and $\mathcal{R}_H$ to the parameters.

Parameters	Sensitivity index($\mathcal{R}_T$)	Parameters	Sensitivity index($\mathcal{R}_T$)	Parameters	Sensitivity index($\mathcal{R}_H$)
β_T	+1.0000	θ	0.0101	β_H	+1.0000
μ	-0.7977	σ	0.0348	μ	-0.6579
μ_T	-0.3235	ρ_2	0.0223	μ_H	-0.5223
κ_1	0.5704	ω	-0.4515	η_1	0.1803
γ_1	-0.0324			ξ_3	0.2548

7.3 Fractional Optimal Control Problem

In this part, the HIV-TB co-infection model (7.3) is extended to a fractional optimal control problem to investigate the impact of time-dependent controls on the dynamics of the diseases. As therapy is available for TB-infected individuals, we present the control $u_1(t)$, which, when administered quickly, will increase the rate of recovery for TB-infected individuals. The administration of antiretroviral drugs, which reduce the viral load in infected people, is one of the most important strategies that can help stop HIV from spreading. We offer this method as the control $u_2(t)$, such that when $u_2(t)$ increases, the viral load decreases, which helps to improve the person's ability to fight off the infection. Consequently, the optimal control problem's extended model is

$$\begin{aligned}
{}_0^C D_t^\alpha S(t) &= \Lambda + \tau R_T - (\lambda_T + \lambda_H)S - \mu S, \\
{}_0^C D_t^\alpha L_T(t) &= \lambda_T S + (1-\theta)\sigma T_T - \lambda_{L_H} L_T - \varphi \lambda_T L_T - (\mu + \kappa_1) L_T, \\
{}_0^C D_t^\alpha I_T(t) &= \kappa_1 L_T + \varphi \lambda_T L_T + \theta \sigma T_T - \lambda_{I_H} I_T - (\omega + u_1 + \mu + \mu_T) I_T, \\
{}_0^C D_t^\alpha T_T(t) &= (\omega + u_1) I_T - (\sigma + \gamma_1 + \mu + \mu_T) T_T, \\
{}_0^C D_t^\alpha R_T(t) &= \gamma_1 T_T - (\mu + \tau) R_T, \\
{}_0^C D_t^\alpha I_H(t) &= \lambda_H S - \lambda_T I_H - (\eta_1 + u_2 + \mu + \mu_H) I_H, \\
{}_0^C D_t^\alpha L_C(t) &= \lambda_T I_H + \lambda_{L_H} L_T - (\kappa_2 + \mu + \mu_H) L_C, \\
{}_0^C D_t^\alpha I_C(t) &= \lambda_{I_H} I_T + \kappa_2 L_C - (\eta_2 + \gamma_2 + \mu + \mu_C) I_C, \\
{}_0^C D_t^\alpha T_H(t) &= (\eta_1 + u_2) I_H + (\eta_2 + \gamma_2) I_C - \mu T_H,
\end{aligned} \tag{7.29}$$

with the initial conditions given as in equation (7.2) and $\lambda_T, \lambda_H, \lambda_{L_H}, \lambda_{I_H}$ are as defined under section (7.2).

The controls $u_j(.), j = 1, 2$, are assumed to be constrained between 0 and u_{jmax}. Because it gives the model a more realistic medical viewpoint, u_{jmax} can never equal 1 in this case. For this reason, we assumed that $u_{jmax} \leq 1 - \delta, j = 1, 2$, where $\delta << 1$ indicates a real number that is positive. When the controls go, no further steps are done to prevent either disease. $u = (u_1, u_2)$ is the notation we employ for convenience and future use.

Our major objective is to reduce the costs and illness burdens associated with HIV and TB treatment. Hence,

$$\mathcal{J}(u) = \int_0^{t_f} \left(K_1 I_T(t) + K_2 I_H(t) + K_3 L_C(t) + K_4 I_C(t) + \frac{1}{2} \sum_{j=1}^{2} W_j u_j^2 \right) dt \to min \tag{7.30}$$

subject to (7.29) with its initial conditions. The weight constants for active TB infec-

tion, HIV infection, HIV-latent TB co-infection, and HIV-active TB co-infection are represented by the positive coefficients K_1, K_2, K_3, and K_4 respectively. The weight constants that quantify the relative costs of the treatments linked to the controls u_1 and u_2 are represented by the parameters W_1 and W_2, respectively.

The higher the W_1 and W_2 numbers, the higher the treatment's implementation cost. The final intervention time is indicated by the fixed constant t_f. The terms $K_1 I_T(t)$, $K_2 I_H(t)$, $K_3 L_C(t)$, and $K_4 I_C(t)$ also denote the expenses related to active TB infection, HIV infection, HIV-latent TB co-infection, and HIV-active TB co-infection, respectively.

In this case, our primary goal is to determine the best control $u^* = (u_1^*, u_2^*)$ of the control functions
$u(t) = (u_1(t), u_2(t))$. The associated state trajectories minimize the cost functional given in (7.30) and represent the solution of the system (7.29) in the intervention time period $[0, t_f]$. More specifically,

$$\mathcal{J}(u^*(t)) = min(\mathcal{J}(u) : u \in \mathcal{U}) \tag{7.31}$$

subject to the system (7.29) where,

$$\mathcal{U} = \{u = (u_1, u_2) \text{ are measurable and } 0 \leq u_j(t) \leq 1, j = 1, 2, \forall_t \in [0, t_f]\} \tag{7.32}$$

The fractional Pontryagin's Minimum Principle given in Mahata et al. (2022); Bergounioux & Bourdin (2020) contributes to the reduction of problems (7.29), (7.30), and (7.32) to a problem of minimizing the Hamiltonian $\mathcal{H}$, which is provided as follows:

$$\mathcal{H} = K_1 I_T(t) + K_2 I_H(t) + K_3 L_C(t) + K_4 I_C(t) + \frac{1}{2}\sum_{j=1}^{2} W_j u_j^2 + \sum_{j=1}^{9} q_j(t) g_j(t, x) \tag{7.33}$$

where $g_j^{'}s$ represents the right hand side of the functions given in equation (7.29) above, $x = (S, L_T, I_T, T_T, R_T, I_H, L_C, I_C, T_H)$ and $q : [0, t_f] \to \mathbb{R}^9$ given by $q = (q_1(t), q_2(t), \cdots, q_9(t))$ is a nontrivial absolutely continuous adjoint vector.

Remark 7.2 *By verifying* $\frac{\partial^2 \mathcal{H}}{\partial u^2} > 0$, *one can observe that the pair* (x^*, u^*) *is a candidate for minimizer.*

Theorem 7.19 *Let* $u \in [0, 1]$ *be a measurable control function on* $[0, t_f]$. *Then an optimal control* u^* *minimizing the objective function* $\mathcal{J}(u)$ *of (7.30) is*

$$u^* = min\left\{max\left\{0, \tilde{u}\right\}, 1\right\},$$

with $\tilde{u} = (\tilde{u_1}, \tilde{u_2}) = \left(\frac{(q_3-q_4)I_T}{W_1}, \frac{(q_6-q_9)I_H}{W_2}\right)$. *Furthermore, from the boundedness of* $u_j^*(t)$ *on* $(0,1)$ *and the minimality condition, we have:*

$$u_1^* = \begin{cases} 0, & if \quad \frac{\partial \mathcal{H}}{\partial u_1} > 0, \\ \frac{(q_3-q_4)I_T}{W_1}, & if \quad \frac{\partial \mathcal{H}}{\partial u_1} = 0, \\ 1, & if \quad \frac{\partial \mathcal{H}}{\partial u_1} < 0. \end{cases} \qquad u_2^* = \begin{cases} 0, & if \quad \frac{\partial \mathcal{H}}{\partial u_2} > 0, \\ \frac{(q_6-q_9)I_H}{W_2}, & if \quad \frac{\partial \mathcal{H}}{\partial u_2} = 0, \\ 1, & if \quad \frac{\partial \mathcal{H}}{\partial u_2} < 0. \end{cases}$$

Proof. Following the same techniques in Mahata et al. (2022); Rosa & Torres (2023), the minimality condition of PMP confirms that the optimal controls are obtained by solving $\frac{\partial \mathcal{H}}{\partial u_j} = 0$ and are given as

$$\begin{cases} u_1(t) = \frac{(q_3-q_4)I_T}{W_1}, \\ u_2(t) = \frac{(q_6-q_9)I_H}{W_2}. \end{cases} \tag{7.34}$$

The adjoint system which is a fractional system of right Riemann–Liouville derivatives can be obtained from the relation

$${}_tD_{t_f}^{\alpha} q_1(t) = \frac{-\partial \mathcal{H}}{\partial S}, \quad {}_tD_{t_f}^{\alpha} q_2(t) = \frac{-\partial \mathcal{H}}{\partial L_T}, \quad {}_tD_{t_f}^{\alpha} q_3(t) = \frac{-\partial \mathcal{H}}{\partial I_T}, \quad {}_tD_{t_f}^{\alpha} q_4(t) = \frac{-\partial \mathcal{H}}{\partial T_T}, \quad {}_tD_{t_f}^{\alpha}$$

$$q_5(t) = \frac{-\partial \mathcal{H}}{\partial R_T}, \ {}_tD_{t_f}^{\alpha} q_6(t) = \frac{-\partial \mathcal{H}}{\partial I_H}, \quad {}_tD_{t_f}^{\alpha} q_7(t) = \frac{-\partial \mathcal{H}}{\partial L_C},$$

$${}_tD_{t_f}^{\alpha} q_8(t) = \frac{-\partial \mathcal{H}}{\partial I_C}, \quad {}_tD_{t_f}^{\alpha} q_9(t) = \frac{-\partial \mathcal{H}}{\partial T_H}$$

More briefly this can be written as

$$\begin{cases} {}_tD_{t_f}^{\alpha} q_1(t) = (\lambda_T + \lambda_H)q_1 - \lambda_T q_2 - \lambda_H q_6, \\ {}_tD_{t_f}^{\alpha} q_2(t) = (\lambda_{L_H} + \varphi\lambda_T + \mu + \kappa_1)q_1 - (\kappa_1 + \varphi\lambda_T)q_3 - \lambda_{L_H} q_7, \\ {}_tD_{t_f}^{\alpha} q_3(t) = -K_1 + \frac{\beta_T S(q_1-q_2)}{N} + \frac{\beta_T \varphi L_T(q_2-q_3)}{N} + \frac{\beta_T I_H(q_6-q_7)}{N} - \lambda_{I_H} q_8 - (\omega + u_1)q_4 \\ \qquad +(\omega + u_1 + \mu + \mu_T)q_3, \\ {}_tD_{t_f}^{\alpha} q_4(t) = \frac{\beta_T \rho_2 S(q_1-q_2)}{N} + \frac{\beta_T \varphi \rho_2 L_T(q_2-q_3)}{N} + \frac{\beta_T \rho_2 I_H(q_6-q_7)}{N} - (1-\theta)q_2 - \theta\sigma q_3 - \gamma_1 q_5 \\ \qquad +(\sigma + \gamma_1 + \mu + \mu_T)q_4, \\ {}_tD_{t_f}^{\alpha} q_5(t) = -\tau q_1 + (\mu + \tau)q_5, \\ {}_tD_{t_f}^{\alpha} q_6(t) = -K_2 + \frac{\beta_H S(q_1-q_6)}{N} + \frac{\beta_H L_T(q_2-q_7)}{N} + \frac{\beta_H I_T(q_3-q_8)}{N} + \lambda_T(q_6-q_7) - (\eta_1 + u_2)q_9 \\ \qquad +(\eta_1 + u_2 + \mu + \mu_H)q_6, \\ {}_tD_{t_f}^{\alpha} q_7(t) = -K_3 + \frac{\beta_H \xi_1 S(q_1-q_6)}{N} + \frac{\beta_H \xi_1 I_T(q_3-q_8)}{N} - \kappa_2 q_8 + (\kappa_2 + \mu + \mu_H)q_7, \\ {}_tD_{t_f}^{\alpha} q_8(t) = -K_4 + \frac{\beta_T \rho_1 S(q_1-q_2)}{N} + \frac{\beta_H \xi_2 S(q_1-q_6)}{N} + \frac{\beta_H \xi_2 L_T(q_2-q_7)}{N} + \frac{\beta_T \varphi \rho_1 L_T(q_2-q_3)}{N} \\ \qquad +\frac{\beta_T \rho_1 I_H(q_6-q_7)}{N} - (\eta_2 + \gamma_2)q_9 + (\eta_2 + \gamma_2 + \mu + \mu_C)q_8, \\ {}_tD_{t_f}^{\alpha} q_9(t) = \frac{\beta_H \xi_3 S(q_1-q_6)}{N} + \frac{\beta_H \xi_3 L_T(q_2-q_7)}{N} + \frac{\beta_H \xi_3 I_T(q_3-q_8)}{N} + \mu q_9. \end{cases} \tag{7.35}$$

In addition to this, the transversality conditions

$$ {}_tD_{t_f}^{\alpha-1} q_j(t)|_{t_f} = 0 \;\Leftrightarrow\; {}_tI_{t_f}^{1-\alpha} q_j(t)|_{t_f} = q_j(t_f) = 0,\; j = 1, 2, \cdots, 9, \tag{7.36} $$

holds true where, ${}_tI_{t_f}^{1-\alpha}$ is the right Riemann–Liouville fractional integral of order $1-\alpha$.

Applying the change of variable $t^{'} = t_f - t$, to equation (7.35) and to the transversality conditions (7.36), we obtain the left Riemann–Liouville fractional initial value problem (Rosa & Torres, 2023):

$$ \begin{cases} {}_0D_{t'}^{\alpha} q_1(t^{'}) = -[(\lambda_T + \lambda_H) q_1 - \lambda_T q_2 - \lambda_H q_6], \\ {}_0D_{t'}^{\alpha} q_2(t^{'}) = -[(\lambda_{L_H} + \varphi\lambda_T + \mu + \kappa_1) q_1 - (\kappa_1 + \varphi\lambda_T) q_3 - \lambda_{L_H} q_7], \\ {}_0D_{t'}^{\alpha} q_3(t^{'}) = -[-K_1 + \frac{\beta_T S(q_1 - q_2)}{N} + \frac{\beta_T \varphi L_T(q_2 - q_3)}{N} + \frac{\beta_T I_H(q_6 - q_7)}{N} - \lambda_{I_H} q_8 - (\omega + u_1) q_4 \\ \qquad + (\omega + u_1 + \mu + \mu_T) q_3], \\ {}_0D_{t'}^{\alpha} q_4(t^{'}) = -[\frac{\beta_T \rho_2 S(q_1 - q_2)}{N} + \frac{\beta_T \varphi \rho_2 L_T(q_2 - q_3)}{N} + \frac{\beta_T \rho_2 I_H(q_6 - q_7)}{N} - (1 - \theta) q_2 - \theta\sigma q_3 - \gamma_1 q_5 \\ \qquad + (\sigma + \gamma_1 + \mu + \mu_T) q_4], \\ {}_0D_{t'}^{\alpha} q_5(t^{'}) = -[-\tau q_1 + (\mu + \tau) q_5], \\ {}_0D_{t'}^{\alpha} q_6(t^{'}) = -[-K_2 + \frac{\beta_H S(q_1 - q_6)}{N} + \frac{\beta_H L_T(q_2 - q_7)}{N} + \frac{\beta_H I_T(q_3 - q_8)}{N} + \lambda_T(q_6 - q_7) - (\eta_1 + u_2) q_9 \\ \qquad + (\eta_1 + u_2 + \mu + \mu_H) q_6], \\ {}_0D_{t'}^{\alpha} q_7(t^{'}) = -[-K_3 + \frac{\beta_H \xi_1 S(q_1 - q_6)}{N} + \frac{\beta_H \xi_1 I_T(q_3 - q_8)}{N} - \kappa_2 q_8 + (\kappa_2 + \mu + \mu_H) q_7], \\ {}_0D_{t'}^{\alpha} q_8(t^{'}) = -[-K_4 + \frac{\beta_T \rho_1 S(q_1 - q_2)}{N} + \frac{\beta_H \xi_2 S(q_1 - q_6)}{N} + \frac{\beta_H \xi_2 L_T(q_2 - q_7)}{N} + \frac{\beta_T \varphi \rho_1 L_T(q_2 - q_3)}{N} \\ \qquad + \frac{\beta_T \rho_1 I_H(q_6 - q_7)}{N} - (\eta_2 + \gamma_2) q_9 + (\eta_2 + \gamma_2 + \mu + \mu_C) q_8], \\ {}_0D_{t'}^{\alpha} q_9(t^{'}) = -[\frac{\beta_H \xi_3 S(q_1 - q_6)}{N} + \frac{\beta_H \xi_3 L_T(q_2 - q_7)}{N} + \frac{\beta_H \xi_3 I_T(q_3 - q_8)}{N} + \mu q_9], \end{cases} \tag{7.37} $$

with initial conditions

$$ p_j(t^{'})|_{t'=0} = 0,\; j = 1, 2, \cdots, 9. \tag{7.38} $$

The initial conditions (7.38) imply that the adjoint system (7.37) can be considered as a system of left Caputo fractional differential equations:

$$\begin{cases}
{}_0^C D_t^\alpha q_1(t) = (\lambda_T + \lambda_H)q_1 - \lambda_T q_2 - \lambda_H q_6, \\
{}_0^C D_t^\alpha q_2(t) = (\lambda_{L_H} + \varphi\lambda_T + \mu + \kappa_1)q_1 - (\kappa_1 + \varphi\lambda_T)q_3 - \lambda_{L_H} q_7, \\
{}_0^C D_t^\alpha q_3(t) = -K_1 + \frac{\beta_T S(q_1 - q_2)}{N} + \frac{\beta_T \varphi L_T(q_2 - q_3)}{N} + \frac{\beta_T I_H(q_6 - q_7)}{N} - \lambda_{I_H} q_8 - (\omega + u_1)q_4 \\
\qquad +(\omega + u_1 + \mu + \mu_T)q_3, \\
{}_0^C D_t^\alpha q_4(t) = \frac{\beta_T \rho_2 S(q_1 - q_2)}{N} + \frac{\beta_T \varphi \rho_2 L_T(q_2 - q_3)}{N} + \frac{\beta_T \rho_2 I_H(q_6 - q_7)}{N} - (1 - \theta)q_2 - \theta\sigma q_3 - \gamma_1 q_5 \\
\qquad +(\sigma + \gamma_1 + \mu + \mu_T)q_4, \\
{}_0^C D_t^\alpha q_5(t) = -\tau q_1 + (\mu + \tau)q_5, \\
{}_0^C D_t^\alpha q_6(t) = -K_2 + \frac{\beta_H S(q_1 - q_6)}{N} + \frac{\beta_H L_T(q_2 - q_7)}{N} + \frac{\beta_H I_T(q_3 - q_8)}{N} + \lambda_T(q_6 - q_7) - (\eta_1 + u_2)q_9 \\
\qquad +(\eta_1 + u_2 + \mu + \mu_H)q_6, \\
{}_0^C D_t^\alpha q_7(t) = -K_3 + \frac{\beta_H \xi_1 S(q_1 - q_6)}{N} + \frac{\beta_H \xi_1 I_T(q_3 - q_8)}{N} - \kappa_2 q_8 + (\kappa_2 + \mu + \mu_H)q_7, \\
{}_0^C D_t^\alpha q_8(t) = -K_4 + \frac{\beta_T \rho_1 S(q_1 - q_2)}{N} + \frac{\beta_H \xi_2 S(q_1 - q_6)}{N} + \frac{\beta_H \xi_2 L_T(q_2 - q_7)}{N} + \frac{\beta_T \varphi \rho_1 L_T(q_2 - q_3)}{N} \\
\qquad +\frac{\beta_T \rho_1 I_H(q_6 - q_7)}{N} - (\eta_2 + \gamma_2)q_9 + (\eta_2 + \gamma_2 + \mu + \mu_C)q_8, \\
{}_0^C D_t^\alpha q_9(t) = \frac{\beta_H \xi_3 S(q_1 - q_6)}{N} + \frac{\beta_H \xi_3 L_T(q_2 - q_7)}{N} + \frac{\beta_H \xi_3 I_T(q_3 - q_8)}{N} + \mu q_9.
\end{cases} \tag{7.39}$$

with initial conditions

$$p_j()|_{t=0} = 0, \ \ j = 1, 2, \cdots, 9. \tag{7.40}$$

7.4 Numerical Simulations and Discussions

Here, we employ the fractional Adams–Bashforth–Moulton PECE technique, which was developed in Diethelm & Freed (1998); Diethelm et al. (2004), to solve numerically the extended fractional optimal control problems (7.29,7.30,7.39,7.40) and the HIV-TB co-infection model (7.3). Using repeated iterations, the controls are updated by a convex combination of the value from (7.34) and the preceding controls. To bolster the analytical findings, we do these numerical simulations using Octave/MATLAB software. $S(0) = 125,900$, $L_T(0) = 141$, $I_T(0) = 135$, $T_T(0) = 128$, $R_T(0) = 118$, $I_H(0) = 563$, $L_C(0) = 135$, $I_C(0) = 40$, and $T_H(0) = 474$ are the initial conditions that we have assumed.

Using the parameter values from Table (7.2), with $\alpha = 0.6$, the basic reproductive values are computed as $\mathcal{R}_T = 1.6406$ and $\mathcal{R}_H = 1.6482$ indicating that both HIV and TB are endemic in the population. On the other hand, the basic reproduction number of the full HIV-TB co-infection model becomes

$$\mathcal{R}_0 = max\{\mathcal{R}_T, \mathcal{R}_H\} = 1.6482 = \mathcal{R}_H > 1.$$

Thus, we can conclude that HIV dominates the complexities of the co-infection model.

The reproduction numbers that result from reducing β_T to 0.1335 and taking $\beta_H = 0.0097$ with $\alpha = 0.6$ are $\mathcal{R}_T = 0.3805$ and $\mathcal{R}_H = 0.2806$. $\mathcal{R}_0 = max\{\mathcal{R}_T, \mathcal{R}_H\} = 0.3805$ is therefore less than unity. These values are all less than unity for each $\alpha \in \{0.7, 0.8, 0.9, 1.0\}$. Numerical evaluation also confirms that $\lambda_i < 0$ for each $i = 1, 2, \cdots, 9$ and $\alpha \in \{0.6, 0.7, 0.8, 0.9, 1.0\}$ satisfying the Matignons' stability condition. Thus, in this instance, the HIV-TB free equilibrium $\mathcal{E}^0$ is obtained, and the local asymptotic stability of the HIV-TB free equilibrium, is shown in Figures (7.2a)–(7.2d).

In Caputo's fractional derivatives, for smaller fractional values, due to their substantial memory effects, the behavior of the dynamical system is strongly influenced by their past and current histories. Because the system responds to perturbations more gradually and is less vulnerable to abrupt changes, it will have slower dynamics and extremely stable as depicted in Figure (7.2). The long-term behavior of an integer-order dynamical system, on the other hand, is only dependent on recent system states and local input data. As a result, the system reacts quickly to disturbances and is significantly impacted by quick changes brought on by input data. Consequently, the system is less stable than a dynamical system of fractional order (Mahata et al., 2022; Oshinubi et al., 2023).

Following WHO guidelines, the values for K_1, K_2, K_3, K_4, W_1, W_2 were chosen. The WHO suggests choosing K_1 between 1.0 and 5.0, K_2 between 1.0 and 4.0, K_3 between 1.0 and 3.0, K_4 between 1.0 and 4.0, W_1 between 0.1 and 2.0, and W_2 between 0.1 and 2.0. Hence, we selected the following values for simulation purposes of the fractional optimal control problem: $K_1 = 3.0, K_2 = 2.5, K_3 = 2.0, K_4 = 2.5, W_1 = 1.06$, and $W_2 = 1.0$ (WHO, 2016a, 2016b). The final intervention time $t_f = 5$ years and $\alpha = 0.6$ are taken into account. We also use $\delta = 0.05$ to limit the maximum values of the control variables. $\beta_T = 0.1335$ and $\beta_H = 0.0097$ are used for this purpose. The values for the remaining parameters are extracted from Table (7.2). The initial conditions for each state variables were taken as before.

Remark 7.3 *The values of co-state functions are zero at the final time $t_f = 5$ years and as a result, all the control variables vanish at this time.*

We present a comparative analysis of the effects of control techniques on disease transmission under the following intervention strategies:

Strategy A: treatment for TB alone ($u_1 \neq 0, u_2 = 0.$)

Strategy B: treatment for HIV alone ($u_1 = 0, u_2 \neq 0.$)

Strategy C: both the controls simultaneously ($u_1 \neq 0, u_2 \neq 0.$)

Efficiency Analysis of the Intervention Strategies

In epidemiological modeling, the number of infection cases averted during the implementation of an intervention plan is used to assess its efficacy; the strategy with the greatest efficiency index is the most successful Olaniyi, Abimbade, et al. (2024). The efficiency index of an intervention strategy $\mathcal{Y}$ is determined as in Olaniyi et al. (2023) by

$$E.I(\mathcal{Y}) = \frac{Total\ infection\ cases\ adverted\ by\ strategy\ \mathcal{Y}}{Total\ infection\ cases\ in\ the\ absence\ of\ intervention\ strategies}, \quad (7.41)$$

where total infection cases adverted by strategy $\mathcal{Y}$ is obtained by subtracting total number of infection cases in the presence of strategy $\mathcal{Y}$ from total infection cases in the absence of strategy $\mathcal{Y}$.

As a consequence, each intervention strategy's E.I. is evaluated using (7.41), and the outcomes are displayed in Table (7.4). With an E.I of 42.68%, the study shows that Strategies C prevents the greatest number of infection cases, while Strategy B with E.I of 17.93% prevents the least number of infection cases. Consequently, Strategy C is the most efficient among the three strategies that were examined. Strategy A is the next most efficient approach. Whereas, Strategy B is the least efficient of all the strategies.

Cost-Effectiveness Analysis of the Intervention Strategies

The implementation of an intervention plan may not be cost-effective, especially when resources are limited, even though it may prevent the highest number of infection cases in the community. In order to evaluate the cost-effectiveness of the three intervention options, this study employed the average cost-effectiveness ratio (ACER) technique. The ACER of an intervention is defined as the ratio of the total cost of implementing that intervention, which we calculate using formula (7.30), to the total number of infection cases that the same intervention adverted Okosun et al. (2013). Specifically,

$$ACER(\mathcal{Y}) = \frac{Total\ cost\ incured\ by\ intervention\ strategy\ \mathcal{Y}}{Total\ infection\ cases\ averted\ by\ intervention\ strategy\ \mathcal{Y}} \quad (7.42)$$

The intervention with the lowest ACER is the most cost-effective, according to the ACER technique of cost analysis. According to Table (7.4), Strategy C, which combines both the two controls is the most cost-effective of the three intervention approaches as it has the lowest ACER of 19.3744. Strategy A is the next most cost-effective approach. With an ACER of 48.7060, Strategy B is the least cost-effective intervention plan.

Table 7.4: Efficiency indices and ACER of the intervention strategies.

Strategy	Total infection averted	E.I	Total cost(in $)	ACER
A : $u_1(t)$ alone	599.71	42.04%	11896	19.8363
B : $u_2(t)$ alone	24.42	17.93%	1189.4	48.7060
C : $u_1(t)u_2(t)$	618.91	42.68%	11991	19.3744

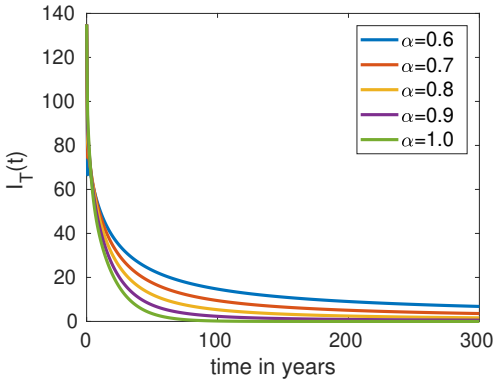

(a) Active TB infected population for $\alpha = (0.6, 0.7, 0.8, 0.9, 1.0)$.

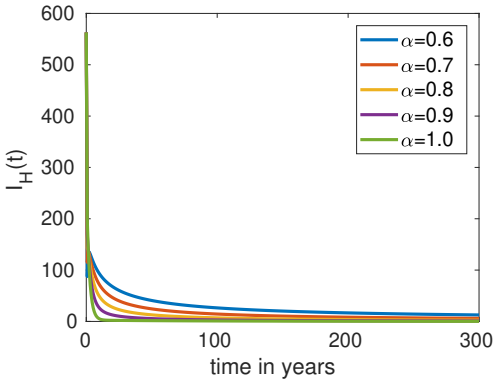

(b) HIV infected population for $\alpha = (0.6, 0.7, 0.8, 0.9, 1.0)$.

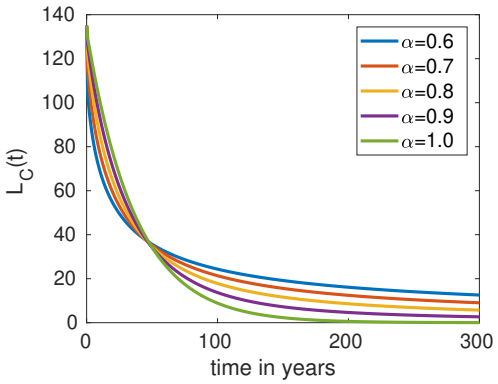

(c) HIV and latent TB co-infected population for $\alpha = (0.6, 0.7, 0.8, 0.9, 1.0)$.

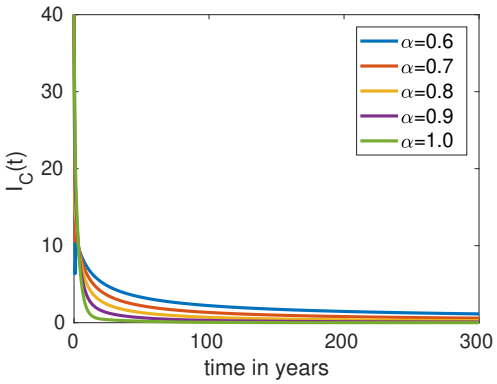

(d) HIV and active TB co-infected population for $\alpha = (0.6, 0.7, 0.8, 0.9, 1.0)$.

Figure 7.2: Graphs demonstrating the local asymptotic stability of the HIV-TB free equilibrium, $\mathcal{E}^0$ when $\lambda_i < 0, \forall_i$ and $\mathcal{R}_0^{(\alpha)} < 1, \forall_\alpha$.

Figures (7.3)–(7.5) show how the dynamics of HIV-TB co-infection are affected by the application of potential control measures. We looked at three strategies to illustrate this. Implementing only TB treatment control ($u_1 \neq 0$ and $u2 = 0$) which is depicted in Figures (7.3a)-(7.3d) is the first strategy. With this strategy, individuals in the I_T compartment decrease from 1314 to 718.9, those in the R_T compartment rises from 111.4 to 188, those in the L_C compartment slightly decreases from 95.84 to 95.07, and those in the I_C compartment decrease from 16.56 to 12.72.

Figures (7.4a)-(7.4d), demonstrate the impact of implementing HIV treatment control alone ($u_1 = 0$; $u_2 \neq 0$) which we considered as the second approach. With this

strategy, the number of infected individuals drop from 23.81 to 13.42 in the I_H compartment, from 95.84 to 84.09 in the L_C compartment, and from 16.56 to 14.28 in the I_C compartment. Moreover the number of HIV treated individuals rises from 178 to 196.6.

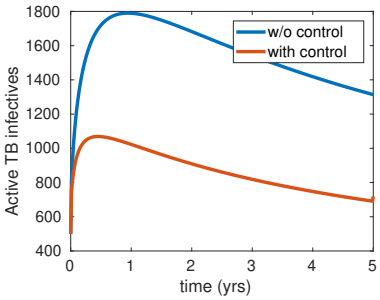

(a) The impact of strategy A on I_T compartment

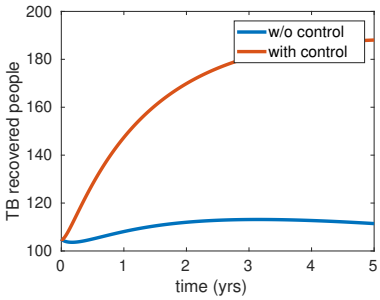

(b) The impact of strategy A on R_T compartment

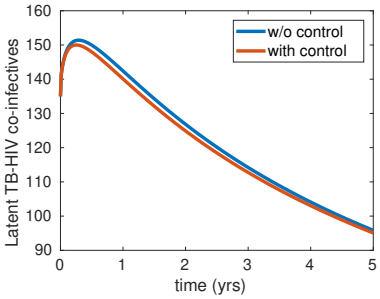

(c) The impact of strategy A on L_C compartment

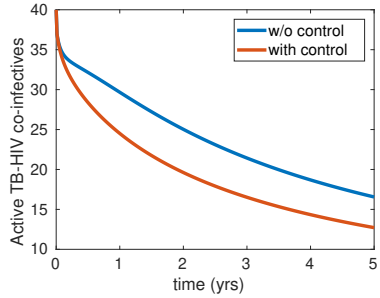

(d) The impact of strategy A on I_C compartment

Figure 7.3: The impact of implementing strategy A on different disease compartments

The third approach, which combines the use of HIV and TB therapies ($u_1 \neq 0$ and $u_2 \neq 0$), is depicted in Figures (7.5a)-(7.5d). By implementing this approach, the number of individuals in I_T compartment decreases from 1314 to 722.1, those in I_H compartment decreases from 23.81 to 13.93, those in I_C compartment falls from 16.56 to 11.29, and the L_C compartment falls from 95.84 to 83.97.

The result of sensitivity analysis indicates that $\mathcal{R}_T^{(\alpha)}$ will decrease with an increase in ω and a decrease in β_T, κ_1. Whereas, lowering β_H and the infectiousness rate η_1 significantly reduces $\mathcal{R}_H^{(\alpha)}$. The optimal control analysis on the other hand shows that combined treatment effort is the most efficient intervention strategy to mitigate the co-infection with minimal cost of implementation. Furthermore, simulation results also demonstrate that by taking memory effects of the disease into account, a Caputo fractional-order provides a deeper understanding of the disease and aids in designing effective prevention and control strategies.

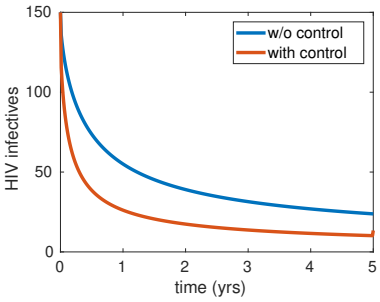

(a) The impact of strategy B on I_H compartment

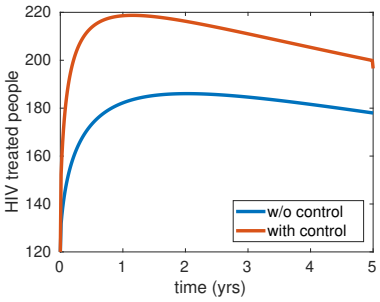

(b) The impact of strategy B on T_H compartment

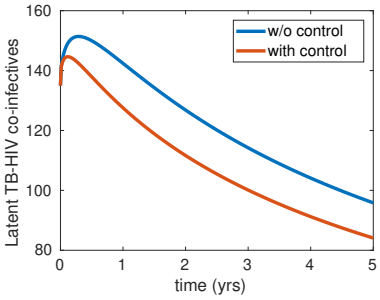

(c) The impact of strategy B on L_C compartment

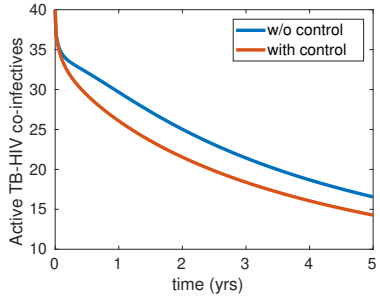

(d) The impact of strategy B on I_C compartment

Figure 7.4: The impact of implementing strategy B on different disease compartments

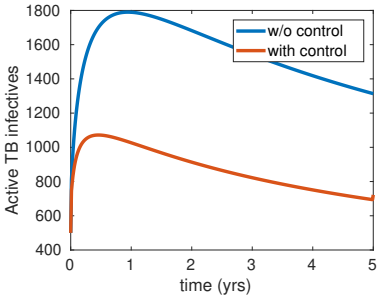

(a) The impact of strategy C on I_T compartment

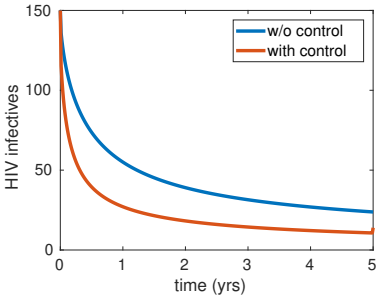

(b) The impact of strategy C on I_H compartment

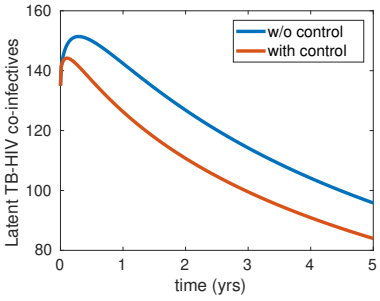

(c) The impact of strategy C on L_C compartment

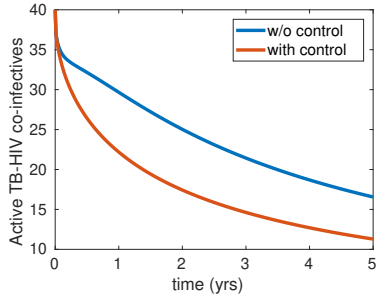

(d) The impact of strategy C on I_C compartment

Figure 7.5: The impact of implementing strategy C on different disease compartments

CHAPTER 8

SUMMARY, CONCLUSION AND RECOMMENDATION

In this chapter, we summarize the study's conclusions and recommendations, as well as outline plans for future work. The primary focus of this dissertation is on developing and analyzing fractional order mathematical models to enhance our understanding of the transmission dynamics of HIV, TB, and their co-infections in human populations. This approach aims to identify the most effective prevention and control strategies. By incorporating relevant biological and epidemiological factors related to both diseases and their co-infections, we have gained several new insights. The key contributions from the findings of this dissertation are summarized and concluded as follows.

8.1 Summary

This dissertation focused on developing and analyzing fractional-order mathematical models to improve our understanding of the transmission dynamics of HIV, TB and their co-infection in human population. By incorporating relevant biological and epidemiological factors, including treatment, vaccination, and prevention strategies, we provided insights into effective disease control and mitigation strategies.

We formulated and analyzed Caputo fractional-order deterministic models for HIV, TB, and HIV-TB co-infection using systems of nonlinear ordinary differential equations. For HIV/AIDS, we extended the classical S-E-I-A model by including PrEP and drug-resistant compartments. The mathematical analysis established fundamental properties such as non-negativity, boundedness, existence, and uniqueness of solutions. The basic reproduction number, $\mathcal{R}_0$, was computed using the next-generation matrix method, and both local and global stability of disease equilibria were investigated using linearization and Lyapunov functions. Real-data from Ethiopia were used to estimate

model parameters, and sensitivity analyses identified key parameters influencing $\mathcal{R}_0$. Numerical simulations assessed the impact of interventions on disease dynamics.

For TB, a Caputo fractional-order model was developed to capture the effects of vaccination and treatment adherence. The model was shown to be mathematically and epidemiologically well-posed. Local and global stability of the disease-free and endemic equilibra were established, and sensitivity analyses highlighted parameters with the greatest impact on TB transmission. An optimal control framework was formulated to determine cost-effective strategies that minimize disease burden while considering limited resources.

Finally, two fractional-order HIV-TB co-infection models were developed. The first model incorporated TB vaccination and treatment compartments for both diseases, while the second extended to an optimal control problem. Using the fractional Pontryagin's Minimum Principle, we characterized the optimal control solutions, identifying strategies that reduce both morbidity and mortality. Parameter estimation from Ethiopian HIV and TB data, sensitivity analyses, and numerical simulation using the fractional Adams–Bashforth–Moulton PECE algorithm in GNU Octave/MATLAB supported our analytical findings.

8.2 Conclusion

This dissertation demonstrates the importance of fractional-order modeling in capturing memory effects and hereditary factors inherent in HIV/AIDS, TB, and co-infection dynamics. Our findings show that reducing the baseline transmission rate, and the drug resistance development rate, improving the ART adherence rates, and increasing the detection rate of symptomatic cases substantially lower HIV prevalence. Moreover, lowering PrEP discontinuation rates and improving PrEP initiation enhance preventive coverage in high-risk populations. On the other hand, increasing vaccination coverage, promoting effective TB treatment, and reducing effective contact rates significantly decrease TB prevalence, with early identification and treatment of latent and active TB reducing transmission and the risk of drug resistance. Combined treatment strategies targeting both HIV and TB on the other side are the most effective interventions, providing significant reductions in co-infection burden.

Cost-effectiveness analysis indicates that TB vaccination alone is the most cost-efficient TB intervention, while integrated strategies for co-infection yield the highest health benefit per unit cost-critical for resource-limited countries such as Ethiopia. Furthermore, the inclusion of memory effects through Caputo fractional derivatives provides a more realistic representation of disease progression, improving predictions

over classical integer-order models. Fractional models allow for more accurate assessment of long-term intervention strategies, supporting better-informed public health policies.

This study also acknwoledges limitations such as the assumption of population homogeneity, potential underestimation of regional heterogeneity, data constraints, and logistical constraints in real-world implementation.

8.3 Recommendation

Based on the findings, the following targeted strategies are recommended to mitigate HIV, TB and their-co-infection, particularly in Ethiopian context:

HIV/AIDS Control:

- Reduce baseline transmission rate and drug resistance development rate: Expand PrEP coverage, improve ART adherence, and promote safe sexual practices. Address stigma and care barriers while monitoring drug resistance.
- Enhance PrEP uptake and retention: Reduce logistical barriers, provide financial assistance, implement follow-up care, and leverage peer support networks.
- Lower ART treatment non-adherence rates: Use patient education, medication reminders, viral load monitoring, and adherence support systems.
- Increase detection rates of symptomatic cases: Implement routine testing, strengthen counseling, provide professional guidance, and secure funding.

TB Control:

- Reduce effective contact rate: Implement preventive measures such as mask-wearing and physical distancing.
- Increase vaccination coverage: Promote widespread TB vaccination to enhance population immunity.
- Improve treatment accessibility: Ensure availability of first- and second-line TB treatments to reduce transmission and prevent treatment failures.
- Early identification and treatment of latent infections: Screen and treat latent TB promptly to reduce progression and transmission.

Integrate HIV-TB Strategies:

Develop and implement healthcare programs that address both diseases simultaneously, maximizing cost savings and overall health outcomes.

8.4 Future Work

Future research should focus on:

- Heterogeneity: Incorporating spatial, demographic, and socio-economic variations to better capture real-world dynamics.
- Multi-strain Dynamics: Extending models to include multiple HIV or TB strains and drug resistance patterns.
- Stochastic Modeling: Introducing stochasticity to account for randomness in transmission and intervention effects.
- Advanced Fractional Stability Theory: Developing new fractional Lyapunov methods for fully nonlinear systems to strengthen global stability proofs.
- Policy-Oriented Modeling: Linking model outputs with health economic evaluations for targeted resource allocations in constrained settings.

REFERENCES

Abbas, U. L., Hood, G., Wetzel, A. W., & Mellors, J. W. (2011). Factors influencing the emergence and spread of hiv drug resistance arising from rollout of antiretroviral pre-exposure prophylaxis (prep). *PloS one*, *6*(4), e18165.

Adeyemo, S., Sangotola, A., & Korosteleva, O. (2023). Modeling transmission dynamics of tuberculosis–hiv co-infection in south africa. *Epidemiologia*, *4*(4), 408–419.

AfricaNews. (2024). Who reports record 8 million tb cases last year. *https://www.africanews.com/2024/10/30/who-reports-record-8-million-tb-cases-last-year/*.

Agarwal, R., Airan, P., & Agarwal, R. P. (2024). Exploring the landscape of fractional-order models in epidemiology: A comparative simulation study. *Axioms (2075-1680)*, *13*(8).

Agbata, B. C., Dervishi, R., Agbebaku, D. F., Cenaj, E., Collins, O. C., Ezeafulukwe, A. U., ... Mbah, G. C. E. (2025). A comprehensive analysis of fractional-order model of tuberculosis with treatment intervention. *BMC Infectious Diseases*, *25*(1), 1070.

Aggarwal, R., Raj, Y. A., et al. (2021). A fractional order hiv-tb co-infection model in the presence of exogenous reinfection and recurrent tb. *Nonlinear Dynamics*, *104*(4), 4701–4725.

Aguila-Camacho, N., Duarte-Mermoud, M. A., & Gallegos, J. A. (2014). Lyapunov functions for fractional order systems. *Communications in nonlinear science and numerical simulation*, *19*(9), 2951–2957.

Ahmed, T., Singh, R., & Ahmad, K. (2022). Modelling, analysis and optimal control to co-dynamics of hiv/aids-tb diseases in homogeneous population. *Jordan Journal of Mathematics and Statistics (JJMS)*, *15*(3B), 741–771.

AIDSMAP. (2019). Resistance to anti-hiv drugs. *https://www.aidsmap.com/about-hiv/resistance-anti-hiv-drugs*.

AIDSMAP. (2022). Prep inequities have worsened in the us over the last decade, both racially and regionally. *https://www.aidsmap.com/news/jul-2022/prep-inequities-have-worsened-us-over-last-decade-both-racially-and-regionally*.

Ajao, S., Olopade, I., Akinwumi, T., Adewale, S., & Adesanya, A. (2023). Understanding the transmission dynamics and control of hiv infection: A mathematical model approach. *Journal of the Nigerian Society of Physical Sciences*, 1389–1389.

Akuka, P. N., Seidu, B., Okyere, E., & Abagna, S. (2024). Fractional-order epidemic model for measles infection. *Scientifica*, *2024*(1), 8997302.

Aldila, D., Ndii, M. Z., & Samiadji, B. M. (2020). Optimal control on covid-19 eradication program in indonesia under the effect of community awareness. *Math. Biosci. Eng*, *17*(6), 6355–6389.

Alfiniyah, C., Soetjianto, W. S. P. A., Aziz, M. H. N., Ghadzi, S. M. S., et al. (2024). Mathematical modeling and optimal control of tuberculosis spread among smokers with case detection. *AIMS Mathematics*, *9*(11), 30472–30492.

Ali, I. (2024). Dynamical analysis of two-dimensional fractional-order-in-time biological population model using chebyshev spectral method. *Fractal and Fractional*, *8*(6), 325.

Allen, L. J. (2017). A primer on stochastic epidemic models: Formulation, numerical simulation, and analysis. *Infectious Disease Modelling*, *2*(2), 128–142.

Almeida, R. (2018). Analysis of a fractional seir model with treatment. *Applied Mathematics Letters*, *84*, 56–62.

Anjam, Y. N., Turki Alqahtani, R., Alharthi, N. H., & Tabassum, S. (2024). Unveiling the complexity of hiv transmission: integrating multi-level infections via fractal-fractional analysis. *Fractal and Fractional*, *8*(5), 299.

Annual. (2022). Top global health issues. *Annual Reviews. https://www.annualreviews.org/page/worldhealththreats*.

Arja, A., Tadesse, S., Agachew, M., Getnet, F., Beksisa, J., Mohammed, S., ... others (2023). The burden of tuberculosis across regions in ethiopia: A systematic subnational analysis for the global burden of disease study 2019. *Ethiopian Journal of Health Development*, *37*(2).

ASHM. (2024). Hiv disease progression. *https://hiv.guidelines.org.au/management/natural-history-of-hiv-infection/disease-progression/*.

Avilov, K., Romanyukha, A., Belilovsky, E., & Borisov, S. (2022). *Mathematical modelling of the progression of active tuberculosis: Insights from fluorography data. infectious disease modelling, 7 (3): 374-386.*

Awoke, T., & Semu, M. (2018). *Optimal control strategy for tb-hiv/aids co-infection model in the presence of behaviour modification. processes 6 (5): 48.*

Ayele, T. K., Doungmo Goufo, E. F., & Mugisha, S. (2024). Co-infection mathematical model for hiv/aids and tuberculosis with optimal control in ethiopia. *PloS one*, *19*(12), e0312539.

Azevedo-Pereira, J. M., Pires, D., Calado, M., Mandal, M., Santos-Costa, Q., & Anes, E. (2023). Hiv/mtb co-infection: from the amplification of disease pathogenesis to an emerging syndemic. *Microorganisms*, *11*(4), 853.

Baba, B. A., & Bilgehan, B. (2021). Optimal control of a fractional order model for the covid–19 pandemic. *Chaos, Solitons & Fractals*, *144*, 110678.

Baggaley, R. F., Garnett, G. P., & Ferguson, N. M. (2006). Modelling the impact of antiretroviral use in resource-poor settings. *PLoS Medicine*, *3*(4), e124.

Baggaley, R. F., Powers, K. A., & Boily, M.-C. (2011). What do mathematical models tell us about the emergence and spread of drug-resistant hiv? *Current Opinion in HIV and AIDS*, *6*(2), 131–140.

Bahaa, G. M. (2017). Fractional optimal control problem for differential system with delay argument. *Advances in difference equations*, *2017*, 1–19.

Barakat, M., Hyder, A.-A., & Almoneef, A. A. (2023). A novel hiv model through fractional enlarged integral and differential operators. *Scientific Reports*, *13*(1), 7764.

Barros, L. C. d., Lopes, M. M., Pedro, F. S., Esmi, E., Santos, J. P. C. d., & Sánchez, D. E. (2021). The memory effect on fractional calculus: an application in the spread of covid-19. *Computational and Applied Mathematics*, *40*, 1–21.

Bergounioux, M., & Bourdin, L. (2020). Pontryagin maximum principle for general caputo fractional optimal control problems with bolza cost and terminal constraints. *ESAIM: Control, Optimisation and Calculus of Variations*, *26*, 35.

Bhattacharjee, A. (2023). A mathematical model of hiv and tb co-infection. *International Journal of Mathematics And its Applications*, *11*(2), 33–50.

Bhatter, S., Kumawat, S., Purohit, S. D., & Suthar, D. (2025). Mathematical modeling of tuberculosis using caputo fractional derivative: a comparative analysis with real data. *Scientific Reports*, *15*(1), 12672.

Bhunu, C., Garira, W., & Mukandavire, Z. (2009). Modeling HIV/AIDS and Tuberculosis Coinfection. *Bulletin of mathematical biology*, *71*(7), 1745.

Bourafa, S., Abdelouahab, M., & Moussaoui, A. (2020). On some extended routh–hurwitz conditions for fractional-order autonomous systems of order $\alpha \in (0, 2)$ and their applications to some population dynamic models. *Chaos, Solitons and Fractals*, *133*, 109623.

Cassels, S., Clark, S. J., & Morris, M. (2008). Mathematical models for hiv transmission dynamics: tools for social and behavioral science research. *JAIDS Journal of Acquired Immune Deficiency Syndromes*, *47*, S34–S39.

Castillo-Chavez, C., & Song, B. (2004). Dynamical models of tuberculosis and their applications. *Mathematical Biosciences & Engineering*, *1*(2), 361–404.

Castillo-Chavez, F. Z. . H. W., C. (2002). On the computation of r 0 and its role on global stability. mathematical approaches for emerging and re-emerging infection diseases: an introduction. , *125*, 31-65.

CCOHS. (2025). Diseases, disorders and injuries. *https://www.ccohs.ca/oshanswers/diseases/mdr-tb.html*.

CDC. (2012). Tb elimination treatment of drug-resistant tuberculosis. *https://www.cdc.gov/tb/publications/factsheets/treatment/drugresistanttreatment.pdf*.

CDC. (2020). HIV TB co-infection. *https://www.cdc.gov/tb/topic/basics/tbhivcoinfection.htm*.

CDC. (2025a). About hiv. *https://www.cdc.gov/hiv/about/index.html*.

CDC. (2025b). Clinical care for people with tb and hiv. *https://www.cdc.gov/tb/hcp/clinical-care/hiv.html*.

Chaisson, R. E., & Churchyard, G. J. (2010). *Recurrent Tuberculosis: Relapse, Reinfection, and HIV* (Vol. 201) (No. 5). The University of Chicago Press.

Chen, S., Robinson, P., Janies, D., & Dulin, M. (2020). Four challenges associated with current mathematical modeling paradigm of infectious diseases and call for a shift. In *Open forum infectious diseases* (Vol. 7, p. ofaa333).

Chen-Charpentier, B. (2025). Mathematical models of epidemics with infection time. *AppliedMath*, *5*(2), 47.

Chinviriyasit, W., Janreung, S., & Chinviriyasit, S. (2018). On the backward bifurcation of an seirs epidemic model with nonlinear incidence rate. *WSEAS Transactions on Systems*, *18*.

Chitnis, N., Hyman, J. M., & Cushing, J. M. (2008). Determining important parameters in the spread of malaria through the sensitivity analysis of a mathematical model. *Bulletin of mathematical biology*, *70*, 1272–1296.

CIDRAP. (2024). Study highlights heavy global burden of infectious diseases :antimicrobial stewardship, hiv/aids, malaria, tuberculosis. *https://www.cidrap.umn.edu/antimicrobial-stewardship/study-highlights-heavy-global-burden-infectious-diseases*.

ContagionLive. (2020). Who identifies urgent challenges to address this decade. *https://www.contagionlive.com/view/who-identifies-urgent-challenges-to-address-this-decade*.

Crepey, P., Noël, H., & Alizon, S. (2022). Challenges for mathematical epidemiological modelling. *Anaesthesia, critical care & pain medicine*, *41*(2), 101053.

Datiko, D. G., Yassin, M. A., Chekol, L. T., Kabeto, L. E., & Lindtjørn, B. (2008). The rate of tb-hiv co-infection depends on the prevalence of hiv infection in a community. *BMC public health*, *8*(1), 266.

David, S. A., Linares, J. L., & Pallone, E. M. d. J. A. (2011). Fractional order calculus: historical apologia, basic concepts and some applications. *Revista Brasileira de Ensino de Física*, *33*, 4302–4302.

Delavari, H., Baleanu, D., & Sadati, J. (2012). Stability Analysis of Caputo Fractional-Order NonLinear Systems Revisited. *Nonlinear Dynamics*, *67*, 2433–2439.

de Oliveira, R. B., Rubio, F. A., Anderle, R., Sanchez, M., de Souza, L. E., Macinko, J., ... Rasella, D. (2022). Incorporating social determinants of health into the mathematical modeling of hiv/aids. *Scientific reports*, *12*(1), 20541.

Diekmann, O., Heesterbeek, J. A. P., & Metz, J. A. J. (1990). On the definition and the computation of the basic reproduction ratio r 0 in models for infectious diseases in heterogeneous populations. *Journal of mathematical biology*, *28*(4), 365–382.

Diethelm, K., Ford, N. J., & Freed, A. D. (2002). A predictor-corrector approach for the numerical solution of fractional differential equations. *Nonlinear Dynamics*, *29*, 3–22.

Diethelm, K., Ford, N. J., & Freed, A. D. (2004). Detailed error analysis for a fractional adams method. *Numerical algorithms*, *36*, 31–52.

Diethelm, K., & Freed, A. D. (1998). The fracpece subroutine for the numerical solution of differential equations of fractional order. *Forschung und wissenschaftliches Rechnen*, *1999*, 57–71.

Dokoumetzidis, A., Magin, R., & Macheras, P. (2010). A commentary on fractionalization of multi-compartmental models. *Journal of pharmacokinetics and pharmacodynamics*, *37*, 203–207.

Dwivedi, A., Dwivedi, V., & Verma, S. (2025). Fractional-order approaches to optimal control in hiv-aids dynamics. *Numerical Algebra, Control and Optimization*, *15*(4), 1286–1320.

E. Alsubaie, N., EL Guma, F., Boulehmi, K., Al-kuleab, N., & A. Abdoon, M. (2024). Improving influenza epidemiological models under caputo fractional-order calculus. *Symmetry*, *16*(7), 929.

Elaydi, S., & Lozi, R. (2024). Global dynamics of discrete mathematical models of tuberculosis. *Journal of Biological Dynamics*, *18*(1), 2323724.

El-Mesady, A., Mahdy, A., & Özköse, F. (2025). A fractional–order model with prevention and isolation optimal control measures to reduce the transmission of tuberculosis. *Journal of Taibah University for Science*, *19*(1), 2475579.

ENA. (2025). Ethiopia registers commendable progress to ending hiv as public health threat: Stakeholders. *https://www.ena.et/web/eng/w/eng-5553532*.

EPHI. (2025). Hiv related estimates and projections in ethiopia for the year 2024-2025. *https://ephi.gov.et/wp-content/uploads/2025/08/Ethiopian-HIV-Estimates-and-projecti-for-the-year-2024-and-2025-EPHI-Augst142025.pdf*.

Escombe, A. R., Moore, D. A. J., Gilman, R. H., Pan, W., Navincopa, M., Ticona, E., ... others (2008). The infectiousness of tuberculosis patients coinfected with hiv. *PLoS medicine*, *5*(9), e188.

Farman, M., Usman, M., Ahmad, A., & Ahmad, M. (2020). Mathematical analysis of fractional order co-infection tb and hiv model. *International Journal of Analysis and Applications*, *18*(1), 16–32.

Fouladi, S., Kohandel, M., & Eastman, B. (2022). A comparison and calibration of integer and fractional-order models of covid-19 with stratified public response. *Math. Biosci. Eng*, *19*(12), 12792–12813.

Frankline, T. K., George, L. O., & Colleta, O. A. (2018). Mathematical analysis of hiv/aids anti-retroviral treatment incorporating adherence.

Fuller, N. M., McQuaid, C. F., Harker, M. J., Weerasuriya, C. K., McHugh, T. D., & Knight, G. M. (2024). Mathematical models of drug-resistant tuberculosis lack bacterial heterogeneity: A systematic review. *PLoS pathogens*, *20*(4), e1011574.

Georgiev, S. (2023). Mathematical identification analysis of a fractional-order delayed model for tuberculosis. *Fractal and Fractional*, *7*(7), 538.

Gómez-Acevedo, H., & Li, M. Y. (2005). Backward bifurcation in a model for htlv-i infection of cd4+ t cells. *Bulletin of Mathematical Biology*, *67*, 101–114.

Grassly, N. C., & Fraser, C. (2008). Mathematical models of infectious disease transmission. *Nature Reviews Microbiology*, *6*(6), 477–487.

Guo, Z., & Zhang, L. (2023). Global dynamics of an age-structured tuberculosis model with vaccine failure and nonlinear infection force. *Axioms*, *12*(9), 805.

Gutowska, S. J., Hoffman, K., & Gurski, K. (2022). The effect of prep uptake and adherence on the spread of hiv in the presence of casual and long-term partnerships. *Mathematical Biosciences and Engineering*, *19*(12).

Habtemariam, T., Tameru, B., Nganwa, D., Beyene, G., Ayanwale, L., & Robnett, V. (2008). Epidemiologic modeling of hiv/aids: use of computational models to study the population dynamics of the disease to assess effective intervention strategies for decision-making. *Advances in systems science and applications*, *8*(1), 35.

Heads, A. M., de Dios, C., An, K., Yoon, J. H., Suchting, R., Gilmore-Thomas, A., & Schmitz, J. M. (2024). Interest in and willingness to use prep: A cross-sectional study of individuals with problematic substance use residing in a high hiv prevalence jurisdiction. *Archives of Sexual Behavior*, *53*(9), 3687–3698.

HIVinfo. (2025). Hiv drug restance. *https://hivinfo.nih.gov/understanding-hiv/fact-sheets/drug-resistance*.

HIVinfo.NIH.gov. (2021). The stages of hiv infection. *https://hivinfo.nih.gov/understanding-hiv/fact-sheets/stages-hiv-infection*.

HIVinfo.NIH.gov. (2025). Hiv prevention: Pre-exposure prophylaxis (prep). *https://hivinfo.nih.gov/understanding-hiv/fact-sheets/pre-exposure-prophylaxis-prep*.

Houben, R. M., Dowdy, D., Vassall, A., Cohen, T., Nicol, M., Granich, R., ... others (2014). How can mathematical models advance tuberculosis control in high hiv prevalence settings? *The International journal of tuberculosis and lung disease*, *18*(5), 509–514.

Inayaturohmat, F., Anggriani, N., Supriatna, A. K., & Biswas, M. H. A. (2024). A systematic literature review of mathematical models for coinfections: tuberculosis, malaria, and hiv/aids. *Journal of Multidisciplinary Healthcare*, 1091–1109.

Khajanchi, S., Das, D. K., & Kar, T. K. (2018). Dynamics of tuberculosis transmission with exogenous reinfections and endogenous reactivation. *Physica A: Statistical Mechanics and its Applications*, *497*, 52–71.

Khalil, H. K., & Grizzle, J. W. (2002). *Nonlinear systems* (Vol. 3). Prentice hall Upper Saddle River, NJ.

Khan, A., Shah, K., Abdeljawad, T., & Amacha, I. (2024). Fractal fractional model for tuberculosis: existence and numerical solutions. *Scientific Reports*, *14*(1), 12211.

Khan, M., Khan, N., Ullah, I., Shah, K., Abdeljawad, T., & Abdalla, B. (2025). A novel fractal fractional mathematical model for hiv/aids transmission stability and sensitivity with numerical analysis. *Scientific Reports*, *15*(1), 9291.

Khan, M. A., Bonyah, E., Hammouch, Z., Shaiful, E. M., et al. (2020). A Mathematical Model of Tuberculosis (TB) Transmission with Children and Adults Groups: A Fractional Model. *AIMS Mathematics*, *5*(4), 2813–2842.

Kheiri, H., & Jafari, M. (2018). Optimal control of a fractional-order model for the hiv/aids epidemic. *International Journal of Biomathematics*, *11*(07), 1850086.

Kim, H., Hanrahan, C., Martinson, N., Golub, J., & Dowdy, D. (2018). Cost-effectiveness of universal isoniazid preventive therapy among hiv-infected pregnant women in south africa. *The International Journal of Tuberculosis and Lung Disease*, *22*(12), 1435–1442.

Kumar, S., & Jain, S. (2018). Assessing the effects of treatment in hiv-tb co-infection model. *The European Physical Journal Plus*, *133*, 1–20.

Lai, H., Li, R., Li, Z., Zhang, B., Li, C., Song, C., ... others (2023). Modelling the impact of treatment adherence on the transmission of hiv drug resistance. *Journal of Antimicrobial Chemotherapy*, *78*(8), 1934–1943.

Lavi, O., Gottesman, M. M., & Levy, D. (2012). The dynamics of drug resistance: a mathematical perspective. *Drug Resistance Updates*, *15*(1-2), 90–97.

Lee, S. (2025). Seir model: The ultimate guide. *Number Analytics. https://www.numberanalytics.com/blog/seir-model-ultimate-guide*.

Letang, E., Ellis, J., Naidoo, K., Casas, E. C., Sánchez, P., Hassan-Moosa, R., ... García-Basteiro, A. L. (2020). Tuberculosis-hiv co-infection: progress and challenges after two decades of global antiretroviral treatment roll-out. *Archivos de bronconeumologia*, *56*(7), 446–454.

Li, Y., Chen, Y., & Podlubny, I. (2009). Mittag–leffler stability of fractional order nonlinear dynamic systems. *Automatica*, *45*(8), 1965–1969.

Li, Y., Chen, Y., & Podlubny, I. (2010). Stability of fractional-order nonlinear dynamic systems: Lyapunov direct method and generalized mittag–leffler stability. *Computers & Mathematics with Applications*, *59*(5), 1810–1821.

Lyons, V. A. S. . C. R. A., R. (2017). Picard's iterative method for caputo fractional differential equations with numerical results. , *5(4), 65*.

Macrotrends. (2024). Ethiopian population 1950-2024.

Mahata, A., Paul, S., Mukherjee, S., Das, M., & Roy, B. (2022). Dynamics of caputo fractional order seirv epidemic model with optimal control and stability analysis. *International Journal of Applied and Computational Mathematics*, *8*(1), 28.

Maina, R. M., Kinyanjui, M. N., Mwalili, S. M., & Kioi, D. G. (2025). An age-stratified mathematical model for human immunodeficiency virus and tuberculosis co-infection with optimal control.

Mallela, A., Lenhart, S., & Vaidya, N. K. (2016). Hiv–tb co-infection treatment: Modeling and optimal control theory perspectives. *Journal of Computational and Applied Mathematics*, *307*, 143–161.

Matignon, D. (1996). Stability results for fractional differential equations with applications to control processing. In *Computational engineering in systems applications* (Vol. 2, pp. 963–968).

Matlob, M. A., & Jamali, Y. (2019). The concepts and applications of fractional order differential calculus in modeling of viscoelastic systems: A primer. *Critical Reviews™ in Biomedical Engineering*, *47*(4).

Mekonen, H., Negesse, A., Dessie, G., Desta, M., Mihiret, G. T., Tarik, Y. D., ... Getaneh, T. (2024). Impact of hiv coinfection on tuberculosis treatment outcomes in ethiopia: a systematic review and meta-analysis. *BMJ open*, *14*(7), e087218.

Michuad, C. M. (2009). Global burden of infectious diseases. *Harvard Initiative for Global Health, Cambridge MA, USA*.

Moya, E. M. D., Rodriguez, R. A., & Pıetrus, A. (2024). A mathematical model for the study of hiv/aids transmission with prep coverage increase and parameter estimation using mcmc with a bayesian approach. *Bulletin of Biomathematics*, *2*(2), 218–244.

Mumbu, A.-R., Mlay, G., Alendal, G., Mayige, M., Senkoro, M., & Shaban, N. (2025). Fractional order derivative modelling dynamics of tuberculosis with treatment and nutrition in tanzania. *Research in Mathematics*, *12*(1), 2517440.

Mwangi, S. M. N., Kitetu, V. M., & Okwany, I. O. (2024). Mathematical modeling of the co-infection dynamics of hiv and tuberculosis incorporating inconsistency in hiv treatment. *Journal of Applied Mathematics and Physics*, *12*(5), 1744–1768.

Naik, P. A., Zu, J., & Owolabi, K. M. (2020). Global dynamics of a fractional order model for the transmission of hiv epidemic with optimal control. *Chaos, Solitons & Fractals*, *138*, 109826.

Nande, A. A. (2021). *Mathematical modeling of drug resistance and the transmission of sars-cov-2* (Unpublished doctoral dissertation). Harvard University.

Navasardyan, I., Miwalian, R., Petrosyan, A., Yeganyan, S., & Venketaraman, V. (2024). Hiv–tb coinfection: current therapeutic approaches and drug interactions. *Viruses*, *16*(3), 321.

Ojo, M. M., Peter, O. J., Goufo, E. F. D., Panigoro, H. S., & Oguntolu, F. A. (2023). Mathematical model for control of tuberculosis epidemiology. *Journal of Applied Mathematics and Computing*, *69*(1), 69–87.

Okosun, K. O., Rachid, O., & Marcus, N. (2013). Optimal control strategies and cost-effectiveness analysis of a malaria model. *BioSystems*, *111*(2), 83–101.

Olaniyi, S., Abimbade, S. F., Ajala, O. A., & Chuma, F. M. (2024). Efficiency and economic analysis of intervention strategies for recurrent malaria transmission. *Quality & Quantity*, *58*(1), 627–645.

Olaniyi, S., Falowo, O., Okosun, K., Mukamuri, M., Obabiyi, O., & Adepoju, O. (2023). Effect of saturated treatment on malaria spread with optimal intervention. *Alexandria Engineering Journal*, *65*, 443–459.

Olaniyi, S., Kareem, G. G., Abimbade, S. F., Chuma, F. M., & Sangoniyi, S. O. (2024). Mathematical modelling and analysis of autonomous hiv/aids dynamics with vertical transmission and nonlinear treatment. *Iranian Journal of Science*, *48*(1), 181–192.

Oshinubi, K., Peter, O. J., Addai, E., Mwizerwa, E., Babasola, O., Nwabufo, I. V., ... Agbaje, J. O. (2023). Mathematical modelling of tuberculosis outbreak in an east african country incorporating vaccination and treatment. *Computation*, *11*(7), 143.

Özalp, N., & Demirci, E. (2011). A fractional order seir model with vertical transmission. *Mathematical and Computer Modelling*, *54*(1-2), 1–6.

Ozanne, M. V., Brown, G. D., Oleson, J. J., Lima, I. D., Queiroz, J. W., Jeronimo, S. M., ... Wilson, M. E. (2019). Bayesian compartmental model for an infectious disease with dynamic states of infection. *Journal of applied statistics*, *46*(6), 1043–1065.

Phillips, A. N., Stover, J., Cambiano, V., Nakagawa, F., Jordan, M. R., Pillay, D., ... Bertagnolio, S. (2017). Impact of hiv drug resistance on hiv/aids-associated mortality, new infections, and antiretroviral therapy program costs in sub–saharan africa. *The Journal of infectious diseases*, *215*(9), 1362–1365.

Podlubny, I. (1998). Fractional Differential Equations: An introduction to Fractional Derivatives, Fractional Differential Equations, to Methods of their Solution and some of their Applications. *Elsevier, California, USA*.

Pooranagangadevi, N., & Padmapriyadarsini, C. (2022). Treatment of tuberculosis and the drug interactions associated with hiv-tb co-infection treatment. *Frontiers in Tropical Diseases*, *3*, 834013.

Pooseh, S., Almeida, R., & Torres, D. F. (2013). Fractional order optimal control problems with free terminal time. *arXiv preprint arXiv:1302.1717*.

Pratap, H., Kumar, S., & Singh, G. (2024). Brief history of fractional calculus: A survey. *Migration Letters*, *21*(7), 238–43.

Pudlubny, I. (1999). Fractional differential equations. *Math. Sci. Eng., Academic Press, New York*.

Rahman, M. u., Karaca, Y., Agarwal, R. P., & Adriani David, S. (2024). Mathematical modelling with computational fractional order for the unfolding dynamics of the communicable diseases. *Applied Mathematics in Science and Engineering*, *32*(1), 2300330.

Raza, N., Irum, S., Niazai, S., Ullah, M. A., Alshahrani, M. Y., & Omame, A. (2025). A mathematical framework of hiv and tb co-infection dynamics. *Scientific Reports*, *15*(1), 11465.

Riaz, M., Khan, Z. A., Ahmad, S., & Ateya, A. A. (2024). Fractional-order dynamics in epidemic disease modeling with advanced perspectives of fractional calculus. *Fractal and Fractional*, *8*(5), 291.

Roberto Telles, C., Lopes, H., & Franco, D. (2021). Sars-cov-2: Sir model limitations and predictive constraints. *Symmetry*, *13*(4), 676.

Roeger, L. I. W., Feng, Z., & Castillo-Chavez, C. (2009). Modeling tb and hiv co-infections.

Ronoh, M., Jaroudi, R., Fotso, P., Kamdoum, V., Matendechere, N., Wairimu, J., ... Lugoye, J. (2016). A mathematical model of tuberculosis with drug resistance effects. *Applied Mathematics*, *7*(12), 1303–1316.

Rosa, S., & Torres, D. F. (2018). Optimal Control of a Fractional Order Epidemic Model with Application to Human Respiratory Syncytial Virus Infection. *Chaos, Solitons & Fractals*, *117*, 142–149.

Rosa, S., & Torres, D. F. (2023). Numerical fractional optimal control of respiratory syncytial virus infection in octave/matlab. *Mathematics*, *11*(6), 1511.

Sado, A. E., Duressa, G. F., & Deressa, C. T. (2025). The fractal-fractional mathematical model analysis of the impact of hiv/aids on the working-class in ethiopia. *Journal of Nonlinear Modeling and Analysis https://journal. global-sci. org/jnma*, *7*(3), 997–1036.

Saeedian, M., Khalighi, M., Azimi-Tafreshi, N., Jafari, G., & Ausloos, M. (2017). Memory effects on epidemic evolution: The susceptible-infected-recovered epidemic model. *Physical Review E*, *95*(2), 022409.

Saqib, S. U., Hasan, A., & Shih, Y.-T. (2025). A novel hybrid fractional approach to nonlinear dynamics of hiv transmission among men who have sex with men in taiwan. *AIMS Mathematics*, *10*(6), 13204–13230.

Saranya Devi, A., Pal, K. K., Tiwari, P. K., Sinha, D. K., & Kang, Y. (2025). Modeling the co-dynamics of hiv, tb and covid-19 using fractional order: Impact of control strategies. *International Journal of Biomathematics*.

Seid, G., Alemu, A., Diriba, G., Zerihun, B., Abebaw, Y., Moga, S., ... Gumi, B. (2024). Routine tuberculosis contact investigation yield and preventive treatment cascade in central ethiopia. *Heliyon*, *10*(10).

Seidu, B., Makinde, O. D., Seini, I. Y., et al. (2023). On the optimal control of hiv-tb co-infection and improvement of workplace productivity. *Discrete Dynamics in Nature and Society*, *2023*.

Sester, M., Giehl, C., McNerney, R., Kampmann, B., Walzl, G., Cuchí, P., ... others (2010). Challenges and perspectives for improved management of hiv/mycobacterium tuberculosis co-infection. *European Respiratory Journal*, *36*(6), 1242–1247.

Shayo, G. A., Chitama, D., Moshiro, C., Aboud, S., Bakari, M., & Mugusi, F. (2017). Cost-effectiveness of isoniazid preventive therapy among hiv-infected patients clinicaly screened for latent tuberculosis infection in dar es salaam, tanzania: A prospective cohort study. *BMC public health*, *18*(1), 35.

Shukla, U. (2025). Role of mathematical modeling to predict aids infection in working women migrants. *International Journal for Multidisciplinary Research*, *7(3)*.

Silva, C. J., & Torres, D. F. (2015). A tb-hiv/aids coinfection model and optimal control treatment. *arXiv preprint arXiv:1501.03322*.

Silva, C. J., & Torres, D. F. (2017). Modeling and optimal control of hiv/aids prevention through prep. *arXiv preprint arXiv:1703.06446*.

Singh, K., Kumari, R., Gupta, S., Tripathi, R., Srivastava, A., Shakya, V., ... Anupurba, S. (2021). Direct Detection of Resistance to Fluoroquinolones/SLIDS in Sputum Specimen by Genotype MTBDR: A Study from Eastern Uttar Pradesh, India. *Annals of Clinical Microbiology and Antimicrobials*, *20*(1), 1–6.

Smith, T., Samandari, T., Abimbola, T., Marston, B., & Sangrujee, N. (2015). Cost-effectiveness of antiretroviral therapy and isoniazid prophylaxis to reduce tuberculosis and death in people living with hiv in botswana. *Journal of acquired immune deficiency syndromes (1999)*, *70*(3), e84.

Suddin, S., & Bano, E. N. (2021). Mathematical modeling and simulation to control the spread of multidrug-resistant tuberculosis. *(IJCSAM) International Journal of Computing Science and Applied Mathematics*, *7*(1), 1–7.

Sun, X., & Hu, B. (2018). Mathematical modeling and computational prediction of cancer drug resistance. *Briefings in bioinformatics*, *19*(6), 1382–1399.

Sweilam, N., Al-Mekhlafi, S., & Baleanu, D. (2019). Optimal control for a fractional tuberculosis infection model including the impact of diabetes and resistant strains. *Journal of advanced research*, *17*, 125–137.

Tanvi A., Y. A. R., Rajiv Aggarwal. (2021). A Fractional Order HIV-TB Co-infection Model in the Presence of Exogenous Reinfection and Recurrent TB. *Nonlinear Dyn.*, *104*, 4701–4725.

TBCAB. (2025). Unaids statement: World tb day: Unite, invest and deliver to end tb. *https://globaltbcab.org/tb-news/unaids-statement-world-tb-day-unite-invest-and-deliver-to-end-tb/*.

Ullah, M. A., & Raza, N. (2024). A simulation-based analysis of a novel hiv/aids transmission model with awareness and treatment. *Nonlinear Dynamics*, *112*(24), 22529–22548.

Ullah, S., Altanji, M., Khan, M. A., Alshaheri, A., & Sumelka, W. (2023). The dynamics of hiv/aids model with fractal-fractional caputo derivative. *Fractals*, *31*(02), 2340015.

Ullah, S., Khan, M. A., Farooq, M., Hammouch, Z., & Baleanu, D. (2020). A fractional model for the dynamics of tuberculosis infection using caputo-fabrizio derivative.

Ullah, S., Ullah, O., Khan, M. A., & Gul, T. (2020). Optimal control analysis of tuberculosis (tb) with vaccination and treatment. *The European Physical Journal Plus*, *135*, 1–27.

UNAIDS. (2025a). Global hiv & aids statistics fact sheet. *https://www.unaids.org/en/resources/fact-sheet*.

UNAIDS. (2025b). Unaids executive director message on world tb day. *https://www.unaids.org/en/resources/presscentre/pressreleaseandstatementarchive*.

Vincent, O. B. (2022). *A mathematical model of hiv and tb co-infection with interventions, a case of siaya county in kenya* (Unpublished doctoral dissertation). Kenyatta University.

Wang, J. (2020). Mathematical models for covid-19: applications, limitations, and potentials. *Journal of public health and emergency*, *4*, 9.

Wang, Y., Cao, J., Xue, C., & Li, L. (2023). Mathematical analysis of epidemic models with treatment in heterogeneous networks. *Bulletin of Mathematical Biology*, *85*(2), 11.

Wangari, I. M., & Stone, L. (2018). Backward Bifurcation and Hysteresis in Models of Recurrent Tuberculosis. *PloS one*, *13*(3), e0194256.

WHO. (2016a). Guidelines for the treatment of tuberculosis in children. who tb guidelines. *WHO*.

WHO. (2016b). Hiv treatment: Guidelines for a test and treat approach. who hiv treatment guidelines. *WHO*.

WHO. (2018). Tuberculosis: Multidrug-resistant tuberculosis (mdr-tb). *https://www.who.int/news-room/questions-and-answers/item/tuberculosis-multidrug-resistant-tuberculosis-(mdr-tb)*.

WHO. (2023a). Global Tuberculosis Report. *WHO*.

WHO. (2023b). HIV and AIDS. *WHO*.

WHO. (2023c). Tuberculosis. *WHO*.

WHO. (2023a). Global tuberculosis report. *WHO*.

WHO. (2023b). Comprehensive tb guidelines for national tuberculosis program, v edition. *WHO*.

WHO. (2024a). Who operational handbook on tuberculosis. mod- ule1:prevention. tuberculosis preventive treatment. *WHO*.

WHO. (2024b). Tuberculosis: Extensively drug-resistant tuberculosis (xdr-tb). *https://www.who.int/news-room/questions-and-answers/item/tuberculosis-extensively-drug-resistant-tuberculosis-(XDR-TB)*.

WHO. (2024c). Tuberculosis: Multidrug-resistant (mdr-tb) or rifampicin-resistant tb (rr-tb). *https://www.who.int/news-room/questions-and-answers/item/tuberculosis-multidrug-resistant-tuberculosis-(mdr-tb).*

WHO. (2025). Hiv treatment and care for people living with hiv diagnosed with tb. *https://tbksp.who.int/en/node/2778*.

WHO. (2025a). Vaccines and immunization. *WHO*.

WHO. (2025b). Infectious diseases. *https://www.emro.who.int/health-topics/infectious-diseases/index.html*.

WHO. (2025c). Global tuberculosis programme: New tb vaccine research. *WHO*.

WHO. (2025d). Hiv and aids. *https://www.who.int/news-room/fact-sheets/detail/hiv-aids*.

WHO. (2025e). Global hiv programme. *https://www.who.int/teams/global-hiv-hepatitis-and-stis-programmes/hiv/prevention*.

Windels, E. M., Wampande, E. M., Joloba, M. L., Boom, W. H., Goig, G. A., Cox, H., ... others (2024). Hiv co-infection is associated with reduced mycobacterium tuberculosis transmissibility in sub-saharan africa. *PLoS pathogens*, *20*(5), e1011675.

Wired. (2020). Who releases global health challenges. *Wired International. https://www.wiredinternational.org/climate-change/who-releases-global-health-challenges/*.

Wolfe, A., Jadhav, P., May, A., Seymour, S., Blanchard, A., & Ali, J. (2024). Latent tb treatment regimens in 2023: Wetmore tb clinic in new orleans. *Journal of Clinical Tuberculosis and Other Mycobacterial Diseases*, *35*, 100443.

Zahli, R., Zeroual, K., & Fatmi, N. I. (2024). Tuberculosis and hiv/aids co-dynamics: a mathematical model and sensitivity analysis. *Commun. Math. Biol. Neurosci.*, *2024*, Article–ID.

Zhu, L., Wang, X., Zhang, H., Shen, S., Li, Y., & Zhou, Y. (2020). Dynamics analysis and optimal control strategy for a sirs epidemic model with two discrete time delays. *Physica Scripta*, *95*(3), 035213.

CONTRIBUTION OF THE DISSERTATION

The dissertation reports original results that contribute knowledge to the scientific advancement in Mathematics. Two of the contributions were published and one is under review, and one is under initial consideration in peer-reviewed journals indexed in Web of Science and Scopus.

P1. Gemeda, A. E., Obsu, L. L., Gurmu, E. D., & Degefa, S. T. (2025). Mathematical modeling of tuberculosis transmission dynamics with vaccination and two lines of treatments: a caputo fractional approach. Journal of Applied Mathematics and Computing, 71(2), 2017-2049. https://doi.org/10.1007/s12190-024-02308-9

P2. Gemeda, A. E., Obsu, L. L., Gurmu, E. D., & Degefa, S. T. (2025). Fractional Order Modeling of HIV/AIDS and TB Co-infection with Vaccination and Treatment Therapies. Journal of Computational Mathematics and Modeling. https://doi.org/10.1007/s10598-025-09621-3

P3. Gemeda, A. E., Obsu, L. L., Gurmu, E. D., & Degefa, S. T. (2025). Fractional Modeling of HIV/AIDS Transmission Dynamics Considering Pre-Exposure Prophylaxis and Drug Resistant Strain. Journal of Applied Mathematics and Computing. (Under Review)

P4. Gemeda, A. E., Obsu, L. L., Gurmu, E. D., & Degefa, S. T. (2025). Fractional Order Modeling of HIV-TB Co-infection with Optimal Control. Journal of Applied Mathematics . (Under Review)

APPENDIX A

Mathematical Preliminaries

A.1 Fractional Calculus

In this part, we go over few of the fundamental terms and ideas in fractional calculus that are useful for the analysis of our model.

Let a real number δ denotes the order of the derivative or integral of u, and let $u : [c, d] \to \mathbb{R}$ be a function. Then, using the definitions (A.1)–(A.3) the Riemann–Liouville fractional integrals and derivatives as well as the Caputo fractional derivatives of u are defined below (Pooseh et al., 2013).

Definition A.1 *For a function u, the left and right Riemann-Liouville fractional integrals can be defined as follows:*

$$ {}_cI_t^{\delta} u(t) = \frac{1}{\Gamma(\delta)} \int_c^t (t-\tau)^{\delta-1} u(\tau) d\tau \ , $$

$$ {}_tI_d^{\delta} u(t) = \frac{1}{\Gamma(\delta)} \int_t^d (t-\tau)^{\delta-1} u(\tau) d\tau. $$

Definition A.2 *For a function u, the left and right Riemann-Liouville fractional derivatives are defined as follows:*

$$ {}_cD_t^{\delta} u(t) = \frac{1}{\Gamma(n-\delta)} \frac{d^n}{dt^n} \int_c^t (t-\tau)^{n-\delta-1} u(\tau) d\tau \ , $$

$$ {}_tD_d^{\delta}u(t) = \frac{1}{\Gamma(n-\delta)}\frac{d^n}{dt^n}\int_t^d (t-\tau)^{n-\delta-1}u(\tau)d\tau. $$

Definition A.3 *The following defines the left and right Caputo fractional derivatives of a function u, respectively:*

$$ {}_c^C D_t^{\delta}u(t) = \frac{1}{\Gamma(n-\delta)}\int_c^t (t-\tau)^{n-\delta-1}u^{(n)}(\tau)d\tau \quad , $$

$$ {}_t^C D_d^{\delta}u(t) = \frac{1}{\Gamma(n-\delta)}\int_t^d (t-\tau)^{n-\delta-1}u^{(n)}(\tau)d\tau, $$

where n is the least integer with $n-1 < \delta \leq n$ and Γ is a gamma function given by:

$$ \Gamma(y) = \int_0^{\infty} t^{y-1}e^{-t}dt \quad , \; y > 0. $$

Definition A.4 *(Delavari et al., 2012) An equilibrium point of the Caputo fractional dynamical system*

$$ D_t^{\delta}x(t) = h(t,\ x(t)),\ \delta \in (0,\ 1] $$

is the constant $\hat{x}$, for which $h(t,\ \hat{x}) = 0$.

Definition A.5 *(Podlubny, 1998) Let q be a function defined above and let ${}_0^C D_t^{\delta}q(t)$ be its Caputo fractional derivative of order δ. Then, we define its Laplace transform by*

$$ \mathcal{L}\left\{{}_0^C D_t^{\delta}q(t)\right\} = s^{\delta}Q(s) - \sum_{k=0}^{n-1} s^{\delta-k-1}q^{(k)}(0), \quad n-1 < \delta \leq n, $$

where $Q(s)$ defined by

$$ Q(s) = \mathcal{L}\{q(t); s\} = \int_0^{\infty} e^{-st}q(t)dt $$

is known as the Laplace transform of the function $q(t)$.

Definition A.6 *(Podlubny, 1998) The two parametric Mittag-leffler function is defined by*

$$ E_{\delta,\psi}(y) = \sum_{k=0}^{\infty}\frac{y^k}{\Gamma(\delta k + \psi)}. $$

With $\delta = \psi = 1$, we have

$$E_{1,1}(y) = \sum_{k=0}^{\infty} \frac{y^k}{\Gamma(k+1)} = \sum_{k=0}^{\infty} \frac{y^k}{k!} = e^y \ ,$$

which is the typical exponential function. However, when $\psi = 1$, the Mittag-Leffler function with one parameter is described by

$$E_\delta = E_{\delta,1}(y) = \sum_{k=0}^{\infty} \frac{y^k}{\Gamma(\delta k + 1)}.$$

Definition A.7 *The integral representation of the Caputo fractional IVP*

$$\begin{cases} {}_{t_0}^{C}D_t^{\alpha} x(t) = \Psi(t,\ x(t)), \\ x(t_0) = x_0,\ \alpha \in (0,1], \end{cases} \tag{A.1}$$

where $\Psi \in C[\mathbb{R}^+ \times \mathbb{R}^n,\ \mathbb{R}^n]$ is given by the integral equation

$$x(t) = x_0 + \frac{1}{\Gamma(\alpha)} \int_0^t (t-\tau)^{\alpha-1} \Psi(\tau,\ x(\tau)) d\tau \tag{A.2}$$

(Lyons, 2017). If the solution of the integral equation (A.2) exists and is unique, then the solution of the IVP (A.1) also exists and is unique.

Lemma A.1 *The integral equation (A.2) is the solution for the IVP (A.1).*

Proof 1 *Multiplying both sides of the given IVP by ${}_{t_0}D_t^{-\alpha}$ and using definition (A.1) we have;*

$${}_{t_0}D_t^{-\alpha} \left({}_{t_0}^{C}D_t^{\alpha} x(t) \right) = {}_{t_0}D_t^{-\alpha} \Psi\left(t,\ x(t)\right),$$

$$x(t) - x_0 = {}_{t_0}I_t^{\alpha} \Psi\left(t,\ x(t)\right),$$

$$x(t) = x_0 + \frac{1}{\Gamma(\alpha)} \int_0^t (t-\tau)^{\alpha-1} \Psi(\tau,\ x(\tau)) d\tau.$$

Hence, the proof is done.

A.2 Jacobian Matrix and the Fractional Stability Criterion

Here, we discuss some of the prominent concepts regarding local stability of the fractional systems.

Definition A.8 *Mahata et al. (2022) The generalized Jacobian matrix $\mathcal{J}$ of a system of equations ${}_{t_0}^{C}D_t^{\alpha}x(t) = f(t,\ x(t))$, where*
$\boldsymbol{x} = (x_1, x_2, \ldots, x_n)^T$, is defined as:

$$\mathcal{J} = \begin{bmatrix} \frac{\partial f_1}{\partial x_1} & \frac{\partial f_1}{\partial x_2} & \cdots & \frac{\partial f_1}{\partial x_n} \\ \frac{\partial f_2}{\partial x_1} & \frac{\partial f_2}{\partial x_2} & \cdots & \frac{\partial f_2}{\partial x_n} \\ \vdots & \vdots & \ddots & \vdots \\ \frac{\partial f_n}{\partial x_1} & \frac{\partial f_n}{\partial x_2} & \cdots & \frac{\partial f_n}{\partial x_n} \end{bmatrix}$$

For stability analysis, we evaluate this Jacobian at the equilibrium point x^*. The equilibrium point is stable if all of the eigenvalues of $\mathcal{J}(x^*)$ are negative or have negative real parts; if any of the eigenvalues have a positive real component, the equilibrium point is unstable. The eigenvalues offer important information in understanding the system's behavior close to equilibrium points.

Definition A.9 *If all the eigenvalues λ_i of the Jacobian matrix $\mathcal{J}$ satisfy the inequality $|arg(\lambda_i)| > \frac{\alpha\pi}{2}$ for each $i = 1, 2, \cdots, n$ and a fractional-order $\alpha \in (0, 1)$, then by the fractional stability criterion (Matignon, 1996), the equilibrium point x^* of the left Caputo fractional system ${}_{t_0}^{C}D_t^{\alpha}x(t) = f(t,\ x(t))$ is locally asymptotically stable and ustable if there exists at least one λ_i such that $|arg(\lambda_i)| < \frac{\alpha\pi}{2}$.*

APPENDIX B

Numerical Algorithms

B.1 The Matlab Algorithm 'fminunc' for Parameter Estimation and Fitting of Figure (4.2)

A MATLAB toolbox called 'fminunc' finds a local minimum of a function of several variables. It is also used to estimate parameters though optimization techniques. Its algorithm is as follows:

1. Initialization:

   - Set values of model parameters:

     $\Lambda_{old} = 1265\ (in\ thousands),\ \mu_{old} = 0.01,\ \tau_{old} = 0.02,\ \rho_{1(old)} = 0.1,$

     $\rho_{2(old)} = 0.2,\ \rho_{3(old)} = 0.3,\ \nu_{old} = 0.05,\ \gamma_{old} = 0.12, \delta_{old} = 0.03,$

     $d_{A(old)} = 0.01.$

   - Define real data and initial conditions:

     real data = [741, 777, 614, 649, 573, 573, 569, 563],

     initial conditions = [125000, 120, 740, 563, 80, 42].

   - Define possible values for σ: $\sigma_{values} = [0.5, 0.6, 0.7, 0.8, 0.9, 1.0]$, where $\sigma \in (0, 1])$ is the order of the derivative.

2. Prepare for Optimization:

- Initialize a results matrix 'results' to store σ and parameters.
- Set best σ to 0 and best result to infinity.

3. Time Span Definition:
   - Define tspan as a linearly spaced vector from 0 to 7 over 150 points.
4. Optimization Loop:
   - For each σ in σ_{values}:

   4.1 Adjust Parameters:
   - Calculate adjusted parameters using:

$$\Lambda = \Lambda^{\sigma}_{old},\ \mu = \mu^{\sigma}_{old},\ \tau = \tau^{\sigma}_{old},\ \rho_1 = \rho^{\sigma}_{1(old)},\ \rho_2 = \rho^{\sigma}_{2(old)},\ \rho_3 = \rho^{\sigma}_{3(old)},$$
$$\nu = \nu^{\sigma}_{old},\ \gamma = \gamma^{\sigma}_{old}, \delta = \delta^{\sigma}_{old},\ d_A = d^{\sigma}_{A(old)}.$$

   4.2 Parameter Optimization:
   - Initialize initial guess for parameters.
   - Optimize parameters using a minimization function to minimize an objective function (sum of squared errors between simulated and real data).

   4.3 Store Results:
   - Save σ and optimized parameters to results.

   4.4 Evaluate Error:
   - Calculate the error for the optimized parameters using the objective function.
   - If the current error is less than best result, update best result, best σ, and best params.

5. Output Results:
   - Print the optimal σ and estimated parameters.

6. Plotting:

   - Create a plot showing estimated values for each σ against the real data.

7. Functions Used:

   ◇ **Model Function:**

   - The model function reflecting the dynamics of HIV/AIDS model is a system of ordinary differential equations:

$$\begin{cases} \frac{dS}{dt} = \Lambda + \eta P - \frac{\beta_0}{N}\left(\rho_1 E + \rho_2 I + \rho_3 R + A\right) S - (\mu + \eta) S, \\ \frac{dP}{dt} = \eta S - (\mu + \epsilon) P, \\ \frac{dE}{dt} = \frac{\beta_0}{N}\left(\rho_1 E + \rho_2 I + \rho_3 R + A\right) S + \nu I - (\mu + \delta) E, \\ \frac{dI}{dt} = \delta E - (\mu + \theta_1 + \nu) I, \\ \frac{dR}{dt} = \phi\gamma\theta_1 I - (\mu + \tau + \theta_2) R, \\ \frac{dA}{dt} = (1 - \phi\gamma)\theta_1 I + \theta_2 R - (\mu + d_A) A. \end{cases} \tag{B.1}$$

   Where:

   S: Susceptible population, P: Population using PrEP,

   E: Asymptomatic, undiagnosed , infectious population,

   I: Symptomatic, diagnosed , infectious population,

   R: Population with HIV drug-resistant strains,

   A: AIDS developed population,

   $N = S + P + E + I + R + A$: Total population.

   ◇ **Objective Function:**

   - The objective function which calculates the sum of squared errors between the simulated data and the real data for each i becomes:

$$\text{error} = \sum \left(simulated\ data - real\ data\right)^2, \tag{B.2}$$

   where simulated data is the simulated data for the exposed population E, and real data is the corresponding observed value.

B.2 The PECE Algorithm for Solving System (5.3)

The algorithm to solve each state variables are derived as follows:

Predictor:

$$
\begin{aligned}
S^p_{k+1} &= S_0 + \frac{1}{\Gamma(\psi)}\sum_{j=0}^{k} b_{j,k+1} f_1(t_j, S_j), \quad & V^p_{k+1} &= V_0 + \frac{1}{\Gamma(\psi)}\sum_{j=0}^{k} b_{j,k+1} f_2(t_j, V_j),\\
E^p_{k+1} &= E_0 + \frac{1}{\Gamma(\psi)}\sum_{j=0}^{k} b_{j,k+1} f_3(t_j, E_j), \quad & I^p_{k+1} &= I_0 + \frac{1}{\Gamma(\psi)}\sum_{j=0}^{k} b_{j,k+1} f_4(t_j, I_j),\\
X^p_{k+1} &= X_0 + \frac{1}{\Gamma(\psi)}\sum_{j=0}^{k} b_{j,k+1} f_5(t_j, X_j), \quad & Y^p_{k+1} &= Y_0 + \frac{1}{\Gamma(\psi)}\sum_{j=0}^{k} b_{j,k+1} f_6(t_j, Y_j),\\
& & R^p_{k+1} &= R_0 + \frac{1}{\Gamma(\psi)}\sum_{j=0}^{k} b_{j,k+1} f_7(t_j, R_j),
\end{aligned}
\tag{B.3}
$$

with

$$
b_{j,k+1} = \frac{h^\psi}{\psi}\left[(k+1-j)^\psi - (k-j)^\psi\right]
$$

Corrector:

$$
\begin{aligned}
S_{k+1} &= S_0 + \frac{1}{\Gamma(\psi)}\left[\sum_{j=0}^{k} a_{j,k+1} f_1(t_j, S_j) + a_{k+1,k+1} f_1(t_{k+1}, S^p_{k+1})\right],\\
V_{k+1} &= V_0 + \frac{1}{\Gamma(\psi)}\left[\sum_{j=0}^{k} a_{j,k+1} f_2(t_j, V_j) + a_{k+1,k+1} f_2(t_{k+1}, V^p_{k+1})\right],\\
E_{k+1} &= E_0 + \frac{1}{\Gamma(\psi)}\left[\sum_{j=0}^{k} a_{j,k+1} f_3(t_j, E_j) + a_{k+1,k+1} f_3(t_{k+1}, E^p_{k+1})\right],\\
I_{k+1} &= I_0 + \frac{1}{\Gamma(\psi)}\left[\sum_{j=0}^{k} a_{j,k+1} f_4(t_j, I_j) + a_{k+1,k+1} f_4(t_{k+1}, I^p_{k+1})\right],\\
X_{k+1} &= X_0 + \frac{1}{\Gamma(\psi)}\left[\sum_{j=0}^{k} a_{j,k+1} f_5(t_j, X_j) + a_{k+1,k+1} f_5(t_{k+1}, X^p_{k+1})\right],\\
Y_{k+1} &= Y_0 + \frac{1}{\Gamma(\psi)}\left[\sum_{j=0}^{k} a_{j,k+1} f_6(t_j, Y_j) + a_{k+1,k+1} f_6(t_{k+1}, Y^p_{k+1})\right],\\
R_{k+1} &= R_0 + \frac{1}{\Gamma(\psi)}\left[\sum_{j=0}^{k} a_{j,k+1} f_7(t_j, R_j) + a_{k+1,k+1} f_7(t_{k+1}, R^p_{k+1})\right],
\end{aligned}
\tag{B.4}
$$

with

$$a_{j,k+1} = \frac{h^{\psi}}{\psi(\psi+1)} \begin{cases} k^{\psi+1} - (k-\psi)(k+1^{\psi}), & if\ j = 0 \\ (k-j+2)^{\psi+1} + (k-j)^{\psi+1} - 2(k-j+1)^{\psi+1}, & if\ 1 \leq k \leq j \\ 1, & if\ j\ = k+1 \end{cases},$$

where, f_r $(r = 1, 2, \cdots, 7)$ denotes the r^{th} equation on the right hand side of system (5.3) and, $k = 0, 1, 2, \cdots, N-1$, and N is the number of required iterations.

B.3 An Algorithm for the PYTHON optimization toolbox called 'minimize' for Parameter Estimation and Fitting of Figure (6.2a)

A PYTHON toolbox called 'minimize' is used a with the L-BFGS-B method to optimize parameters. Its algorithm is as follows:

1. Initialization:

   - Define constants:

     $\Lambda_{\text{old}} = 1265$ (in thousands), $\mu_{\text{old}} = 0.01$, $\mu_{T(old)} = 0.0767$,
     $\epsilon_{\text{old}} = 0.7$, $\xi_{\text{old}} = 0.1$, $\phi_{\text{old}} = 0.01$, $\theta_{1(old)} = 0.2959$, $\sigma_{\text{old}} = 0.1$.

   - Set α (correction factor): $\alpha = 1$ (can be adjusted)

   - Correct parameters based on α:

     $\Lambda = \Lambda_{\text{old}}^{\alpha}$, $\mu = \mu_{\text{old}}^{\alpha}$, $\mu_T = \mu_{T(old)}^{\alpha}$, $\epsilon = \epsilon_{\text{old}}^{\alpha}$,
     $\xi = \xi_{\text{old}}^{\alpha}$, $\phi = \phi_{\text{old}}^{\alpha}$, $\theta_1 = \theta_{1(old)}^{\alpha}$, $\sigma = \sigma_{\text{old}}^{\alpha}$.

2. Define the System of ODEs:

   - Let S, V, E_T, I_T, R_T be the state variables representing:
     - S: Susceptible population, V: Vaccinated population,
     - E_T: Exposed population, I_T: Infected population

- R_T: Recovered population.

- Define total population:

  $N = S + V + E_T + I_T + R_T$.

- The ODEs is defined as:

$$\begin{cases} \frac{dS}{dt} = \Lambda + \sigma V + \phi R_T - \frac{\beta_T S I_T}{N} - (\mu + \xi)S, \\ \frac{dV}{dt} = \xi S - \frac{\beta_T (1-\epsilon) V I_T}{N} - (\mu + \delta)V, \\ \frac{dE_T}{dt} = \frac{\beta_T S I_T}{N} + \frac{\beta_T (1-\epsilon) V I_T}{N} - (\mu + \theta_1 + \kappa_1)E_T, \\ \frac{dI_T}{dt} = \kappa_1 E_T - (\mu + \mu_T + \theta_2)I_T, \\ \frac{dR_T}{dt} = \theta_1 E_T + \theta_2 IT - (\mu + \phi)R_T. \end{cases} \tag{B.5}$$

3. Set Initial Conditions:

   - Define initial conditions:

     initial conditions = [123005, 1800, 205, 126, 117] (in thousands).

4. Define Time Points and Data:

   - Set the time range:

     $t = \text{range}(2016, 2024)$

   - Define observed data:

     data = [126, 117, 110, 111, 108, 103, 114, 135].

5. Initial Parameter Guesses:

   - Set initial guesses for parameters:

     initial params = [0.1, 0.15, 0.01, 0.02].

6. Define Parameter Bounds:

   - Set bounds for parameters (0 to 1.525):

     param bounds = $[(0, 1.525)] \times \text{length(initial\_params)}$

7. Define the Objective Function:

    - The objective function calculates the error between model outputs and observed data:
        - Solve the ODE system using the 'odeint' function.
        - Extract the infected population I_T the solution.
        - Calculate error as:

$$\text{error} = \sum (I_T \text{ solution} - \text{data})^2. \tag{B.6}$$

8. Perform Parameter Optimization:

    - Use the 'minimize' function with the 'L-BFGS-B' method to optimize parameters:
    - Minimize the objective function within defined bounds.

9. Output Results:

    - Print the optimized parameters.

10. Solve ODEs with Optimized Parameters:

    - Re-solve the ODEs using the optimized parameters.

11. Plot Results:

    - Create a plot showing:
        - The observed data points.
        - The fitted model output for I_T.

APPENDIX C

GNU Octave/Matlab and Python Codes

C.1 Python Code for Figure 6.2(b)

```
#!/usr/bin/env python3
# -*- coding: utf-8 -*-
"""
Created on Wed Jan  8 18:41:17 2025 by Abdurkadir Edeo Gemeda

@author: phd
"""

import numpy as np
from scipy.integrate import odeint
from scipy.optimize import minimize
import matplotlib.pyplot as plt
# Define the parameters
#Lambda=1265270
alpha=1
#alpha=0.9
#alpha=0.8
```

```
#alpha=0.7
Lambda_old=1265 #in thousands
mu_old=0.01
mu_H_old=0.0154
rho_3_old=0.45
rho_4_old=0.4
eta_old=0.33
#kappa_3_old=0.0217
mu_A_old=0.0256
#correction of parameters
Lambda=Lambda_old**alpha #in thousands
mu=mu_old**alpha
mu_H=mu_H_old**alpha
rho_3=rho_3_old**alpha
rho_4=rho_4_old**alpha
#kappa_3=kappa_3_old**alpha
eta=eta_old**alpha
mu_A=mu_A_old**alpha
# Define the system of ODEs
def odes(y, t, params):
S, IH, TH, A = y
NH=S+IH+TH+A
#beta_H,eta,mu_H = params
beta_H,kappa_3 = params
dS_dt = Lambda-beta_H*S*(IH+rho_3*TH+rho_4*A)/NH-mu*S
dIH_dt = beta_H*S*(IH+rho_3*TH+rho_4*A)/NH-(eta+mu+mu_H)*IH
dTH_dt = eta*IH-(mu+kappa_3)*TH
dA_dt = kappa_3*TH-(mu+mu_A)*A
return [dS_dt, dIH_dt, dTH_dt, dA_dt]
```

```
# Initial conditions
#initial_conditions = np.array([123005217,3000000,141188,
#134616,117654])
# Initial conditions in thousands
#initial_conditions = np.array([123005,563,474,42])
initial_conditions = np.array([123005,741,394,42])

# Time points and data
day1 = 2016
day_end = 2023
t = np.arange(day1, day_end + 1)
#data=[125826,116725,110675,110961,107846,102876,113633,134616]
#data in thousands
data=[741,777,614,649,573,573,569,563]
# Initial parameter guesses
initial_params = np.array([0.01, 0.1])

# Parameter bounds (0 to 1 for all parameters)
param_bounds = [(0, 0.35)] * len(initial_params)
#param_bounds = [(0, 0.29)] * len(initial_params)
#param_bounds = [(0, 1.3)] * len(initial_params)
#param_bounds = [(0, 0.3)] * len(initial_params)
#param_bounds = [(0, 0.3)] * len(initial_params)

# Define the objective function
def objective(params):
solution = odeint(odes, initial_conditions, t,
args=(params,))
```

```
IH_solution = solution[:, 1]
error = np.sum((IH_solution - data)**2)
return error

# Perform the optimization with bounds
result = minimize(objective, initial_params, method='L-BFGS-B',
bounds=param_bounds)

# Print the optimized parameters
optimized_params = result.x

print("Optimized parameters:", optimized_params)

# Solve the ODEs with optimized parameters
solution_optimized = odeint(odes, initial_conditions, t,
args=(optimized_params,))
IH_solution_optimized = solution_optimized[:, 1]
plt.figure(figsize=(10, 6))
plt.xlabel('Time in years', fontsize=20)
plt.ylabel('HIV cases per thousands', fontsize=20)
plt.plot(t, data, '*', label='Data', markersize=16)
plt.plot(t, IH_solution_optimized, '-', label='Fitted',
linewidth=4)
plt.legend()
plt.show()
```

C.2 GNU Octave/Matlab Code for Figure 6.5(d)

```
% A PECE MATLAB code for the numerical simulation of HIV-TB coinfection
%model without control
%considering vaccination for TB and treatment for HIV
%without optimal control by Abdurkadir E.
% Last modified April 21,2025
function [t,y] = manusc3_dfelocalstab(N,alpha)
% Values of parameters
miu_old = 0.01; Lambda_old=1265;
beta_T_old=1.525;%R_T=0.8992  <1,TB free steady state
%beta_T_old=1.525;
miu_T_old=0.0767; kappa_1_old=0.1142; kappa_2_old=0.0017; kappa_3_old=0.35;
theta_1_old=0.2959; theta_2_old=0.2506;
%beta_H_old=0.1855;
%beta_H_old=0.0655;
beta_H_old=0.0455;%R_HA=0.6783<1,HIVA free state, TB is dominant in this case.
miu_H_old=0.0154; miu_C_old=0.2096;
miu_A_old=0.0256; delta_old=1.525; phi_old=0.01;
eta_old=0.33; rho_1_old=0.2;rho_2_old=0.3; rho_3_old=0.45; rho_4_old=0.4;
xi_old=0.1; epsilon_old=0.7; sigma_old=0.1;
%tfinal = 5;
%tfinal = 100;% for I_T and I_H compartments
%tfinal = 50;% for I_C compartment
tfinal=250;% for A compartment
%t0=0; tfinal=100;
%initial conditions where population is in thousands
%N=400;
S0 = 123005; V0=1800; ET0 = 205; IT0 = 126; RT0 = 117;
```

```
IH0 = 741; EC0 = 60; IC0 = 37; TH0 = 394; A0=42;
N0=S0+V0+ET0+IT0+RT0+IH0+EC0+IC0+TH0+A0;
N0_star=1; %total population
% correction of parameter values
%alpha_values=[0.5, 0.7, 0.9, 1.0]
%indx=length(alpha_values)
%for m=1:indx
%alpha=alpha_values(m)
miu=miu_old^alpha
Lambda=Lambda_old^alpha;
beta_T=beta_T_old^alpha;
miu_T=miu_T_old^alpha;
kappa_1=kappa_1_old^alpha;kappa_2=kappa_2_old^alpha; kappa_3=kappa_3_old^alpha;
beta_H=beta_H_old^alpha;
miu_H=miu_H_old^alpha;eta=eta_old^alpha;
miu_C=miu_C_old^alpha;
rho_1=rho_1_old^alpha;rho_2=rho_2_old^alpha; rho_3=rho_3_old^alpha;
rho_4=rho_4_old^alpha;epsilon=epsilon_old^alpha; xi=xi_old^alpha;
miu_A=miu_A_old^alpha; delta=delta_old^alpha; phi=phi_old^alpha;
theta_1=theta_1_old^alpha; theta_2=theta_2_old^alpha; sigma=sigma_old^alpha;

q_1 = miu + xi; q_2 = miu + delta; q_3 = miu + theta_1 + kappa_1;
q_4 = theta_2 +miu + miu_T;
q_5 = miu + phi; q_6 = eta + miu + miu_H; q_7 = theta_1 + kappa_2 + q_6;
q_8 = eta + theta_2 + miu + miu_C; q_9 = miu + kappa_3; q_10 = miu + miu_A;
xi_1=beta_T*(miu+delta)/(miu+delta+xi);xi_2=beta_H*(miu+delta)/(miu+delta+xi);
xi_3=beta_T*xi*(1-epsilon)/(miu+delta+xi);
% Analysis of the HIV Sub-model, its steady states and basic reproduction number
HIVAFE=[Lambda/miu;0;0;0]
```

```
R_HA=(beta_H)/(eta+miu+miu_H)*(1+(eta*rho_3)/(miu+kappa_3)+(eta*kappa_3*rho_4)...
/((miu+kappa_3)*(miu+miu_A)))
K=[-miu -beta_H -beta_H*rho_3 -beta_H*rho_4;0 beta_H-(eta+miu+miu_H) beta_H...
*rho_3 beta_H*rho_4;...
0 eta -(miu+kappa_3) 0;0 0 kappa_3 -(miu+miu_A)]
lambda_k=eig(K)
% Analysis of the TB Sub-model, its steady states and basic reproduction number
TBFE=[Lambda*(miu+delta)/miu*(miu+xi+delta);Lambda*xi/miu*(miu+xi+delta);0;0;0]
R_T = (beta_T*kappa_1*(miu+delta+xi-epsilon*xi))/((miu+theta_1+kappa_1)...
*(miu+theta_2+miu_T)*(miu+delta+xi))


%Analysis, steady states and basic reproduction number of HIV-TB coinfection
%model

E_0=[Lambda*(miu+delta)/miu*(miu+xi+delta);Lambda*xi/miu*(miu+xi+delta)
...;0;0;0;0;0;0;0;0]
R_0=max(R_T,R_HA)
L=[-q_1 delta 0 -xi_1 -phi -xi_2 -rho_1*xi_1 -(sigma*xi_1+rho_2*xi_2) -...
rho_3*rho_2 -rho_4*xi_2;...
xi_2 -q_2 0 -xi_3 0 0 0 -sigma*xi_3 0 0;0 0 -q_3 xi_1+xi_3 0 0 0 0 0 0;...
0 0 kappa_1 -q_4 0 0 0 0 0 0;...
0 0 theta_1 theta_2 -q_5 0 0 0 0 0;0 0 0 0 0 -q_6 rho_1*xi_2 rho_2*xi_2 ...
rho_3*xi_2 rho_4*xi_2;...
0 0 0 0 0 0 -q_7 0 0 0;0 0 0 0 0 0 kappa_2 -q_8 0 0;0 0 0 0 0 eta eta+...
theta_1 eta+theta_2 -q_9 0;...
0 0 0 0 0 0 0 0 kappa_3 -q_10]
lambda=eig(L)
critical_angle = alpha * pi/2;
```

```
critical_angle_deg = critical_angle * 180/pi;

fprintf('For alpha = %.1f:\n', alpha);
fprintf('  Critical angle: %.1f\n', critical_angle_deg);

% Check stability
%is_stable = true;
for j = 1:length(lambda)
arg_deg = abs(angle(lambda(j))) * 180/pi;
if arg_deg > critical_angle_deg
is_stable = true;
fprintf('  |arg(lambda(j))| = %.1f> %.1f ', arg_deg, critical_angle_deg);
else
is_stable =false;
fprintf('  |arg(lambda(j))| = %.1f <= %.1f ', arg_deg, critical_angle_deg);
end
end

if is_stable
stable_text = 'YES';
title_color = 'black';
else
stable_text = 'NO';
title_color = 'black';
end
%%%%%%%%%%%%%%%%%%%%%%%%%%%%%%%%%%%%%%%%%%%%%%%%%%%%%%%%%%%%%%%%%%%%%%%%%%%%%%%%%%%
% Initialization of variables
t = linspace(0,tfinal,N); h = tfinal/N; init = zeros(1,N);
%beta = fbeta(t); lambda = flambda(t);
```

```
S = init; V=init; ET = init; IT = init; RT = init; IH = init;
EC = init; IC = init; TH = init; A=init;
b = init; a = init;
S(1) = S0; V(1)=V0; ET(1) = ET0; IT(1) = IT0; RT(1) = RT0; IH(1) = IH0;
EC(1) = EC0; IC(1) = IC0; TH(1) = TH0; A(1)=A0;
%N(1)=N0;
Sp = S; Vp=V; ETp = ET; ITp = IT; RTp = RT; IHp = IH; ECp = EC;
ICp = IC; THp = TH; Ap=A; Np = N0;
% computation of coefficients a_k and b_k
for k = 1:N
b(k) = k^alpha-(k-1)^alpha;
a(k) = (k+1)^(alpha+1)-2*k^(alpha+1)+(k-1)^(alpha+1);
end
for j = 2:N
% First part: prediction
aux_s = 0; aux_v = 0; aux_et = 0; aux_it = 0; aux_rt = 0; aux_ih = 0;
aux_ec = 0; aux_ic = 0; aux_th = 0; aux_a=0; aux_n = N0;
for k = 1:j
% Differential system of equations of the model
aux_s = aux_s+b(j-k+1)*(Lambda+delta*V(k)+phi*RT(k)-(beta_T*S(k)*(IT(k)+...
sigma*IC(k)))/(N0)...
-(beta_H*S(k)*(IH(k)+rho_1*EC(k)+rho_2*IC(k)+rho_3*TH(k)+rho_4*A(k)))...
/(N0)-(miu+xi)*S(k));
aux_v = aux_v+b(j-k+1)*(xi*S(k)-(beta_T*(1-epsilon)*V(k)*(IT(k)+sigma*IC(k)))...
/(N0)-(miu+delta)*V(k));
aux_et = aux_et+b(j-k+1)*((beta_T*S(k)*(IT(k)+sigma*IC(k)))/(N0)+(beta_T*...
(1-epsilon)*V(k)*(IT(k)...
+sigma*IC(k)))/(N0)-(beta_H*ET(k)*(IH(k)+rho_2*IC(k)+rho_3*TH(k)+rho_4*A(k)))...
/(N0)-(miu+kappa_1+theta_1)*ET(k));
```

```
aux_it = aux_it+b(j-k+1)*(kappa_1*ET(k)-(beta_H*IT(k)*(IH(k)+rho_1*EC(k)+rho_3*...
TH(k)+rho_4*A(k)))/(N0)-(miu+theta_2+miu_T)*IT(k));
aux_rt = aux_rt+b(j-k+1)*(theta_1*ET(k)+theta_2*IT(k)-(miu+phi)*RT(k));
aux_ih = aux_ih+b(j-k+1)*((beta_H*S(k)*(IH(k)+rho_1*EC(k)+rho_2*IC(k)+rho_3*TH(k)+.
rho_4*A(k)))/(N0)-(beta_T*IH(k)*(IT(k)+sigma*IC(k)))/(N0)-(eta+miu+miu_H)*IH(k));
aux_ec = aux_ec+b(j-k+1)*((beta_T*IH(k)*(IT(k)+sigma*IC(k)))/(N0)...
+(beta_H*ET(k)*(IH(k)+rho_1*EC(k)+rho_2*IC(k)+rho_3*TH(k)+rho_4*A(k)))/(N0)-...
(eta+kappa_2+theta_1+miu+miu_H)*EC(k));
aux_ic = aux_ic+b(j-k+1)*(kappa_2*EC(k)+(beta_H*IT(k)*(IH(k)+rho_1*EC(k)+rho_2*...
IC(k)+rho_3*TH(k)+rho_4*A(k)))/(N0)-(eta+theta_2+miu+miu_C)*IC(k));
aux_th = aux_th+b(j-k+1)*(eta*IH(k)+(eta+theta_1)*EC(k)+(eta+theta_2)*IC(k)-...
(miu+kappa_3)*TH(k));
aux_a = aux_a+b(j-k+1)*(kappa_3*TH(k)-(miu+miu_A)*A(k));
end
Sp(j)=S0+h^alpha/gamma(1+alpha)*aux_s;
Vp(j)=V0+h^alpha/gamma(1+alpha)*aux_v;
ETp(j)=ET0+h^alpha/gamma(1+alpha)*aux_et;
ITp(j)=IT0+h^alpha/gamma(1+alpha)*aux_it;
RTp(j)=RT0+h^alpha/gamma(1+alpha)*aux_rt;
IHp(j)=IH0+h^alpha/gamma(1+alpha)*aux_ih;
ECp(j)=EC0+h^alpha/gamma(1+alpha)*aux_ec;
ICp(j)=IC0+h^alpha/gamma(1+alpha)*aux_ic;
THp(j)=TH0+h^alpha/gamma(1+alpha)*aux_th;
Ap(j)=A0+h^alpha/gamma(1+alpha)*aux_a;
Np(j)=Sp(j)+Vp(j)+ETp(j)+ITp(j)+RTp(j)+IHp(j)+ECp(j)+ICp(j)+THp(j)+Ap(j);
% Second part: correction
aux_ss = Lambda+delta*Vp(j)+phi*RTp(j)-(beta_T*Sp(j)*(ITp(j)+sigma*ICp(j)))
.../(Np(j))...
-(beta_H*Sp(j)*(IHp(j)+rho_1*ECp(j)+rho_2*ICp(j)+rho_3*THp(j)+rho_4*Ap(j)))
```

```
.../(Np(j))-(miu+xi)*Sp(j);
aux_vv= xi*Sp(j)-(beta_T*(1-epsilon)*Vp(j)*(ITp(j)+sigma*ICp(j)))
.../(Np(j))-(miu+delta)*Vp(j);
aux_etet = (beta_T*Sp(j)*(ITp(j)+sigma*ICp(j)))
.../(Np(j))+(beta_T*(1-epsilon)*Vp(j)*(ITp(j)+sigma*ICp(j)))
.../(Np(j))-(beta_H*ETp(j)*(IHp(j)+
...rho_2*ICp(j)+rho_3*THp(j)+rho_4*Ap(j)))/(Np(j))...
-(miu+kappa_1+theta_1)*ETp(j);
aux_itit=kappa_1*ETp(j)-(beta_H*ITp(j)*(IHp(j)+rho_1*ECp(j)+rho_3*THp(j)+
...rho_4*Ap(j)))/(Np(j))...
-(miu+theta_2+miu_T)*ITp(j);
aux_rtrt = theta_1*ETp(j)+theta_2*ITp(j)-(miu+phi)*RTp(j);
aux_ihih = (beta_H*Sp(j)*(IHp(j)+rho_1*ECp(j)+rho_2*ICp(j)+rho_3*THp(j)+
...rho_4*Ap(j)))
/(Np(j))...
-(beta_T*IHp(j)*(ITp(j)+sigma*ICp(j)))/(Np(j))-(eta+miu+miu_H)*IHp(j);
aux_ecec = (beta_T*IHp(j)*(ITp(j)+sigma*ICp(j)))/(Np(j))...
+(beta_H*ETp(j)*(IHp(j)+rho_1*ECp(j)+rho_2*ICp(j)+rho_3*THp(j)
+rho_4*Ap(j)))/(Np(j))-(eta+kappa_2...
+theta_1+miu+miu_H)*ECp(j);
aux_icic= kappa_2*ECp(j)+(beta_H*ITp(j)*(IHp(j)+rho_1*ECp(j)+rho_2*ICp(j)
+rho_3*THp(j)...
+rho_4*Ap(j)))/(Np(j))-(eta+theta_2+miu+miu_C)*ICp(j);
aux_thth = eta*IHp(j)+(eta+theta_1)*ECp(j)+(eta+theta_2)*ICp(j)-
(miu+kappa_3)*THp(j);
aux_aa=kappa_3*THp(j)-(miu+miu_A)*Ap(j);

auxx=((j-1)^(alpha+1)-(j-1-alpha)*j^alpha);
aux_s0 = auxx*(Lambda+delta*Vp(1)+phi*RTp(1)-(beta_T*Sp(1)*(ITp(1)+
```

```
...sigma*ICp(1)))/(N0)...
-(beta_H*Sp(1)*(IHp(1)+rho_1*ECp(1)+rho_2*ICp(1)+rho_3*THp(1)
+rho_4*Ap(1)))/(N0)-(miu+xi)*Sp(1));
aux_v0 = auxx*(xi*Sp(1)-(beta_T*(1-epsilon)*Vp(1)*(ITp(1)+sigma*ICp(1)))
/(N0)-(miu+delta)*Vp(1));
aux_et0 = auxx*((beta_T*Sp(1)*(ITp(1)+
sigma*ICp(1)))
/(N0)+(beta_T*(1-epsilon)*Vp(1)*(ITp(1)...
+sigma*ICp(1)))
/(N0)-(beta_H*ETp(1)*(IHp(1)+rho_2*ICp(1)+rho_3*THp(1)+rho_4*Ap(1)))
/(N0)...
-(miu+kappa_1+theta_1)*ETp(1));
aux_it0 = auxx*(kappa_1*ETp(1)-(beta_H*ITp(1)*(IHp(1)+rho_1*ECp(1)+
rho_3*THp(1)+rho_4*Ap(1)))/(N0)...
-(miu+theta_2+miu_T)*ITp(1));
aux_rt0 = auxx*(theta_1*ETp(1)+theta_2*ITp(1)-(miu+phi)*RTp(1));
aux_ih0 = auxx*((beta_H*Sp(1)*(IHp(1)+rho_1*ECp(1)+rho_2*ICp(1)+rho_3*THp(1)
+rho_4*Ap(1)))/(N0)...
-(beta_T*IHp(1)*(ITp(1)+sigma*ICp(1)))/(N0)-(eta+miu+miu_H)*IHp(1));
aux_ec0 = auxx*((beta_T*IHp(1)*(ITp(1)+sigma*ICp(1)))/(N0)...
+(beta_H*ETp(1)*(IHp(1)+rho_1*ECp(1)+rho_2*ICp(1)+rho_3*THp(1)
+rho_4*Ap(1)))/(N0)-(eta+kappa_2...
+theta_1+miu+miu_H)*ECp(1));
aux_ic0 = auxx*(kappa_2*ECp(1)+(beta_H*ITp(1)*(IHp(1)+rho_1*ECp(1)
+rho_2*ICp(1)+rho_3*THp(1)...
+rho_4*Ap(1)))/(N0)-(eta+theta_2+miu+miu_C)*ICp(1));
aux_th0 = auxx*(eta*IHp(1)+(eta+theta_1)*ECp(1)+(eta+theta_2)*ICp(1)
-(miu+kappa_3)*THp(1));
aux_a0 = auxx*(kappa_3*THp(1)-(miu+miu_A)*Ap(1));
```

```
aux_s = 0; aux_v=0; aux_et = 0; aux_it = 0; aux_rt = 0; aux_ih = 0;
aux_ec = 0; aux_ic = 0; aux_th = 0; aux_a=0;
for k = 1:j-1
% Differential system of equations of the model
aux_s = aux_s+a(j-k)*(Lambda+delta*V(k)+phi*RT(k)-(beta_T*S(k)*(IT(k)
+sigma*IC(k)))/(N0)...
-(beta_H*S(k)*(IH(k)+rho_1*EC(k)+rho_2*IC(k)+rho_3*TH(k)+rho_4*A(k)))
/(N0)-(miu+xi)*S(k));
aux_v = aux_v+a(j-k)*(xi*S(k)-(beta_T*(1-epsilon)*V(k)*(IT(k)+sigma*IC(k)))
/(N0)-(miu+delta)*V(k));
aux_et = aux_et+a(j-k)*((beta_T*S(k)*(IT(k)+sigma*IC(k)))/(N0)+(beta_T*
(1-epsilon)*V(k)*(IT(k)...
+sigma*IC(k)))/(N0)-(beta_H*ET(k)*(IH(k)+rho_2*IC(k)+rho_3*TH(k)
+rho_4*A(k)))/(N0)...
-(miu+kappa_1+theta_1)*ET(k));
aux_it = aux_it+a(j-k)*(kappa_1*ET(k)-(beta_H*IT(k)*(IH(k)+rho_1*EC(k)
+rho_3*TH(k)+rho_4*A(k)))/(N0)...
-(miu+theta_2+miu_T)*IT(k));
aux_rt = aux_rt+a(j-k)*(theta_1*ET(k)+theta_2*IT(k)-(miu+phi)*RT(k));
aux_ih = aux_ih+a(j-k)*((beta_H*S(k)*(IH(k)+rho_1*EC(k)+rho_2*IC(k)
+rho_3*TH(k)+rho_4*A(k)))/(N0)...
-(beta_T*IH(k)*(IT(k)+sigma*IC(k)))/(N0)-(eta+miu+miu_H)*IH(k));
aux_ec = aux_ec+a(j-k)*((beta_T*IH(k)*(IT(k)+sigma*IC(k)))/(N0)...
+(beta_H*ET(k)*(IH(k)+rho_1*EC(k)+rho_2*IC(k)+rho_3*TH(k)
+rho_4*A(k)))/(N0)-(eta+kappa_2+theta_1+miu+miu_H)*EC(k));
aux_ic = aux_ic+a(j-k)*(kappa_2*EC(k)+(beta_H*IT(k)*(IH(k)+rho_1*EC(k)
+rho_2*IC(k)+rho_3*TH(k)...
```

```
+rho_4*A(k)))/(N0)-(eta+theta_2+miu+miu_C)*IC(k));
aux_th = aux_th+a(j-k)*(eta*IH(k)+(eta+theta_1)*EC(k)+(eta+theta_2)*IC(k)
-(miu+kappa_3)*TH(k));
aux_a = aux_a+a(j-k)*(kappa_3*TH(k)-(miu+miu_A)*A(k));
end
S(j)=S0+h^alpha/gamma(2+alpha)*(aux_ss+aux_s0+aux_s);
V(j)=V0+h^alpha/gamma(2+alpha)*(aux_vv+aux_v0+aux_v);
ET(j)=ET0+h^alpha/gamma(2+alpha)*(aux_etet+aux_et0+aux_et);
IT(j)=IT0+h^alpha/gamma(2+alpha)*(aux_itit+aux_it0+aux_it);
RT(j)=RT0+h^alpha/gamma(2+alpha)*(aux_rtrt+aux_rt0+aux_rt);
IH(j)=IH0+h^alpha/gamma(2+alpha)*(aux_ihih+aux_ih0+aux_ih);
EC(j)=EC0+h^alpha/gamma(2+alpha)*(aux_ecec+aux_ec0+aux_ec);
IC(j)=IC0+h^alpha/gamma(2+alpha)*(aux_icic+aux_ic0+aux_ic);
TH(j)=TH0+h^alpha/gamma(2+alpha)*(aux_thth+aux_th0+aux_th);
A(j)=A0+h^alpha/gamma(2+alpha)*(aux_aa+aux_a0+aux_a);
end
y(1,:) = S; y(2,:) = V; y(3,:) = ET; y(4,:) = IT; y(5,:) = RT;
y(6,:) = IH; y(7,:) = EC; y(8,:) = IC; y(9,:) = TH; y(10,:) = A;

plot(t,y(10,:),'Linewidth', 2.5);
xlabel('time in years'); ylabel('A(t)');
%title(sprintf('Stability Regions (Order = %.2f)', alpha), 'FontWeight', 'bold');
legend_handle=legend({'\alpha=0.5', '\alpha=0.7', '\alpha=0.9', '\alpha=1.0'});
set(legend_handle, 'FontSize', 16);
% Set font size for axes ticks
ax = gca;
ax.FontSize = 16; % Adjust this value as needed
hold on
end
```